



Universidad de Valladolid

FACULTAD DE CIENCIAS/ I. U. CINQUIMA

**DEPARTAMENTO DE QUÍMICA FÍSICA Y QUÍMICA
INORGÁNICA**

TESIS DOCTORAL

**The transmetalation step in Pd-catalyzed
processes: Understanding the role of the classical
nucleophile, the ligands and the synthetic
potential of a third metal**

Presentada por **Juan del Pozo del Valle** para optar al
grado de Doctor por la Universidad de Valladolid

Dirigida por

Prof. Dr. Juan A. Casares González
Prof. Dr. Pablo Espinet Rubio

Valladolid, 2015

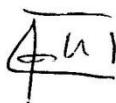
AUTORIZACIÓN DE LOS DIRECTORES DE TESIS

(Art. 2.1. c de la Normativa para la presentación y defensa de la Tesis Doctoral en la UVa)

D. Pablo Espinet Rubio, con D.N.I. nº 17176361F y D. Juan Ángel Casares González, con D.N.I. nº 09740156R, Catedráticos de Universidad del Departamento de Química Física y Química Inorgánica de la Facultad de Ciencias, como Directores de la Tesis Doctoral titulada “The transmetalation step in Pd-catalyzed processes: Understanding the role of the classical nucleophile, the ligands and the synthetic potential of a third metal”, presentada por D. Juan del Pozo del Valle, alumno del programa: “Doctorado en Química: Química de síntesis, métodos de separación, catálisis y materiales avanzados” impartido por el Instituto Universitario CINQUIMA, autorizan la presentación de la misma, considerando que cumple todos los requisitos para ello

Valladolid, 14 de octubre de 2015

Los Directores de la Tesis



Fdo. Pablo Espinet Rubio



Fdo. Juan A. Casares González

Table of contents

Abbreviations and acronyms	1
Abbreviations and symbols used for NMR	2
General scheme of the Memory	3
General Introduction: The key role of the transmetalation step in Pd-catalyzed cross-coupling reactions.....	5
1. Pd-catalyzed cross-coupling reactions	7
1.1. Catalysts for cross-coupling reactions.....	8
1.2. The general mechanism of Pd-catalyzed cross-coupling reactions.....	9
2. The transmetalation reaction.....	11
2.1. Mechanisms of the transmetalation: A Ligand Substitution at Pd ^{II}	12
3. Factors controlling the transmetalation.....	15
3.1. Polarization of the M-C bond Basicity and nucleophilicity:.....	16
3.2. Thermodynamics of the transmetalation: M-C and M-X bond strength.....	18
3.3. Kinetics: factors controlling the transition state	21
4. Objectives	24
5. References.....	26
Chapter I: The gold co-catalyzed Stille reaction.....	30
1. Introduction.....	31
1.1. Background.....	32
1.2. Structural features of organostannanes	32
1.3. Nature of the Sn/Pd transmetalation.....	34
2. Gold co-catalysis makes Stille coupling involving bulky groups feasible.....	42
2.1. Results and discussion	43
2.2. Conclusions.....	52
3. The decisive role of ligand metathesis in Au/Pd bimetallic catalysis	53
3.1. Results and Discussion	54
3.2. Conclusions.....	62
4. Experimental section	63
4.1. General methods.....	63

4.2. Synthesis of the compounds	63
4.3. General procedure of the Stille cross-coupling reactions co-catalyzed by gold and palladium complexes.....	65
4.4. General procedure for ligand exchange reactions between gold and palladium complexes.....	65
4.5. Computational Details.....	72
5. References.....	73

Chapter II: Bimetallic Hiyama cross-coupling of bulky groups promoted by CuF₂..78

1. Introduction.....	81
1.1. Background.....	81
1.2. Nature of the Si/Pd transmetalation	82
1.3. Mechanisms of the Si/Pd transmetalation: evidences for different Si/Pd transmetalation scenarios.....	89
1.4. Extending the scope of the silicon-based cross-coupling reactions.....	95
2. Results and discussion.....	98
2.1. Mechanistic Studies and considerations	108
2.2. Proposed mechanistic cycle for the cross-coupling reaction	120
3. Conclusions.....	120
4. Experimental section.....	122
4.1. General methods.....	122
4.2. Synthesis of bulky (aryl)triethoxysilanes	122
4.3. Synthesis of Palladium complexes	125
4.4. General procedure of the cross-coupling reactions	126
4.5. Mechanistic Studies.....	129
4.6. Additional experiments	132
5. References.....	133

Chapter III: Study of the secondary transmetalations in the Negishi reaction140

1. Introduction.....	141
1.1. Background.....	142
1.2. Structural features of organozincs	143
1.3. Nature of the Zn/Pd transmetalation.....	146

1.4. Mechanistic studies of the Zn/Pd transmetalation	151
1.5. The hot spot of the Negishi reaction: sp ³ couplings.....	156
2. Organometallic nucleophiles and Pd: What makes ZnMe ₂ different?	159
2.1. Results and discussion.....	164
2.2. What is special in ZnMe ₂ (or ZnEt ₂) compared to other Zn organometallics? .	173
2.3. Conclusions.....	179
3. Study of Zn/Pd secondary (R ² for R ¹) transmetalations of [PdR ¹ R ²] complexes	180
3.1. Results and discussion.....	180
3.2. Conclusions.....	187
4. Experimental section.....	189
4.1. General Methods.....	189
4.2. Synthesis of the complexes	189
4.3. Spontaneous isomerization of <i>cis</i> -[PdArMe(PPh ₃) ₂] (1) to <i>trans</i> -[PdArMe(PPh ₃) ₂] (2)	189
4.4. Transmetalation reaction between <i>cis</i> -[PdArMe(PPh ₃) ₂] (1) or <i>trans</i> - [PdArMe(PPh ₃) ₂] (2) and ZnMe ₂	193
4.5. Computational methods	198
5. References.....	200
Chapter IV: Unexpected instability of Pd–Phosphine–Olefin complexes	206
1. Introduction.....	209
2. Results and discussion.....	210
2.2. Computational examination of the olefin insertion into the Pd–Aryl bond.....	212
2.3. Effect of the groups in the migration process	214
3. Conclusions.....	216
4. Experimental section.....	218
4.1. General methods.....	218
4.2. Synthesis of the compounds	218
4.3. Decomposition studies.....	222
4.4. DFT calculations.....	222
4.5. Computational optimization	222
5. References.....	224

Chapter V: Mechanism of the N–H oxidative addition/reductive elimination of anilines	227
2. Results and discussion	234
2.1. Study of the reductive elimination of [(PCP)Ir(H)(NHPH)]	234
2.2. Study of the oxidative addition	245
2.3. Equilibration of [(PCP)Ir(H)(Ph)] with anilines and [(PCP)Ir(H)(NHAr–R)]	247
2.4. Additional experiments	250
3. Conclusions.....	251
4. Experimental section	253
4.1. General Considerations	253
4.2. General synthesis of complexes [(PCP)Ir(H)(NHAr)].....	253
4.3. Kinetic runs.....	254
4.4. Study of the reductive elimination	255
4.5. Study of the oxidative addition	256
4.6. Equilibration of [(PCP)Ir(H)(Ph)] (5) with anilines and [(PCP)Ir(H)(NHAr-R)] (1n)	256
4.7. DFT calculations.....	256
5. Reference	257
Resumen en español.....	261

Abbreviations and acronyms

Ar	aryl
BDE	bond Dissociation Energy
bipy	2,2'-bipyridine
Bu	butyl
COD	1,5-cyclooctadiene
dba	dibenzylideneacetone
DFB	difluorobenzene
DFT	density Functional Theory
DMF	dimethyl formamide
dppf	1,1'-Bis(diphenylphosphino)ferrocene
Et	ethyl
EWO	Electron-withdrawing olefin
IDM	1,3-dimethyl- imidazoline-2-ylidene
HOMO	highest Occupied Molecular Orbital
KIE	kinetic Isotope Effect
<i>i</i> -Pr	isopropyl
L	monodentate neutral ligand
LUMO	lowest Unoccupied Molecular Orbital
M	metal in general
Me	methyl
Mes	mesityl
NHC	nitrogen Heterocyclic Carbene
Nu	nucleophile
OTf	trifluoromethanesulfonate (CF ₃ SO ₃)

Ph	phenyl
Pf	pentafluorophenyl (C ₆ F ₅)
PEWO	Phosphine–Electron-withdrawing olefin
R	organic group in general
Rf	3,5-dichlorotrifluorophenyl (3,5-C ₆ Cl ₂ F ₃)
RT	room Temperature
S	solvent in general
SET	single electron transfer
THF	tetrahydrofuran
tht	tetrahydrothiophene
TS	transition State
X	halogen

Abbreviations and symbols used for NMR

s	singlet
bs	broad singlet
d	doublet
t	triplet
m	multiplet
dd	doublet of doublets
dt	doublet of triplets
dm	doublet of multiplets
ddd	doublet of doublet of doublets
ppm	parts per million
δ	chemical shift
J	spin-spin coupling constant

General scheme of the Memory

This Memory contains the results of the research that I have developed in the Institute CINQUIMA (Department of Inorganic Chemistry) at the University of Valladolid during my thesis work. Essentially it is a contribution on synthetic and mechanistic studies in Pd-catalyzed cross-coupling reactions, mainly focused on the transmetalation step. The ultimate goal of our investigations is the rational design of new reactions and catalysts in order to provide enhanced reactivity for synthetic applications. Some of the results are published in scientific journals and part of the contents and figures may be coincident.

This Thesis is organized in a General Introduction and four independent chapters. The main purpose of the General Introduction is to define in a general way the basic concepts that affect the nature of the transmetalation step. These concepts will be repeated throughout the Doctoral Thesis and are worth commenting beforehand. All chapters of this thesis are organized in the same way: introduction, results and discussion, conclusions, references and experimental part, and they are very independent of one another. The individual introductions of each chapter review the state of the art and the particular factors conditioning each transmetalation. The bibliographical references have been included at the end of every chapter. Footnotes are used to provide relevant explanations when considered appropriate.

Chapters I and II study the use of metals from Group X of the Periodic table (Au and Cu respectively) to promote efficient Pd-catalyzed cross-coupling of bulky groups from organotin (Chapter I) and organosilanes (Chapter II) with aryl halides. The corresponding bimetallic systems are explored synthetically and mechanistically, focusing on the enhanced transmetalation as the source of improved reactivity. Chapter I was carried out in collaboration with other researchers: Desirée Carrasco studied experimentally the Sn/Au transmetalation equilibria. This chapter includes a DFT study of the Sn/Au, Sn/Pd and Au/Pd

transmetalation carried out in collaboration with Max García Melchor and Rosana Álvarez.

Chapter III deals with the Zn/Pd transmetalation. It provides a fundamental perspective of an undesired group exchange that decreases the efficiency of the Negishi coupling, addressing in great detail the Pd/Zn interactions governing the group transfer. The computational work described in this chapter was carried out by Dr. Rosana Álvarez at the University of Vigo.

Chapter IV contains work carried out throughout the Doctoral studies, in a different topic that is being studied in the group of Valladolid. It consists of a computational and experimental investigation of a phosphine-olefin ligand designed in our group with the aim of enhancing the reactivity of palladium catalysts for challenging syntheses. Part of this work was carried out in a collaboration of the group with Dr. Vladimir V. Grushin of the Institute of Chemical Research of Catalonia.

Chapter V involves an experimental investigation of the mechanisms of the N-H oxidative addition of anilines to [(PCP)Ir] complexes. This work was carried out at Rutgers University (New Jersey, USA) under the supervision of Alan S. Goldman as required for the International Doctor Mention. The experimental work of this chapter is not finished and further experimentation is ongoing in Goldman's group.

We thank all the collaborators for their contributions to this Doctoral Thesis and valuable discussions.

This Memory is presented to obtain the International Ph.D. It was chosen to write the Memory in English, including a brief summary of the results and general conclusions in Spanish.

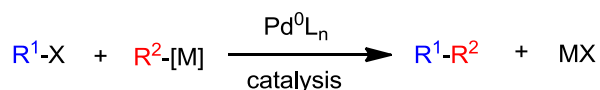
General Introduction

**The key role of the
transmetalation step in Pd-
catalyzed cross-coupling
reactions**

1. Pd-catalyzed cross-coupling reactions

The C-C cross-coupling reactions are undoubtedly one of the most important and useful reactions in organic synthesis and organometallic chemistry, since all kinds of moieties can be coupled from readily accessible reactants under mild conditions.¹ These reactions consist of two main reagents: an organic electrophile (R^1-X) and an organometallic nucleophile (R^2-M) in the presence of a metal catalyst.

It will be the interest of this Doctoral Thesis the cross-coupling reactions that are catalyzed by palladium, as they have been extensively used and studied in both academic and industrial fields. As a result of their huge impact on Organic Chemistry, the 2010 Nobel Prize in Chemistry was awarded jointly to Professor Richard F. Heck (University of Delaware, USA), Professor Ei-ichi Negishi (Purdue University, USA) and Professor Akira Suzuki (Hokkaido University, Japan), acknowledging their great contribution to the development and understanding of a field that has revolutionized the way chemists design and construct molecules.²



X = halide, triflate, tosylate...

[M] = Al, B, Cu, In, , Li, Mg, Si, Sn, Zn, Zr, etc.

Scheme Intro-1. General equation of Pd-catalyzed cross-coupling reactions.

Apart from the widely employed organometallic nucleophiles, there are other very important transformations not including these counterparts. Cross-coupling reactions can involve olefins (Heck reaction), amines (Buchwald-Hartwig amination) and almost any other nucleophile,³ leading to selective C-O, C-P, C-S, C-B and C-F formation.⁴ In this regard, the role of ligands needs to be highlighted as the key factor that has allowed chemists for the development of all kinds of cross-coupling reactions. However, as reviewing all the chemistry that can be carried out by

palladium could take a lifetime, only those that involve transmetalation of the organic group from an organometallic nucleophile will be the subject of this doctoral thesis. Furthermore, the transmetalation step will be considered with special care and will be analyzed from both a mechanistic and synthetic perspective.

1.1. Catalysts for cross-coupling reactions

Although typically cross-coupling reactions involve a nucleophile and an electrophile,^{*,5} they only take place in the presence of a catalyst. Generally, the most widely used catalysts in cross-coupling are Pd and Ni complexes, although several efficient examples have been reported with Cu, Fe, or Co.⁶

The key feature for an efficient catalyst in cross-coupling is the ease of redox exchange of the metal center. All these metals coincide in this characteristic, but Pd and Ni are by far the ones that allow for the most efficient redox switch. A number of advantages can be found in the use of nickel instead of palladium: lower price, greater availability and more facile oxidative addition are characteristics of Ni catalysts and very important concerns for the industry. Aryl chlorides are more easily activated by nickel than by palladium, and they are certainly the most attractive aryl halides for synthetic applications on an industrial scale.⁷ Nevertheless, Pd-catalyzed reactions have shown so far more advantages for cross-coupling than those of Ni. For example, they tend to be less sensitive to oxygen and great differences in selectivity have been reported in certain reactions.³ This behavior comes from the difference in the mechanism and the elementary steps.

Mechanistically, palladium and nickel show some similarities as they are close neighbors in the periodic table. However, Ni possesses a greater number of readily available oxidation states. Although Ni⁰/Ni^{II} catalytic cycles are widespread, the easy accessibility of Ni^I and Ni^{III} oxidation states allows for a richer mechanistic picture. The higher relative stability of Ni^I opens the door to the existence of radical

* There are examples of reactions involving two nucleophiles or two electrophiles, in the presence of oxidants or reductants, respectively. See ref 5 for selected examples.

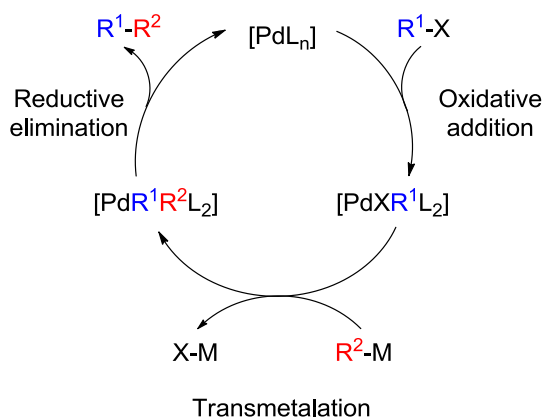
mechanisms via Single Electron Transfer (SET) reactions.^{*8} On the contrary, Pd^I and Pd^{III} are rare and hardly accessed oxidation states, which means that most of its chemistry follows a polar (non-radical) Pd⁰/Pd^{II}.³ The fact that SET processes are disfavored increases the selectivity of the catalyst, as radical reactions are usually not very selective. Finally, it is also worth giving a few words to Pt as catalyst for cross-coupling reactions. The ease of redox switching is severely hindered by the great kinetic inertness of Pt, due to the fact that the *d* orbitals are stabilized when going down in a group of the periodic table. As well, this metal is very expensive and the industrial applicability is more limited.

Currently, Pd-catalyzed methods appear to be generally superior to the rest of active transition metals in its scope, stereo, regio, and chemoselectivities, but in the last decade, the number of cross-coupling reports using Ni has boomed due to the greater understanding of the mechanism.⁹ Nevertheless, it is less understood than the Pd-catalyzed variant and it deserves special attention on its own. Accordingly, it will not be covered in this thesis, which will be focused on the Pd-catalyzed cross-coupling reactions and in particular, on the transmetalation step. For further information of the features of cross-coupling using nickel catalysis, abundant literature is available concerning the mechanisms of the elementary steps.^{10,11}

1.2. The general mechanism of Pd-catalyzed cross-coupling reactions

These reactions are generally proposed to proceed through a mechanism that involves three main steps:¹

* Indeed, the oxidative addition of aryl halides to Ni(PEt₃)₄ has been proven to follow a radical mechanism, in which the rate limiting step is a SET transfer from the Ni⁰ donor, to the aryl halide acceptor. See ref 8.



Scheme Intro-2. Simplified mechanistic cycle of the Pd-catalyzed cross-coupling reactions.

1. *Oxidative addition* of the organic electrophile to the metal center.¹²

2. *Transmetalation*, in which an organic fragment is transferred from an organometallic nucleophile (usually main group element) to the metal catalyst, replacing the halide or pseudohalide with the organic group. Several different reagents can be used for this step, and the mechanism for the process is expected to show differences depending on the steric and electronic properties of this counterpart.¹³

3. *Reductive elimination* of the new R^1-R^2 bond to afford the reaction product and the concomitant regeneration of the palladium catalyst in oxidation state zero.¹⁴ Although other reactions have been demonstrated to follow a $\text{Pd}^{\text{II}}/\text{Pd}^{\text{IV}}$ redox cycle, these are rare and only take place with strong oxidants.¹⁵

This is a simplistic picture of the catalytic cycle. Nevertheless, it is worth commenting that the actual scenario can be a lot more complicated. For example, palladium complexes can present cis-trans isomers. Although frequently overlooked, this can play a key role in the success or failure of a coupling reaction. Oxidative addition and transmetalation can provide any of the two isomers, but reductive elimination can take place only from a cis isomer. In some cases, an *isomerization step* should be considered as a very important part of a catalytic cycle.¹⁶

The oxidative addition and reductive elimination steps are common to all the different catalytic cross-coupling processes and have been studied in depth by both experimental and computational methods.¹²⁻¹⁴ As it was pointed out by Stille, these two steps were reasonably well understood even back in 1986.¹⁷ Conversely, the transmetalation has been studied more recently. It depends on the nucleophile used, and important differences in the mechanism have been noted. These features are closely related to the nature of the transition states of the group transfer, as it will be discussed along this manuscript.

2. The transmetalation reaction

The transmetalation reaction consists in the transfer of an organic group R (alkyl, aryl, vinyl, alkyne, etc) from an organometallic nucleophile (metal or semimetal) to the palladium catalyst.¹⁸

Among the numerous advantages of the C-C reactions, it is remarkable the broad variety of organometallic reagents that can be employed for this purpose. The metal or semimetal involved determines the particular nuances of each reaction and also the transmetalation mechanism. The nature of the nucleophile defines important features such as the transmetalation rate, the need for additives, the tolerance of functional groups and reaction conditions. Each variation receives a name which usually corresponds to the discoverer's name (Scheme Intro-3).

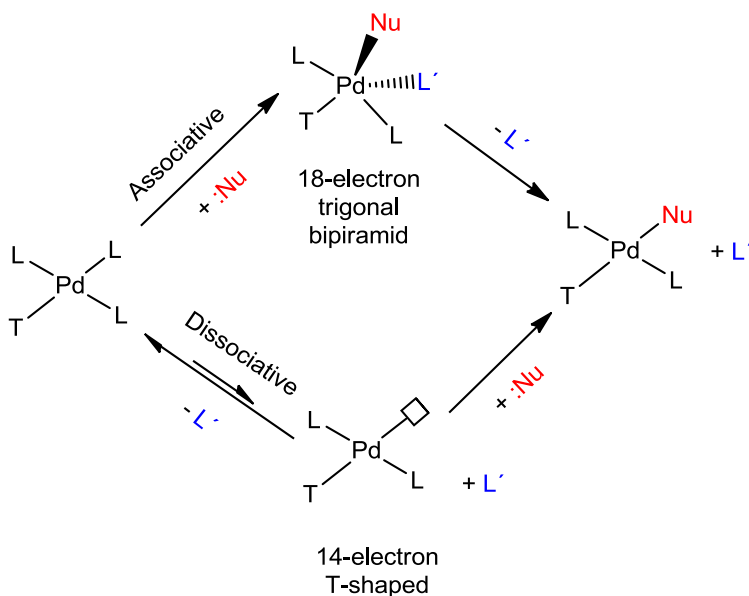


(M) = B (Suzuki-Miyaura)
 Sn (Stille)
 Si (Hiyama)
 Zn (Negishi)
 Mg (Kumada)...

Scheme Intro-3. General scheme for the transmetalation in cross-coupling reactions.

2.1. Mechanisms of the transmetalation: A Ligand Substitution at Pd^{II}

Before going into details concerning the different transmetalation mechanisms that can be found in the rich chemistry of the Pd-catalyzed reactions, it is interesting to realize from the beginning that the very nature of the transmetalation is that of a ligand substitution on a Pd^{II} complex.¹⁹ These complexes are usually tetracoordinated square-planar 16-electron species and can undergo ligand-substitution processes by the two pathways depicted in Scheme Intro-4.^{18,20,*}



Scheme Intro-4. Mechanisms of the ligand substitution in Pd^{II} complexes.

The dissociative pathway involves a 14-electron T-shaped intermediate, and usually takes place at the position of the most labile ligand. As well, the ligand with the highest trans influence plays a role at determining at which position the

* The palladium catalyst neither changes its oxidation number (it remains Pd^{II}) nor its final coordination number, because 16-electron complexes are recovered. It is depicted as a "Metal exchange mechanism", different from the "Redox mechanism" or the "ate complex mechanisms", usually evoked in classical organometallic texts. See for instance ref 20.

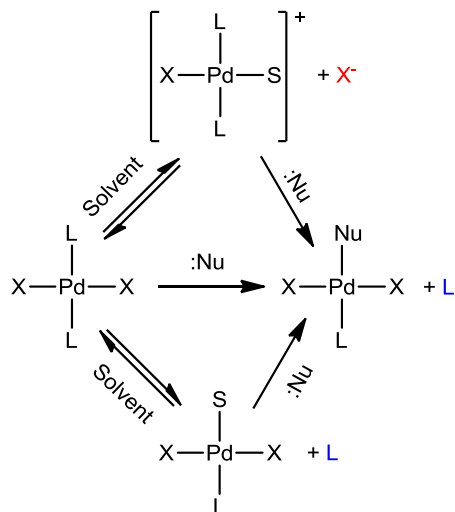
substitution occurs, weakening the bond trans to it and contributing to the dissociation equilibrium.

The associative pathway goes through an 18-electron trigonal bipyramidal complex either as intermediate or transition state, and the position at which the substitution occurs is determined by the ligand with the highest trans effect, which determines the lowest-energy transition state. $[\text{PdRXL}_2]$ complexes seem to follow this pathway in most cases. Often the associative mechanism includes two parallel pathways: direct substitution and solvent-assisted substitution (see Scheme Intro-5).

In the case of the solvent assisted substitution, the leaving ligand is firstly substituted associatively by a molecule of solvent, which has to be able to behave as a Lewis base. The substitution is favored by the very large concentration of the solvent in the reaction field. This is followed by substitution of the coordinated solvent by the corresponding nucleophile, via a less energetic pathway than the direct substitution. It is more facile for good donor solvents, such as NMP, DMF or HMPA.* A molecule of solvent may replace either a neutral ligand or a halide. In the latter case, the transmetalation takes place via cationic Pd intermediates, which are usually more reactive towards the transmetalation than the homologous neutral species, as they are more electrophilic.^{†,21}

* Note that in the solvent-assisted pathway both the substitution of L for S and that of S for Nu are usually associative. A coordinating solvent is simply a ligand and contributes two electrons to the complex. Thus, a $[\text{PdRXL}(\text{S})]$ complex is a 16-electron species. Olefins, adventitious water, and agostic bonds can play a similar role as ligands.

† Replacement of X⁻ is less costly for good leaving ligands. It usually follows the trend $\text{Cl} < \text{Br} < \text{I} \ll \text{OTf}$. Indeed, *trans*- $[\text{PdRXL}_2]$ complexes are found to be in equilibrium with $[\text{PdRSL}_2]^+$ or $[\text{PdRL}_3]^+$. See ref.21.



Scheme Intro-5. Direct substitution versus solvent assisted substitution.

In a first step, the organometallic nucleophile needs to coordinate to Pd either associatively or dissociatively, as illustrated in Scheme Intro-4. The actual group transfer between the metals can take place through two different pathways:

i) Coordination of the nucleophile to the palladium catalyst and the group transfer take place simultaneously, via pentacoordinate transition states. The presence of free ligand L would not affect the rate of the reaction.

ii) It can take place at a tetracoordinate intermediate in which the neutral ligand has been previously released: A first step of neutral ligand substitution by the nucleophile is followed by a second step where the actual group transfer takes place. The first step is hindered by the presence of additional free L. As a result, the addition of external ligand has been shown to slow down the transmetalation reaction in these cases.^{*22,23}

The particular case of bulky phosphines and NHC carbenes ligands should be commented in detail. They have become ubiquitous in catalysis with palladium and their use should be regarded as a breakthrough in the development of effective

* This fact was initially taken as an indication of prior dissociation of neutral ligand, but it is perfectly compatible with an associative mechanism. See ref. 23.

protocols for challenging cross-coupling reactions.²⁴ The steric bulk is one of the key features of the success of these ligands. As the volume occupied by the ligand is increased, palladium intermediates bearing only one ligand are favored.^{24a} This fact has very important implications in oxidative addition and reductive elimination,* but also in the transmetalation step.

Three-coordinate [PdRXL] are proposed to be the actual species that undergo transmetalation when bulky ligands are involved. Their chemistry is dramatically different because they favor a 16e–14e–16e dissociative mechanism over the most common 16e–18e–16e associative substitution operating in the usual square planar [Pd^{II}RXL₂] complexes.[†] Thus, additional advantages are provided by these ligands: three-coordinate palladium complexes are more electrophilic than the equivalent tetracoordinated ones with one additional neutral ligand. This facilitates the reaction with less-strong nucleophiles. As an extra bonus, the problem associated with the formation of cis and trans isomers in the palladium complex is circumvented (see section 1.2).

Indeed, depending on the solvent and nature of the ancillary ligands, the two pathways (associative and dissociative) may contribute to the rate of substitution, and the reaction kinetics may become more complex.

3. Factors controlling the transmetalation

One can imagine a mechanism by which the metal center of the nucleophile would initially coordinate to the halogen and simultaneously assist dissociation of the halogen while delivering the carbon nucleophile to the palladium metal center

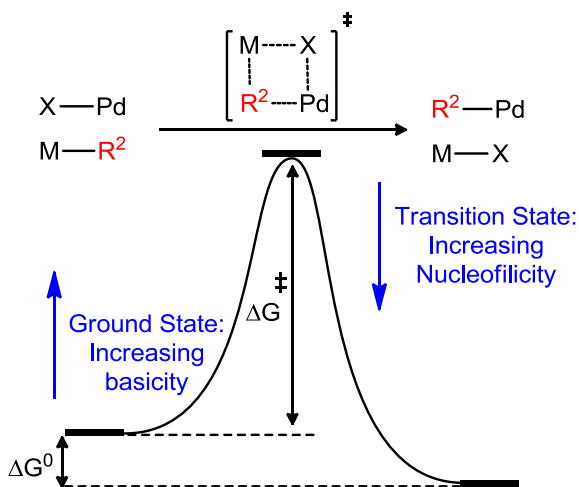
* Pd⁰L species are more reactive towards oxidative addition than the homologous Pd⁰L₂. As well, reductive elimination from 3-coordinate [PdR₂L] is faster than that of [PdR₂L₂]. As a matter of fact, several reductive eliminations have been reported to dissociate a ligand prior to the coupling. That would be favored if ligand dissociation is energetically feasible.

[†] The strict consideration of these complexes as 14-electron three-coordinate Pd(II) complexes can be questioned; the vast majority of them show C–H, or other weak agostic coordination to the hypothetically empty coordination position on Pd. Agostic interactions can be easily dissociated at very low energy cost and lead to short-lived tricoordinated intermediates with an empty low-lying Pd orbital.

(see Scheme Intro-6). However, the mechanism by which less polar and less electrophilic organosilanes, stannanes, and boronates undergo transmetalation has been shown to be more complex.¹³ In any case, this depiction is accurate enough to introduce some of the common and fundamental concepts of the transmetalation.

3.1. Polarization of the M-C bond Basicity and nucleophilicity:

The reactivity of nucleophiles is defined by kinetic and thermodynamic features that make them different to one another. In a general way, it is generally favored with the increasing difference of electronegativity between the metal center and the carbon atom and thus with the ionic character of the carbon-metal bond (see Scheme Intro-7).²⁵ This is a simplified consequence of two generally handled concepts in organometallic reactions: basicity and nucleophilicity.



Scheme Intro-6. Potential energy surface of the transmetalation.

Lewis acidity and basicity are thermodynamic concepts related to the energy of the corresponding empty or full frontier orbitals (with appropriate symmetry) in the fundamental state of the reagents and products.²⁶ Electrophilicity and nucleophilicity are kinetic concepts that, in addition to the fundamental orbital acidity and basicity, can be importantly influenced by steric factors in the approach of the nucleophile to the electrophile or by factors conditioning the energy of the

transition states, such as changes of the reaction mechanism (e.g., associative vs. dissociative), changes of the atoms involved (e.g., inert Pt vs. labile Pd) and others.^{*,26}

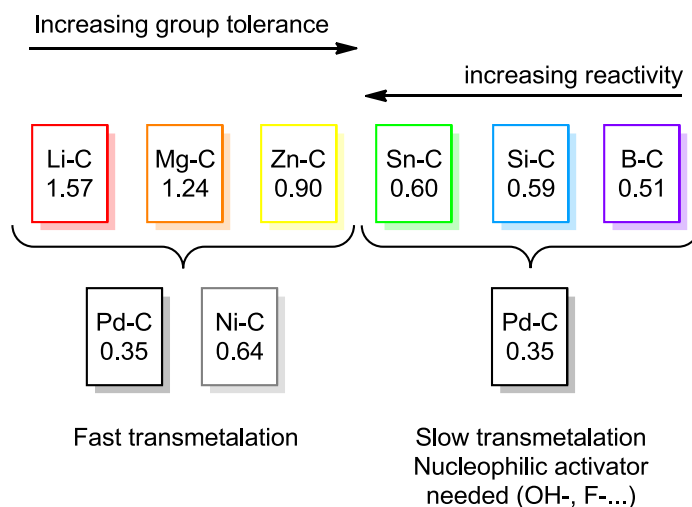
Advantages and disadvantages can be found in using more reactive nucleophiles. The transmetalation step is much faster when the highly polar organometallics are used. For example, the very reactive organolithium compounds undergo efficient transmetalation at temperatures as low as -78 °C.[†] This allows for easy coupling under mild conditions of very unreactive systems in other conditions, such as hindered nucleophiles.²⁷ At the other side of the scale, organoboron and organosilicon counterparts do not transmetalate in the absence of the corresponding activator, usually a base or a fluoride.²⁸

On the other hand, highly reactive organometallics are not compatible with all functional groups. For example, carbonyls are not well-tolerated, as they easily react with Li and Mg organometallics. Rather on the contrary, Suzuki, Stille and Hiyama couplings are tolerant to almost all kinds of groups, thus these are the reactions of choice for late-stage functionalization of complicated molecules, such as natural products.²⁹

According to the M-C differences in electronegativity of the Pauling scale, three main groups of M-C bond polarity can be envisioned:

* Nucleophilicity scales have been defined based on kinetic determinations on ligand substitution reactions, particularly in four-coordinated square-planar complexes (Pt^{II} and Au^{III}). See reference 26.

† For instance, [Pd(C₆F₃Cl₂)₂(COD)] is synthesized by transmetalation of C₆F₃Cl₂Li to [PdCl₂(COD)] at -78°C. See : Ref. 31c.



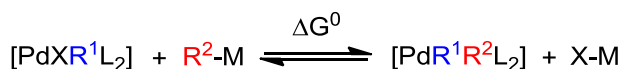
Scheme Intro-7. Electronegativity differences (Pauling scale) between selected organometallic reagents.

- High polarity: Organolithium and organomagnesium reagents (Kumada reaction). Low group tolerance
- Medium polarity: Zn (Negishi reaction) and Cu (Sonogashira reaction). The polarity of the C-M bond can be considered as moderate. They exhibit a medium group tolerance.
- Low polarity: Organoboron (Suzuki reaction), stannanes (Stille reaction) and silanes (Hiyama reaction). Practically, all kinds of groups are tolerated.

3.2. Thermodynamics of the transmetalation: M-C and M-X

bond strength

In a simplified view, these reactions entail the cleavage of a M-C and a Pd-X bond and the concomitant formation of a new Pd-C and a M-X bond. The thermodynamics of the process will be governed by the relative stability of the metal-carbon bonds and the metal-X bonds of the started and produced organometallic compounds.



Scheme Intro-8. Thermodynamics of the transmetalation at Pd^{II} complexes.

As a result, strong M-C bonds will difficult the transmetalation step whereas highly stable M-X compounds will play in favor of the process. In Table Intro-1, selected M-C and M-Cl Bond Dissociation Energies (BDE) are gathered.

Table Intro-1. Averaged Bond Dissociation Energies of selected M-C and M-Cl bonds.^{30,*}

M-C bond	Energy (kcal·mol) ⁻¹	M-Cl bond	Energy (kcal·mol) ⁻¹
Li-C	51.3	Li-Cl	112
Mg-C	60.5	Mg-Cl	112.4
Zn-C	63.7	Zn-Cl	87.5
Sn-C	70.5	Sn-Cl	101.6
B-C	107	B-Cl	106.3
Si-C	94.2	Si-Cl	117.1
Pd-C	61.6	Pd-Cl	91.9

Li and Mg are highly electropositive metals and the strength of the M-C bond is poor. The M-X product is stabilized by the ionic component of the bond between the more electropositive metal and the electronegative group X.[†] Another driving force is the fact that MX salts of these organometallics are usually poorly soluble in non-polar solvents, and they usually precipitate out of reaction fields with low dielectric constant. These properties cause the equilibrium in Scheme Intro-8 to lie far to the right in these cases.

* In this table, the BDEs are averaged values for Li, Mg and B. In the case of Sn, Si, Zn and Pd, the BDEs have been obtained from selected real molecules that would be good models of those taking part in actual reactions (see the corresponding chapter for further details). Experimental values are preferred when available. See reference 30.

[†] The ionic component of a bond is very dependent on the X involved, and usually follows the general trend: M-Cl > M-Br > M-I. That is: the fact that M-Cl is formed in place of a M-I bond usually favors the thermodynamics of the transmetalation. See for instance the effects of Cl⁻ in the Sn/Au transmetalation equilibria in ref 34.

However, this is not the general case and it is more the exceptional situation of highly polar organometallics. For other less polarized M-C bonds, the transmetalation to Pd is a reversible reaction, or even slightly endergonic, depending on the subtle balance of both reagents and products. For example, ZnMe_2 and ZnMeCl were compared in the transfer of Me to *trans*-[PdMeCl(PMePh₂)₂] by means of kinetic experimental and theoretical investigations in the context of the Negishi coupling.³¹ The equilibrium in Scheme Intro-8 for the Zn/Pd transmetalation is displaced to the right for the highly basic and nucleophilic ZnMe_2 , whereas if ZnMeCl is used, the starting reagents are more stable than the products.³¹ Indeed, the fact that the transmetalation step in some systems is fast and quickly reversible has important implications in catalysis. For example, ZnMeCl catalyzes the isomerization of [PdMe₂(PMePh₂)₂] via quick and reversible transmetalation/retrotransmetalation sequences, a process that otherwise would take place very slowly.³¹ This same phenomenon has been observed with other metals, such as Au or Sn.³² Fast retrotransmetalations can originate group scrambling, leading to the formation of byproducts that reduce the efficiency of the coupling and should not be overlooked.³³

On the other hand, less electropositive reagents such as Si, B or Sn derivatives do not have a very strong ionic interaction in the final product. As a matter of fact, additives are needed to push forward the equilibrium: the presence of a base is needed for the Suzuki coupling, F^- is a very common promoter of the Hiyama reaction and LiCl (and others) has been shown to benefit the Sn/Au and the Sn/Pd transmetalation equilibrium.^{16,34}

Due to the fact that the transmetalation step is usually reversible or endergonic,^{31,35} the coupling sometimes proceeds thanks to the irreversible step of reductive elimination. The formation of a highly exergonic C-C bond pulls forward the catalytic cycle, but a kinetically feasible transmetalation is critical not to act as bottleneck of the coupling.

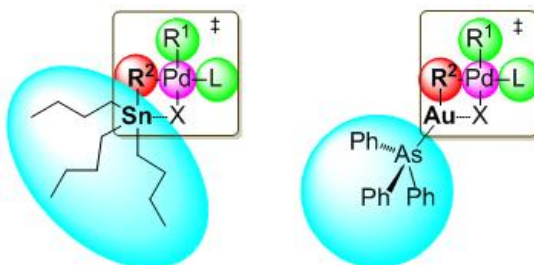
3.3. Kinetics: factors controlling the transition state

As it has been discussed, the group transfer from M to Pd is likely to take place through bimetallic transition states in which association of the nucleophile and the catalyst has taken place prior to the group transfer.

Although very difficult to quantify, there is an entropic cost associated with any bimolecular association that is a consequence of degrees of freedom of motion lost when two molecules are rigidly constrained within a complex.³⁶ Thus, all factors contributing to stabilize/destabilize the association will play a role in the kinetics of the transmetalation, compensating the entropic penalty of the formation of the bimetallic transition state.

a) *Volume of the nucleophile*

The transition state of the transmetalation is very sensitive to steric effects, and the size of every group participant in every partner should be considered:



Scheme Intro-9. Effect of the steric hindrance in the transition state.

The steric crowding may inhibit nucleophile coordination to the Pd complex, making the TS too high in energy and inaccessible under the reaction conditions. In this regard, the size of group taking part in the transfer is particularly important (R^2), since it has to be located very close to the palladium center. Transmetalation of bulky groups is slower and usually remains a challenge for cross-coupling reactions.³⁷ In a similar manner, the size of ancillary ligands in the palladium catalyst could be

detrimental for the transmetalation rate (L and R¹).^{38,*} Finally, the intrinsic volume of the organometallic reagent can be crucial for a successful group transfer. As depicted in Scheme Intro-9, the steric requirements of the nucleophile might hinder its own approach to the Pd complex.

b) Metal-metal interactions

There are strong evidences of the existence of metal-metal interactions that might contribute to hold the two metals in close proximity when d¹⁰ organometallics are involved, by a labile d⁸-d¹⁰ metallophilic bond.^{†,39} These bonds are a topic of increasing interest and debate.^{‡,40} There are a lot of examples in which abnormally short distances between metals are observed, both in the ground state of several bimetallic complexes and in transition states of transmetalation reactions. These interactions range from very weak forces to moderate forces that are in the order of the strongest hydrogen bonds.

This attraction is shown to originate from dispersion (van der Waals) interactions. It is especially strengthened by relativistic effects for heavy elements such as gold. Thus, aurophilicity is the best-known interaction of this kind as it is among the strongest,⁴¹ but they have been described between all closed-shell metals. These take place between d¹⁰-d¹⁰ metal ions, but also square-planar d⁸ complexes can be regarded as closed shells if the crystal-field splittings are large. In fact, d⁸-d¹⁰ interactions have been found in a variety of compounds between Pd and Pt with Cu, Ag and Au.⁴²

In this case, the interaction is constituted by an electron-rich Pt^{II} or Pd^{II} center and a Lewis-acidic coinage metal. They are thought to have a significant donor-

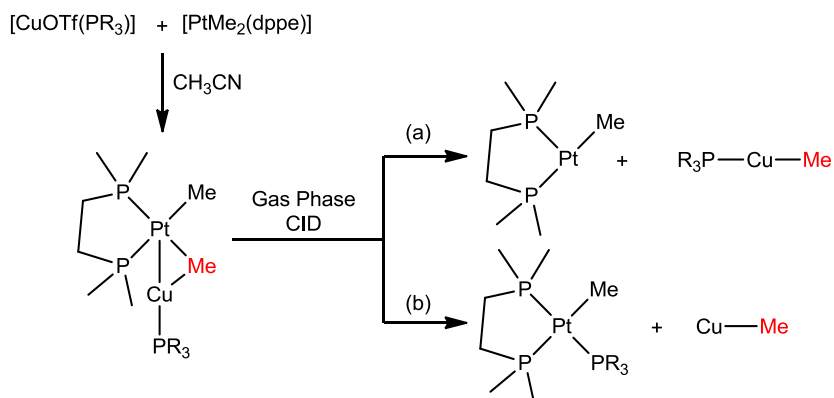
* This has to be taken with care, because as commented above, bulky ligands might promote dissociative mechanisms of transmetalation. This affirmation is only valid in systems of the same coordination number.

† By metallophilic bonds, we do not refer to covalent M-M bonds found in other systems, which can be rather strong. See ref. 39.

‡ They are a matter of debate due to the theoretical challenge of accurately describing them. However, they cannot be neglected, as they can be in the order of hydrogen bonding, which has a tremendous impact in the properties of molecules.

acceptor character and thus are often referred to as dative bonds.^{42a,*} These interactions have been shown to have implications in the transmetalation by the group of Chen.⁴³ They reported the methyl transfer from platinum to copper in the gas phase by collision-induced dissociation (CID). It takes place from a Pt/Cu bimetallic cation, which is stable enough for X-Ray characterization due to the existence of this M-M interaction and a Me-bridging bond.

They proposed two types of transmetalations from the bimetallic complex (Scheme Intro-10). In the first one, the methyl ligand is transferred from Pt to Cu, while PMe_3 remains coordinated to Cu^{I} (pathway (a)). In the second pathway, a platinum cation is formed by migration of PMe_3 from Cu to Pt, with concerted formation of CuMe (pathway (b)).



Scheme Intro-10. Transmetalation from a stable bimetallic Pd/Cu complex.

The same interpretation is valid for the Pt/Au transmetalation in analogous systems.^{43b} In this regard, our group reported recently a mechanistic investigation of the Pd/Au transmetalation of aryls. Therein, computational evidence was obtained about the existence of a strong metallophilic interaction between Pd and Au, which might contribute to reduce the energetic barrier of the transmetalation. This interaction has been also found in the context of the Negishi coupling between

* As commented above, these interactions are stronger when heavier metals are involved, and that is the reason why most bimetallic d^8-d^{10} complexes have been isolated with platinum.

Pd and Zn although the nature of the interaction could be somewhat different. Zn complexes are usually good Lewis acids, thus these interactions are presumed to have a greater acid/base character.^{31,44}

4. Objectives

Starting with these precedents, it was the purpose of our research group to develop bimetallic systems which could enhance the reactivity of reactions whose transmetalation step is not facile (Stille and Hiyama). For this purpose, we selected metals whose participation in transmetalation reactions is expected to be easier due to reduced steric hindrance, the presence of metallophilic interactions and others (Au and Cu). As explained along this introduction, these reactions present very important advantages, such as great functional compatibility and are very useful due to the high chemical stability and availability of the nucleophiles.

Another objective of the group was gaining a greater understanding of Zn/Pd undesired transmetalations. We wanted to carry out insights into the nature of the transition state, which possesses an important metallophilic component as that of Au and Cu. Our group has been involved in the study of this reaction for several years with great success and a good general picture of it is now available. However, selectivity issues are still present, preventing further application of the reaction in certain contexts. A greater understanding of the transmetalation step could contribute to the design of more efficient catalytic processes of interest for both academic fields and industry.

Other goals out of the main topic of this Doctoral Thesis consisted in the study of the feasibility of a Pd-catalyzed process of fluorination and trifluoromethylation of aryl halides based on PEWO ligands. As well, the oxidative addition of N-H bonds to iridium complexes has been evaluated by means of experimental and computational techniques. A better understanding of these fundamental processes could trigger the development of efficient catalytic reactions of great industrial importance.

5. References

1. (a) De Meijere, A.; Dietrich, F.; *Metal-Catalyzed Cross-Coupling Reactions*, 2nd ed. **2004**, Wiley-VCH: Weinheim. (b) Miyaura, N.; *Cross-Coupling Reactions: A practical Guide*; in *Topics in Current Chemistry*, Series 219; **2002**, Springer, Berlin. (c) Buchwald, S. L.; *Acc. Chem. Res.* **2008**, *41*, 1439.
2. Colacot, T. J. *Platin. Met. Rev.* **2011**, *55*, 84–90.
3. Negishi, E-i.; *Handbook of Organopalladium Chemistry for Organic Synthesis*, Wiley-Interscience, New York, **2002**.
4. Watson, D. A.; Su, M.; Teverovskiy, G.; Zhang, Y.; García-Fortanet, J.; Kinzel, T.; Buchwald, S. L. *Science* **2009**, *325*, 1661–1664.
5. For an example of oxidative cross-coupling: David R. Stuart, K. F. *Science* **2007**, *316*, 1172–1176. For an example of coupling of two electrophiles in the presence of a reducing agent: Ackerman, L. K. G.; Lovell, M. M.; Weix, D. J. *Nature* **2015**, *524*, 454–457.
6. For the use of other metals than Pd and Ni (they will be commented separately) see the following publications: (a) Hammann, J. M.; Haas, D.; Knochel, P. *Angew. Chem. Int. Ed.* **2015**, *54*, 4478–4481. (b) Thapa, S.; Kafle, A.; Gurung, S. K.; Montoya, A.; Riedel, P.; Giri, R. *Angew. Chem. Int. Ed.* **2015**, *54*, 8236–8240. (c) Reddy, C. K.; Knochel, P. *Angew. Chem. Int. Ed.* **1996**, *35*, 1700–1701.
7. (a) Grushin, V. V.; Alper, H. *Chem. Rev.* **1994**, *94*, 1047–1062. (b) Littke, A. F.; Fu, G. C. *Angew. Chem. Int. Ed. Engl.* **2002**, *41*, 4176–4211.
8. Tsou, T. T.; Kochi, J. K. *J. Am. Chem. Soc.* **1979**, *101*, 6319–6332.
9. Tasker, S. Z.; Standley, E. a; Jamison, T. F. *Nature* **2014**, *509*, 299–309.
10. The following reviews contain a detailed picture of Ni chemistry and seminal references can be found therein: (a) Hu, X. *Chem. Sci.* **2011**, *2*, 1867. (b) Phapale, V. B.; Cárdenas, D. J. *Chem. Soc. Rev.* **2009**, *38*, 1598–1607. These articles include uncovered mechanistic information in the reviews: (c) Schley, N. D.; Fu, G. C. *J. Am. Chem. Soc.* **2014**, 16588. (d) Zheng, B.; Tang, F.; Luo, J.; Schultz, J. W.; Rath, N. P.; Mirica, L. M. *J. Am. Chem. Soc.* **2014**, *136*, 6499–6504.
11. (a) Jin, L.; Xin, J.; Huang, Z.; He, J.; Lei, A. *J. Am. Chem. Soc.* **2010**, *132*, 9607–9609. (b) Nicolas, E.; Ohleier, A.; D'Accriscio, F.; Pécharman, A.-F.; Demange, M.; Ribagnac, P.; Ballester, J.; Gosmini, C.; Mézailles, N. *Chem. Eur. J.* **2015**, *21*, 7690–7694.

12. Amatore, C.; Jutand, A. *Acc. Chem. Res.* **2000**, *33*, 314–321.
13. García-Melchor, M.; Braga, A.g; Lledós, A.; Ujaque, G.; Maseras, F. *Acc. Chem. Res.* **2013**, *46*, 2626–2634.
14. (a) Gillie, A.; Stille, J. K.; *J. Am. Chem. Soc.*; **1980**, *102*, 4933-4941. (b) Saillard, Y.-I.; Hoffmann, R. *J. Am. Chem. Soc.* **1984**, *106*, 2006–2026. (c) Tatsumi, K.; Hoffmann, R.; Yamamoto, A.; Stille, J. K. *Bull. Chem. Soc. Jpn.* **1981**, *54*, 1857–1867.
- 15.(a) Xu, L.-M.; Li, B.-J.; Yang, Z.; Shi, Z.-J. *Chem. Soc. Rev.* **2010**, *39*, 712–733. (b) Canty, A. J.; *Acc. Chem. Res.* **1992**, *25*, 83-90.
16. Pérez-Temprano, M. H.; Gallego, A. M.; Casares, J. A.; Espinet, P. *Organometallics* **2011**, *30*, 611-617.
17. Stille J. K. *Angew. Chem.Int. Ed.* **1986**, *25*, 508-524.
18. Espinet, P.; Echavarren, A. M. *Angew. Chem. Int. Ed.* **2004**, *43*, 4704–4734.
19. Casares, J. A.; Espinet, P.; Salas, G.; *Chem. Eur. J.* **2002**, *8*, 4843-4853.
20. Osakada, K. *Fundamentals of Molecular Catalysis; Current Methods in Inorganic Chemistry*, **2003**, Elsevier: Amsterdam, Chapter 5.
21. (a) Nova, A.; Ujaque, G.; Maseras, F.; Lledós, A.; Espinet, P. *J. Am. Chem. Soc.* **2006**, *128*, 14571–14578.(b) Casado, a. L.; Espinet, P.; Gallego, A. M. *J. Am. Chem. Soc.* **2000**, *122*, 11771–11782.
22. (a) Farina, V.; Krishnan, B.; Marshall, D. R.; Roth, G. P.; *J. Org. Chem.* **1993**, *58*, 5434. (b) Louie, J.; Hartwig, J. F.; *J. Am. Chem. Soc.* **1995**, *117*, 11598-11599.
23. Casado, A. L.; Espinet, P. *J. Am. Chem. Soc.* **1998**, *120*, 8978-8985.
24. (a) Martin, R.; Buchwald, S. L. *Acc. Chem. Res.* **2008**, *41*, 1461–1473. (b) Kantchev, E. A. B.; O'Brien, C. J.; Organ, M. G. *Angew. Chem. Int. Ed.* **2007**, *46*, 2768–2813.
25. Boudier, A.; Bromm, L. O.; Lotz, M.; Knochel, P. *Angew. Chem. Int. Ed. Engl.* **2000**, *39*, 4414
26. A presentation of the topic and some seminal contributions can be found in: (a) Lewis, G. N. *Valence and the Structure of Atoms and Molecules*; Chemical Catalogue Co., Inc.: New York, **1923** (b) Tobe, M. L. *Comprehensive Coordination Chemistry*, 1st ed.; Wilkinson, G., Gillard, R. D., McCleverty, J. A., Eds.; Pergamon Press: Oxford, England, **1987**; Vol. 1, p 312. (c) Belluco, U.; Cattalani, L.; Basolo, F.; Pearson, R. G.; Turco, A. *J. Am. Chem. Soc.* **1965**, *87*, 241–246. (d) Belluco, U.; Martelli, M.; Orio, A.

- Inorg. Chem.* **1966**, *5*, 582–586. (e) Pearson, R. G.; Sobel, H.; Songstad, J. *J. Am. Chem. Soc.* **1968**, *90*, 319–326.
27. Giannerini, M.; Hornillos, V.; Vila, C.; Fañanás-Mastral, M.; Feringa, B. L. *Angew. Chem. Int. Ed.* **2013**, *52*, 13329–13333.
28. (a) Miyaura, N.; Suzuki, A. *Chem. Rev.* **1995**, *95*, 2457–2483. (b) Denmark, S. E.; Sweis, R. F. *Organosilicon Compounds in Cross-Coupling Reactions*; **2008**; pp. 163–216. Wiley-VCH Verlag GmbH & Co. KGaA, Weinheim, Germany.
29. (a) Nicolaou, K. C.; Bulger, P. G.; Sarlah, D. *Angew. Chem. Int. Ed.* **2005**, *44*, 4442–4489. (b) Denmark, S. E.; Liu, J. H. C. *Angew. Chem. Int. Ed.* **2010**, *49*, 2978–2986.
30. BDE values have been obtained from: (a) Ruo, Y.-L.; *Comprehensive Handbook of Chemical Bond Energies*; CRC Press; 1 edition, **2007**. BDEs of the silicon compounds: (b) Walsh, R. *Acc. Chem. Res.* **1981**, *1537*, 246–252. The Pd-C bond dissociation energy was extracted from: (c) Simoes, J. A. M.; Beauchamp, J. L. *Chem. Rev.* **1990**, *90*, 629–688. The Pd-halogen bond dissociation energy was obtained from: Lan, Y.; Liu, P.; Newman, S. G.; Lautens, M.; Houk, K. N. *Chem. Sci.* **2012**, *3*, 1987. Experimental information concerning Pd-halide dissociation can be obtained herein: Casares, J. A.; Coco, S.; Espinet, P.; Lin, Y. *Organometallics*, **1995**, 3058–3067.
31. (a) García-Melchor, M.; Fuentes, B.; Lledós, A.; Casares, J. a.; Ujaque, G.; Espinet, P. *J. Am. Chem. Soc.* **2011**, *133*, 13519–13526. (b) Fuentes, B.; García-Melchor, M.; Lledós, A.; Maseras, F.; Casares, J. A.; Ujaque, G.; Espinet, P. *Chem. Eur. J.* **2010**, *16*, 8596–8599. (c) Casares, J. A.; Espinet, P.; Fuentes, B.; Salas, G. *J. Am. Chem. Soc.*, **2007**, *129*, 3508–3509.
32. (a) Carrasco, D.; Pérez-Temprano, M. H.; Casares, J. a.; Espinet, P. *Organometallics* **2014**, *33*, 3540–3545. (2) Casado, A. L.; Espinet, P. *Organometallics* **1998**, *17*, 3677–3683.
33. (a) Gioria, E.; Martínez-Ilarduya, J. M.; Espinet, P. *Organometallics* **2014**, *2*, 140814163405008. (1) Liu, Q.; Lan, Y.; Liu, J.; Li, G.; Wu, Y. D.; Lei, A. *J. Am. Chem. Soc.* **2009**, *131*, 10201–10210.
34. delPozo, J.; Carrasco, D.; Pérez-Temprano, M. H.; García-Melchor, M.; Álvarez, R.; Casares, J. A.; Espinet, P. *Angew. Chem. Int. Ed.* **2013**, *52*, 2189–2193.
35. (a) Pérez-Temprano, M. H.; Nova, A.; Casares, J. A.; Espinet, P. *J. Am. Chem. Soc.* **2008**, *130*, 10518–10520. (b) Cotter, W. D.; Barbour, L.; McNamara, K. L.; Hechter, R.; Lachicotte, R. J. *J. Am. Chem. Soc.* **1998**, *120*, 11016–11017.
36. Searle, M. S.; Williams, D. H. *J. Am. Chem. Soc.* **1992**, *114*, 10690–10697.
37. Fu, G. C.; Schwarz, L.; Littke, A. F. *J. Am. Chem. Soc.* **2002**, *5*, 6343–6348.

38. Ariafard, A.; Yates, B. F. *J. Am. Chem. Soc.* **2009**, *131*, 13981–13991.
39. Cotton, F. A. *Acc. Chem. Res.* **1968**, *2*, 240–247.
40. Pyykkö, P. *Chem. Rev.* **1997**, *97*, 597–636.
41. Gorin, D. J.; Toste, F. D. *Nature* **2007**, *446*, 395–403.
42. (a) Moret, M. E.; Chen, P. *J. Am. Chem. Soc.* **2009**, *131*, 5675–5690. (b) Xia, B.-H.; Zhang, H.-X.; Che, C.-M.; Leung, K.-H.; Phillips, D. L.; Zhu, N.; Zhou, Z.-Y. *J. Am. Chem. Soc.* **2003**, *125*, 10362–10374.
43. (a) Moret, M. E.; Serra, D.; Bach, A.; Chen, P. *Angew. Chem. Int. Ed.* **2010**, *49*, 2873–2877. (b) Serra, D.; Moret, M. E.; Chen, P. *J. Am. Chem. Soc.* **2011**, *133*, 8914–8926.
44. (a) Álvarez, R.; De Lera, A. R.; Aurrecochea, J. M.; Durana, A. *Organometallics* **2007**, *26*, 2799–2802. (b) González-Pérez A. B.; Álvarez, R.; Nieto Faza O.; de Lera, A. R.; Aurrecochea, J. *Organometallics* **2012**, *31*, 2053–2058.

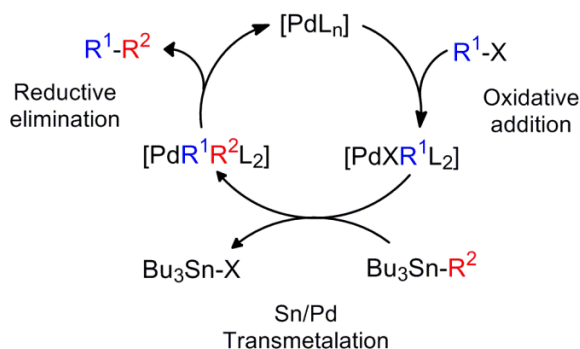
Chapter I

**The gold co-catalyzed Stille
reaction**

1. Introduction

The Stille reaction belongs to the family of Pd-catalyzed cross-coupling reactions. It consists in the coupling of organic electrophiles (R^1-X) with organostannanes (R^2-SnBu_3).¹ The popularity of this reaction is based on mild reaction conditions required to create C–C bonds. The high functional-group compatibility of organotin and the fact that can be carried out in mild and neutral conditions makes it particularly effective for transformation of highly functionalized molecules in the synthesis of complex natural products.²

The mechanism of the Pd-catalyzed Stille reaction is among the best-known of all Pd-catalyzed catalytic processes and every step of the cycle has been deeply studied. It follows the same general sequence of the rest of the family of cross-coupling reactions, gathered in Scheme I-1.³



Scheme I-1. Classic simplified mechanism of the Stille reaction

Our group has published the most extensive reviews dealing with the Stille reaction,⁴ and the last update of the work has been reported very recently.⁵ The most relevant pieces of research for this Thesis will be commented along this text, but further information is provided in these reviews and the corresponding references included therein.

1.1. Background

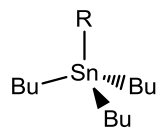
The first examples of the coupling of organostannanes with organic electrophiles were disclosed during the period 1976-1977 by the research groups of Eaborn⁶ and Kosugi.⁷ These early works preceded the first report by Milstein and Stille,⁸ but it was the extensive synthetic and pioneer mechanistic work carried out by this group the reason why organostannanes became standard reagents in cross-coupling reactions.³ The emergence of bulky ligands has also powered the use of the Stille reaction in synthesis, making it compatible with all kinds of groups under mild conditions.^{5,9}

Stille carried out a thorough mechanistic study on all the different steps involved in the catalytic cycle and gathered all the information available at the time in a seminal review published in 1986.¹⁰ In that Review, Stille considered that the oxidative-addition and reductive elimination sequences were reasonably well understood, whereas further investigation was still required to understand the ins and outs of the transmetalation. In this regard our group has played a central role, by understanding its nature,^{11,12} both experimentally and computationally (in collaboration with the group of Maseras, Ujaque and Lledós).¹³ All these advances have led to the current state of the Stille reaction, which is probably the most understood one of the family of Pd-catalyzed cross-coupling reactions.

1.2. Structural features of organostannanes

The most commonly used organostannanes employed in the Stille reaction are trialkyl tin derivatives $\text{RSn}(\text{Alkyl})_3$. These compounds are usually tetrahedral and can be formally considered as Sn^{IV} molecules.¹⁴ The selected R group can be transferred selectively from tin, as different groups undergo transmetalation with different rates. Alkyl chains are chosen as ancillary groups because they have the slowest transfer rate. Thus, by using a trimethyl or tributyl organotin reagent, the group

other than the alkyl chain transfers exclusively.* In particular, tri-n-butyltin derivatives are more employed than trimethyl or any other variant, due to their decreased toxicity with regard to organotins bearing shorter chains.^{†,10}



Scheme I-2. Structure of a common organotin employed in Stille couplings.

Although they have their four electrons occupied in forming 4 σ -carbon bonds, they can expand their coordination accepting electron density from additional ligands (this is: they behave as weak Lewis acids, leading to hypervalent stannanes).¹⁴ Lewis bases can coordinate to Sn and provide enhanced nucleophilic reactivity, although they are reactive enough by themselves.[‡]

One of the reasons for the popularity of the Stille reaction in modern organic synthesis is the fact that trialkyl organotin species are readily available, quite air and moisture stable, and tolerate many functional groups.³ These properties are mostly due to the low polarity of the Sn–C bond, and condition the transmetalation mechanism and the reactivity of organotins.

* Relative rates of transfer: alkynyl > alkenyl > aryl > allyl and benzyl > $-\text{CH}_2\text{COCH}_3$ > alkyl. See ref 10.

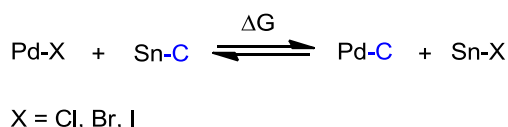
[†] The toxicity of tributyl organotins is in the range of 100-300 mg kg^{-1} . At present, there are several approaches that have contributed to reduce the content in tin of the products, such as catalytic use of stannanes or polymer immobilized stannanes. For further information, see ref. 5.

[‡] The mechanisms by which these molecules expand their valence and how this fact affects the reactivity will be considered in Chapter II for the particular case of organosilicon compounds. Similar conclusions can be withdrawn for the case of organotins, as very similar orbitals are involved.

1.3. Nature of the Sn/Pd transmetalation

a) Thermodynamics of the Sn/Pd transmetalation

The thermodynamic balance of a Sn/Pd transmetalation can be interpreted according to the following Scheme I-3:



Scheme I-3. Thermodynamic balance of the Sn/Pd transmetalation.

In a simplified manner, Sn–C and Pd–X bonds are broken and Pd–C and Sn–X bond are formed. Concerning the tin species, experimental data of various Sn–C and Sn–X bond dissociation energies (BDE) are available.¹⁵ In the case of Pd–halogen bonds in real complexes, only calculated energies are available.¹⁶

Table I-1. Mean calculated Bond dissociation energies of selected tin bonds in Kcal·mol⁻¹.

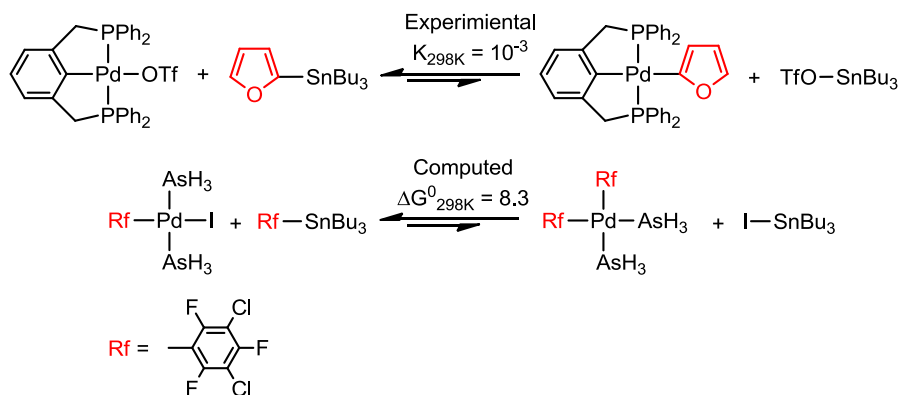
Sn–C Bond	BDE
Me–SnMe ₄	70.5
Ph–SnPh ₃	65.5
Cl–SnMe ₃	101.6
I–SnMe ₃	76.5
HO–SnMe ₃	116.6
F–SnMe ₃ ^{15b}	130

Table I-2. Calculated bond dissociation energies (Kcal·mol⁻¹) of selected Pd compounds.

Bond	BDE
Pd–C	59.0
Pd–Cl	91.9
Pd–Br	81.1
Pd–I	72.8

As it can be deduced from the table, products are not clearly favored in the energetic balance. It is dependent on the halide taking part in the transfer, as it is

more favored for $X = \text{Cl}$ than for $X = \text{I}$.^{*} As well, F^- and OH^- are commonly used as promoters of the Stille reaction, due to the fact that they form very stable bonds with tin.^{9,17} These anions are beneficial for the energetic balance and displace the transmetalation reaction to the right. If they are not present, the Sn to Pd transmetalation has been proved endergonic experimentally¹⁸ and computationally.¹²



Scheme I-4. Selected Sn/Pd transmetalation equilibria.

In the absence of any additive of this kind, the Stille reaction relies on the large concentration of the tin nucleophile with regard to the palladium catalyst (20:1 ratios are common) to provide significant concentration of the [Pd–C] transmetalated species. As well, the irreversible reductive elimination step acts as a thermodynamic driving force of the catalytic cycle.

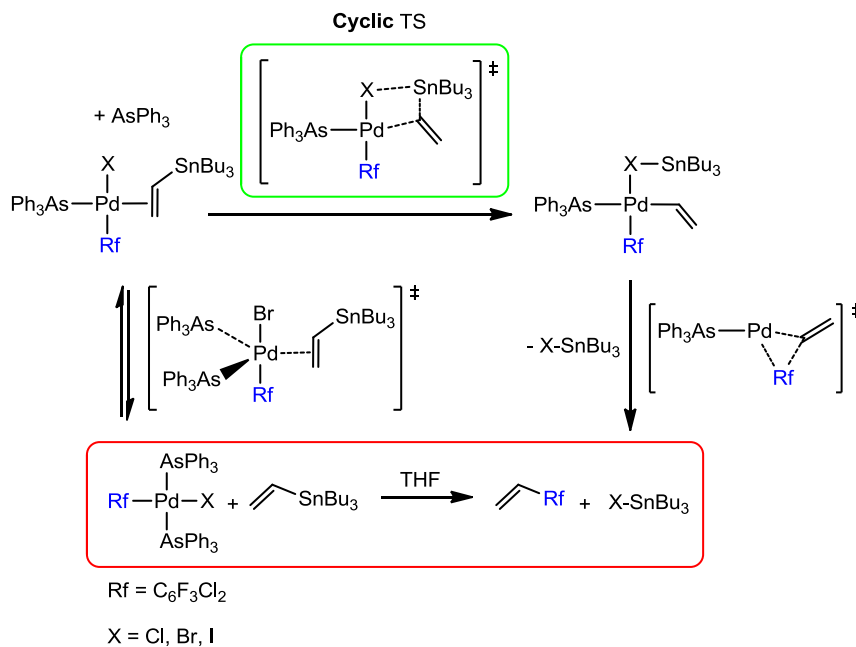
b) Kinetics and nature of the Transition State

Two mechanisms, named as *cyclic* and *open*, have been proposed to accommodate the fact that the transmetalation of chiral stannanes could take place with retention or inversion of the configuration in the α carbon of the products.¹⁹ These observations were key to provide a detailed picture of the interaction between the palladium Rf complex and the organotin in the transition state.

^{*} Overall $\Delta G_0 = -1.8 \text{ kcal}\cdot\text{mol}^{-1}$, $X = \text{Cl}$; $\Delta G_0 = -7.8 \text{ kcal}\cdot\text{mol}^{-1}$, $X = \text{I}$. Of course, these values cannot be taken as valid (experimental values of real molecules should be available for a significant calculation), but tendencies are probably right.

Our group studied in detail the catalytic coupling of vinyl tin derivatives with aryl halides in non-polar or medium-polar solvents, and also the isolated transmetalation step.^{11a} The experimental evidences suggested a stepwise mechanism: the first step is an equilibrium in which it takes place the associative substitution of the L ligand by the stannane group. The second one corresponds to the group transfer from the stannane to the palladium center.* Computational work supports this view, and no transition state could be found without prior release of a neutral ligand.²⁰ The geometry of the transmetalation transition state is concerted: the X and R² ligands are bridging the two metal atoms. Once the group transfer has taken place, the corresponding tin halide is released, providing a *cis* configuration of a three-coordinate Pd center, from which the coupling takes place directly. This mechanism would explain processes with retention of configuration at the transmetalated carbon.¹⁹ Giving much support to this proposal, the post-intermediate of concerted transmetalation *cis*-[PdR¹R²L(I-SnBu₃)] could be detected by ¹⁹F NMR in the study of the retrotransmetalation reaction of fluorinated groups. These groups undergo reductive elimination very slowly, allowing for the study of the transmetalation in the opposite sense as it takes place in the Stille reaction.¹²

*The activation parameters found for the reaction in Scheme I-5 support an associative mechanism ($\Delta S^\ddagger = -115 \text{ J}\cdot\text{K}^{-1}\cdot\text{mol}^{-1}$). It was found that the addition of AsPh₃ retarded the reaction, suggesting a pre-equilibrium to release one molecule of ligand as first step See ref 11a. Although initially dissociative mechanisms were proposed to account for this fact, it is perfectly compatible with an associative mechanism. See ref 4.

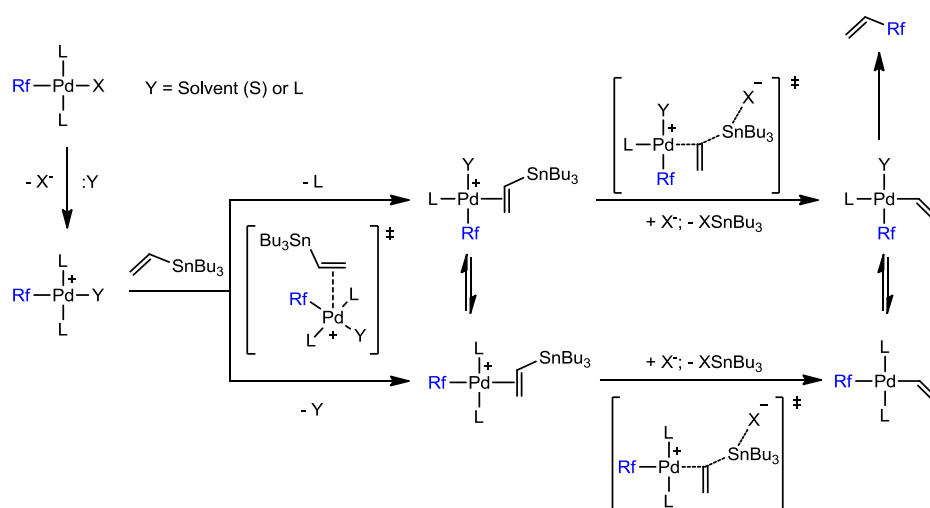


Scheme I-5. Transmetalation via open transition states. Reaction of vinyl stannanes with aryl halides catalyzed by $[\text{PdRfX}(\text{AsPh}_3)_2]$ in THF.

The open transmetalation mechanism is the only possible pathway in the absence of bridging ligands, but it can also operate in the presence of such ligands when the coupling is carried out in polar, coordinating, non-bridging solvents.⁴ The ionic pathway is in fact, the most frequent subcategory of the open pathway (which can proceed also through neutral species, but it is less common). Under these circumstances, the anionic ligand X^- is replaced by a molecule of solvent or neutral ligand, generating cationic complexes $[\text{PdR}^1(\text{S})\text{L}_2]^+$ or $[\text{PdR}^1\text{L}_3]^+$, respectively.^{11b} The formation of this highly electrophilic intermediate is key to stabilize the transition state of the nucleophilic attack of the poorly nucleophilic α carbon of the stannane. Consequently, good leaving anions at the Pd center (such as OTf^-) and strongly-coordinating solvents favor the formation of this intermediate and thus the open pathway.*

* Experimentally, complexes $\text{trans}-[\text{PdR}(\text{OTf})\text{L}_2]$ formed after oxidative addition of aryl triflates are found to be in equilibrium with $[\text{PdR}^1(\text{S})\text{L}_2]^+$ and $[\text{PdR}^1\text{L}_3]^+$. See ref 11b.

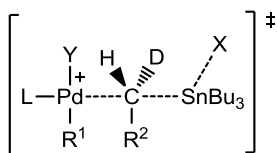
Although the initial proposal of this mechanism considered transmetalation at a pentacoordinate Pd transition state, calculations propose that one ligand is eventually released.²⁰ Further evolution of the reaction leads to competitive formation of both *cis* and *trans* isomers of the palladium product of transmetalation, at differential rates governed by the different *trans* effects of the rest of the ligands. This fact now implies the addition of an isomerization step for the *trans* isomer in order for the coupling to take place, which can be problematic in certain circumstances.²¹ This pathway is less strongly retarded by added L.*



Scheme I-6. Formation pathways of the complexes *cis* and *trans* in the open transmetalation with vinyl stannane.

In the case of alkyl stannanes and other derivatives with sp^3 configured α carbon atoms, the transmetalation leads to inversion of configuration (see Scheme I-7), as it has been reported in multiple instances in the literature.

* The influence of the neutral ligand on the reaction rate is more difficult to analyze in this mechanism. Calculations predict that the rate limiting step is L for Sn substitution, but as well, added ligand favors the formation of cationic $[\text{PdR}^1\text{L}_3]^+$. See ref 20.



Scheme I-7. Open transition state of sp^3 carbons. This pathway leads to inversion in the configuration of the α Carbon.

Interestingly, the computed Sn/Pd distances in the TSs of the transmetalation available in the literature are very long in all cases, suggesting no interaction between both metals beyond weak dispersion forces.^{20,22} It is worth reminding that the nature of the transition state is very dependent on the conditions: the group involved in the transfer, solvent, and auxiliary ligands can play a role at determining which transition state is preferred. For example, the steric properties of L have a profound effect on the kinetics of the transmetalation step: strong and/or bulky ligands can be very detrimental for the coordination of the organotin to the palladium center, so a judicious choice of the reaction conditions and partners is very important for the success of the coupling.²³

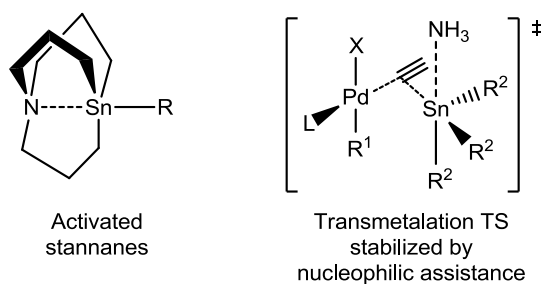
c) Role of additives

As mentioned in section 1.3.a), additives containing fluoride and hydroxide anions enhance the reactivity of organostannates.^{9,17} Although there is a certain thermodynamic benefit of the use of these additives, the reasons for the enhanced reactivity possess a very important kinetic background.

The role of F^- in the transmetalation was evaluated computationally by Ariafard and Yates in the $Pd(P^tBu_3)_2$ -catalyzed cross-coupling of vinyltributyltin with chlorobenzene.^{9,23} They found an effective rate enhancement of transmetalation via $[PdR(F)(P^tBu_3)]$ intermediates formed after chloride displacement. The greater reactivity of these palladium fluorides was attributed to the stronger coordination

ability of the F^- to Sn that would stabilize the cyclic transition state by making a stronger bridge.*

In other instances, the nucleophilic activation mechanism has shown to be very effective. Coordination of a nitrogen atom present in the structure of certain designed stannanes results in enhanced reactivity of the substrate for transmetalation.²⁴



Scheme I-8. Nucleophilic assisted transmetalation.

A very interesting computational work reported that the stabilization effect produced on the transition state of the transmetalation by nucleophilic assistance of NH_3 at Sn could be close to $10 \text{ kcal}\cdot\text{mol}^{-1}$.²⁵ The authors suggested that coordination expansion at tin plays a major role in facilitating the group transfer. Intuitively, pentacoordination would render organotins more nucleophilic than the homologous tetrahedral counterparts.²⁶ It is likely that highly electronegative nucleophiles (F^- and OH^-) could stabilize more efficiently the hypervalent state of organotins.[†] With these considerations, the role of polar and coordinating solvents should be revisited, as they might act as nucleophilic promoters of the

* In this work, the role of the F^- as an external nucleophilic activator to form pentacoordinate $[Sn(\text{vinyl})(Me_3)F]^-$ was also taken into account, but it took place with greater activation barriers than those of the Pd–F mechanism. The nucleophilic assisted mechanism cannot be discarded with smaller ligands in tetracoordinate Pd complexes.

[†] This situation is critical for the coupling with organosilanes in the Hiyama reaction, and since Sn and Si are close neighbors in the periodic table, a similar description of the transition state could be at play. For full description of the hypervalency phenomenon, see Chapter II. One important difference should be pointed out: the larger size of Sn with regard to Si plays in favor of the expansion of the coordination of Sn. As a matter of fact, hypervalent complex $SnMe_5^-$ is known, but the corresponding silicon one is unstable. See ref. 14.

transmetalation by coordination to Sn. Important rate enhancements have been reported in the presence of such solvents.¹⁰

In the particular case of poorly reactive organotins in synthesis (e.g. bulky stannanes), fluoride activators are very important for a successful coupling.^{7,27} This fact results in a big drawback: the presence of the strongly basic F^- reduces the group tolerance of the coupling, which is on the other hand, the main reason for choosing the Stille reaction instead of any other cross-coupling reaction.

d) The Copper effect on the Stille reaction

A remarkable phenomenon in Stille coupling reactions is the effect of the addition of Cu^I salts, which has been shown to accelerate couplings in certain instances.²⁸ This so-called “copper effect” was first studied by the research groups of Farina and Liebeskind.²⁹ In their initial investigation, they propose “a dual mechanistic role for cocatalytic copper in the Stille reaction”.

First, they concluded that the role of CuI in their systems catalyzed by $[PdL_4]$ was to act as scavenger of free ligand,^{*} which retards the coupling by shifting to the left the rate determining coordination of the stannane to the palladium catalyst (it is an equilibrium in which free ligand is released, see section 1.3.b) Consequently, the effect of the addition of copper salts was more efficient for those ligands in which the binding constant to copper was greater, these are “strong” ligands (such as PPh_3) rather than “soft” ligands (e. g. $AsPh_3$), in which minimal rate accelerations were found.³⁰

In their initial study, Farina, Liebeskind and co-workers proposed that in very polar solvents Sn/Cu transmetalation was taking place.²⁹ Thus, organocopper species were participating in the reaction. The feasibility of this transmetalation has been demonstrated in the context of Cu-catalyzed (or promoted) Pd-free cross-coupling reactions.³¹

^{*} $[PdL_4]$ complexes undergo oxidative addition providing $[PdRXL_2]$ and 2 equivalents of free L per palladium atom.

Several effective coupling systems were later developed based on the Sn/Cu/Pd proposal, achieving the coupling of otherwise unreactive organotins in the presence of both catalytic and stoichiometric conditions of copper salts. The enhanced reactivity is based on the premise that the resulting organocopper species would transmetalate to Pd at a higher rate than the stannane itself.³² As commented in the introduction, this hypothesis is supported by the smaller size of organocuprates and the greater polarity of the C–Cu bond. However, for challenging cases, the efficiency of the system is limited, and large quantities of CuX are usually needed to allow for sufficient reactivity (sometimes, the use of up to 5-fold excess of CuX has been reported).^{32b} Nevertheless, the development of bimetallic catalytic systems seemed promising for promoting enhanced reactivity of unreactive organotins.

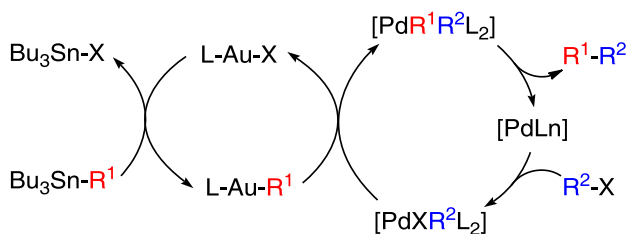
2. Gold co-catalysis makes Stille coupling involving bulky groups feasible

There is a growing interest in bimetallic catalysis, a synthetic approach combining two or more non main-group metal catalysts working in tandem.³³ A main-group metal is often involved as the nucleophilic reagent. The aim of bimetallic catalysis is to take advantage of the specific behavior of each catalyst in new one-pot synthetic routes. For the Au/Pd couple it is known that the Au/Pd transmetalation, a step hoped to connect the Pd and the Au catalytic cycles, is kinetically feasible,^{34,35} even for fairly bulky groups,³⁶ but so far only a few Au/Pd bimetallic catalyzed processes have been reported, including the Sonogashira-like cross-coupling,³⁷ the carbometalation of alkynes,³⁸ and processes combining cyclization with cross-coupling steps.^{39,40} Here we examine the potential of the Au/Pd pair in a Stille reaction modified with Au co-catalysis. Sn is a third metal involved in the system, providing the nucleophile.

As commented above, the Stille reaction is sometimes co-catalyzed by addition of CuX salts. The so-called “copper effect” is frequently deemed to be due to copper(I) mediating aryl transfer from organotin to palladium,^{28,31,32} although it has

been shown also that in some cases the kinetic effect observed is simply due to the ability of the copper(I) to sequestrate the excess of ligand in solution.^{29,30} Blum has succeeded recently in using gold as vinyl carrier from Sn to Pd in the carbostannylation of alkynes.^{38a,33b}

We speculated that using AuXL complexes as the transmetalation co-catalyst to PdR¹XL₂ intermediates (both L being identical), instead of CuX salts, we might produce a Stille reaction co-catalyzed with gold(I) instead of copper(I). Moreover, should this co-catalysis happen, we could skip any L sequestering “copper effect like” or any ligand scrambling effect (for different ligands on Pd and Au) on the reaction and observe the non perturbed catalytic effect of Au on the transmetalation. Furthermore, this reaction might be a good model to check the compatibility of Pd and Au as co-catalysts, and to explore the thermodynamic and kinetic parameters controlling this bimetallic system. In fact the results show that the intermediacy of gold can be critical to make Stille reactions involving bulky stannanes feasible.



Scheme I-9. Proposal of a gold-cocatalyzed Stille reaction

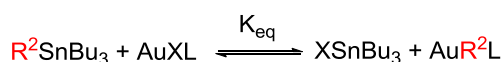
2.1. Results and discussion

a) Thermodynamics of the Au/Sn transmetalation equilibria

There are only very few reports of isolated transmetalations from Sn to Au or vice versa. The transmetalation of Ar groups from SnArMe_3 (Ar = Ph, naphthyl, 8-iodonaphthyl) to $[\text{AuCl}(\text{EPh}_3)]$ (E = P, As) complexes has been reported, whereas the same reaction fails with SnPhBu_3 .⁴¹ Attempts at performing Ar transmetalations

with SnAr_4 or SnAr_3Cl ($\text{Ar} = \text{C}_6\text{F}_5, \text{C}_6\text{F}_3\text{Cl}_2, \text{C}_6\text{Cl}_5$) were also unsuccessful.⁴² These results suggest that the thermodynamics of the Sn/Au transmetalation might be shifted towards either side, depending on the specific groups involved.

We have studied the equilibrium for different combinations of reagents ($\text{X} = \text{Cl}, \text{I}$; $\text{R} = \text{vinyl}, \text{aryl}, \text{alkynyl}$) and ligands ($\text{L} = \text{PPh}_3, \text{AsPh}_3$).^{*} However, this work corresponds to another doctoral thesis and it will not be commented in detail.⁴³ All these results were published together with Au-Pd co-catalyzed reactions that are discussed below; and numerical values can be found therein.⁴⁴



Scheme I-10. Sn/Au transmetalation equilibria

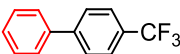

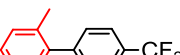
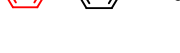
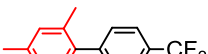
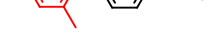
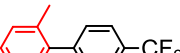
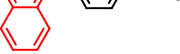
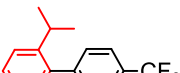
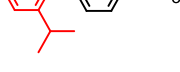

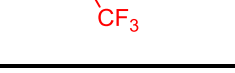
As suspected, the picture obtained was more complex than known so far. These results showed that for $\text{X} = \text{I}$ all the equilibria studied are shifted to the left, that is: the desired transmetalation from Sn to Au is counter-thermodynamic. This shift is very pronounced for vinyl and most aryls, and less marked for alkynyl groups and for mesityl. Electronic and steric factors can tune or modify importantly this observed trend. Thus for $\text{L} = \text{AsPh}_3$ all the equilibria are less shifted to the left than for $\text{L} = \text{PPh}_3$, probably because the better σ -donor PPh_3 renders more electron-rich the corresponding AuXL than the weaker AsPh_3 , and makes less favorable the transfer of another strong σ -donor. The halide is very influential, and these equilibria shift markedly more to the right for $\text{X} = \text{Cl}$. This effect is mostly due to the energetic balance of the very different Sn-X bond energies ($\text{Sn}-\text{Cl} = 101 \text{ kcal}\cdot\text{mol}^{-1}$; $\text{Sn}-\text{I} = 76 \text{ kcal}\cdot\text{mol}^{-1}$) versus similar Au-X bond energies ($\text{Au}-\text{Cl} = 67 \text{ kcal}\cdot\text{mol}^{-1}$; $\text{Au}-\text{I} = 62 \text{ kcal}\cdot\text{mol}^{-1}$).^{15,45} Steric features of the transmetalated group are also influential: for bulky R^2 groups (entries 4, 5) the equilibrium is more shifted to the right than for electronically similar but smaller R^2 groups, probably because some steric constrain

^{*} Most equilibria were reached within 5 minutes (for $\text{L} = \text{AsPh}_3$) or 24 hours (for $\text{L} = \text{PPh}_3$) at room temperature, and they took longer for aryl groups with high steric hindrance. Numerical values could be obtained for a few cases with PPh_3 as ligand, by ^{31}P NMR integration of the two Au complexes at equilibrium.

of gold co-catalyst clearly opens a more efficient pathway for the coupling with bulky stannylated groups.

The fluoromesityl group (entries 11, 12) could not be coupled with Au co-catalyst, even using long reaction times. Interestingly in the conditions of the co-catalyzed reaction important amounts of the homocoupling product (**2**) and the hydrolysis product 1,3,5-(CF₃)₃C₆H₃ (**5**) were formed, which are almost absent in the reactions attempted without gold co-catalyst. Homocoupling byproducts like (**2**) are typically formed in classic Stille reactions where a slow coupling allows for undesired transmetalations.^{8,32b,30} In our experience hydrolysis byproducts like (**5**) (and also C₆F₅H) are formed also in processes involving frustrated coupling, (e.g. [Pd(C₆F₅)₂L₂] hardly undergoes reductive elimination to C₆F₅-C₆F₅). Thus, it looks that the unsuccessful co-catalysis in entry 11 is due to frustration of the process at the final reductive elimination step, rather than at any of the two successive transmetalation steps.

Table I-3. Pd-catalyzed cross-coupling of *p*-CF₃C₆H₄I (**1**) with several ArSnBu₃ compounds to ArC₆H₄CF₃, with L = AsPh₃, added LiCl and with or without gold co-catalyst.

Entry	Au Co-cat	ArC ₆ H ₄ CF ₃ product	Time (h)	Yield (4) (%)	Other products (%)
1	Yes		5	83	2 (7), 3 (10)
2	No		5	68	1 (22), 2 (5), 3 (5)
3	Yes		6	89	2 (8), 3 (3)
4	No		6	4	1 (80), 2 (3), 3 (12)
5	Yes		24	84	1 (<1), 2 (8), 3 (6)
6	No		24	<1	1 (85), 2 (3), 3 (10)
7	Yes		24	90	2 (4), 3 (6)
8	No		24	0	1 (81), 2 (5), 3 (11)
9	Yes		48	64	1 (1), 2 (19), 3 (1)
10	No		48	0	1 (19), 2 (38), 3 (29)
11	Yes		48	0	1 (22), 2 (36), 5 (42)
12	No		48	0	1 (90), 2 (2), 5 (2)

General reaction conditions: solvent MeCN; temperature 80 °C; [*p*-CF₃C₆H₄I] = 0.10 M; [SnR₃SnBu₃] = 0.11 M; [AsPh₃] = 4.07 × 10⁻³ M; [LiCl] = Saturated solution. Pd catalyst: [PdCl₂(AsPh₃)₂] = 2 × 10⁻³ M; Au catalyst: [AuCl(AsPh₃)] = 2 × 10⁻³ M. The reactions were monitored until total conversion of the initial reagent, or for the time indicated. Yields were determined by ¹⁹F NMR integration and are average of two runs.

Further experiments were carried out to check the influence of added LiCl, the L ligand, and other effects (Table I-4).

Table I-4. Results of the cross-coupling experiments between *p*-CF₃C₆H₄-I and mesityltributyltin to produce *p*-CF₃-C₆H₄-Mes (**5**) in other conditions.^(a)

Entry	Pd catalyst Au co-catalyst? LiCl?	Time (h)	Yield %
5	[PdCl ₂ (AsPh ₃) ₂] [AuCl(AsPh ₃)], LiCl	24	84
13	[Pd(C ₆ H ₄ CF ₃)I(AsPh ₃) ₂] [AuCl(AsPh ₃)], LiCl	24	84
14	[Pd(C ₆ H ₄ CF ₃)I(AsPh ₃) ₂] [AuI(AsPh ₃)], no LiCl	24	<1
15	[PdCl ₂ (AsPh ₃) ₂] [AuCl(AsPh ₃)], no LiCl	24	33
16	[Pd(C ₆ H ₄ CF ₃)I(PPh ₃) ₂] [AuI(PPh ₃)], no LiCl	110	58(+5)
17	[Pd(C ₆ H ₄ CF ₃)I(PPh ₃) ₂] [AuI(PPh ₃)], LiCl	110	75
18	[PdCl ₂ (PPh ₃) ₂] [AuCl(PPh ₃)], LiCl	310	96
19	[Pd(C ₆ H ₄ CF ₃)I(AsPh ₃) ₂] CuCl, LiCl	24	13

^(a) General reaction conditions as in Table 2, except for the catalysts used and for the addition or not of LiCl, as indicated.

The reactions can be carried out with similar good yields of *p*-CF₃-C₆H₄-Mesityl (5) using indistinctly [Pd(C₆H₄CF₃)I(AsPh₃)₂] (the intermediate formed after the first oxidative addition to Pd (prepared independently), or [PdCl₂(AsPh₃)₂], as far as excess LiCl is used (entries 5, 13). The suppression of added LiCl is very detrimental for the Au co-catalyzed reaction with AsPh₃: it is lethal when there is no other source of Cl⁻ in the system (entry 14), and the process still works, although poorly, when Cl⁻ is coming with the Pd and Au catalysts (entry 15), but fails completely when these catalysts come with iodide and there is no Cl⁻ in the system (entry 14). This is clearly related to the fact that the oxidative addition step to Pd⁰ complexes with weak ligands such as arsanes does not take place without addition of chloride.^{4,11,46}

In fact, the coupling reaction using PPh₃ catalysts runs perfectly, although very slowly (entry 16). In this case a 5% of undesired homocoupling product *p*-CF₃C₆H₄-C₆H₄CF₃-*p* is formed initially but does not grow on prolonged time. This undesired product was not formed when LiCl was added (entry 17). The reactions with PPh₃ still continued slowly after 110 h. With added LiCl the homocoupling disappears and the reaction is as efficient as with AsPh₃, although noticeably slower (entry 13 vs. 17 and 5 vs. 18). This effect is well known in the classic Stille process, and is due to the easier ligand displacement of weaker ligands during the associative transmetalation to Pd.^{11a} Other positive effects of a large excess of LiCl are that it exchanges I for Cl in the metals. This reduces the energetic barrier of the Sn to Pd transmetalation step.^{11b,47,*} Also, the excess of LiCl helps to keep the gold co-catalyst in the form [AuCl(AsPh₃)][†] which, as shown section 2.1.a), shifts the Sn to Au transmetalation equilibrium towards the gold arylated compound. Furthermore, LiCl improves the overall thermodynamic balance of the coupling (whether classic or Au co-catalyzed) because of the higher stability of SnClBu₃ as compared to that of SnIBu₃.

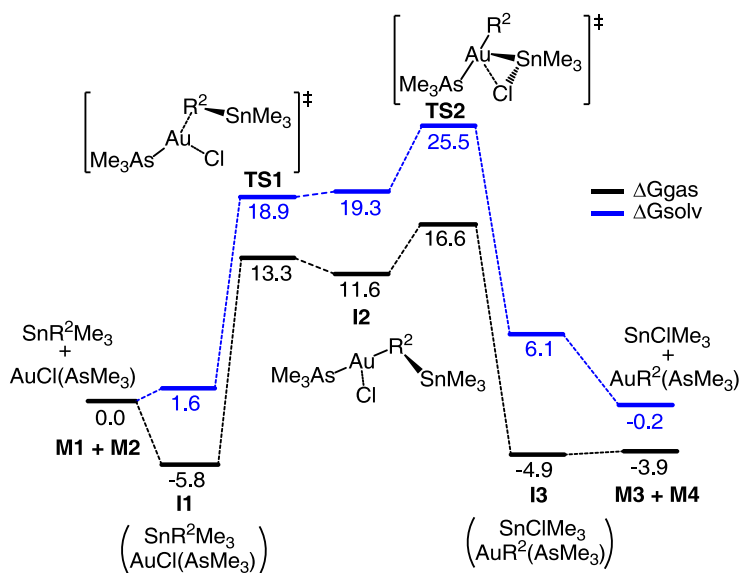
* Probably the effect on the Sn to Au transmetalation should be similar, as this barrier is much related to the electrophilicity of the M center. See ref. 47.

† The coupling reaction is continuously producing ISnBu₃. Should no other source of Cl be available, this ISnBu₃ would react with AuCl(AsPh₃) to give ClSnBu₃ and AuI(AsPh₃), which is undesired.

Finally, it is interesting that, under similar experimental conditions, [AuCl(AsPh₃)] or [AuCl(PPh₃)] were much more efficient co-catalysts than CuCl (entries 5, 13, 17, 18 vs. 19), as shown by the yields achieved in entries 13, 16 (84% for the gold complex versus 13% for CuCl).

The ability of gold to promote the cross-coupling of sterically encumbered aryltin derivatives is remarkable. So far, these cross-coupling processes required the use of bulky and strongly σ -donor phosphanes able to draw the reaction through tricoordinate palladium intermediates.^{9,48} Apparently, when Au (and expectedly when Cu) complexes act as intermediates in the transmetalation, the steric hindrance for direct transmetalation with tetracoordinated Sn and Pd compounds is circumvented by the less demanding linear gold complexes which in addition brings the bulky substituents one bond farther away from the critical exchange bridging zone in the transmetalation transition states (see Figure I-1). This improvement allows for the process to occur using Pd complexes with inexpensive common ligands.

Our hypothesis was confirmed by DFT calculations, which estimated the energy of the transmetalation transition states from Sn to Pd (involved in the direct Stille reaction), or from Sn to Au and from Au to Pd (involved in the gold co-catalyzed pathway). The calculations were performed for the formation of (2-methyl-1-(4-(trifluoromethyl)phenyl)naphthalene (Table I-4, entry 7) with the real molecules, except for the SnBu₃ group, which was simplified to SnMe₃. The transmetalation mechanisms from Sn to Pd and from Au to Pd have been studied before for sterically non demanding groups.^{20,35} The transmetalation mechanism from Sn to Au, has not been studied so far, and it is depicted in Scheme I-12.



Scheme I-12. DFT calculated pathway for the tin to gold transmetalation.

The structures of the three rate determining transition states and their free energies in vacuum and in MeCN are shown in Figure I-1.

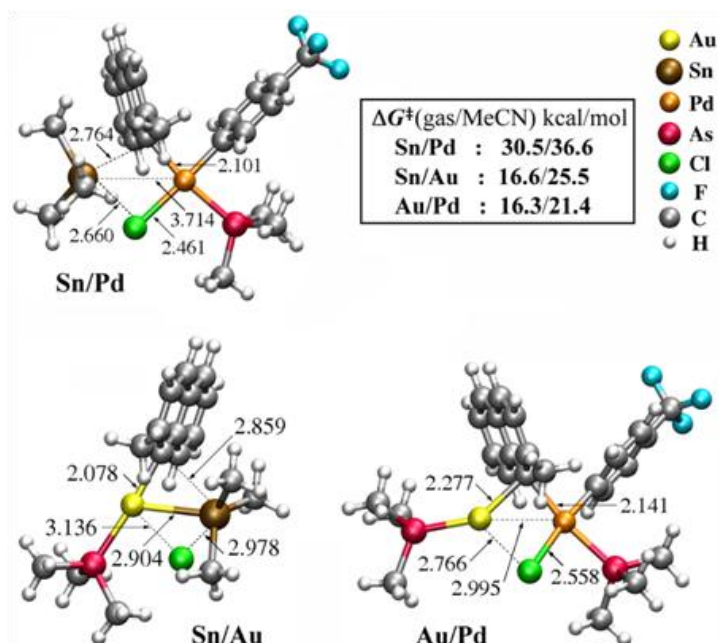


Figure I-1. Transition states and ΔG^\ddagger for the transmetalations.

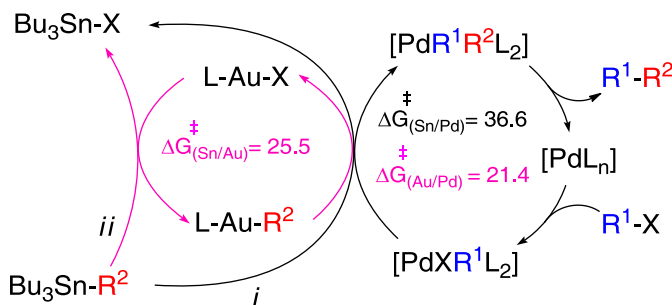
The transition energies very clearly show that there is a considerable difference in favor of the bimetallic pathway, thus predicting that, for this case, the direct Stille transmetalation should not take place, and the bimetallic process should be facile, as observed. Interestingly the two transition states involving gold show intermetallic distances much shorter than the sum of the van der Waals radii (in fact not far from the sum of covalent radii) for Sn–Au (2.904 versus 3.83 Å) and for Pd–Au (2.995 versus 3.29 Å),⁴⁹ thus suggesting metallophilic interactions in the transition states. In contrast, the sum of the van der Waals radii is found for Sn–Pd (3.714 versus 3.80 Å), thereby suggesting no interaction.

2.2. Conclusions

This study shows that gold(I) complexes in the presence of LiCl catalyze efficiently the transmetalation step of bulky groups from tin to palladium making possible some cross-couplings that would not proceed under the classical Stille reaction conditions. The effect of gold in the reaction might be limited by the unfavorable thermodynamics of the transmetalation equilibrium from organotin to gold if the concentrations of the aryl–gold intermediate were kinetically insufficient for the process to go on to the next step. Fortunately this transmetalation, which involves the replacement of aryl–Sn for X–Sn bonds, is favored in the presence of LiCl due to high Sn–Cl bond energy, and is also more favorable for hindered aryl groups on the stannane, when the mediation of gold is more necessary. Thus the combination of a gold co-catalyst and LiCl provides an interesting upgrade of the Stille process for its application to bulky reagents that were not accessible so far in the classic way.

DFT calculations for the classic Stille and the two successive transmetalations in the bimetallic processes have been carried out, including the first study of a Sn to Au transmetalation. It is shown that, for a fairly bulky aryl group, the intermediacy of gold drives the reaction through transition states much lower in energy than the classic direct Stille processes (Scheme I-13). This reduction of the energetic barrier is associated to a lower crowding that additionally allows formation of Au–Pd and Au–Sn stabilizing interactions, which are non-existent in the Sn–Pd transition state of

the classic process. Obviously the effect of gold is expected to be very important for crowded systems, and less so for conventional aryls where the classic process is still sufficiently fast, as observed.



Scheme I-13. Pathways for (i) the classical Stille and (ii) the Au co-catalyzed processes, including the transition state energies for the rate determining step when X = Cl and R^2 = 2-methyl-naphthalene.

3. The decisive role of ligand metathesis in Au/Pd bimetallic catalysis

As it has been shown in Section 2, bimetallic processes based on Au/Pd cocatalysis can lead to very interesting reactivity.³⁶⁻⁴⁰ However, designing appropriate bimetallic systems is not an easy task and sometimes the reaction conditions needed for effective catalysis with one metal are incompatible with those required by the other metal. In the particular case of Au/Pd bimetallic systems, redox incompatibilities have been reported as a possible cause of the failure of these systems.⁵⁰ As shown in that work, the ancillary ligands can be very important for tuning the specific reactivity of each metal.* It is logical to think that if different metals carry out different tasks within a catalytic cycle, they would have different steric and electronic requirements, thus the appropriate ligand could be different for each catalyst.

* Therein, it was demonstrated that the accumulation of Pd(0) is pernicious for the life of the coupling. The reaction is ruined by a Pd(0)/Au(I) redox reaction that generates a gold mirror and Pd(II). Strong ligands contribute to stabilize Au(I) species. See ref. 50.

In the initial experimental and DFT mechanistic study of section 2, AsPh₃ was utilized as ligand for the two metals, in order to skip possible observational complications arising from scrambling of the ancillary ligands.* The reaction also worked with PPh₃, but much more slowly due to the fact that transmetalations on Pd are slower for phosphine than for arsine complexes.⁴ Transfer under cocatalytic conditions of PPh₃ from Au to Pd (by HRMS), and from [Pd(PPh₃)₄] to Au to form catalytically less active [(PPh₃)₂Au]⁺ (by NMR) has been observed before but it has never been studied comprehensively or carefully.^{38a}

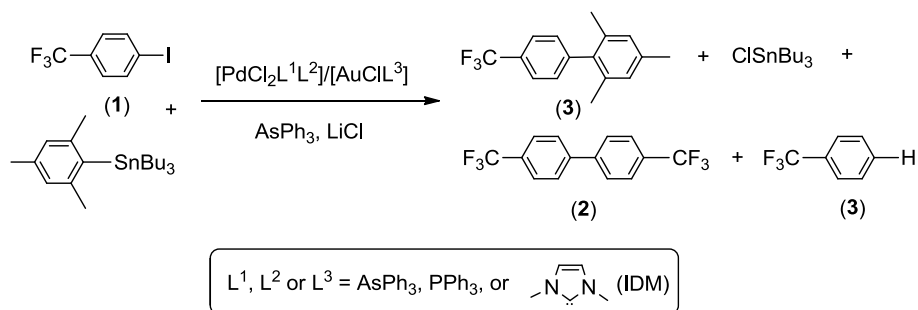
Having established the basic framework of the mechanism of the Au-cocatalyzed Stille process, it is now possible to address the effect of the changing the ancillary ligands (a typical strategy used in synthesis optimization) from a mechanistic point of view. This study uncovers aspects such as the thermodynamic preference of each metal for different ligands, the kinetics of ligand scrambling, and the importance of the several mechanistic steps in the process using three representative ancillary ligands, PPh₃, AsPh₃, and IDM (IDM = 1,3-dimethyl-imidazol-2-ylidene),⁵¹ and their combinations by pairs.[†]

3.1. Results and Discussion

Our model is the coupling of *p*-CF₃C₆H₄I (**1**) with the sterically demanding nucleophile MesSnBu₃ (Bu = *n*-butyl, Mes = mesityl), catalyzed with [PdCl₂L¹L²₂] and [AuClL³] (L¹, L², or L³ = AsPh₃, PPh₃, or IDM). This coupling works only in the presence of gold co-catalysis. AsPh₃ and LiCl were added in all the mechanistic tests, in order to keep the reaction conditions constant. The experimental kinetic conditions were Pd:Au:Cl⁻:As_{added} = 1:1:saturated:2, where Pd and Au stand for the Pd and Au catalyst used, with the corresponding ligand in each case (Scheme I-14).

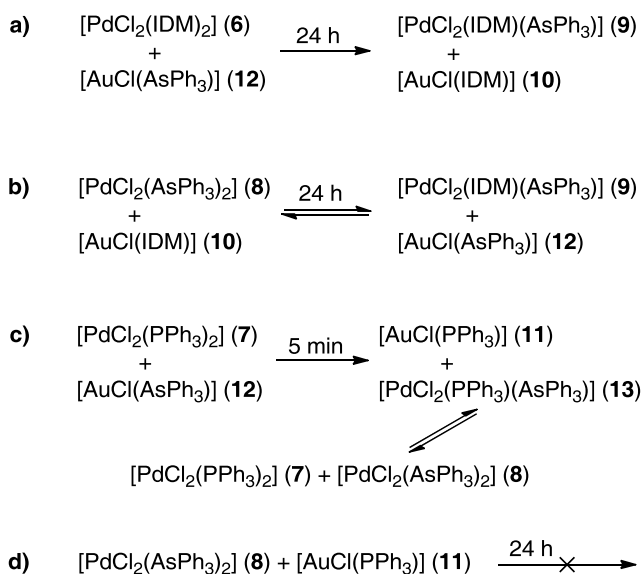
* The undesired ligand exchange between metals can be avoided by using a chelate ligand. See ref. 36a.

† NHC carbenes are considered to be strong σ -donors. In comparison, PPh₃ would be categorized as moderate σ -donor and AsPh₃ as weak σ -donor. See ref 51.



Scheme I-14. Summary of experiments

The initial catalytic tests using combinations of metal complexes with different ligands revealed that in the final mixture the complexes not always corresponded to the initial ones. Sometimes ligand rearrangement was occurring during the catalytic process, and the scrambling rate could be fast or slow. This scrambling had to be studied apart, stoichiometrically, in order to understand the catalytic performance. The ligand exchange processes observed stoichiometrically are shown in Scheme I-15. All the spectra are shown in the supporting information at the end of this chapter. All the complexes are labelled in order to facilitate the reading (see also Table I-5).



Scheme I-15. Ligand scrambling processes

For instance, the stoichiometric reaction between $[\text{PdCl}_2(\text{IDM})_2]$ (**6**) and $[\text{AuCl}(\text{AsPh}_3)]$ (**12**) (Scheme I-15, entry a) leads to $[\text{AuCl}(\text{IDM})]$ (**10**) and the mixed palladium complex $[\text{PdCl}_2(\text{IDM})(\text{AsPh}_3)]$ (**9**). Thus, Pd transfers half of the IDM ligand available, in exchange for AsPh_3 . However, starting from $[\text{PdCl}_2(\text{AsPh}_3)_2]$ (**8**) and $[\text{AuCl}(\text{IDM})]$ (**10**) (Scheme 3, b), an equilibrium is reached by partial transfer of IDM ligand from Au to Pd. These equations show how delicate the thermodynamic balance is for these systems, but also suggests that, in the equilibrium, a Pd with two strongly coordinating ligands will have be prone to transfer one to gold if the starting Au complex has a more weakly coordinating ligand. Monitoring of this ligand exchange shows that it takes about 24 h at 80 °C (the temperature used in the catalytic process) for completion of the ligand rearrangement, as shown in Figure I-2. Thus, this rearrangement is unexpectedly slow, with a rate comparable to that of the catalytic process. It is worth warning that it may be frequent that, in similar cases, the actual catalytic systems will contain mixtures of catalytic species changing along the catalysis.

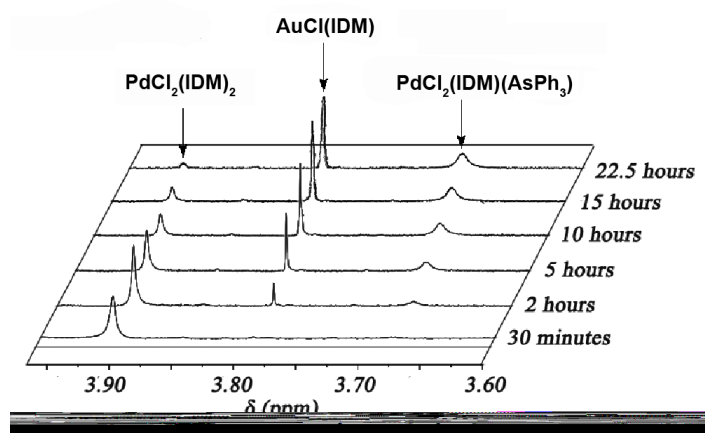


Figure I-2. Ligand exchange between $[\text{PdCl}_2(\text{IDM})_2]$ and $[\text{AuCl}(\text{AsPh}_3)]$, at 80 °C in CD_3CN , monitored by ^1H NMR on the Me signals of IDM.

The $\text{PPh}_3/\text{AsPh}_3$ metathesis is much faster than the IDM/AsPh_3 exchange, but shows further complications. The reaction of $[\text{PdCl}_2(\text{PPh}_3)_2]$ (**7**) with $[\text{AuCl}(\text{AsPh}_3)]$

(12) (Scheme I-15, c) is complete after five minutes at 80 °C,* leading to the formation of [AuCl(PPh₃)] (11) and [PdCl₂(PPh₃)(AsPh₃)] (13) (again, Au takes one strongly coordinating ligand from Pd), but (13) disproportionates in part to [PdCl₂(PPh₃)₂] (7) and [PdCl₂(AsPh₃)₂] (8). In acetonitrile as the reaction solvent, the gold complex [AuCl(PPh₃)] (12) is observed by ³¹P NMR, but fast ligand/solvent exchange in palladium complexes precludes the observation of the individual Pd complexes. Yet our assignment is supported by the following observations:

i) evaporation of the acetonitrile and dissolution in CDCl₃ (where ligand/solvent exchange does not occur) allows for the observation of [PdCl₂(PPh₃)₂] (7) and [PdCl₂(PPh₃)(AsPh₃)] (13).

ii) The same problem in observation by ³¹P NMR is found with an equimolar mixture of [PdCl₂(PPh₃)₂] (7) and [PdCl₂(AsPh₃)₂] (8) in acetonitrile.

iii) the reaction of [PdCl₂(PPh₃)₂] (7) with [AuCl(AsPh₃)] (12) in tetrachloroethane-d₂ at 80 °C also gives [AuCl(PPh₃)] (11) and a mixture of [PdCl₂(PPh₃)(AsPh₃)] (13), [PdCl₂(PPh₃)₂] (7), and [PdCl₂(AsPh₃)₂] (8).

No reaction is observed when [AuCl(PPh₃)] (11) and [PdCl₂(AsPh₃)₂] (8) are mixed in acetonitrile, showing the very high preference of gold for PPh₃ (Scheme I-15, d).

Considering the previous results, not only homogeneous but also mixed-ligand complexes were tested as catalysts. The results of all cross-coupling catalytic experiments are gathered in Table I-5.

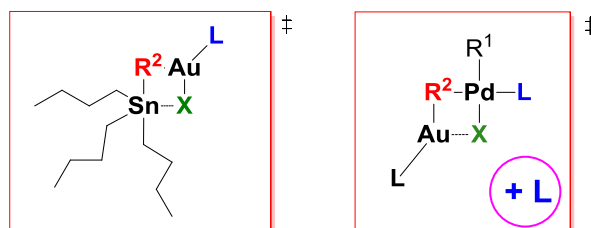
* [PdCl₂(PPh₃)₂] is not soluble in acetonitrile at room temperature.

Table I-5. Pd/Au co-catalyzed cross-coupling reaction of p-CF₃C₆H₄-I (**1**) with Mes-SnBu₃ to give p-Mes-C₆H₄-CF₃ (**4**), with different ligands in the initial gold and palladium cocatalysts, as shown in Scheme 2 above.

Entry	L ¹ , L ² , (Pd cat.)	L ³ (Au cat.)	(4) (%) [*] (24h)	Final conversion ^{**}
				4g: 2: 3: 1: other % ratio (hours)
1	2 IDM, (6)	IDM (10)	0	0 : 0: 0: 0 (48)
2	2 PPh ₃ , (7)	PPh ₃ (11)	14	96 : 3: 1: 0 (310) ^a
3	2 AsPh ₃ , (8)	AsPh ₃ (12)	84	84 : 8: 6: 2 (24) ^a
4	2 IDM, (6)	AsPh ₃ (12)	44	65 : 16: 10: 9 (72) ^b
5	IDM, AsPh ₃ , (9)	IDM (10)	66	89 : 7: 0: 4 (48)
6	IDM, AsPh ₃ , (9)	AsPh ₃ (12)	76	87 : 8: 4: 1 (48)
7	2 AsPh ₃ , (8)	IDM (10)	78	90 : 10: 0: 0 (38)
8	2 PPh ₃ , (7)	AsPh ₃ (12)	59	96 : 3: 1: 0 (84)
9	2 AsPh ₃ , (8)	PPh ₃ (11)	43	75 : 14: 7: 0 (250) ^b
10 ^c	2 AsPh ₃ , (8)	AsPh ₃ (12)	40	53 : 26: 13: 3: 5 (89)
11 ^c	IDM, AsPh ₃ , (9)	IDM (10)	37	81 : 15: 0: 0: 4 (89)
12 ^c	IDM, AsPh ₃ , (9)	AsPh ₃ (12)	60	81 : 15: 0: 0: 4 (89)
13 ^c	2 AsPh ₃ , (8)	IDM (10)	71	86 : 12: 0: 0: 2 (89)
14 ^c	2 PPh ₃ , (7)	AsPh ₃ (12)	29	83 : 2: 0: 15: 0 (89)
15 ^d	IDM, AsPh ₃ , (9)	IDM (10)	26	52 : 5: 0: 40: 0 (115)
16 ^d	IDM, AsPh ₃ , (9)	AsPh ₃ (12)	41	53 : 6: 0: 34: 7 (115)
17 ^d	2 AsPh ₃ , (8)	IDM (10)	28	39 : 2: 0: 34: 1 (115)

Procedure: NMR tubes were charged with solutions containing: solvent MeCN saturated with LiCl; temperature 80 °C; [p-CF₃C₆H₄-I] = 0.10 M; [SnRBU₃] = 0.11 M; [AsPh₃] = 4x10⁻³ M. [Pd] = 2x10⁻³ M; [Au] = 2x10⁻³ M. The reactions were monitored until total conversion of the initial reagent, or for the time indicated. Yields were determined by ¹⁹F NMR integration and are average of two runs. *Percentage of 3 formed in 24h. **Final conversion is the conversion achieved up to the moment when last measurement is taken (hours), and is the difference to 100 of the percentage of unreacted (1). a) Taken from Table I-4. b) Deposition of metal was observed. c) No added AsPh₃. d) No added AsPh₃ and no LiCl.

Entries 1–3 show the results of reactions with the same ligand on both metals.* In each of these three entries the possible occurrence of ligand scrambling is, expectedly, kinetically irrelevant since it does not produce chemical changes in the catalysts. We find that the carbene ligand totally blocks the Au/Pd catalyzed coupling (entry 1). PPh_3 gives only slow reaction rates (entry 2) compared to AsPh_3 (entry 3), which gives the fastest reaction. These results are easily understood in view of the prior mechanistic study of section 2: Since the transmetalation to Pd (whether associative or dissociative) implies release of one ligand from the palladium catalyst,^{11,20} the R^1 (Au-to-Pd) transmetalation step is rate determining when the ligand to be displaced is a strongly coordinating one. Rather on the contrary, our studies suggest that Sn/Au transmetalation does proceed without ligand release. Both scenarios are gathered in Scheme I-16.



Scheme I-16. Representation of the transition states of the Sn/Au and Au/Pd transmetalation.

Consistently, very good donors such as IDM block efficiently the catalysis at that point; the slightly weaker donor PPh_3 produce slow transmetalation (14% in 24 h); and the more weakly coordinating ligand AsPh_3 gives the fastest transmetalation (84% in 24h). Although AsPh_3 is faster, the highest yield after total conversion, and the highest selectivity to **(4)**, is found for PPh_3 , but only after 310 h (entry 2). We have shown before that homocoupling products such as **(2)** are formed from undesired R^1/R^2 transmetalations,⁵² and these seem to be disfavoured with PPh_3 , as compared to AsPh_3 .

* Entries 2 and 3 are taken from Table I-4, entries 18 and 5, respectively.

The formation of mixed-ligand palladium complexes (Scheme I-15) explains the catalytic activity observed for the other systems in Table I-5. Thus, entries 4 and 5 are closely related because the initial system in entry 4 must be slowly evolving to the initial system used in entry 5 along the reaction progress. Initially, the reaction in entry 4 is inefficient because complex (6) is blocking the process. Only when (9) starts to be formed the transmetalation and coupling can complete the second catalytic cycle, and the reaction runs at a progressively increasing rate as the concentration of active (9) increases to its equilibrium value. One AsPh_3 ligand in the palladium complex (as in (9)) is enough to provide a kinetically active coordination site (protected with an easily leaving ligand), that allows for the Au to Pd transmetalation and subsequent coupling reaction to occur.

The slowness of the ligand metathesis has the undesired side effect observed in entry 4: since arylgold complexes are not thermally stable in solution at 80 °C, the $[\text{AuR}^1\text{L}]$ intermediates initially formed by Sn/Au transmetalation do not find a palladium complex suitable for transmetalation. For this reason, considerable decomposition of the gold catalyst is observed during the initial period of the reaction, which reduces the overall catalytic activity of the system and leads to lower yields and lower percentage of the cross-coupling product. The problem disappears when the Pd complex used from the beginning has one labile AsPh_3 ligand (entry 5).^{*} In fact not much difference is made whether Au comes with an inert or with a labile (entry 6) ligand because the ligand on Au is not supposed to dissociate during the process.[†] The rate and yields in heterocoupling compound (4) of the catalysis can still be noticeably improved using two labile (and weak) ligands on Pd, which increases the electrophilicity of the Pd centre, and an inert (and strong) ligand on Au, which improves the stability of the gold intermediates (entry 7). In fact IDM seems to be the best stabilizer for gold, and the formation of the

* $[\text{PdCl}_2(\text{IDM})(\text{AsPh}_3)]$ (9) is stable and is easily prepared, see preparation in the experimental part.

† The R^1 transmetalation from Sn to linear Au occurs through a 3-coordinate transition state (see reference 44). Preliminary studies show no variation of the rates of Sn/Au transmetalation at different concentrations of neutral ligand.

reduction product (**3**) is totally suppressed by the use of [AuCl(IDM)] (entries 5 and 7).*

For entry 8 we expect, as in entry 4, ligand rearrangement (fast in this case) to produce [AuCl(PPh₃)] (**11**). Thus the gold intermediates are fairly well stabilized and decomposition via hydrolysis is almost absent. As shown in equation c of Scheme I-15, part of the palladium catalyst remains sequestered in the kinetically slow form, which is detrimental to the overall catalytic rate of the system. In spite of that, this combination turns out to be as selective as entry 2, with the best cross-coupling selectivity, and four times faster, providing probably the most convenient catalytic system.

Somehow to our surprise the catalysts combination in entry 9 makes a bad system, showing bad selectivity to (**3**). Entries 9 and 4 have in common that noticeable reduction to metal is observed at the beginning and then the catalysis yields noticeable amounts of homocoupling and reduction products. It is not easy to understand in the case of entry 9 but the observation of metal deposition suggests that these combinations might be less protected against redox incompatibility, perhaps in minor intermediates produced by ligand dissociation.⁵⁰

The best catalytic combinations were tested sparing the AsPh₃ stabilizing additive (entries 10-14). Then, those still working fine were tested without LiCl (entries 15-17). The results in Table I-5 show that, for the selected reactions, the suppression of adding AsPh₃ produces an increase of homocoupling, but in the best combination ([PdCl₂(AsPh₃)₂] + [AuCl(IDM)]) the suppression of added AsPh₃ has no cost. In all cases the suppression of LiCl is lethal and has a very detrimental effect on the conversion.†

* Mesitylene is a byproduct produced by hydrolysis of the gold intermediates [Au(Mes)L] (see ref. 44).

† LiCl has an important thermodynamic effect, converting ISnBu₃ in ClSnBu₃, as it was discussed.

3.2. Conclusions

In summary, although often ignored or overlooked, ligand metathesis is probably a frequently operating process in homogeneous catalysis, which can become decisive for the success of the reaction when different metals and ligands are involved in a bimetallic catalysis. Ligand exchanges can be slow, with the consequence that the catalytic system is changing during the reaction. The use of the most stable ligand combination from the beginning, or preformed catalysts with mixed ligands, is advised for these cases, thus skipping its cumbersome or sluggish formation in solution and long preactivation times, preventing undesired side reactions. However, if the ligand rearrangement is fast compared to the catalyzed reaction, as in entry 9, this precaution is not necessary.

For the cases studied the ligand scrambling led to catalysts with the best σ -donor ligand ($IDM > PPh_3 > AsPh_3$) on the gold atom, which is very convenient since it produces a palladium complex with at least one labile ligand ($AsPh_3$), and a gold complex coordinated with the best and more stabilizing ligand (IDM or PPh_3). According to the first part of this work, the transmetalation step from Sn to Au is much easier than the Sn to Pd transmetalation and occurs without ligand dissociation. Hence, the coordination of the best ligand to gold has many advantages, improving its stability and minimizing the formation of hydrolysis products that might occur on gold.³⁸ On the other hand, the Au to Pd transmetalation to Pd is rate determining for strongly coordinating ligands and having one weaker, easier to displace ligand in the coordination sphere of Pd strongly reduces the activation energy of this transmetalation, and increases the overall rate of the catalysis.* The combination of these two conditions leads to the best catalytic systems.

* Note that, in general, other steps in a cross-coupling cycle (for instance reductive elimination) could be rate determining depending on the reagents. See ref. 19 and 36.

4. Experimental section

4.1. General methods

All reactions were carried out under N₂ or Ar, in THF dried using a Solvent Purification System (SPS). NMR spectra were recorded on a Bruker AV 400 instrument equipped with a VT-100 variable-temperature probe, or a Varian 400-MR. Chemical shifts are reported in ppm from tetramethylsilane (¹H), CCl₃F (¹⁹F), or 85% H₃PO₄ (³¹P), with positive shifts downfield, at ambient probe temperature unless otherwise stated. The temperature for the NMR probe was calibrated using ethylene glycol (T > 300K) and methanol (T < 300K) as temperature standards. In the ¹⁹F and ³¹P spectra measured in non-deuterated solvents, a coaxial tube containing acetone-*d*₆ was used for the lock ²H signal. The Gas Chromatography-Mass analyses were performed in a Thermo-Scientific DSQ II GC/MS Fows GL. Combustion CHN analyses were made on a Perkin-Elmer 2400 CHN microanalyzer. Unless specified, all the compounds were used from commercial sources and used without further purification. The compounds [AuCl(tht)],⁵³ [AuCl(PPh₃)],⁵⁴ [AuCl(AsPh₃)],⁵⁵ [AuCl(IDM)],⁵⁶ [PdCl₂(AsPh₃)₂],⁵⁷ [PdCl₂(PPh₃)₂],⁵⁸ [PdCl₂(IDM)₂],⁵⁹ *ortho*-tolyltributyltin,⁶⁰ mesityltributyltin,⁶¹ 2-methyl-1-naphthyltributyltin,⁶² 2,4,6-(CF₃)₃(C₆H₄)SnBu₃⁶³ were prepared by literature methods.

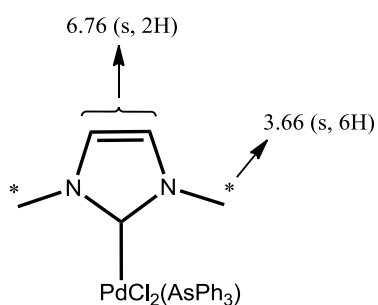
4.2. Synthesis of the compounds

trans-[Pd(C₆H₄CF₃)I(AsPh₃)₂]

[Pd₂dba₃]-CHCl₃ (600 mg, 0.58 mmol) and AsPh₃ (774 mg, 2.53 mmol) were dissolved in 20 mL of deoxygenated THF in a Schlenk flask and stirred for 30 minutes. A color change from deep purple to brown occurred. IC₆H₄CF₃ (295 μL, 2.55 mmol) was added and the solution was stirred for one extra hour, after which the solvent was removed under reduced pressure. The beige solid, containing the palladium compound and dba, was washed five times with cold Et₂O (10 mL) in an ice bath until the dba was removed. The resulting brown solid (930 mg) consists of a mixture of [Pd(C₆H₄CF₃)I(AsPh₃)₂] and the dimer [Pd₂(C₆H₄CF₃)₂(μ-I)₂(AsPh₃)₂]. In order to obtain the monomeric complex, the mixture was dissolved in CH₂Cl₂ (15 mL). To this solution 280 mg (0.91 mmol) of AsPh₃ were added, the solution was filtered through Celite to remove small amounts of metallic palladium, and 15 mL EtOH were added. Orange crystals were produced after concentrating in rotaevaporator to 15 mL and cooling the solution at -20 °C for 12 h. The solid was filtered, washed with cold ethanol and vacuum dried. Yield 745 mg (66 %). In solution, [Pd(C₆H₄CF₃)I(AsPh₃)₂] is in equilibrium with the dimer [Pd₂(C₆H₄CF₃)₂(μ-I)₂(AsPh₃)₂] and free AsPh₃ (K_{eq}(297 K) = 7.3·10⁻⁴ mol·L⁻¹), as reported for other palladium complexes with AsPh₃.^{12,64} ¹H NMR: δ 7.45 (dd, *J* = 8.0, 1.0 Hz, 1H), 7.42 – 7.22 (m, 2H), 6.87 (d, *J* = 8.4 Hz, 1H), 6.86 – 6.80 (m, 1H), 6.49 (d, *J* = 8.4 Hz, 1H). ¹⁹F NMR (376 MHz, CD₂Cl₂) δ -62.35 (s) (dimer, integral = 0.23), -62.52 (s) (monomer, integral = 1). Anal. Calcd for C₄₃H₃₄As₂F₂IPd: C, 52.12; H, 3.46. Found: C, 52.27; H 3.75.

[PdCl₂(IDM)(AsPh₃)]

A two necked flask was charged with [PdCl₂(AsPh₃)₂] (102 mg 0.129 mmol) and [PdCl₂(IDM)₂] (369 mg 0.129 mmol) dissolved in 100 mL of CH₃CN. The solution was stirred at 80 °C for 30 hours. The resulting yellow solution was filtered through Celite and the solvent was removed under reduced pressure giving a brown oil. This residue was dissolved in 1 mL of CH₂Cl₂ and crystallized by the addition of 5 mL of EtOH. The solid was filtered, washed with cold EtOH (3 mL) and vacuum dried. Yield 69% (102 mg). Anal. Calcd for C₂₃H₂₃As₂Cl₂N₂Pd: C, 47.55; H, 4.00; N, 4.83. Found: C, 47.29; H 3.70; N, 4.99. ¹H NMR (500 MHz, CD₃CN) δ 7.57 (dd, *J* = 8.1, 1.2 Hz, 6H), 7.55 – 7.50 (m, 3H), 7.47 – 7.42 (m, 6H), 6.76 (s, 2H), 3.66 (s, 6H). ¹³C NMR (126 MHz, CDCl₃) δ 157.62, 133.17, 130.22, 129.09, 123.16, 37.64.

**2,6-Diisopropylphenyl-tributyltin**

A two-necked flask was charged with 2,6-diisopropyl-1-bromo-benzene (1.078 g, 4.47 mmol) and 20 mL of Et₂O. The mixture was cooled to -78 °C and a 1.5 M solution of Li^tBu in hexanes (3.3 mL, 4.92 mmol) was added dropwise. The solution was stirred for one hour at this temperature, then for 15 minutes more at room temperature. The solution was cooled again to -78 °C and SnBu₃ (1.42 mL, 4.47 mmol) was added dropwise. The solution was allowed to warm to room temperature overnight, then it was quenched with a saturated aqueous solution of NH₄Cl (30 mL). The aqueous layer was decanted and extracted with Et₂O (3x30 mL). All the organic layers were combined, washed with brine (3x60 mL) and dried over MgSO₄. The solvent was removed under reduced pressure. The product was purified by chromatography in silica, with hexane as eluent, to give a colorless liquid, identified as a mixture of 2,6-diisopropylphenyl-tributyltin and 1,3-diisopropylbenzene. The final product was obtained by distilling off the 1,3-diisopropylbenzene at 160 °C under reduced pressure. A colorless liquid was obtained (yield: 665 mg, 34%). ¹H NMR (500 MHz, CDCl₃) δ 7.33 (t, *J* = 7.6 Hz, 1H), 7.19 (d, *J* = 7.6 Hz, 2H), 2.94 (m, *J* = 6.98 Hz, 2H), 1.64 – 1.52 (m, 6H), 1.40 (m, *J* = 14.6, 7.3 Hz, 6H), 1.29 (d, *J* = 6.8 Hz, 12H), 1.21 – 1.04 (m, 6H), 0.95 (m, 9H). ¹³C NMR (126 MHz, CDCl₃) δ 156.14 (s), 141.23 (s), 128.73 (s), 122.64 (s), 36.87 (s), 29.26 (s), 27.48 (s), 25.25 (s), 13.66 (s), 13.13 (s). ¹¹⁹Sn NMR (186 MHz, CDCl₃) δ -61.22 (s). GC-MS: MS (EI+, 70 eV): *m/z* (%): 395 (100) [M-Bu]⁺, 339 (20), 281 (45) [M-Bu₃]⁺.

4.3. General procedure of the Stille cross-coupling reactions co-catalyzed by gold and palladium complexes

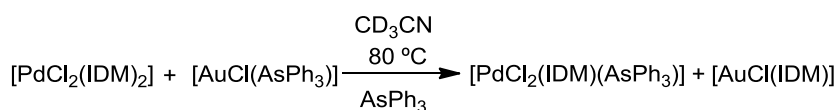
A stock solution 2.0×10^{-3} M in the specified gold catalyst was prepared using as solvent CH_3CN saturated in LiCl at rt. (solubility about 1.8 g/L). For experiments with Cl-Au-AsPh_3 as co-catalyst, AsPh_3 was added to reach a concentration of 4×10^{-3} M in the ligand. A NMR tube was charged with 1 mg ($1.2 \cdot 10^{-3}$ mmol) of the specified Pd catalyst, 0.061 mmol of the corresponding aryl halide, and 0.068 mmol of the corresponding aryltributyltin. 0.6 mL of the stock solution ($1.2 \cdot 10^{-3}$ mmol of AuXL and 2.4×10^{-3} mmol of AsPh_3 if $\text{AuCl(AsPh}_3)$ was used) were added via syringe, and the tube was heated at 80°C until completion of the reaction or specified time. All reactions were monitored by ^{19}F NMR. The yields of the products in Table 2 were obtained by ^{19}F NMR integration.

4.4. General procedure for ligand exchange reactions between gold and palladium complexes

A solution in CD_3CN (0.6 mL) of concentration $2.0 \cdot 10^{-3}$ M in the gold catalyst, $2.0 \cdot 10^{-3}$ M in the palladium catalyst and $4.1 \cdot 10^{-3}$ M in AsPh_3 was prepared in a NMR tube under nitrogen atmosphere. The tube was sealed and heated in an oil bath at 80°C until completion of the reaction or specified time. All reactions were monitored by ^1H NMR or ^{31}P .

The following spectra correspond to Scheme I-15 in "Decisive Ligand Metathesis Effects in Au/Pd Bimetallic Catalysis".

Reaction between $[\text{PdCl}_2(\text{IDM})_2]$ and $[\text{AuCl(AsPh}_3)]$



Corresponding to reaction "a" in Scheme I-15 in the main text.

The reaction between $[\text{PdCl}_2(\text{IDM})_2]$ and $[\text{AuCl(AsPh}_3)]$ produces quantitatively $[\text{AuCl(IDM)}]$ and $[\text{PdCl}_2(\text{IDM})(\text{AsPh}_3)]$ in 24 hours.

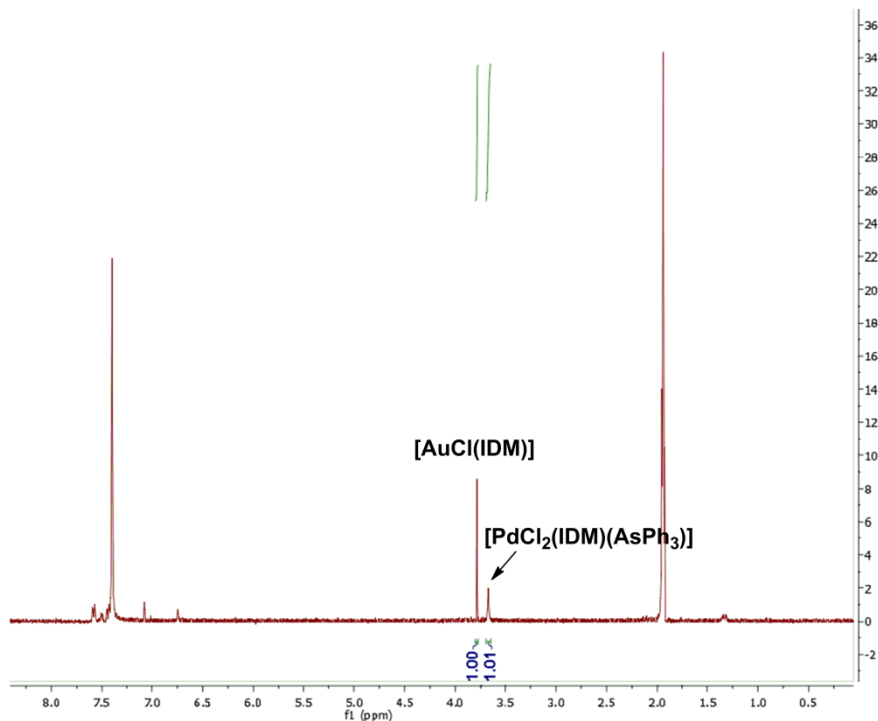
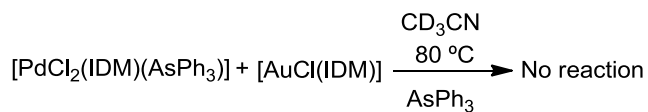


Figure I-3. Spectra of $[\text{PdCl}_2(\text{IDM})_2]$ and $[\text{AuCl}(\text{AsPh}_3)]$ after 24 h in CD_3CN at 80°C . The signals from the methyl IDM groups in both metals (marked with arrows) have been used for quantitative purposes.

Reaction between $[\text{PdCl}_2(\text{IDM})(\text{AsPh}_3)]$ and $[\text{AuCl}(\text{IDM})]$



Corresponding to reaction "a" in Scheme I-15 in the main text.

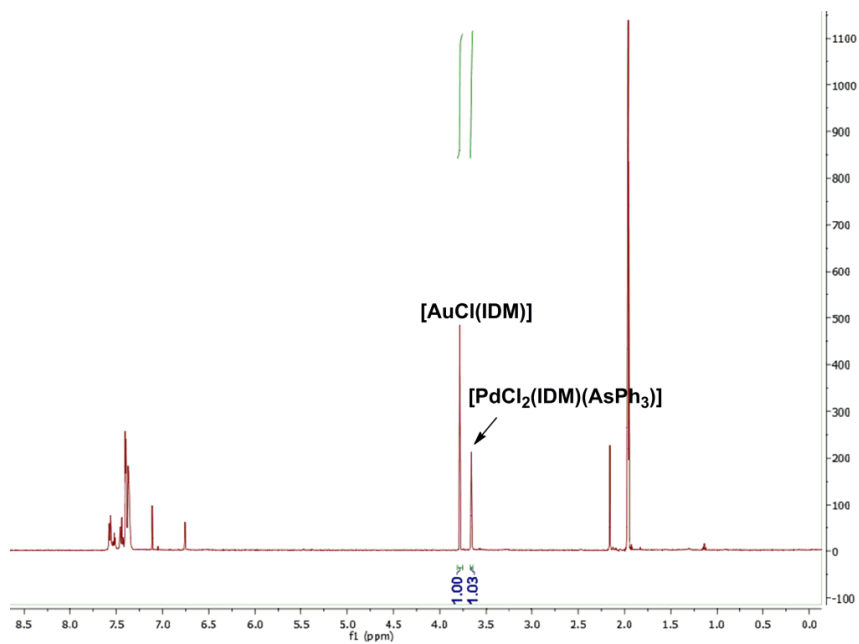
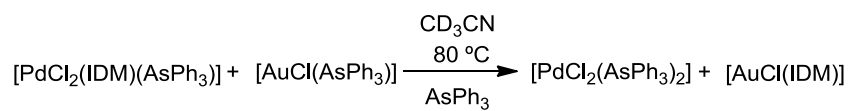


Figure I-4. Spectra of $[\text{PdCl}_2(\text{IDM})(\text{AsPh}_3)]$ and $[\text{AuCl}(\text{IDM})]$ after 24 h in CD_3CN at 80°C .

Reaction between $[\text{PdCl}_2(\text{IDM})(\text{AsPh}_3)]$ and $[\text{AuCl}(\text{AsPh}_3)]$

Corresponding to reaction "b" in Scheme I-15 in the main text.



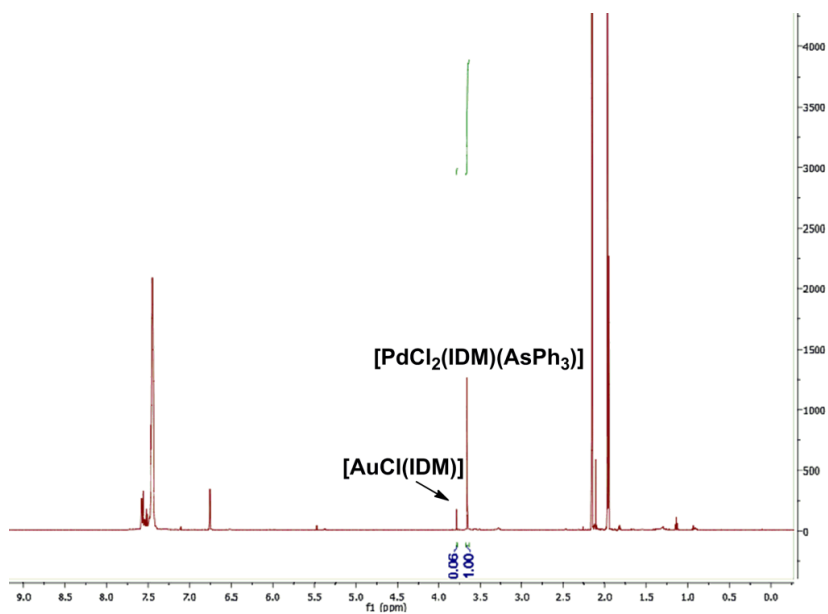
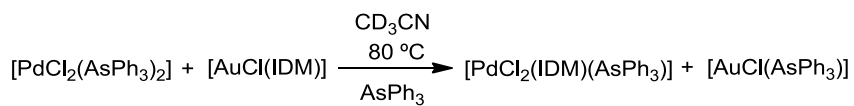


Figure I-5. Spectrum of $[\text{PdCl}_2(\text{IDM})(\text{AsPh}_3)]$ and $[\text{AuCl}(\text{AsPh}_3)]$ after 24 h in CD_3CN at 80°C .

Reaction between $[\text{AuCl}(\text{IDM})]$ and $[\text{PdCl}_2(\text{AsPh}_3)]$



Corresponding to reaction "b" in Scheme I-15 in the main text.

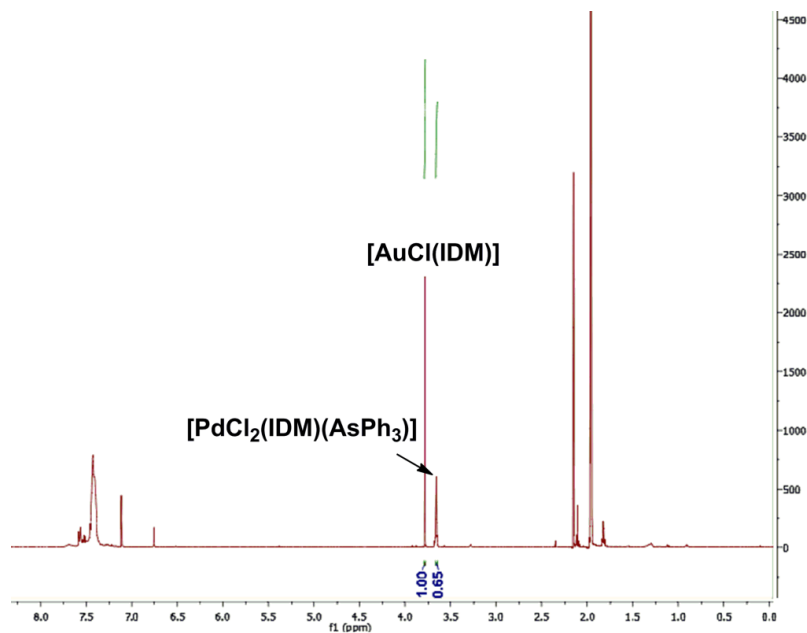
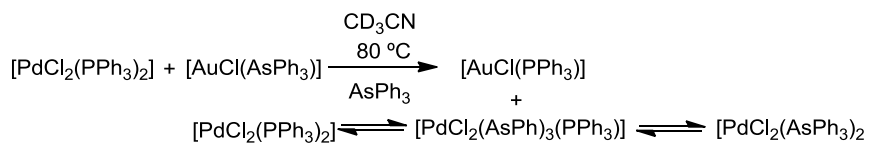


Figure I-6. Spectrum of [AuCl(IDM)] and [PdCl₂(AsPh₃)] after 24 h in CD₃CN at 80°C.

Reaction between [PdCl₂(PPh₃)₂] and [AuCl(AsPh₃)]:



Corresponding to reaction "c" in Scheme I-15 in the main text.

a) In CD_3CN

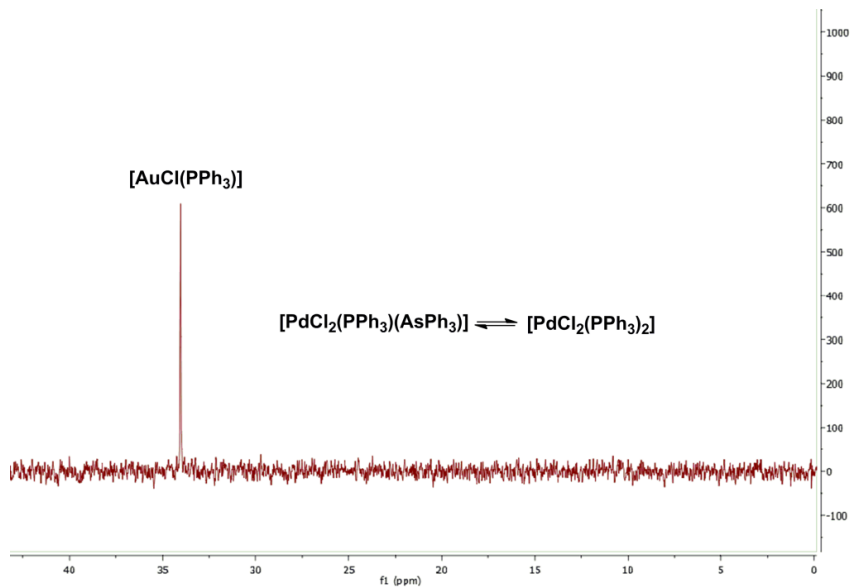


Figure I-7. Spectrum of $[\text{PdCl}_2(\text{PPh}_3)_2]$ and $[\text{AuCl}(\text{AsPh}_3)]$ in CD_3CN at 80°C after 5 minutes.

b) After evaporating the CD_3CN and dissolving the residue in CDCl_3 .

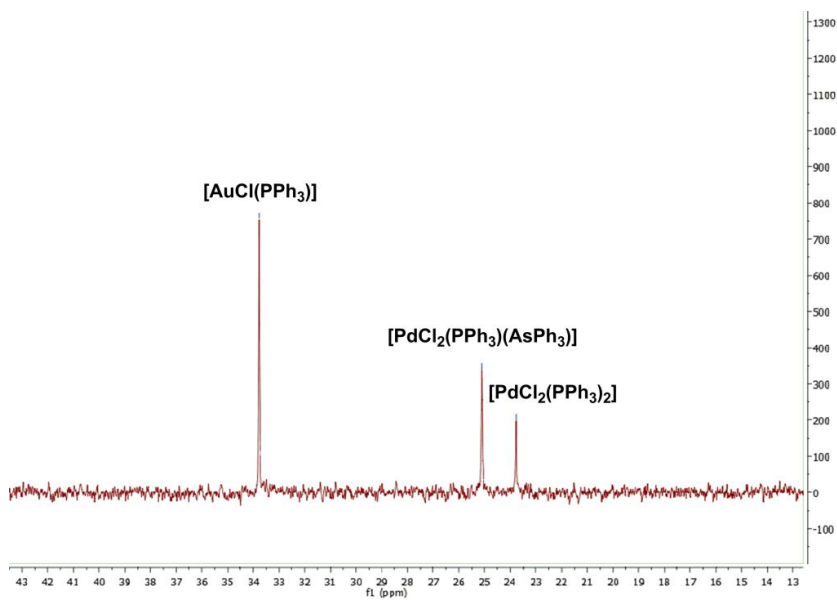
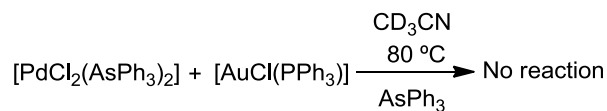


Figure I-8. Spectrum of $[\text{PdCl}_2(\text{PPh}_3)_2]$ and $[\text{AuCl}(\text{AsPh}_3)]$ in CDCl_3 .

Reaction between [PdCl₂(AsPh₃)₂] and [AuCl(PPh₃)]

Corresponding to reaction "c" in Scheme I-15 in the main text.



The reaction between [PdCl₂(AsPh₃)₂] and [AuCl(PPh₃)] in the reported conditions provided only [AuCl(PPh₃)] after 5 minutes in the ³¹P spectra, either in CD₃CN or CDCl₃.

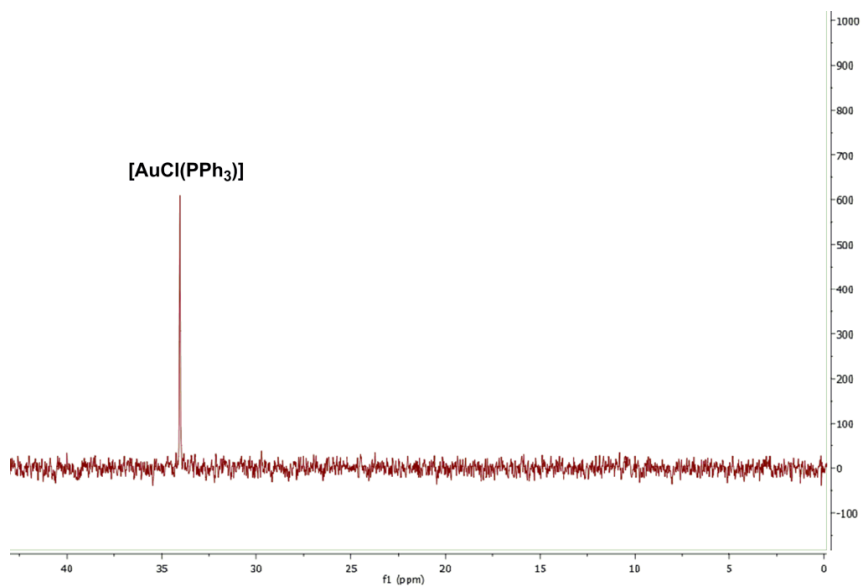


Figure I-9. Spectrum of [PdCl₂(AsPh₃)₂] and [AuCl(PPh₃)] in CD₃CN after 5 minutes at 80°C.

4.5. Computational Details

Density Functional Theory (*DFT*) calculations were performed using the *Gaussian 09* program package⁶⁵ and the wB97X-D hybrid functional of Head-Gordon and co-workers,⁶⁶ which includes empirical long-ranged correlation corrections. Geometry optimizations and harmonic force constants were computed at the 6-31G**^{*}-LANL2DZ level.^{67,*} The optimized transition state structures were confirmed by having a unique imaginary frequency and correlating the corresponding reactants and products. Solvent effects (MeCN, $\epsilon = 35.688$) were introduced through single point calculations at optimized gas-phase geometries by means of a continuum method, the *SMD* solvation model⁶⁸ implemented in *Gaussian 09*. Relative Gibbs energies in MeCN were obtained by adding the gas-phase Gibbs energy corrections of the solute calculated at $T = 298.15$ K and $P = 1$ atm to the energies in solution. *Trans*-[Pd(C₆H₄CF₃)Cl(AsMe₃)₂], [Au(AsMe₃)Cl] and R²SnMe₃ (R² = 2-methyl-1-naphthalene) were used as the model complexes. The optimized Cartesian coordinates will not be included herein for short, but they can be consulted in the corresponding publication.⁴⁴

* This is the methodology that produced the best results in our previous study of a Pd/Au transmetalation. See ref. 35.

5. References

1. (a) De Meijere, A.; Dietrich, F.; *Metal-Catalyzed Cross-Coupling Reactions*, 2nd ed. **2004**, Wiley-VCH: Weinheim. (b) Miyaura, N.; *Cross-Coupling Reactions: A practical Guide; in Topics in Current Chemistry, Series 219; 2002*, Springer, Berlin.
2. For a recent example of the use of the Stille reaction in the synthesis of a complex natural product, see: Neuhaus, C. M.; Liniger, M.; Stieger, M.; Altmann, K.-H. *Angew. Chem. Int. Ed.* **2013**, *52*, 5866–5870.
3. Farina, V., Krishnamurthy, V., Scott, W. K.; *The Stille Reaction*, Wiley: New York, **2004**.
4. Espinet, P.; Echavarren, A. M.; *Angew. Chem. Int. Ed.* **2004**, *43*, 4704-4734.
5. Cordovilla, C.; Bartolomé, C.; Martínez-Ilarduya, J. M.; Espinet, P. *ACS Catal.* **2015**, 3040–3053.
6. Azarian, D.; Dua, S. S.; Eaborn, C.; Walton, D. R. M. *J. Organomet. Chem.* **1976**, *117*, C55-C75.
7. (a) Kosugi, M.; Sasazawa, K.; Shimizu, Y.; Migita, T. *Chem. Lett.* **1977**, 301-302. (b) Kosugi, M.; Shimizu, Y.; Migita, T. *Chem. Lett.* **1977**, 1423-1424.
8. Milstein, D.; Stille, J. K.; *J. Am. Chem. Soc.* **1979**, *101*, 4992-4998.
9. (a) Fu, G. C.; Schwarz, L.; Littke, A. F. *J. Am. Chem. Soc.* **2002**, *5*, 6343–6348. (b) Naber, J. R.; Buchwald, S. L. *Adv. Synth. Catal.* **2008**, *350*, 957–961. (c) Littke, A. F.; Fu, G. C. *Angew. Chem. Int. Ed.* **1999**, *38*, 2411–2413. (d) Valente, C.; Çalimsiz, S.; Hoi, K. H.; Mallik, D.; Sayah, M.; Organ, M. G. *Angew. Chem. Int. Ed.* **2012**, *51*, 3314–3332.
10. Stille, J. K. *Angew. Chem. Int. Ed.* **1986**, *25*, 508–524.
11. (a) Casado, A. L.; Espinet, P.; *J. Am. Chem. Soc.* **1998**, *120*, 8978-8985; (b) Casado, A. L.; Espinet, P.; *J. Am. Chem. Soc.* **2000**, *122*, 11771-11782.
12. Pérez-Temprano, M. H.; Nova, A.; Casares, J. a.; Espinet, P. *J. Am. Chem. Soc.* **2008**, *130*, 10518–10520.
13. García-Melchor, M.; Braga, A.; Lledós, A.; Ujaque, G.; Maseras, F. *Acc. Chem. Res.* **2013**, *46*, 2626–2634.
14. Davies, A. G.; Gielen, M.; Pannell, K. H.; Tiekink, E. R. T.; *Tin Chemistry: Fundamentals, Frontiers and Applications*, John Wiley & Sons, **2008**, Ltd, Chichester.

15. (a) Ruo, Y.-L.; *Comprehensive Handbook of Chemical Bond Energies*; CRC Press; 1 edition, 2007. The BDE of FSnMe_3 is computed and can be found herein: (b) Adams, M. R.; Bushnell, E. a. C.; Bruce Grindley, T.; Boyd, R. J. *Comput. Theor. Chem.* **2014**, *1050*, 7–14.
16. The Pd-C bond dissociation energy was extracted from: Simoes, J. A. M.; Beauchamp, J. L. *Chem. Rev.* **1990**, *90*, 629–688. The Pd-halogen bond dissociation energy was obtained from: Lan, Y.; Liu, P.; Newman, S. G.; Lautens, M.; Houk, K. N. *Chem. Sci.* **2012**, *3*, 1987. Experimental information concerning Pd-halide dissociation can be obtained herein: Casares, J. A.; Coco, S.; Espinet, P.; Lin, Y. *Organometallics*, **1995**, 3058–3067.
17. For coupling reactions with fluorostannates, see: (a) García-Martínez, A.; Barcina, J. O.; de Fresno Cerezo, A.; Subramanian, L. R. *Synlett* **1994**, 1047-1048; (b) García-Martínez, A.; Barcina, J. O., Colorado Heras, M. R.; de Fresno Cerezo, A. *Org. Lett.* **2000**, *2*, 1377-1378.
18. Bhatt, R. K.; Ye, J. *J. Am. Chem. Soc.* **1995**, *117*, 5973–5982.
19. For an example of transmetalation with inversion of the configuration of the α -C of a chiral stannane see: (a) Labadie, J. W.; Stille, J. K. *J. Am. Chem. Soc.* **1983**, *105*, 6129-6137. For examples reporting retention see: (b) Ye, J.; Bhatt, R. K.; Falck, J. R. *J. Am. Chem. Soc.* **1994**, *116*, 1-5; (c) Ye, J.; Bhatt, R. K.; Falck, J. R. *Tetrahedron Lett.* **1993**, *34*, 8007-8010.
20. Nova, A.; Ujaque, G.; Maseras, F.; Lledós, A.; Espinet, P. *J. Am. Chem. Soc.* **2006**, *128*, 14571–14578.
21. For the isomers arising from the transmetalation and their isomerization see the following paper and references therein: Pérez-Temprano, M. H.; Gallego, A. M.; Casares, J. A.; Espinet, P.; *Organometallics*, **2011**, *30*, 611-617.
22. (a) Álvarez, R; Faza, O. N.; López, C. S.; de Lera, A. R. *Org. Lett.* **2006**, *8*, 35–38. (b) Ariaifard, A.; Lin, Z.; Fairlamb, I. J. S. *Organometallics* **2006**, *25*, 5788–5794.
23. Ariaifard, A.; Yates, B. F. *J. Am. Chem. Soc.* **2009**, *131*, 13981–13991.
24. (a) Vedejs, E.; Haight, A. R.; Moss, W. O. *J. Am. Chem. Soc.* **1992**, *114*, 6556-6558. (b) Jensen, M. S.; Yang, C.; Hsiao, Y.; Rivera, N.; Wells, K. M.; Chung, J. Y. L.; Yasuda, N.; Hughes, D. L.; Reider, P. J. *Org. Lett.* **2000**, *2*, 1981-1984; (c) Sebahar, H. L.; Yoshida, K.; Hegedus, L. S. *J. Org. Chem.* **2002**, *67*, 3788-3795.
25. Napolitano, E.; Farina, V.; Persico, M. *Organometallics* **2003**, *22*, 4030–4037.
26. For the transmetalation of hyper coordinate aryl trialkyl silanes and aryl trialkyl stannanes with Pd^{II} and Pt^{II} complexes, see: Steenwinkel, P.; Jastrzebski, J. T. B. H.;

- Deelman, B.; Grove, D. M.; Kooijman, H.; Veldman, N.; Smeets, W. J. J.; Spek, A. L.; van Koten, G. *Organometallics* **1997**, *16*, 5486–5498.
27. Dowlut, M.; Mallik, D.; Organ, M. G. *Chem. Eur. J.* **2010**, *16*, 4279–4283.
28. Early examples of this effect: (a) Liebeskind, L. S.; Fengl, R. W. *J. Org. Chem.* **1990**, *55*, 5359. (b) Johnson, C. R.; Adams, J. P.; Braun, M. P.; Senanayake, C. B. W. *Tetrahedron Lett.* **1992**, *33*, 919. (c) Ye, J.; Bhatt, R. K.; Falck, J. R. *J. Am. Chem. Soc.* **1994**, *116*, 1.
29. Farina, V.; Kapadia, S.; Krishnan, B.; Wang, C.; Liebeskind, L. S. *J. Org. Chem.* **1994**, *59*, 5905–5911.
30. Casado, A. L.; Espinet, P.; *Organometallics*. **2003**, *6*, 1305–1309;
31. (a) Bhatt, R. K.; Ye, J. *J. Am. Chem. Soc.* **1995**, *117*, 5973–5982. (b) Allred, G. D.; Liebeskind, L. S. *J. Am. Chem. Soc.* **1996**, *118*, 2748–2749. (c) Piers, E.; Wong, T. *J. Org. Chem.* **1993**, *58*, 3609–3610.
32. (a) Benson, C. L.; West, F. G. *J. Org. Chem.* **2004**, *69*, 220–223. (b) Han, X.; Stoltz, B. M.; Corey, E. J. *J. Am. Chem. Soc.* **1999**, *121*, 7600–7605.
33. Recent reviews: (a) Pérez-Temprano, M. H.; Casares, J. A.; Espinet, P.; *Chem. Eur. J.* **2012**, *18*, 1864–1884; (b) Blum, S. A.; Hirner, J. J.; Shi, Y.; *Acc. Chem. Res.* **2011**, *44*, 603–613.
34. Casado, A. L.; Espinet, P.; *Organometallics* **1998**, *17*, 3677–3683.
35. Pérez-Temprano, M.; Casares, J. A.; de Lera, A. R.; Álvarez, R.; Espinet, P.; *Angew. Chem. Int. Ed.* **2012**, *51*, 4917–4920.
36. a) Hashmi, A. S. K.; Lothschütz, C.; Döpp, R.; Rudolph, M.; Ramamurthi, T. D.; Rominger, F.; *Angew. Chem. Int. Ed.* **2009**, *48*, 8243–8246. b) Hashmi, A. S. K.; Döpp, R.; Lothschütz, C.; Rudolph, M.; Riedel, D.; Rominger, F.; *Adv. Synth. Catal.* **2010**, *352*, 1307–1314.
37. For Sonogashira-like cross-coupling employing palladium-gold instead of palladium-copper systems see: (a) Lauterbach, T.; Livendahl, M.; Rosellón, A.; Espinet, P.; Echavarren, A. M. *Org. Lett.* **2010**, *12*, 3006–3009. (b) Jones, L. A.; Sanz, S.; Laguna, M.; *Catal. Today*, **2007**, *122*, 403–406. (c) Panda, B.; Sarkar, T. K.; *Tetrahedron Lett.* **2010**, *51*, 301–305.
38. a) Shi, Y.; Peterson, S. M.; Haberaecker III, W. W.; Blum, S. A.; *J. Am. Chem. Soc.* **2008**, *130*, 2168–2169; b) Shi, Y.; Ramgren, S. D.; Blum, S. A.; *Organometallics*, **2009**, *28*, 5, 1275–1277.

39. a) Shi, Y. Roth, K. E.; Ramgren, S.D.; Blum, S.A.; *J. Am. Chem. Soc.* **2009**, *131*, 18022–18023; b) Shi, Y.; Ramgren, S. D.; Blum, S. A., *Organometallics*, **2011**, *30*, 4811–4813.
40. Hashmi, A. S. K.; Lothschütz, C.; Döpp, R.; Ackermann, M.; Becker, J. D. B.; Rudolph, M.; Scholz, C.; Rominger, F.; *Adv. Synth. Catal.* **2012**, *354*, 133–147.
41. Meyer, N.; Sivanathan, S.; Mohr, F.; *J. Organomet. Chem.* **2011**, *696*, 1244–1247.
42. Bojan, R. V.; López-de-Luzuriaga, J. M.; Monge, M.; Olmos, M. E.; *J. Organomet. Chem.* **2010**, *695*, 2385–2393.
43. Doctoral thesis of Desirée María Carrasco Fernández. Manuscript in preparation.
44. The results of this section have been published herein: delPozo, J.; Carrasco, D.; Pérez-Temprano, M. H.; García-Melchor, M.; Álvarez, R.; Casares, J. A.; Espinet, P. *Angew. Chem. Int. Ed.* **2013**, *52*, 2189–2193.
45. The Au-Cl bond was extracted from: Lide, David R.; ed., *CRC Handbook of Chemistry and Physics, Internet Version 2005*, CRC Press, Boca Raton, FL, **2005**.
46. Álvarez, R.; Pérez, M.; Nieto-Faza, O.; de Lera, A. R.; *Organometallics*, **2008**, *27*, 3378–3389.
47. Ariafard, A.; Lin, Z.; Fairlamb, I. J. S.; *Organometallics*, **2006**, *25*, 5788–5794.
48. (a) Fu, G.C.; *Acc. Chem. Res.*, **2008**, *41*, 1555–1564; (b) Martin, R.; Buchwald, S. L. *Acc. Chem. Res.* **2008**, *41*, 1461–1473.
49. Bondi, A. J. *Phys. Chem.* **1964**, *68*, 441–451.
50. Weber, D.; Gagné, M. R.; *Chem. Commun.* **2011**, *47*, 5172–5174-
51. Dröge, T.; Glorius, F. *Angew. Chem. Int. Ed.* **2010**, *49*, 6940–6952.
52. (a) Casares, J. A.; Espinet, P.; Fuentes, B.; Salas, G.; *J. Am. Chem. Soc.* **2007**, *129*, 3508–3509. (b) Fuentes, B.; García-Melchor, M.; Lledós, A.; Maseras, F.; Casares, J. A.; Ujaque, G.; Espinet, P.; *Chem. Eur. J.* **2010**, *16*, 8596–8599.
53. Usón, R.; Laguna, M.; *Inorg. Synth.* **1989**, *26*, 85.
54. Sinha, P.; Wilson, A. K.; Omary, M. A.; *J. Am. Chem. Soc.* **2005**, *127*, 12488–12489.
55. Nieto-Oberhuber, C.; López, S.; Echavarren, A. M.; *J. Am. Chem. Soc.* **2005**, *127*, 6178–6179.

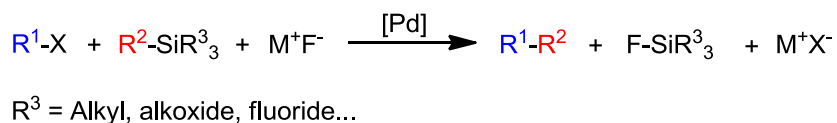
56. Wang, H. M. J.; Sekhar Vasam, C.; Tsai, T. Y. R.; Chen, S.; Chang, A. H. H.; Lin, I. J. B.; *Organometallics*, **2005**, *24*, 486-493.
57. Norbury, A. H.; Sinha, A. L. P.; *J. Inorg. Nucl. Chem.* **1973**, *35*, 1211-1218.
58. Miyaura, N.; Suzuki, A.; *Org. Synth. Coll.* **1993**, *Vol. 8*, 532, (note 8).
59. Lee, E.; Yandulov, D. V.; *J. Organometallic Chem.* **2011**, 696, 4095-4103.
60. Gligorich, K. M.; Cummings, S. A.; Sigman, M. S. *J. Am. Chem. Soc.* **2007**, *129*, 14193-14195.
61. Littke, A. F.; Schwarz, L.; Fu, G. C.; *J. Am. Chem. Soc.* **2002**, *124*, 6343-6348.
62. Weisemann, C.; Schmidtberg, G.; Brune, H.; *J. Organomet. Chem.* **1988**, *361*, 3, 299-307.
63. Vij, A.; Kirchmeier, R. L.; Willett, R. D.; Shreeve, J. M. *Inorg. Chem.* **1994**, *33*, 5456-5462.
64. Casares, J. A.; Espinet, P.; Salas, G.; *Chem. Eur. J.*, **2002**, *8*, 4843-4853.
65. Gaussian 09, Revision C.01, Frisch, M. J.; Trucks, G. W.; Schlegel, H. B.; Scuseria, G. E.; Robb, M. A.; Cheeseman, J. R.; Scalmani, G.; Barone, V.; Mennucci, B.; Petersson, G. A.; Nakatsuji, H.; Caricato, M.; Li, X.; Hratchian, H. P.; Izmaylov, A. F.; Bloino, J.; Zheng, G.; Sonnenberg, J. L.; Hada, M.; Ehara, M.; Toyota, K.; Fukuda, R.; Hasegawa, J.; Ishida, M.; Nakajima, T.; Honda, Y.; Kitao, O.; Nakai, H.; Vreven, T.; Montgomery, Jr., J. A.; Peralta, J. E.; Ogliaro, F.; Bearpark, M.; Heyd, J. J.; Brothers, E.; Kudin, K. N.; Staroverov, V. N.; Kobayashi, R.; Normand, J.; Raghavachari, K.; Rendell, A.; Burant, J. C.; Iyengar, S. S.; Tomasi, J.; Cossi, M.; Rega, N.; Millam, J. M.; Klene, M.; Knox, J. E.; Cross, J. B.; Bakken, V.; Adamo, C.; Jaramillo, J.; Gomperts, R.; Stratmann, R. E.; Yazyev, O.; Austin, A. J.; Cammi, R.; Pomelli, C.; Ochterski, J. W.; Martin, R. L.; Morokuma, K.; Zakrzewski, V. G.; Voth, G. A.; Salvador, P.; Dannenberg, J. J.; Dapprich, S.; Daniels, A. D.; Farkas, Ö.; Foresman, J. B.; Ortiz, J. V.; Cioslowski, J.; Fox, D. J. Gaussian, Inc., Wallingford CT, 2009.
66. Chai, J.-D.; Head-Gordon, M. *Phys. Chem. Chem. Phys.* **2008**, *10*, 6615-20.
67. (a) Hay, P. J.; Wadt, W. R.; *J. Chem. Phys.*, **1985**, *82*, 270-283; (b) Hay, P. J.; Wadt, W. R.; *J. Chem. Phys.*, **1985**, *82*, 299-310.
68. Marenich, A. V.; Cramer, C. J.; Truhlar, D. G. *J. Phys. Chem. B*, **2009**, *113*, 6378-6396.

Chapter II

Bimetallic Hiyama cross-coupling of bulky groups promoted by CuF_2

1. Introduction

The palladium-catalyzed cross-coupling of organosilicon compounds with organic electrophiles is also known as the Hiyama reaction. Unlike the Stille and Negishi reactions, which require no activation, or the Suzuki reaction, which requires only heating with mild bases, silicon-based cross-coupling reactions often require the presence a nucleophilic activator due to the low polarizability of the C–Si bond.¹ This activator is a fluoride source in most cases, but in certain examples bases have been used efficiently.²



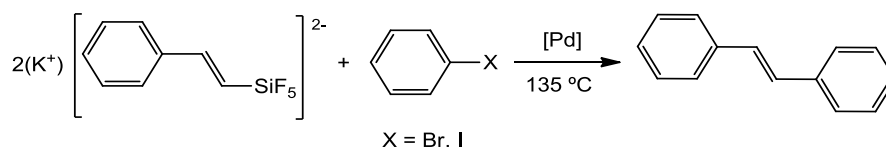
Scheme II-1. General scheme of the Hiyama reaction.

For cross-coupling, the Hiyama reaction is particularly attractive due to the low cost, ease of synthesis, low toxicity, and high chemical stability of the silicon compounds used as cross-coupling partners. All this great advantages of silicon nucleophiles usually come with a negative feature: The need of fluoride activators (or strong bases) presents many drawbacks, such as the high cost of organic soluble fluoride sources, the corrosive nature of fluoride the evident incompatibility with certain groups. In this regard, great achievements have been reported since the initial works, such as the incorporation of the more reactive alkoxy silanes,³ to the latest silanolates developed by Denmark and coworkers, which allow for mild Hiyama coupling under fluoride free and base free conditions.²

1.1. Background

The first example of a coupling reaction involving a silicon transmetalating agent was reported by Kumada's group in 1982. In that work, a hexavalent siliconate was able to transmetalate to Pd in the absence of any fluoride promoter,

demonstrating the feasibility of hypervalent silanes as transmetalating counterparts, whereas neutral tetravalent silanes were inefficient.^{*,4,5}



Scheme II-2. Early reports of cross-coupling with hypervalent siliconates.

A decisive push for the development of this reaction was the introduction of external fluoride sources that could generate the siliconate species *in situ*.⁶ By employing stable and easy-to-synthesize tetracoordinate silanes, the substrate scope could be significantly expanded. These findings were developed by Hiyama and collaborators and they constituted the origin of the silicon cross-coupling chemistry the way it is used today in most examples. These breakthroughs triggered the study of the fundamentals of the silicon based cross-coupling, which have stimulated the development of milder and more diverse conditions for organosilicon cross-coupling reactions. In these regard, seminal work has been carried out by the group of Denmark. In recognition to their brilliant contribution to the field, this reaction is often identified as Hiyama-Denmark coupling.

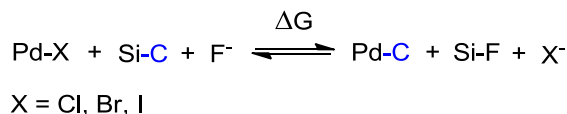
1.2. Nature of the Si/Pd transmetalation

All the efforts concerning the mechanisms of the Hiyama reaction have been focused on the Si/Pd transmetalation step. They have been studied by means of experimental techniques and DFT calculations and they will be discussed in detail.

* However, it cannot be discarded that in this example, the siliconate reacts with the palladium catalyst, forming a palladium fluoride complex. Hypervalent silicon-fluoride sources are good fluorinating agents. A good example of this is tetrabutylammonium difluorotriphenylsilicate (TBAT) (ref 5). The implication of palladium fluorides in the mechanism of the Hiyama reaction will be discussed later.

a) *Thermodynamics of the Si/Pd transmetalation*

The thermodynamic balance of a Si/Pd transmetalation can be interpreted according to the following Scheme II-3:



Scheme II-3. Thermodynamic balance of the Si/Pd transmetalation.

In a simplistic manner, Si–C and Pd–X bonds are broken and Pd–C and Si–F bond are formed. Concerning the silicon species, experimental data of various Si–X bond dissociation energies (BDE) are available.⁷ Considering X–Si dissociation energies in the X–SiMe₃ series, the Si–C bond dissociation energy (BDE) is 85 kcal·mol⁻¹, whereas the formed Si–F energy is 158 kcal·mol⁻¹. The affinity of F⁻ for silicon centers is indeed well known, and it acts as the thermodynamic driving force of the transmetalation. In fact the Si–F bond in SiF₄ is probably the strongest formally single bond known (160 kcal·mol⁻¹, much stronger than the F–C BDE in the analogous CF₄). It is also worth commenting that oxygen promoters are also good driving forces (Si–O BDE, 128 kcal·mol⁻¹).

In the case of Pd–halogen bonds of actual complexes, only calculated energies are available.⁸ The energy balance between the Pd–X and the Pd–C bonds is slightly endergonic, (from about 14 kcal·mol⁻¹ for Pd–I, up to 30 kcal·mol⁻¹ if a Pd–Cl bond is broken, see Table II-2). Nevertheless, much smaller differences are handled if compared with the silicon ones, which would have a greater contribution to the overall ΔG . Under a thermodynamic point of view, the role of the promoters and specially fluoride promoters is a push in free energy towards the breaking of the considerable inert Si–C bond⁷.

Table II-1. Experimental bond dissociation energies ($\text{kcal}\cdot\text{mol}^{-1}$) of selected silicon compounds.⁷

Bond	BDE
F ₃ Si-F	160
F ₃ C-F	130
Me ₃ Si-F	158
Me ₃ Si-Cl	109
Me ₃ Si-OH	133
Me ₃ Si-Me	94.2

Table II-2. Calculated bond dissociation energies ($\text{kcal}\cdot\text{mol}^{-1}$) of selected Pd compounds.⁸

Bond	BDE
Pd-C	59.0
Pd-Cl	91.9
Pd-Br	81.1
Pd-I	72.8

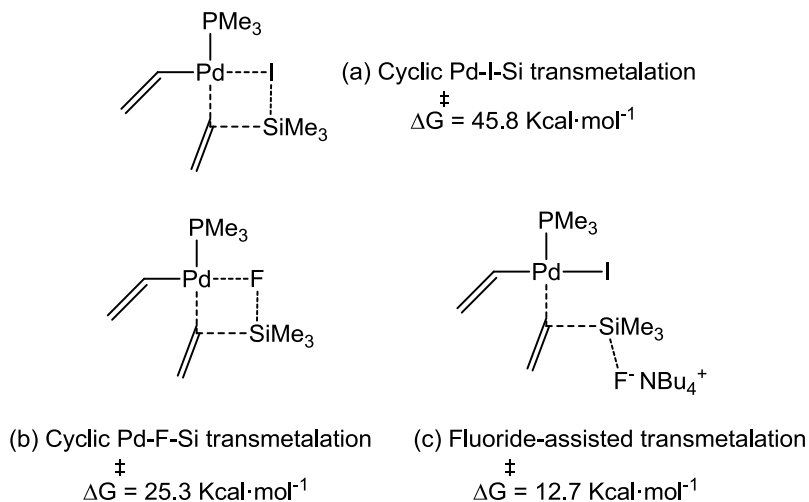
However, in a multistep reaction the whole balance of ΔG does not depend only on the transmetalation step, but also on the other steps. A cross-coupling reaction involves the formation of a C-C bond, which is enough driving force for the overall balance in most cases. As a matter of fact, usually the transmetalation is reversible,⁹ but the coupling proceeds as the irreversible reductive elimination pulls forward the catalytic cycle. As a consequence, kinetic factors are usually more relevant than thermodynamic ones, if the transmetalation itself is not too much disfavored.

b) Kinetics and nature of the Transition State

The intrinsic nature of the Si-C bond makes relatively challenging the use of organosilicon compounds for the transmetalation of carbon groups in palladium-catalyzed cross-coupling reactions. They are rather kinetically inert due to the low polarity of the Si-C bond (the difference in electronegativity of silicon and carbon is only 0.65 in the Pauling scale).¹⁰

Formation of hypervalent silicon species via fluoride coordination was thought to be a key requirement in the activation of the poorly polarized Si-C bond prior to the transmetalation step.¹¹ However, when fluoride is added as an external source, this initial view of transmetalation via prior formation of pentacoordinate siliconates was questioned for certain silanes, supported by experimental measurements and DFT calculations.¹² Theoretical and experimental work by the group of Sakaki

beautifully illustrates the nature of the possible TSs of a Si/Pd transmetalation, which is worth commenting in detail. It was found that vinyl-SiMe₃ does not take hypervalency prior to transmetalation, but the promoter plays a crucial role in the transition state when the carbon group is being transferred.



Scheme II-4. Nature of the TS of the fluoride promoted Si/Pd transmetalation.

It was concluded that activator-free transmetalation is not feasible (pathway a), since all the explored transition states showed activation barriers prohibitory large.¹² In addition, the thermodynamic ΔG of the whole process is very endergonic (25.6 kcal·mol⁻¹). By contrast, two other mechanisms are proposed as feasible when fluoride is involved: (b) cyclic transition state with a palladium fluoride intermediate, (c) external fluoride attack to the silane coordinated to the palladium complex. Both transition states are possible and which one is preferred depends on the nature of the silane reagent in use, and they have both been confirmed by experimental studies. No substantial interaction is detected in any TS between the Si and Pd centers, getting placed far away from one another (3.16 Å in pathway b, and 3.74 Å in pathway c).

On one hand, vinylic silanes have shown faster transmetalation kinetics than the homologous aryl counterparts.¹³ This is reasonable because the π electron density of an olefin is greater than that of an aryl (which is delocalized due to aromatization

throughout the whole aromatic ring), and facilitates the interaction with the metal center. As it was found in the DFT study,¹² the silane first coordinates to the Pd center via the olefinic moiety. From this Pd–Si complex, the calculated transmetalation is faster via nucleophilic activation of the silicon nucleophile. When there is no group that can act as linkage between the Pd and the silicon centers, the transmetalation would take place from a Pd–F intermediate, which would create a Pd–F–Si bridge in the transition state, eventually triggering the transmetalation. This is the case of aryl–Si nucleophiles, and that is the reason why they usually show slower kinetics of transmetalation of the aryl group than alkenyl counterparts, as they interact less efficiently with the palladium center.

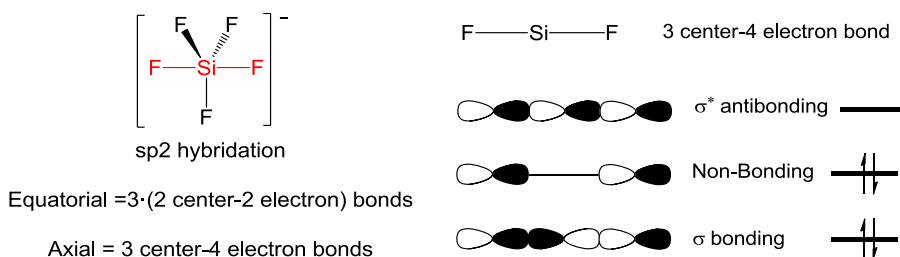
Both possible situations have a common feature: *the silane becomes pentavalent in the transition state*.¹⁴ This is the key reason why fluoride makes the transmetalation kinetically feasible. The formation of a very strong Si–F bond stabilizes the hypervalent Si center of the TS. The expansion of the coordination of the Si is only possible when stabilized by highly electronegative groups. Consistently, OH[−] or other oxygen anions (alkoxides or KOSiMe₃) are able to promote Si–Pd transmetalation in a similar manner, but they are less efficient promoters as they are less electronegative than fluoride.^{11b,15}

c) *Molecular Orbital description of hypervalent silanolates*

But what is the reason for the stabilization of higher coordination numbers of Si by the fluoride anion? Very relevant information can be withdrawn from the molecular orbitals and the Lewis structure of these species. The structure of pentacoordinate or hexacoordinate silicon that takes place in these transition states implies formation of 3-center 4-electron bonds.^{*,11,16}

* Early considerations of hypervalent molecules of the second-row elements usually referred to the "important contributions to the bonding" made by the d orbitals, an idea that was useful to explain the unknown nature of hypervalency. However, theoretical calculations have shown no support for the view that diffuse d orbitals on the central atom take part in bonding. The inclusion of d functions is important to describe the p orbitals better, as polarization functions, but not to describe the bonding. See ref 16.

$[\text{SiF}_5]^-$ can be used as a model to construct a qualitative image of the molecular orbitals involved. A simplified way to describe the structure is to consider a sp^2 hybridization for the silicon atom.^{*,17} Three simple σ bonds are formed in the equatorial plane between three sp^2 hybrids and the p HOMO of the three F, with participation of 6 electrons. The bonds of the axial plane are formulated in terms of the valence p_z atomic orbital of the silicon atom (not considered for the hybridization), and 2 p HOMO orbitals of the two F, involving 4 electrons.[†] They form a linear arrangement of three atoms that yields three MOs: a σ bonding orbital, a Non-Bonding orbital and an antibonding σ^* (Scheme II-5).



Scheme II-5. Molecular orbital diagram of a 3-center 4-electron bond of a F–Si–F fragment.

The consequence is that a nonbonding orbital centered on the ligands needs to be filled.[‡] That is the reason why hypervalent silicon species are only found with highly electronegative ligands (such as fluoride or alkoxides), which are able to stabilize this non bonding orbital, which normally would be high in energy.[§] As a

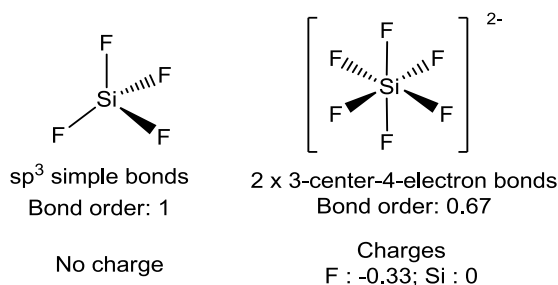
* A more accurate description of the MO of $[\text{SiF}_5]^-$ can be extrapolated from the analogous PH_5 , whose Molecular Orbital diagram was described by Hoffman et al. with extended Hückel calculations. The MO diagram describes the 3-center 4-electron bond, delocalized among all the H ligands, and not only between the axial ones. Full description of the molecule is beyond the interest of this test. See ref 17.

† There are two possible considerations of the Lewis structure of the 3-center 4-electron bond of $[\text{SiF}_5]^-$: 2 electrons come from the Si^- and one from each F atom. An alternative view is that 1 electron comes from Si, another one from a neutral F (constituting a neutral SiF_4 molecule), and 2 electrons come from F^- acting as a Lewis base towards the acidic SiF_4 .

‡ Extended Hückel calculations have shown slight antibonding character of this NB orbital in PH_5 , because it has two nodal surfaces. See ref 17.

§ The molecular orbitals of the hypervalent PH_5 have been studied and the instability of the molecule was attributed to the inability of the donor H ligands to stabilize the high-lying

result, significant weakening of Si–F bond is produced in these 3-center 4 electron linkages. The bond order is decreased below the unity as only 2 electrons of the four are hosted in a bonding orbital.*



Scheme II-6. Lewis structure of a tetrahedral silane, compared to a hypervalent silicate.[†]

We can extend these concepts to a silicate $[\text{Si}(\text{vinyl})(\text{Me})_3\text{F}]^-$ analogous to that of the TS in Scheme II-4. Hypervalency in the TS results in enhanced nucleophilic character of the carbon atom, whereas the charge at the silicon atom remains unaffected, or even increased (due to the inductive effects of the highly electronegative substituents).^{‡,18} This results in effective polarization of the Si–C bond. All these changes in the orbital structure of the silane facilitate the cleavage

nonbonding orbital derived from a three-center-4 electron bond. Analogous interpretation is valid for $[\text{SiF}_5]^-$. See ref 17.

* For calculation of the bond order, only the electrons in bonding orbitals are considered, whereas those in antibonding orbitals contribute negatively. An alternative and more realistic view can be obtained considering that this NB orbital is indeed slightly antibonding, as commented above. The fact that this orbital is occupied significantly weakens the Si–F bond.

† Calculating the Bond Order of SiF_4 is straightforward, 4 pairs of electrons are located in 4 bonding orbitals. Although the full MO description is complicated for $[\text{SiF}_6]^{2-}$, the bond order can be calculated considering that 4 electron pairs are hosted by 4 bonding orbitals, whereas 2 pairs go to NB orbitals (two 3-center 4-electron bonds are needed to expand the Si valency). That provides an average BO of 0.67 in the six bonds equivalents by symmetry.

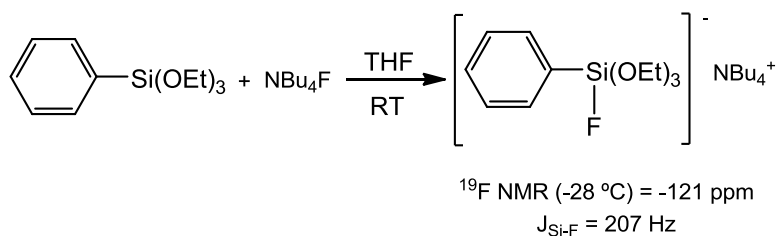
‡ This situation seems to contradict chemical intuition. One might anticipate the silicon center to be more negatively polarized upon expansion of the coordination shell, since more ligands are donating electron density. However, ab initio calculations on SiF_5^- and related molecules suggest that silicon atoms are more positively charged (Mulliken) in pentacoordinate structures than in the neutral tetracoordinate analogues. However, this tendency is not reproduced in all examples found in the literature, and others found that little change occurs upon expansion of the coordination. See ref 18.

of the Si–C linkage, thus enabling transmetalation to a transition metal, or any other reaction where silicon derivatives are used as nucleophiles.

1.3. Mechanisms of the Si/Pd transmetalation: evidences for different Si/Pd transmetalation scenarios

a) Fluoride-promoted Si/Pd transmetalation

As commented before, both mechanistic pathways (b and c, section 1.2.b) have been experimentally confirmed depending on the nature of the silicon nucleophile. Great difference in the properties of the silicon center is made by the spectator substituents that come with the transferring group. The reactivity of Si towards F^- can change importantly if more electronegative groups contribute to stabilize the hypervalent species. For instance, as commented above, vinyl–SiMe₃ does not form pentacoordinate species in the presence of F^- prior to transmetalation.¹² Rather on the contrary, the presence of alkoxy ligands contribute to the stabilization of the pentacoordinate $[F-SiPh(OEt)_3]^-$, as it takes place upon mixing of Ph–Si(OEt)₃ with NBu₄F in THF (Scheme II-7).¹⁹ Alkoxysilanes are now one of the most common sources since they were introduced by the group of Tamao, due to the ease of synthesis from the inexpensive Si(OEt)₄ and their high efficiency on the coupling.³



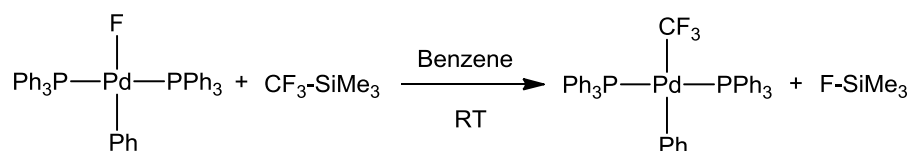
Scheme II-7. Formation of pentacoordinate arylalkoxysilanes with NBu₄F.

Contrary to what was previously thought, recent studies by Amatore and Jutand have demonstrated that the preformed $[F-SiPh(OEt)_3]^-$ is inefficient at transmetalating to $[Pd(Br)(PhCN)(PPh_3)_2]$.²⁰ This remarkable finding fights the

established idea that hypervalent siliconates were in all cases the actual transferring agents in cross-coupling with silicon derivatives.¹¹

It was found that the fastest Si/Pd transmetalation takes place between $[\text{Pd}(\text{F})(\text{PhCN})(\text{PPh}_3)_2]$ and the neutral $\text{PhSi}(\text{OEt})_3$, detecting the palladium fluoride in catalytic coupling conditions with voltamperometric techniques. The inefficiency of $[\text{F}-\text{SiPh}(\text{OEt})_3]^-$ to transmetalate to Pd explains the bell-type curves of the reaction rate dependence on the concentration of NBu_4F , obtained in their kinetic data. F^- is able to sequester the active $\text{PhSi}(\text{OEt})_3$ in the form of $[\text{F}-\text{SiPh}(\text{OEt})_3]^-$, thus decreasing the reaction rate when $(\text{F}^-/\text{PhSi}(\text{OEt})_3)$ ratios are too high.

Great support to this proposal can be found as well in the synthesis of the complex $[\text{Pd}(\text{Ph})(\text{CF}_3)(\text{PPh}_3)_2]$ developed by Grushin, via clean and fast Si/Pd transmetalation involving $[\text{Pd}(\text{Ph})(\text{F})(\text{PPh}_3)_2]$ and the Ruppert silane.²¹

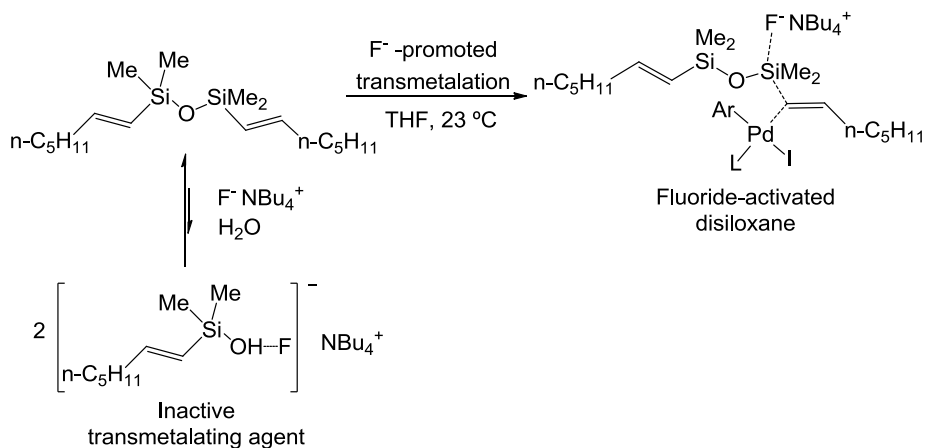


Scheme II-8. Transmetalation of the CF_3 group from Ruppert silane to a palladium fluoride complex.

Hammett analysis of the Si/Pd transmetalation with substituted aryl(triethoxy)silanes have shown a positive slope ($\rho = 1.4$) in competition experiments, providing faster coupling of electron-withdrawing substituents in the alkoxy silane.²² This can be interpreted in terms of the greater stabilization of the hypervalent silicon center of the key Pd–F–Si intermediate, due to the greater electrophilicity of the silicon atom when carrying more electron-withdrawing groups (see Scheme II-6).

Seminal mechanistic investigations concerning Si/Pd transmetalation have been carried out by Denmark's group, using silanols or silanolates as nucleophiles in both TBAF-promoted and fluoride-free cross-coupling reactions.²³ As the authors stated, different mechanisms seem to be operating in each process.

If the fluoride-promoted cross-coupling is examined, the rate-limiting transmetalation is achieved through a fluoride-activated disiloxane (Scheme II-9).^{23b} Formation of this key intermediate is dependent on the structure and steric features of the silanol precursor and the amount of TBAF employed. The negative dependence on [TBAF] at high concentration is consistent with a hydrogen-bonded complex between the silanol and the fluoride anion, which sequesters the silanol and precludes formation of the active transmetalating disiloxane. No pentacoordinate silicon species were detected by ¹⁹F NMR and ²⁹Si NMR when different silanols were reacted with TBAF, suggesting that the role of the fluoride anion is to stabilize the transmetalation TS via nucleophilic-assistance (Scheme II-4, pathway c).



Scheme II-9. Mechanisms of the fluoride-promoted transmetalation with silanols to Pd.

b) Fluoride free transmetalation

Denmark's group mechanistic studies concerning the fluoride free cross-coupling of silanols and silanolate have been very meaningful to the field. When silanols and silanolate are involved, the presence of the Si-O⁻ functional group plays a pivotal role as demonstrated by careful insight into the kinetic data. Initial studies suggested that the Si/Pd transmetalation was assisted by the formation of a complex bearing a Si-O-Pd linkage.^{23c} Decisive evidence of this pathway was

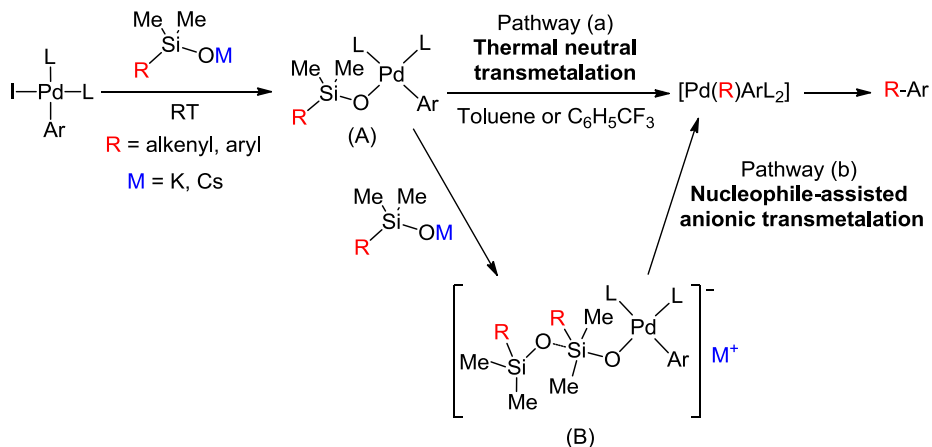
obtained when they succeeded in the isolation and X-Ray characterization of adducts $[\text{Pd}(\text{Ph}-\text{F})(\text{O}-\text{SiMe}_2\text{Ar})(\text{P}^t\text{Bu}_3)]$ (A, Scheme II-10)d.^{23d}

Thermal decomposition at 50 °C of the aryl–palladium silanolate resulted in the formation of the biaryl product in quantitative yields and Pd^0 , proving the mechanistic relevance of this intermediate. The silicon center in these transmetalation precursors is tetrahedral, once again contrary to the accepted idea that transmetalation from silicon to palladium only could take place through anionic and hypervalent silicate species, as stated in the early works.¹¹

More recently, they succeeded in the isolation of a family of complexes aryl–Pd–O–Si, with both alkenyl and aryl silanolates, bearing monodentate and chelate phosphine ligands.²⁴ They carried out a very deep mechanistic study through the combination of reaction kinetics and computational analysis to demonstrate the existence of two different mechanistic pathways:

(a) Direct Si/Pd transmetalation via neutral aryl–Pd^{II}–silanolate complexes.

(b) Transmetalation via anionic species or transition states, with nucleophile-activated silanolates. Both of them are possible and which one is preferred depends on the nature of the silanolate (alkenyl or aryl) and the counteranion (cesium or potassium were examined).



Scheme II-10. Mechanisms of the fluoride-free transmetalation from silanolates to Pd.

The isolation of intermediate (A) permitted the study of the effect of the ancillary ligands on the thermal transmetalation (pathway a). When these complexes bearing monodentate ligands such as PPh₃ are heated, much higher reaction rates of transmetalation are obtained than those bearing chelate ligands. Moreover, the reaction was inhibited or even suppressed in the presence of substoichiometric amounts of added ligand and greatly accelerated in the presence of ligand scavengers such as Cu(thiophene-2-carboxylate). These data suggest that reversible ligand displacement by the α carbon involved in the transmetalation does occur prior to transmetalation. (see mechanisms of the Stille reaction in Chapter I)

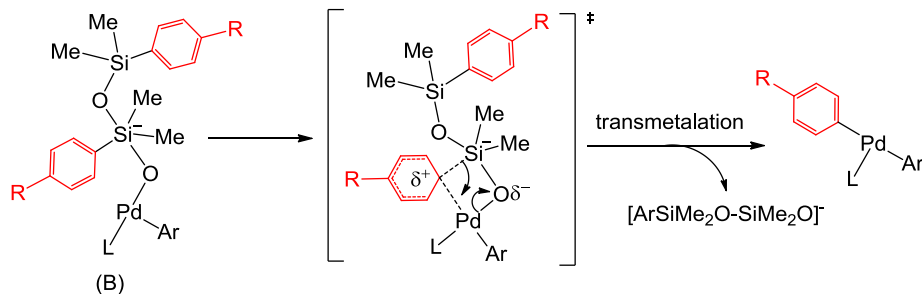
As commented above, transmetalation of alkenyl groups is usually faster than transmetalation of aryl groups. Denmark's group findings unveiled that potassium salts of alkenyl silanolates react via neutral intermediates (pathway a), as this pathway is faster with these nucleophiles. Interestingly, the more nucleophilic cesium alkenylsilanolates transmetalate via the anionically activated route (pathway b, Scheme II-10). The presence of the less coordinating counterion enhances the nucleophilicity of the silanolate, and facilitates the formation of the anionically activated intermediate (B).

In the case of arylsilanolates, both mechanisms were equally demonstrated depending on the [Si]/[Pd] ratio. The neutral pathway is favored at [Si]/[Pd] ratio \leq

1, but at higher ratios, transmetalation takes place via anionic pathway b. Under conditions usually employed in catalysis ([Si]/[Pd] ratio > 5), the transmetalation showed saturation kinetics of added silanolate, suggesting that the catalyst is saturated as intermediate (B). Additional support for the anionic mechanism is that greater reaction rates are obtained when the more nucleophilic activator CsO–SiMe₂Ar is used.

Furthermore, theoretical calculations of both possible reaction pathways confirmed the greater stability of the TS of the anionic transmetalation for the transfer of aryl groups (pathway b) than the neutral transmetalation (pathway a). DFT calculations provided a difference in activation energies between these two pathways of 1.8 kcal·mol⁻¹. This result is in good agreement with the experimental difference obtained by kinetic measurements of 1.6 kcal·mol⁻¹. Although these computational results only permit qualitative comparison with the experimental ones, they provide compelling support for the experimentally documented observations.

Hammett analysis of the transmetalation of substituted aryl-silanolates revealed a negative slope ($\rho = -0.8$), obtaining faster transmetalations when electron-donating groups were present.²⁵ These studies were carried out in high concentrations of silanolate, mimicking catalytic conditions and forcing the group transfer to take place via nucleophilic assistance (pathway b). In these conditions, the greater electron density on the hypervalent siliconate moiety, the more facile the transmetalation as the activated silanolate is more nucleophilic. This phenomenon can be rationalized as an electrophilic aromatic substitution at the carbon bearing the silicon fragment. Electron donating groups would contribute to stabilize the partial positive charge generated in the aryl ring throughout the group transfer (Scheme II-11).



Scheme II-11. Nature of the TS of the transmetalation, depicted as an electrophilic substitution at the α -carbon.

1.4. Extending the scope of the silicon-based cross-coupling reactions

Although this silicon based cross-coupling is now broadly used in synthesis of complicated molecules,²⁶ much fewer examples of its use for these purposes can be found in the literature than that of the homologous Suzuki or Stille reactions.²⁷ The reason for this is the lack of robust procedures when the coupling gets challenging. As far as we know, there is no precedent in the literature of the use of diorthosubstituted-aryl silanes or alkoxy silanes in the Hiyama coupling, and very few examples concerning the use of any hindered silane.^{*,28} This reactivity is not surprising if the mechanism of the Si/Pd transmetalation is considered. As it was discussed above, the silicon center has to increase its coordination number at the transition state, and this is very disfavored if there is too much steric constriction around the relatively small silicon center. Consistently, all the processes involving transient hypervalent silanes or TS are extremely disfavored when bulky groups are present, such as nucleophilic substitution of Si-Cl bonds by organolithium or organomagnesium reagents or oxidation with peroxides to form alcohols.²⁹

Compounds containing bulky aryls are interesting targets because they are found as components of many natural products.³⁰ They find use in medicinal

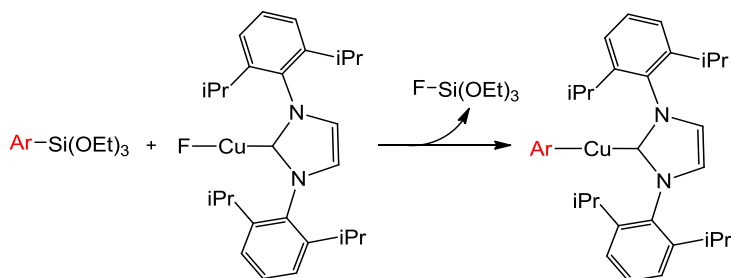
* The use of hindered ally-vinyl silanols has been reported, see ref 28. However, vinyl silanols undergo transmetalation to Pd much faster than the corresponding aryl congeners (see reference 13 and 24a), so the use of the latter is more challenging.

chemistry since they improve the lipophilicity and metabolic stability of drugs.³¹ Additionally, they play a pivotal role in ligand design, as they are ubiquitously present in NHC carbenes or phosphines that have shown to be very effective at promoting special reactivity or stabilizing rare compounds.³² However, when bulky groups are involved, cross-coupling reactions become highly challenging.³³ Heterocoupling of hindered aryls can be achieved using lithium,³⁴ magnesium,³⁵ or zinc derivatives,³⁶ but these strongly basic reagents severely narrow the scope of application, as they are less compatible with many functional groups. Suzuki reactions have been occasionally used,³⁷ but voluminous boronic acids are very prone to protodeboronation and are difficult to synthesize and purify.³⁸ Indeed, Suzuki reactions involving transmetalation of bulky groups are extremely challenging: fine tuning of the reaction and optimization for every substrate is usually needed. As a matter of fact, all the reported examples rely on the use of bulky and electron-rich ligands, which can be expensive or not readily available. Simpler robust methodologies are still lacking.³⁹

In the previous chapter, we have reported the use of gold as a transmetalation cocatalyst for the Stille reaction with bulky groups. It enabled a less energetic pathway for the transmetalation of bulky groups to Pd, via smaller linear gold aryls that were able to carry the bulky group to the palladium cocatalyst through a less encumbered transition state than the classical Pd/Sn one (via tetravalent organotin).^{40,41} Unfortunately our attempts, at the beginning of this work, at extending this Au^I co-catalysis to the Hiyama reaction have been unsuccessful. Copper is a very tempting alternative to gold, as it is inexpensive. Yet there is no direct parallelism of gold and copper, due to the richer variety of accessible oxidation states and coordination geometries for the latter.

The first step that one has to consider to set up this chemistry is the feasibility of Si/Cu transmetalation.⁴² In this regard, much attention should be paid to the seminal work carried out by Ball's group.⁴³ Therein, a number of stable Cu^I aryls are obtained when the NHC-stabilized Cu^I-F is treated with arylalkoxysilanes in excellent yields (Scheme II-12). They could develop a copper-catalyzed procedure for the arylation of aldehydes and vinyl epoxides, applying the Si/Cu transmetalation

idea.⁴⁴ Although there are some rare examples of fluoride free Si/Cu transmetalation,⁴⁵ they take place slowly and it seemed to us that the chances of developing a fluoride-free system were scarce.



Scheme II-12. Si/Cu transmetalation of aryl groups.

The second step of the catalytic cycle would involve Cu/Pd transmetalation. The number of precedents concerning this step is large, as it can be found in the Sonogashira coupling,⁴⁶ or in carboborations.⁴⁷ If the particular case of aryl-Cu^I/Pd transmetalations is considered, the number of examples is more limited but still well preceded in decarboxylative coupling⁴⁸ and others.⁴⁹

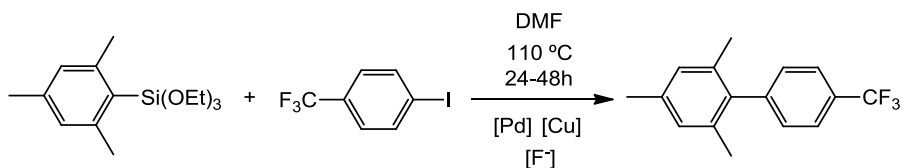
Cu/Pd is probably one of the most frequently applied combinations in bimetallic catalysis.⁵⁰ However, the precise effects of Cu salts in these transformations are not fully understood. The use of copper⁵¹ or silver⁵² salts to enhance the performance in the particular case of the Hiyama coupling has been reported, but there is no study of the actual role of these metals in the catalytic cycle. In these examples, the Cu additive only improved moderately the yield of the cross-coupling product and there is no proof of the actual function of these salts beyond the increase in selectivity of the catalytic reaction.

Herein, we report a copper promoted Hiyama coupling that makes feasible for the first time the use of diortosubstituted arylalkoxysilanes. The coupling is highly versatile, accepting both electron withdrawing and electron donating substituents, and also sensitive moieties. Moreover, a detailed experimental mechanistic study is presented, which allows not only to shed some light to the actual role of copper

salts in the Hiyama coupling, but also to the chemical features of organocopper reagents in cross-coupling.

2. Results and discussion

In a methodical testing of Pd/Cu systems with different copper additives and fluoride sources for the mesityl-aryl cross-coupling (Scheme II-13 and Table II-3), we found some interesting results. Several Cu sources in stoichiometric and sub-stoichiometric conditions relative to the mesityltris(ethoxy)silane were tested, combined or not with different external fluoride sources.⁴² As well, the palladium-free Hiyama reaction catalysed by CuI, CsF, and P,N ligands has been reported.⁵³ However, chemical systems analogous to all those mentioned above were in our hands inefficient for the cross-coupling of ortho-disubstituted arylsilanes (see experimental).



Scheme II-13. Model reaction between a bulky aryl alkoxy silane and an aryl iodide for reaction optimization.

Table II-3. Experiments with different Cu sources, using [PdCl₂(AsPh₃)₂] as catalyst.

Entry	Cu source	Cu % ^[a]	F ⁻	Yield %
1	None	0	CsF or NBu ₄ F	<5
2	CuI	50	CsF	4
3	Cu(^t OBu)	100	None	0
4	CuF ₂	100	None	88
5	CuF ₂ ·3H ₂ O ^[b]	100	None	81
6	Cu(OH) ₂	100	None	0
7	Cu(OAc) ₂ ·H ₂ O	25	CsF	27
8	Cu(OTf) ₂	25	CsF	25
9	CuF ₂	25	CsF	17

[a] Reaction conditions: 1 mol *p*-I-Ph-CF₃, 2 mol MesSi(OEt)₃ in DMF at 110 °C for 24-48 h; 2 mol% [Pd] = [PdCl₂(AsPh₃)₂]; the specified amount of Cu promoter (mol% relative to *p*-I-Ph-CF₃); 2 mol of CsF when specified. Termination of the reaction and yields were determined by ¹⁹F NMR integration. [b] The reaction proceeds at 90 °C in 24h.

Mesityl(triethoxy)silane does not react with *p*-I-C₆H₄-CF₃ under typical Hiyama conditions (that is, in the absence of a Cu promoter) (entry 1). Copper(I) compounds CuI and Cu(O^tBu), hoped to form CuMes (Mes = mesityl) and transmetalate Mes to Pd, gave poor results or showed to be ineffective (entries 2-3). In contrast the reactions with CuF₂ in stoichiometric amount proceeded in good yield (entries 4, 5) without added CsF. A oxygenated source of Cu^{II}, Cu(OH)₂, which is in theory good for the transfer, failed to work in the absence of fluoride (entry 6). The addition of CsF activated the reaction of copper sources with labile anions (entries 7, 8) but could not make the process catalytic in copper. In all active conditions (entries 4, 5, 7-9) the amount of *p*-I-C₆H₄-CF₃ converted to *p*-Mes-C₆H₄-CF₃ was stoichiometric relative to the amount of Cu^{II} used, or fairly close to it.

Thus, although we failed to find conditions for a process catalytic in copper (it is catalytic in Pd) a very interesting atom economical transformation stoichiometric in

CuF₂ was found (Table II-3, entry 4). The need for a stoichiometric amount of CuF₂ might look a disadvantage but, much on the contrary, it has several advantages. As discussed later it provides stoichiometrically the exact amounts of Cu^I-Ar and fluoride needed for the reaction, sparing the need for any other source of fluoride used in typical Hiyama couplings (e.g. CsF or (NBu₄)F). Moreover, CuF₂ is of similar cost or cheaper (per F atom) than other fluoride sources, and is easier to handle than, for instance, the very hygroscopic (NBu₄)F.

Anhydrous CuF₂ is a moderately hygroscopic white solid leading to the green complex CuF₂·3H₂O when hydrated. Using the latter as copper additive (Table II-3, entry 5) also gave excellent cross-coupling yield, showing that the reaction is fairly compatible with water,^{*} although it produced about 10% of the homocoupling biphenyl *p*-F₃C-C₆H₄-C₆H₄-CF₃-*p* (a byproduct not easy to separate), and a larger amount of Mes-H by hydrolysis of the silane. By contrast, in optimized conditions with the anhydrous CuF₂, the cross-coupling product *p*-Mes-C₆H₄CF₃ could be easily purified by extraction with ether and filtration through a short pad of silica (see experimental information for details). Somewhat high temperature is needed to perform the coupling. The reason for this might be the poor solubility of anhydrous CuF₂. Other solvents such as THF, dioxane, toluene and CH₃CN were tested with no formation of the cross-coupling product, even under reflux, due to the fact that anhydrous CuF₂ is poorly soluble in DMF but insoluble in almost any other solvent.

Other palladium precatalysts were checked (Table II-4) in the model reaction of Scheme II-13, using CuF₂ as promoter to optimize the reaction.

^{*} The hydrated CuF₂·3H₂O is slightly more soluble in DMF. With this promoter, it was observed an important increase of the rate of the coupling. The reaction can be carried out at 90 °C in only 24 hours

Table II-4. Palladium catalyst optimization. ($R^1 = \text{Mes}$; $R^2 = p\text{-CF}_3\text{-C}_6\text{H}_4$).

Entry	Pd precatalyst	Yield % $R^1\text{-}R^2$	Other % $R^2\text{-}R^2/R^2\text{-}H$
1	[Pd(OAc) ₂] + 2 eq. Xphos (1)	12	66/0
2	[PdCl ₂ (ⁱ Pr-carb.)(3-Clpy)] (2)	< 5	70/0
3	[PdCl ₂ (AsPh ₃) ₂] (3)	87	5/7
4	[PdCl ₂ (dppf)] (4)	88	5/5
5	[PdCl₂(IDM)(AsPh₃)] (5)	> 98	0/0
6	[PdCl ₂ (IDM)(3-Clpy)] (6)	87	10/0
7	[PdCl(μ-Cl)(IDM)] ₂ (7)	81	9/0 ^b
8	[PdCl₂(PPh₃)₂] (8)	96	2/0

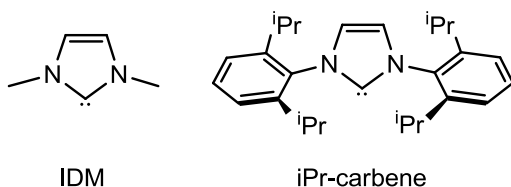
[a] Reaction conditions: 2 mol% of [Pd], 1 equivalent of CuF₂, 1 *p*-CF₃C₆H₄I, 2 mol MesSi(OEt)₃ in DMF at 110 °C for 24-48 h. [b] 11% unreacted ArI and some black Pd are observed. Termination of the reaction and yields were obtained by ¹⁹F NMR integration and GC-MS using Ph-Ph as internal standard. Good correlation was found in all cases.

A blank experiment without Pd catalyst confirmed that CuF₂ alone does not activate the cross-coupling process. Remarkably, for catalysts bearing bulky ligands (Table II-4, entries 1 and 2), very efficient in other instances, almost no reaction was observed, while other palladium precatalysts used were very efficient for the cross-coupling process (Table II-4, entries 3-8).^{*} Not surprisingly from our previous experience with stannanes,⁴⁰ the mixed complex [PdCl₂(IDM)(AsPh₃)] showed excellent performance (Table II-4, entry 5). The formation of F₃CC₆H₄C₆H₄CF₃ was eliminated (Table II-4, entry 5) or highly diminished (Table II-4, entry 8) with the most efficient catalysts.

It might seem that Pd complexes with any other weak ligand instead of AsPh₃ could be used if arsine is to be avoided, but this is not quite true: the use of 3-Clpy in place of AsPh₃ (Table II-4, entry 6) affords worse results. Similarly, (μ-Cl)₂[PdCl(IDM)]₂, which probably splits in DMF solution to give [PdCl₂(IDM)(DMF)],

^{*} Note that the Pd complexes used need to get reduced to Pd⁰ before the first catalytic cycle can start.

gives worse results accompanied by catalyst decomposition that leaves 11% Ar-I unreacted (Table II-4, entry 7). Thus, the ancillary weak ligand has some effect, which will be commented in the mechanistic considerations. For the moment we will concentrate on some steric effects with synthetic consequences that are obvious from the very direct comparison between the excellent performance of $[\text{PdCl}_2(\text{IDM})(\text{AsPh}_3)]$ (**5**) and the fairly good of $[\text{PdCl}_2(\text{IDM})(3\text{-Clpy})]$ (**6**) against the bad results of the electronically related PEPPSI catalyst $[\text{PdCl}_2(\text{}^i\text{Pr-carbene})(3\text{-Clpy})]$ (**2**). The three complexes have an easy leaving ligand and a heterocyclic carbene that remains strongly coordinated to Pd along the process, but the steric requirements of the IDM and $\text{}^i\text{Pr-carbene}$ are very different (Scheme II-14).



Scheme II-14. Carbene ligands in entries 5,6 (left) and 2 (right) of Table II-4

The commonly accepted understanding of reductive elimination suggests that eventually the cross-coupling should take place *via* a palladium $[\text{PdMes}(\text{C}_6\text{H}_4\text{CF}_3)(\text{carbene})]$ intermediate. The results in Table II-4 show that, in our reaction involving a poor Cu^{I} nucleophile,* acceding to form this tricoordinate intermediate and the subsequent transition state is very critically dependent on the steric factors of all the coordinated groups:[†] a smaller ancillary carbene ligand IDM is more compatible with the participation of the bulky aryl Mes than a bulkier carbene ligand $\text{}^i\text{Pr-carbene}$ (Table II-4, entries 5, 6 vs. 2). The same problem must be

* Nucleophilicity is a function of basicity of the nucleophile and steric hindrance in the transmetalation step. Although we speak for short of the crowding and accessibility of the tricoordinated intermediate, it should be understood that we refer only to the reaction conditions where the final R^{I} transfer to Pd comes from a moderate nucleophile CuR^{I} . In fact similarly crowded aryls can be transferred using more basic nucleophiles such as Li, Mg, or Zn derivatives, as we said in the introduction.

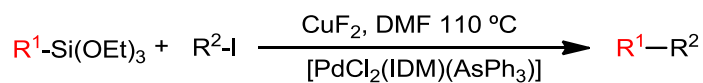
[†] As discussed later, kinetic problems can also be operating in other steps previous to the final reductive elimination.

affecting the bulky Xphos in entry 4 compared to PPh₃ in entry 8. The steric compatibility or incompatibility of coupling groups and ligands of diverse sizes dominates the transmetalation rate and the feasibility of the subsequent coupling step.

The requirement of steric compatibility is also clearly seen in the following case of stoichiometric syntheses: The stoichiometric reaction of PhSi(OEt)₃ with the isolated complex [Pd(C₆H₄CN-*p*)F(PPh₃)₂], has been reported to yield easily PhC₆H₄CN-*p* and FSi(OEt)₃,²⁰ by direct exchange of Ph for F. In contrast, all our attempts to react the bulkier MesSi(OEt)₃ with the isolated complex [Pd(C₆H₄CF₃-*p*)F(PPh₃)₂] failed (see below).

In our initial choice of possible catalysts we did not consider the common catalyst [PdCl₂(PPh₃)₂] (**8**), driven by our previous experiences showing that: *i*) in the gold co-catalysed Stille reaction of bulky groups, [PdCl₂(IDM)(AsPh₃)] behaved very well but [PdCl₂(PPh₃)₂] performed extremely slow, as expected from the use of a strong ligand not easy to release during transmetalation;⁴⁰ and *ii*) we were aware that PPh₃ coordinates strongly to Cu^I whereas AsPh₃ does not.^{*54} So we were concerned about possible detrimental interactions of copper and PPh₃. However, when we tried it (last entry in Table II-4) we were surprised and delighted to see that [PdCl₂(PPh₃)₂] (**8**) performed almost as good as [PdCl₂(IDM)(AsPh₃)] (**5**).

In order to check the scope of the process, the reactivity of other differently substituted bulky arylalkoxysilanes as nucleophiles was studied, with the best catalyst (**5**) and, for some reactions, with (**8**).

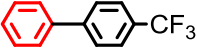
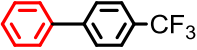
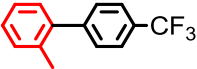
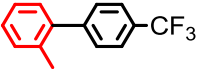
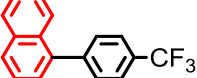
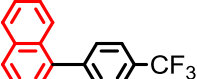
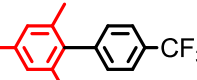
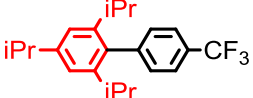
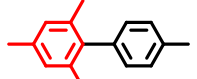
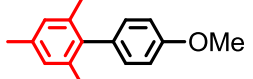
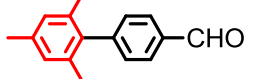
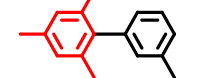
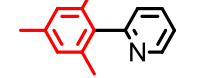


Scheme II-15. CuF₂-promoted Hiyama coupling of substituted aryls. The results are gathered in Table II-5.

* The different coordination behavior of PPh₃ and AsPh₃ towards Cu^I is well demonstrated: In a 50:1 AsPh₃:PPh₃ ratio, Cu^I will coordinate PPh₃ and not AsPh₃. This is in part responsible for the copper effect in Stille reactions. See ref. 54.

The cross-coupling results are gathered in Table II-5. At that point, the excellent performance of **(5)** towards bulky groups was found to be quite general, whereas **(8)** turned out to be less efficient or very little efficient in other couplings (see entries 2, 3, 6, 11 in Table II-5). It might appear that the molecular composition of $[\text{PdCl}_2(\text{IDM})(\text{AsPh}_3)]$ were announcing a contaminant and not easily accessible catalyst, but in fact it is very easy to make in two steps from simple precursors,^{40b} and the isolated cross-coupling reaction products analysed by the ICP-MS show that the palladium or arsenic concentrations in the product are $< 1 \mu\text{g/g}$ (see experimental part for details).

Table II-5. CuF₂-promoted Hiyama coupling of substituted aryls.

Entry	Product R ¹ -R ²	Yield	Other products ^f
1a		73	R ² -R ² : 14%; also R ¹ -R ¹
1b		70 ^h	
2		71	R ² -R ² : 21%; also R ¹ -R ¹
		35 ^h	
3		95	
4		> 98	
5		> 98 > 95 ^d 54 ^{d,e}	
6		78 71 ^h	
7		> 95 ^g 90 ^c	
8		> 95 ^g 87 ^c	
9		> 95 ^g 88 ^b	
10		> 95 ^g 90 ^c	
11		> 95 ^g 88 ^{e,c} 25 ^h	

[a] Reaction conditions: 2 mol% of (**5**); CuF₂:R²I: R¹Si(OEt)₃ = 1:1:2, in DMF at 110 °C for 24-48h. [b] CuF₂ was substituted by 2 equivalents of CsF. [c] Isolated yield. [d] Yield (% from R²-I) determined by ¹⁹F NMR. [e] R²-Br was used instead of R²I. [f] Byproducts for 1a. [g] GC-MS yield, using biphenyl as internal standard. [h] [PdCl₂(PPh₃)₂] (**8**) was used instead of [PdCl₂(IDM)(AsPh₃)] (**5**).

As shown in Table II-5, the reactions with (5) as catalyst afford excellent yields for the coupling of mesityl and naphthyl derivatives (entries 3-5), which do not work under the normal Hiyama protocols. The good result obtained for 2,4,6-triisopropyltris(ethoxy)silane (Table II-5, entry 6) is noteworthy considering the extreme bulkiness of this substrate. Suzuki couplings using the much more reactive boronic counterpart usually fail for similarly bulky aryls.³⁷ It is also worth commenting that the procedure with CuF_2 tolerates equally well electron-withdrawing (Table II-5, entries 5, 6, 9) and electron-donating (Table II-5, entries 7-8) substituents. Sensitive groups difficult to access otherwise, such as aldehydes (Table II-5, entry 9), and pyridyl (Table II-5, entry 11) can be effectively coupled.

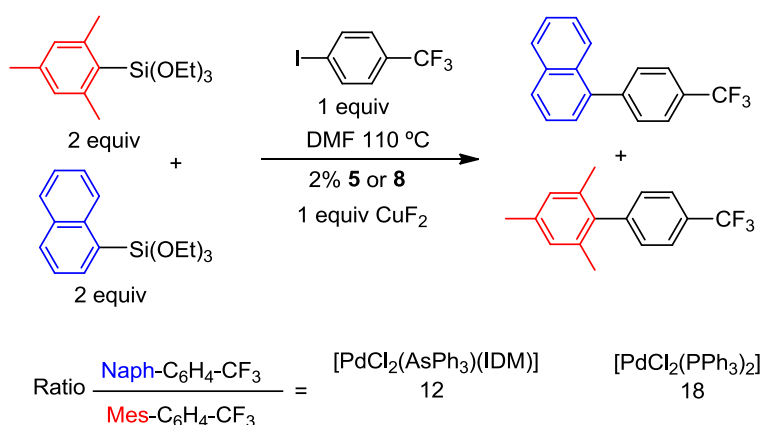
While the yield of desired cross-coupling product $\text{R}^1\text{-R}^2$ is very good for the bulky arylalkoxysilanes, as found initially for $\text{MesSi}(\text{OEt})_3$ (virtually quantitative yield by NMR, Table II-5, entries 3-11), it is noticeably lower for aryls of conventional size (Table II-5, entries 1-2). This apparently surprising behaviour makes sense when examination of the products reveals (Table II-5, entries 1-2) that this lower yield is mostly due to a loss of coupling selectivity producing a significant percentage of $\text{R}^1\text{-R}^1$ and $\text{R}^2\text{-R}^2$ homocoupling products. In fact using CsF instead CuF_2 in Table II-5, entry 1b improved the yield of $\text{PhC}_6\text{H}_4\text{CF}_3$. This confirms that CsF succeeds to produce cross-coupling with arylalkoxysilanes of conventional bulk, while CsF fails and CuF_2 is required when the coupling involves a bulky arylalkoxysilane.

The formation of homocoupling products with arylalkoxysilanes of conventional bulk is easily explained assuming that the bimetallic Cu-mediated Hiyama process facilitates also undesired transmetalations that eventually can generate homocoupling products.⁹ Thus, when the arylalkoxysilane has a conventional size all $[\text{PdR}^1\text{R}^2(\text{L})]$, $[\text{PdR}^2\text{R}^2(\text{L})]$, and $[\text{PdR}^1\text{R}^1(\text{L})]$ transition states are kinetically accessible and can generate $\text{R}^1\text{-R}^2$, $\text{R}^2\text{-R}^2$, and $\text{R}^1\text{-R}^1$, respectively.* However, when R^1 is bulky the formation of $[\text{PdR}^1\text{R}^1(\text{L})]$ is made inaccessible at some point of the process (as discussed later) and the rate of formation of $\text{R}^1\text{-R}^1$ drops to zero. The positive

* $\text{R}^1\text{-R}^1$ can proceed also from coupling on Cu^{II} , as discussed later.

consequence of this is that the reaction becomes very selective in favour of the heterocoupling product.

In principle a fine combination of R^1 , R^2 , and L groups should allow for tuning of selectivity of the reactions as controlled by the kinetic accessibility of the corresponding $[PdR^1R^2(L)]$ intermediate. For instance, a smaller ligand might allow for further improvement of the reaction in Table II-5 entry 6. Similarly, competitive reactions coupling differently sized arylalkoxysilanes should show selectivity of the alkoxysilane towards the less encumbered intermediate.

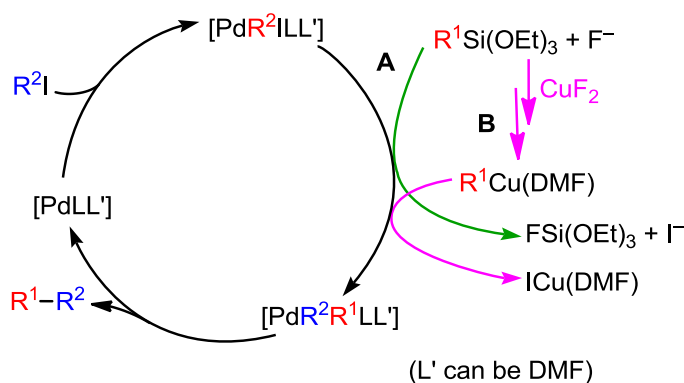


Scheme II-16. Selectivity of naphthyl vs. mesityl coupling with 5 or 8 as catalyst.

As a proof of principle, the competitive reaction in Scheme II-16 afforded highly selective coupling (12:1 ratio) of the less hindered arylalkoxysilane (1-naphthyl) using complex (5). With complex (8) the reaction was somewhat slower and correspondingly more selective (18:1 ratio). This shows how much the size influence on the nucleophilicity of these Si reagents (and their corresponding Cu^I intermediates), is determinant for processes when it has to proceed through critically crowded species.

2.1. Mechanistic Studies and considerations

With the evidence provided so far, two pathways are possible for the Hiyama coupling, depending on how the nucleophilic moiety R^1 reaches the Pd cycle (Scheme II-17):



Scheme II-17. Simplified picture of direct Hiyama-Denmark (A) and Cu-mediated (B) catalyses. Ligand exchanges (L/L'/DMF) are possible.

(A) directly from the Si reagent in the conventional process (which requires a ionized source of F^-); or (B) as proposed in Scheme II-17, *via* CuR^1 , formed stoichiometrically *in situ* in the CuF_2 mediated non-catalytic steps of the process. The conversion of CuF_2 into CuR^1 requires a change in oxidation state of copper. Sufficiently bulky R^1 groups will have essentially zero rate via (A), and consequently will need CuF_2 as reagent to follow pathway (B). In this case other fluoride sources can be spared. Pathway (B) is slow (therefore high temperature and long time are required), but efficient for the heterocoupling on Pd. In the case of conventional R^1 groups, which hetero-couple well via pathway (A) using sources of ionic fluoride, the presence of undesired homocoupling products when CuF_2 is used suggests that CuF_2 is not a good source of ionized F^- and it is unable to make path (A) efficient;* this also supports that in pathway (B) there is some reversibility of the Cu^I/Pd^{II} transmetalation, giving rise to undesired transmetalations as the source of R^2-R^2

* Conductivity measurements of CuF_2 in DMF suggest that this compound is not dissociated in solution.

and, at least in part, R^1-R^1 .⁹ From now on we will centre our attention on pathway (B).

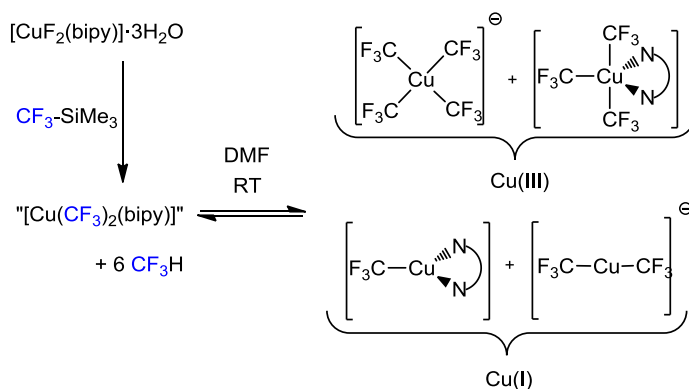
The Pd catalysed cycle that closes the coupling process can be read in a rather conventional way, and we have already discussed above how the coupling rates depend on the size of the groups to be coupled, as well as on the coordinating strength and size of the ancillary ligands. The ancillary ligands can influence every step of this cycle. For instance, phosphines can slow down the transmetalation, as compared to $AsPh_3$; the stability of the Pd^0 intermediate, which is critical for the protection of the catalyst working under harsh conditions depends on these ligands, as it happens also with the barrier to oxidative addition. Consequently it is not surprising that the nature of the ligands (also the weak ones) has a direct effect on the efficiency of the reaction.

Can we propose a reaction scheme for the non-catalytic part of the process and a plausible mode of reaction of CuF_2 consistent with all the products and byproducts observed? Fortunately, studies available from literature and experiments discussed below allow us to get a convincing picture of this non-catalytic part of the reaction. In this respect there are reports in the literature where Cu^{II} fluorides react with organosilicon compounds. For instance, Lam *et al.* have reported the use of $Cu(OAc)_2 + NBu_4F$ to promote the coupling of amines with arylsilanes.⁵⁵

Cu^{II} organometallics have been proposed as transient species in several chemical processes.⁵⁶ However, their intrinsic unstability usually precludes detection or characterization of these intermediates. Cu^{II} -aryls readily disproportionate into Cu^I and Cu^{III} complexes, as it was elegantly demonstrated by the group of Lobet and Ribas with the use of a macrocyclic ligand.^{57a} There are also examples that show that the reductive elimination from Cu^{III} is usually easy and fast.⁵⁸

Very recently, Nebra and Grushin have studied the reaction of $[CuF_2(bipy)] \cdot 3H_2O$ with CF_3SiMe_3 .⁵⁹ They have concluded very convincingly that the transmetalation of CF_3 to copper generates the NMR-indetectable

"[Cu(CF₃)₂(bipy)]". This Cu^{II} organometallic spontaneously disproportionates leading to a reversible equilibrium between Cu^I + Cu^{III} and Cu^{II} species that can be observed because the CF₃-CF₃ coupling is not feasible. The detectable species only account for 40% of the mass balance, suggesting that 60% were still in the Cu^{II} form (Scheme II-18).



Scheme II-18. Disproportionation equilibrium of "[Cu(CF₃)₂(bipy)]" reported by Nebra and Grushin.^{57b}

The reason for the instability of Cu^{II} organometallics has been addressed by computational means. It was found that Cu^{II}-alkyl compounds were very prone to undergo reduction to Cu^I and disproportionation via bimolecular SET reactions.⁶⁰ As a result, only a few examples of Cu^{II} compounds, bearing a Cu-C bond, are known to date.^{61,62}

a) Reaction of Copper (II) salts and aryl(triethoxy)silanes

If CuF₂ and Mes-Si(OEt)₃ are heated in DMF at 110 °C for 24-48 h in the absence of any Pd catalyst and aryl-iodide, full consumption of the silane was obtained, along with formation of Mes-H, Mes-OEt and Mes-Mes (only traces). These products are likely to come from hydrolysis of a copper organometallic (Mes-H), and Chan-Lam-Evans reaction (Mes-OEt),⁶³ which must take place from an intermediate containing a CuMes(OEt) moiety.⁶⁴ All this reactivity is well precedented in the literature since the early discovery of the Ullmann reaction,⁶⁵ and it does suggest the intermediacy Cu^{III} organometallics present in our reaction

field. GC-MS analysis of the reaction products of the reactions in entries 7-11 of Table II-5 revealed in all cases the formation of the two main byproducts. These side products are not specified in Table II-5, and are the reason for the need to use some excess of the aryl(alkoxy)silane.

We have obtained mechanistic hints of this disproportionation from experiments using CuF_2 and pentafluorophenyltris(ethoxy)silane.* Thus, a suspension of CuF_2 was stirred in the absence of Pd catalyst with 3 equivalents of $(\text{C}_6\text{F}_5)\text{Si}(\text{OEt})_3$ in DMF for 24 hours at RT. After this time, the ^{19}F NMR spectrum of the reaction mixture (Figure II-1) showed signals corresponding to the Cu^{I} complex $[\text{Cu}(\text{C}_6\text{F}_5)(\text{DMF})_n]^\dagger$, along with decafluorobiphenyl and $\text{C}_6\text{F}_5\text{H}$ (originated by hydrolysis).

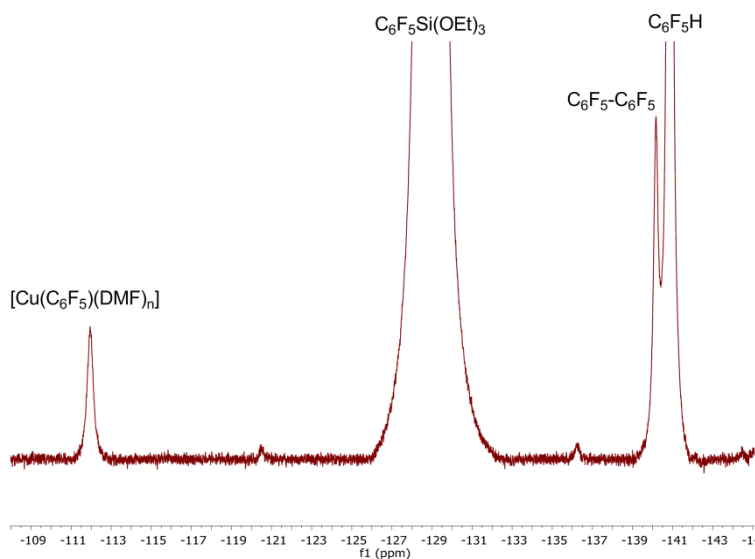
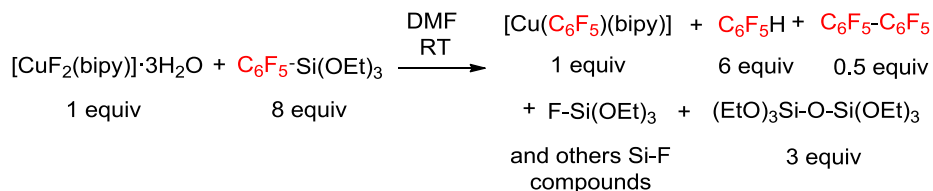


Figure II-1. ^{19}F NMR of the Reaction of CuF_2 with $(\text{C}_6\text{F}_5)\text{Si}(\text{OEt})_3$ at RT.[‡]

* C_6F_5 is used because it is easy to observe by ^{19}F NMR, facilitating the observation of intermediates.

[†] The preparation of CuC_6F_5 in DMF has been reported (however, it seems to us that a more likely structure of this complex should include one or more molecules of coordinated DMF as $[\text{CuC}_6\text{F}_5(\text{DMF})_n]$). See: MacNeil, K. J.; Burton, D. J. *J. Org. Chem.* **1993**, *58*, 4411.

[‡] CuF_2 did not react completely after 24 hours at RT. Due to the presence of paramagnetic Cu^{II} , the signals in the ^{19}F were broad. *Meta* and *para* fluorines of $[(\text{C}_6\text{F}_5)\text{Cu}(\text{DMF})_n]$ were overlapped with *para* and *meta* fluorine atoms of $(\text{C}_6\text{F}_5)\text{Si}(\text{OEt})_3$ and $\text{C}_6\text{F}_5\text{H}$. *Ortho* fluorine atoms were well resolved.



Scheme II-21. Reaction of $[\text{CuF}_2(\text{bipy}) \cdot 3\text{H}_2\text{O}]$ with $(\text{C}_6\text{F}_5)\text{Si}(\text{OEt})_3$ in DMF at RT.

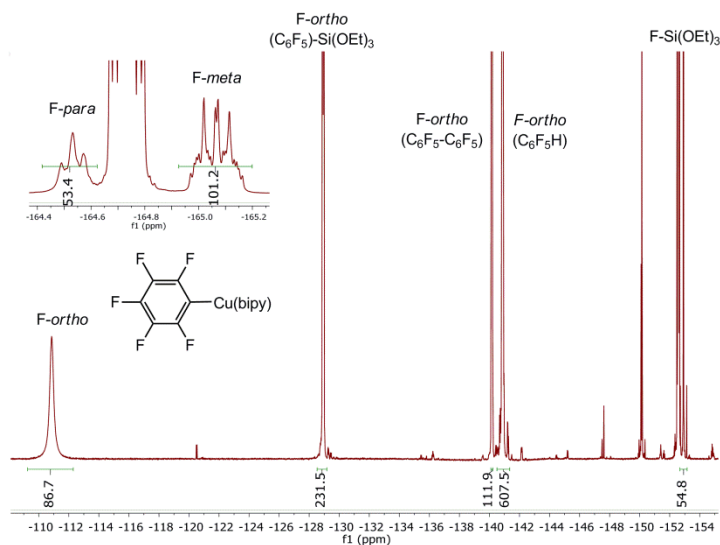


Figure II-2. ^{19}F NMR of the Reaction of $[\text{CuF}_2(\text{bipy}) \cdot 3\text{H}_2\text{O}]$ with $(\text{C}_6\text{F}_5)\text{Si}(\text{OEt})_3$ in DMF at RT. The spectrum was acquired at -50°C . Integrals are referred to an internal standard (Ph-CF_3).

$\text{C}_6\text{F}_5\text{H}$ is probably formed by hydrolysis with the water molecules coming with $[\text{CuF}_2(\text{bipy}) \cdot 3\text{H}_2\text{O}]$. $\text{F-Si}(\text{OEt})_3$ is clearly identified as the mayor product containing a Si-F bond (accounting for about 55% of the F-Si formed), along with some other Si-F signals. * $\text{C}_6\text{F}_5\text{-C}_6\text{F}_5$ was formed right after mixing, suggesting that C-C reductive elimination is fast.

These results are formally analogous to those of Grushin and Nebra.⁵⁹ However, reaction of $[\text{CuF}_2(\text{bipy}) \cdot 3\text{H}_2\text{O}]$ with an excess of $g(\text{C}_6\text{F}_5)\text{Si}(\text{OEt})_3$ leads to quantitative

* $\text{F-Si}(\text{OEt})_3$ was identified by spiking an authentic sample of it in the NMR tube. The other F-Si products might be oligomers or some other products of complicated structure. The presence of $(\text{EtO})_3\text{Si-O-Si}(\text{OEt})_3$ was detected by GC-MS.

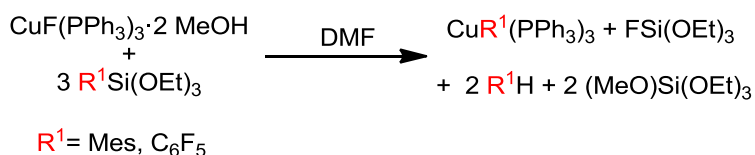
formation of $[\text{Cu}(\text{C}_6\text{F}_5)(\text{bipy})]$ (that is, quantitative reduction of Cu^{II}), whereas in their system a disproportionation equilibrium was found. The reason for this might be that $\text{Cu}^{\text{III}}(\text{CF}_3)_2$ complexes are stable and reluctant to undergo reductive elimination, so an equilibrium between all the stable species is found. In our system, the formation of $\text{C}_6\text{F}_5\text{-C}_6\text{F}_5$ is irreversible.

Note that, at variance with Scheme II-19, as the reduction of Cu^{III} produces Mes-OEt instead of Mes-Mes, only 25% of the initial $\text{MesSi}(\text{OEt})_3$ plays the role of reducing agent, keeping the electrophile:nucleophile stoichiometry for the reaction 1:1.5 (Scheme II-20). This lower consumption of $\text{MesSi}(\text{OEt})_3$ maintains a higher concentration of it up to the end of the process, in spite of some hydrolysis, and prevents the competition of homocoupling processes.

b) Examination of Cu^{I} promoters

The formation of the second molecule of CuMes finds also a different origin in Scheme II-20 than in Scheme II-19, consisting of the direct arylation of a $\text{Cu}^{\text{I}}\text{F}$ intermediate. This is supported by a parallel experiment in which, reacting $[\text{CuF}(\text{PPh}_3)_3] \cdot 2\text{MeOH}$ in place of CuF_2 for the experiment defined in Table 3 entry 5, gives $\text{MesC}_6\text{H}_4\text{CF}_3$ in 83% yield, not producing Mes-OEt. This suggests that $\text{Cu}^{\text{I}}\text{F}$ is able to undergo direct $\text{Cu}^{\text{I}}/\text{Si}$ transmetalation to give $\text{R}^{\text{I}}\text{Cu}$. It also reveals that the Mes-OEt formed as byproduct in Table II-5 is produced on a different oxidation state of Cu, as discussed.

We could also verify that complexes of $\text{Cu}^{\text{I}}\text{F}$ are easily arylated by arylalkoxysilanes, whether bulky or small, in DMF at room temperature, as for instance in Scheme II-22:



Scheme II-22. Reaction of $[\text{CuF}(\text{PPh}_3)_3 \cdot 2\text{MeOH}]$ with 3 equivalents of $\text{R}^{\text{I}}\text{Si}(\text{OEt})_3$

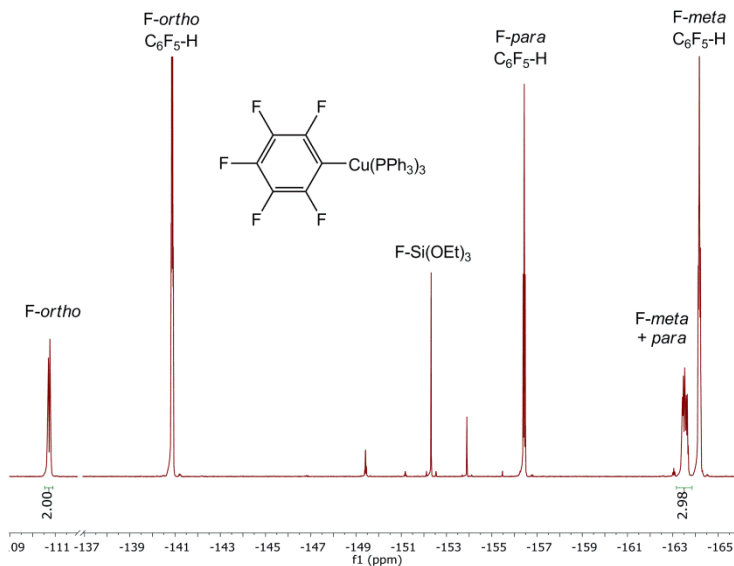
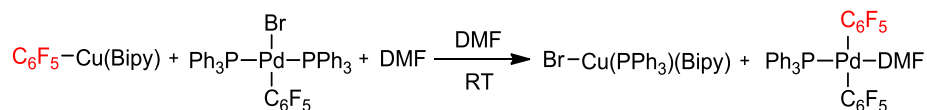


Figure II-3. ^{19}F NMR spectrum of $[\text{CuF}(\text{PPh}_3)_3 \cdot 2\text{MeOH}]$ and two equivalents of $\text{C}_6\text{F}_5\text{-Si}(\text{OEt})_3$ in DMF at $-50\text{ }^\circ\text{C}$. The ^{19}F spectra at RT showed broadening of the signals. Integrals are referred to an internal standard (Ph-CF_3).

c) *Cu/Pd and Si/Cu/Pd transmetalation experiments*

A freshly prepared solution of $[\text{Cu}^I(\text{C}_6\text{F}_5)(\text{bipy})]$ was transferred to an NMR tube containing a substoichiometric amount of *trans*- $[\text{Pd}(\text{C}_6\text{F}_5)(\text{Br})(\text{PPh}_3)_2]$ (Cu/Pd ratio = 5). Full transmetalation of the C_6F_5 group was observed upon mixing at RT by ^{19}F NMR, leading to a new complex consistent with the formulation *trans*- $[\text{Pd}(\text{C}_6\text{F}_5)_2(\text{DMF})(\text{PPh}_3)]$.*



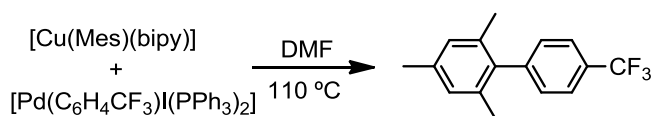
Scheme II-23. Transmetalation of $[\text{Cu}^I(\text{C}_6\text{F}_5)(\text{bipy})]$ to $[\text{Pd}(\text{C}_6\text{F}_5)(\text{Br})(\text{PPh}_3)_2]$.

Interestingly, 1 equivalent of PPh_3 is sequestered from the Pd complex by the Cu species, showing one broad signal at typical chemical shifts for Cu-PPh_3

* ^{31}P NMR spectrum shows a Pd-PPh_3 complex as a quintuplet, confirming the coupling of the P to two equivalent C_6F_5 groups.

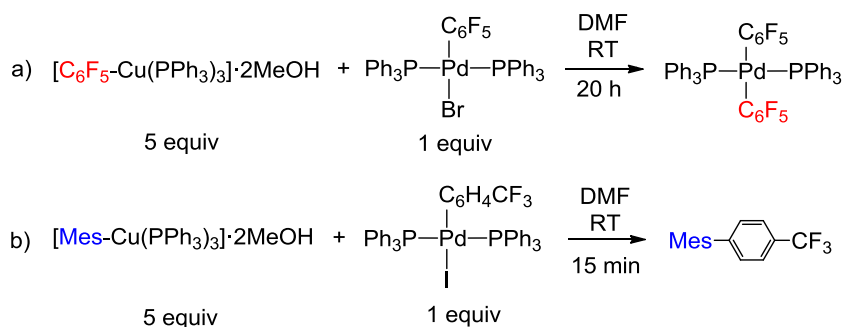
complexes. Cu complexes with mixed N-chelated ligands and PPh_3 have been reported as well.⁶⁸

Similarly, $[\text{Cu}(\text{Mes})(\text{bipy})]$ can be generated in situ by treating $[\text{CuF}_2(\text{bipy})\cdot 3\text{H}_2\text{O}]$ with an excess of $(\text{Mes})\text{Si}(\text{OEt})_3$. When a preformed solution of this organometallic in DMF is transferred to a flask containing $[\text{Pd}(\text{C}_6\text{H}_4\text{CF}_3)\text{I}(\text{PPh}_3)_2]$ and heated to 110°C for an hour, quantitative formation of $\text{Mes-C}_6\text{H}_4\text{CF}_3$ is observed. This experiment confirms that a Cu^{I} organometallics transmetalate effectively the bulky aryl to the palladium catalyst.



Scheme II-24. Transmetalation of $[\text{Cu}^{\text{I}}(\text{Mes})(\text{bipy})]$ to *trans*- $[\text{Pd}(\text{C}_6\text{H}_4\text{CF}_3)\text{I}(\text{PPh}_3)_2]$.

Ligand scrambling can be avoided if PPh_3 is the ancillary ligand in both Pd and Cu complexes. The corresponding $[\text{CuR}^1(\text{PPh}_3)_3]$ complexes generated in situ transmetalate effectively C_6F_5 or Mes to the palladium catalysts $[\text{Pd}(\text{C}_6\text{F}_5)\text{Br}(\text{PPh}_3)_2]$ and $[\text{Pd}(\text{C}_6\text{H}_4\text{CF}_3)\text{I}(\text{PPh}_3)_2]$, respectively (Scheme II-25).

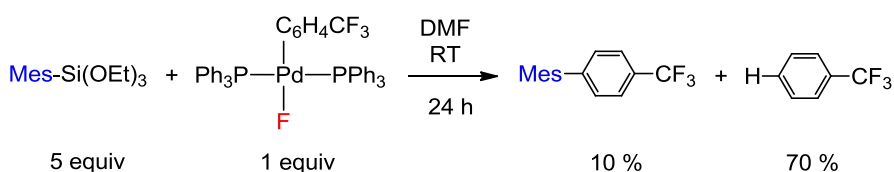


Scheme II-25. Si/Cu/Pd Transmetalation experiments. The reactions were monitored by ^{19}F and ^{31}P NMR.

d) Direct Si/Pd transmetalation of bulky groups

After having proven the feasibility of the Si/Cu/Pd transmetalation one question arises: is the Si/Pd transmetalation impossible with bulky groups or the catalytic reaction fails due to any other problem? An indirect proof of the inefficiency of the direct Si/Pd direct transmetalation when bulky groups are involved can be obtained from the fact that CsF is unable to promote the coupling under catalytic conditions of I-Ph-CF₃ with Mes-Si(OEt)₃ (Table II-3, entry 1), but high yields of cross-coupling product are obtained with Ph-Si(OEt)₃ in the same conditions (Table II-5, entry 1).

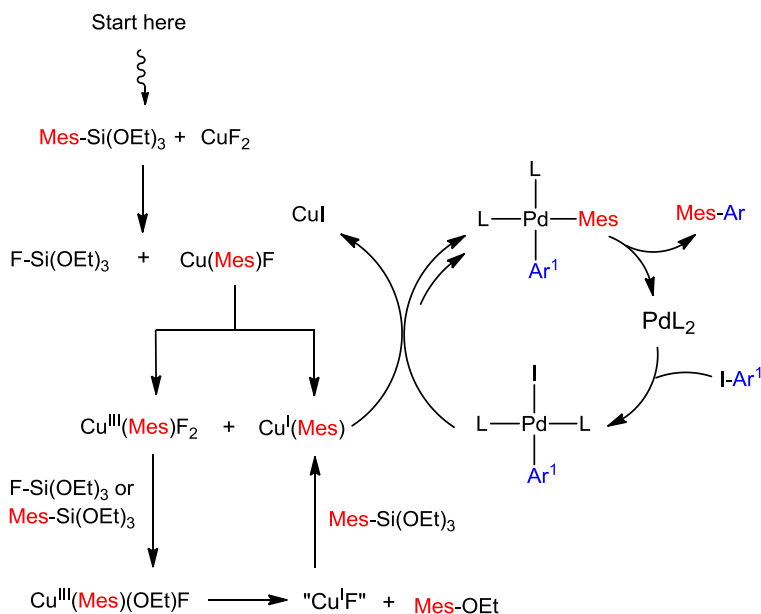
To get further insight into the Si/Pd direct transmetalation, it should be considered that palladium fluorides have been recognized as the actual intermediates that undergo transmetalation in the Hiyama coupling when arylSi(OEt)₃ are involved.²⁰ If the silane is not bulky, the Si/Pd transmetalation was reported to be fast and selective.²¹ The inefficiency of the Si/Pd transmetalation with hindered silicon sources was demonstrated by attempting a Cu-free reaction of [Pd(F)(C₆H₄CF₃)(PPh₃)₂] and Mes-Si(OEt)₃ (Scheme II-26). Reaction of these two partners in DMF took place slowly. It took one day to go to completion and showed a very poor selectivity towards the cross-coupling product.



Scheme II-26. Direct Si/Pd transmetalation experiments with bulky groups. The reactions were monitored by ¹⁹F and ³¹P NMR.

2.2. Proposed mechanistic cycle for the cross-coupling reaction

Scheme II-27 summarizes our mechanistic proposal. A route to the formation of all the observed products is proposed:



Scheme II-27. Proposed reaction pathway of the cross-coupling reaction of bulky silanes with aryl iodides promoted by copper fluorides.

3. Conclusions

In summary, a bimetallic synthetic procedure involving Si/Cu/Pd aryl transfers has been developed that makes the Hiyama reaction useful for the coupling of bulky aryl(alkoxy)silanes for the first time. It uses stoichiometric CuF_2 in an atom-economical way, as the only source of the two important reagents required for the aryl transmetalations in the reaction, namely: i) fluoride, for the initial Si-to-Cu transmetalation step; and ii) Cu^{I} , for the transmetalation from Cu(aryl) to Pd. Very interestingly, using easily accessible catalysts very simple to prepare from readily available materials, the reaction affords excellent yields, has a wide scope of application. The reaction is compatible with active functional groups such as aldehydes or pyridine that, for hindered substrates, often fail with other cross-

coupling alternatives. Moreover, it shows size selectivity and offers the possibility of tuning for selective size competing couplings.

Future investigations concerning this reaction should include the exploration and development of other Cu^I fluorides. In principle, a dry, soluble and stable Cu^I fluoride would be the ideal source to undertake this coupling. In addition, there is room for further improvements if the Cu^I-F complex can be regenerated in situ, allowing for the development of a bimetallic cocatalytic system. This approach would preclude stoichiometric use of the silicon nucleophile as reductant of the copper promoter.

4. Experimental section

4.1. General methods

All reactions were carried out under N₂ or Ar. DMF was purchased anhydrous from Alfa Aesar. Prior to its use, it was degassed by the freeze-pump-thaw procedure and stored over 3 Å molecular sieves for a week. All other solvents were used dried by standard techniques.⁶⁹ NMR spectra were recorded on a Bruker AV 400 instrument equipped with a VT-100 variable-temperature probe, or a Varian 500-MR. Chemical shifts are reported in ppm from tetramethylsilane (¹H), CCl₃F (¹⁹F), or 85% H₃PO₄ (³¹P), with positive shifts downfield, at ambient probe temperature unless otherwise stated. The temperature for the NMR probe was calibrated using ethylene glycol (T > 300K) and methanol (T < 300K) as temperature standards.⁷⁰ In the ¹⁹F and ³¹P spectra measured in non-deuterated solvents, a coaxial tube containing acetone-*d*₆ was used for the lock ²H signal. The Gas Chromatography-Mass analyses were performed in a Thermo-Scientific DSQ II GC/MS Fows GL. Combustion CHN analyses were made on a Perkin-Elmer 2400 CHN microanalyzer. Unless specified, all the compounds were used from commercial sources and used without further purification. The compounds [PdCl₂(AsPh₃)₂],⁷¹ [PdCl₂(PPh₃)₂],⁷² [PdCl₂(IDM)₂],⁷³ [PdCl₂(AsPh₃)(IDM)],^{40b} [PdCl₂(dppf)],⁷⁴ PEPPSI,⁷⁵ *trans*-[Pd(C₆F₅)(Br)(PPh₃)₂],⁷⁶ *trans*-[Pd(C₆H₄CF₃)(I)(PPh₃)₂],⁷⁷ *trans*-[Pd(C₆H₄CF₃)(F)(PPh₃)₂],⁷⁸ [CuF₂Bipy]·3H₂O,⁷⁹ Cl-Si(OEt)₃,⁸⁰ and the P-N ligand 1-(2-(diphenylphosphino)phenyl)-N,N-dimethylmethanamine⁸¹ were prepared by literature methods. Anhydrous CuF₂ was purchased from Alfa Aesar, Ph-Si(OEt)₃ was purchased from Aldrich and (C₆F₅)Si(OEt)₃ from Fluorochem. The rest of the silanes were synthesized according to the procedure described in this supporting information. LiCl used for the syntheses was dried under vacuum at 250 °C overnight.

4.2. Synthesis of bulky (aryl)triethoxysilanes

Bulky (aryl)triethoxysilanes were prepared by treating Si(OEt)₄ with the corresponding LiCl-activated organomagnesium reagent,⁸² according to the procedure published by DeShong et al.⁸³

General procedure for the synthesis of Ar-Si(OEt)₃

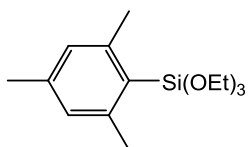
a) Synthesis of the activated bulky aryl Grignard reagents

A three-necked flask was charged with 2.9 g of dry LiCl (0.065mol), Mg turnings and an I₂ crystal, and set under N₂ atmosphere. The I₂ crystal was sublimated with a heat gun, and released out of the flask under a strong current of nitrogen, with the aim of activating the magnesium turnings. Once all the iodine had been released, 10 mL of THF were added via syringe. A solution of the corresponding Ar-Br was added dropwise to the refluxing mixture (0.065 mol in 50 mL of THF), using an addition funnel. Once the addition was finished, the reaction was monitored by TLC until full consumption of the aryl-Br was achieved (usually 20 hours were needed).

b) Reaction of the Grignard reagent with $\text{Si}(\text{OEt})_4$

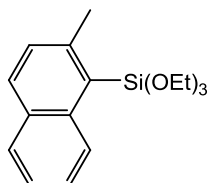
A separate flask containing 0.19 mol of $\text{Si}(\text{OEt})_4$ in 50 mL of THF was cooled down to $-30\text{ }^\circ\text{C}$. The solution of Br-Mg-Ar-LiCl was cannulated dropwise to the flask containing the $\text{Si}(\text{OEt})_4$. When the addition was finished, the reaction was allowed to warm to RT and stirred for 8 hours. To make sure that it was completed, the mixture was refluxed overnight. After this time, the reaction was quenched with a saturated solution of NH_4Cl (40mL) and the organic layer was decanted. The aqueous layer was extracted with Et_2O (3 x 50mL). All organic layers were combined, washed with brine (2 x 100mL) and dried over MgSO_4 . The solvent was removed under reduced pressure to obtain a yellowish oil.

All (aryl)triethoxysilanes were purified by distillation under vacuum (1 mbar). The excess of $\text{Si}(\text{OEt})_4$ was recovered at $90\text{ }^\circ\text{C}$, whereas the pure (aryl)triethoxysilane was obtained at about $160\text{ }^\circ\text{C}$ as an oil.

(Mesityl)triethoxysilane

13.1 grams of colorless oil were isolated. Yield: 73%.

^1H NMR (500 MHz, CDCl_3) δ 6.84 (s, 2H), 3.85 (q, $J = 7.0$, 6H), 2.52 (s, 6H), 2.27 (s, 3H), 1.30 – 1.18 (q, $J = 7.0$, 9H). ^{13}C NMR (126 MHz, CDCl_3) δ 145.90, 139.76, 128.79, 124.99, 58.10, 23.72, 21.07, 18.14. GC-MS: MS (EI+, 70 eV): m/z (%): 282 (15) $[\text{M}]^+$, 237 $[\text{Mes-Si}(\text{OEt})_2]^+$ (5), 281 $[\text{Mes-Si-O}]^+$ (100). Elemental analysis calculated for $\text{C}_{15}\text{H}_{16}\text{O}_3\text{Si}$: C, 63.78; H, 9.28. Found: C, 63.63; H, 9.13.

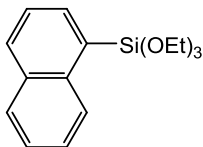
(2-methyl-1-naphthyl)triethoxysilane

15.8 g were obtained as yellowish oil. Yield: 80%.

^1H NMR (500 MHz, CDCl_3) δ 8.77 (d, $J = 8.7$ Hz, 1H), 7.82 – 7.73 (m, 2H), 7.46 (ddd, $J = 8.6, 6.8, 1.6$ Hz, 1H), 7.39 (ddd, $J = 8.0, 6.7, 1.2$ Hz, 1H), 7.30 (d, $J = 8.4$ Hz, 1H), 3.88 (q, $J = 7.0$ Hz, 6H), 2.76 (s, 3H), 1.25 (t, $J = 7.0$ Hz, 9H). ^{13}C NMR (126 MHz, CDCl_3) δ 145.86, 138.18, 131.58, 130.82, 129.57, 128.49, 128.27, 125.90, 124.49, 109.99, 58.38, 24.19, 18.13. GC-MS: MS (EI+, 70 eV): m/z (%): 304 (30) $[\text{M}]^+$, 259

(5) [2-Me-Naph-Si(OEt)₂]⁺, 147 (100). Elemental analysis calculated for C₁₇H₂₄O₃Si: C, 67.06; H, 7.95. Found: C, 66.99; H, 7.98.

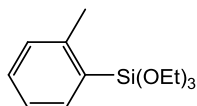
(1-Naphtyl)triethoxysilane



0.052 mmol of 1-Bromonaphtalene were used in this synthesis, keeping the proportions of the rest of the reagents as established in the general procedure. 13.8 g were obtained as colorless oil. Yield: 93%

¹H NMR (500 MHz, CDCl₃) δ 8.41 – 8.32 (d, *J* = 8.2 Hz, 1H), 8.02 (d, *J* = 6.8 Hz, 1H), 7.93 (d, *J* = 8.2 Hz, 1H), 7.85 (d, *J* = 7.4 Hz, 1H), 7.56 – 7.45 (m, 3H), 3.91 (q, *J* = 7.0 Hz, 6H), 1.26 (t, *J* = 7.0 Hz, 9H). ¹³C NMR (126 MHz, CDCl₃) δ 136.20, 133.24, 131.09, 128.62, 128.56, 126.23, 125.57, 124.96, 58.74, 18.23. GC-MS: MS (EI⁺, 70 eV): *m/z* (%): 290 (45) [MZ]⁺, 243 (15) [Naph-Si(OEt)₂]⁺, 147 (100). Elemental analysis calculated for C₁₆H₂₂O₃Si: C, 66.17; H, 7.64. Found: C, 67.11; H, 7.62.

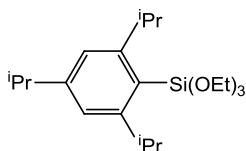
(2-tolyl)triethoxysilane



0.020 mmol of 2-Bromotoluene were used in these synthesis, keeping the proportions of the rest of the reagents as established in the general procedure. 3.9 g of colorless oil were obtained. Yield: 77%

¹H NMR (400 MHz, CDCl₃) δ 7.72 (m, 1H), 7.32 (t, *J* = 7.6, 1H), 7.18 (d, *J* = 7.6 Hz, 2H), 3.86 (d, *J* = 7.0 Hz, 6H), 2.51 (s, 3H), 1.26 (d, *J* = 7.0 Hz, 9H). ¹³C NMR (126 MHz, CDCl₃) δ 144.50, 136.45, 130.44, 129.68, 124.63, 59.14, 22.39, 18.09. GC-MS: MS (EI⁺, 70 eV): *m/z* (%): 254 (15) [MZ]⁺, 243 (10) [2-tol-Si(OEt)₂]⁺, 147 (100). Elemental analysis calculated for C₁₃H₂₂O₃Si: C, 61.38; H, 8.72. Found: C, 61.29; H, 8.91.

(2,4,6-triisopropylphenyl)triethoxysilane



0.054 mol of (2,4,6-triisopropylphenyl)Mg-Br·LiCl in 50 mL of THF (prepared the same way as the other Grignard reagents) were canulated dropwise to a flask containing with 0.069 mmol of Cl-Si(OEt)₃ in 50 mL of THF at -30 °C. When the addition-finished, the reaction was allowed to warm to RT and stirred for 8 hours.

To make sure that it was completed, the mixture was refluxed overnight. After this time, the reaction was quenched with a saturated solution of NH_4Cl (40 mL) and the organic layer was decanted. The aqueous layer was extracted with Et_2O (3 x 50 mL). All the organic layers were combined, washed with brine (2 x 100 mL) and dried over MgSO_4 . The solvent was removed under reduced pressure to obtain a yellowish oil. After distillation at low pressure (160 °C, 1 mBar), 9.6 g of (2,4,6-triisopropylphenyl)triethoxysilane were obtained in 80% purity, which accounts for 48 % yield in the arylalkoxysilane. NMR and GC-MS analysis revealed the presence of a byproduct present in the reagent. The byproduct was identified as (2,4,6-triisopropylphenoxy)triethoxysilane. All efforts to separate these materials were unsuccessful, due to their similar polarity and structure. However, in the conditions of the cross-coupling reactions, this byproduct showed no reactivity. Thus, it was used in catalysis without further purification, taking into account the purity of the siloxane for the calculation of the quantities.

^1H NMR (500 MHz, CDCl_3) δ 7.03 (s, 2H), 3.86 (q, $J = 7.1$ Hz, 7H), 3.72 (sept, $J = 6.7$ Hz, 2H), 2.85 (sept, $J = 6.7$ Hz, 1H), 1.28 – 1.19 (m, 27H). GC-MS: MS (EI+, 70 eV): m/z (%): 266 (10) $[\text{MZ}]^+$, 243 (10), 163 (100) $[\text{Si}(\text{OEt})_3]^+$.

4.3. Synthesis of Palladium complexes

$[\text{PdCl}_2(\text{IDM})(3\text{-Clpy})]$

This palladium complex was synthesized according to the reported synthesis of $[\text{PdCl}_2(\text{IDM})(\text{py})]$ using 3-chloropyridine as solvent instead of pyridine.⁸⁴

^1H NMR (500 MHz, CDCl_3) δ 9.05 (dd, $J = 2.4, 0.6$ Hz, 1H), 8.95 (dd, $J = 5.5, 1.4$ Hz, 1H), 7.78 (ddd, $J = 8.2, 2.4, 1.3$ Hz, 1H), 7.33 (ddd, $J = 8.2, 5.5, 0.7$ Hz, 1H), 6.90 (s, 2H), 4.14 (s, 6H). ^{13}C NMR (126 MHz, CDCl_3) δ 150.23, 149.13, 147.75, 138.07, 124.84, 123.07, 37.94. Elemental analysis calculated for $\text{C}_{10}\text{H}_{12}\text{Cl}_3\text{N}_3\text{Pd}$: C, 31.04; H, 3.13 N, 10.86. Found: C, 31.28; H, 3.11; N, 11.02.

$[\text{PdCl}(\mu\text{-Cl})(\text{IDM})]_2$

In air, a flask was charged with 36 mg of PdCl_2 (0.186 mmol) and 68.4 mg of $[\text{PdCl}_2(\text{IDM})_2]$ (0.186 mmol). The mixture of solids was refluxed for 36 hours in 50 mL of acetone. The solution was filtered through a pad of Celite. The crude and the pad were washed with abundant boiling acetone (3 x 20 mL). The solvent was removed until 2 mL of acetone remained in the solution. At this volume, fine orange crystals started to form. Slow addition of 30 mL of hexane led to the formation of 76 mg of an orange solid, which was filtered and dried under vacuum. Yield: 75%.

^1H NMR (500 MHz, CDCl_3) δ 6.89 (s, 2H), 4.19 (s, 6H). ^{13}C NMR (126 MHz, CDCl_3) δ 141.11, 123.42, 38.09. Elemental analysis calculated for $\text{C}_{10}\text{H}_{16}\text{Cl}_4\text{N}_4\text{Pd}_2$: C, 21.96; H, 2.95 N, 10.24. Found: C, 22.12; H, 3.01; N, 10.43.

4.4. General procedure of the cross-coupling reactions

The organic products obtained in the catalytic cross-coupling reactions are common products reported in the literature. In all cases, the NMR chemical shifts matched the ones reported in the literature. GC-MS analyses were used in all cases to confirm the expected molecular weight and structure.

Optimization of the Cu source (Table II-3). A screw-capped Schlenk flask was charged with the appropriate amount of the Cu salt and the fluoride promoter specified in each entry of the table. The solids were stored under N₂ atmosphere in the flask with a magnetic stir bar. Under a strong current of N₂, 1 mL of a separately prepared stock solution in DMF was transferred via syringe, containing 0.061 mmol of I-Ph-CF₃, and 0.12 mmol of MesSi(OEt)₃ and 0.0012 mmol of [PdCl₂(AsPh₃)₂]. The flask was heated at 110 °C until completion of the reaction or specified time. The reactions were monitored by ¹⁹F NMR on samples taken under N₂ atmosphere.

Yields of reactions in Table 1 were determined by ¹⁹F NMR integration. The products could also be isolated after chromatography on silica with hexane as eluent.

Optimization of the Pd source (Table II-4)

A screw-capped Schlenk flask was charged with the appropriate amount of the Pd catalyst (0.0012 mmol) (and 0.0024 mmol of XPhos for entry 5) specified in each entry of the table and 0.061 mmol of CuF₂ weighed in air as fast as possible. The solids were stored under N₂ atmosphere in the flask with a magnetic stir bar. Under a strong current of N₂, 1 mL of a separately prepared stock solution in DMF was transferred via syringe, containing 0.061 mmol of I-Ph-CF₃, and 0.12 mmol of Mes-Si(OEt)₃. The flask was heated at 110 °C until completion of the reaction or specified time. The reactions were monitored by ¹⁹F NMR on samples taken under N₂ atmosphere.

Yields of reactions in Table 2 were determined by ¹⁹F NMR integration. The products were isolated after chromatography on silica with hexane as eluent.

Copper-promoted Hiyama coupling of I-Ar with various ArSi(OEt)₃

Stock solutions were used to measure accurately the quantities of all the reagents. Identical results are obtained if they are added independently.

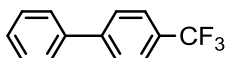
A screw-capped Schlenk flask was charged with 0.061 mmol of CuF₂ weighed in air as fast as possible. The solid was stored under N₂ atmosphere in the flask with a magnetic stir bar. Under a strong current of N₂, 1 mL of a separately prepared stock solution in DMF was transferred via syringe, containing 0.061 mmol of I-Ar, 0.12 mmol of the appropriate silane and 0.0012 mmol of [PdCl₂(IDM)(AsPh₃)]. The flask was heated at 110 °C until completion of the reaction or specified time. All reactions were monitored by ¹⁹F NMR on samples taken under N₂ atmosphere.

Termination of the reaction and yields were determined by GC-MS using Ph-Ph as internal standard of the reaction mixture or ^{19}F NMR integration when possible, of samples taken under N_2 atmosphere. Good correlation was found in all cases. The products could also be isolated after chromatography on silica with hexane as eluent.

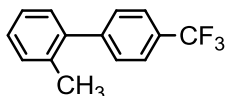
Isolation of the organic products

Determination of the isolated yields was carried out running the reactions in double scale (0.122 mmol of aryl iodide). After termination of the reaction, 1 mL of a 2M solution of KF was added and the reaction crude was heated at 110 °C for one hour. A saturated NH_4Cl solution in water was added until neutralization (usually 2 mL are required). The aqueous phase was extracted with Et_2O (3x 10mL). All the organic layers were gathered and dried over MgSO_4 . The solvent was removed under reduced pressure and the sample was dissolved in hexane and filtered through a short pad of silica. After solvent evaporation, the product is usually obtained pure. The products could also be isolated after chromatography on silica with hexane as eluent.

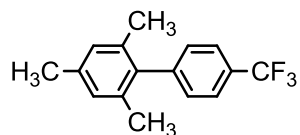
The isolated products were found exempt of AsPh_3 at the detection level of GC-MS. Selected isolated products were analyzed by the ICP-MS technique. In all cases the palladium and arsenic concentration in the cross-coupling products was found to be $< 1 \mu\text{g/g}$.



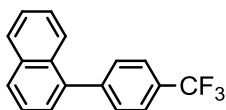
^1H NMR (500 MHz, CDCl_3): $\delta = 7.70\text{--}7.65$ (m, 4H), 7.63–7.55 (m, 2H), 7.50–7.35 (m, 3H). ^{19}F NMR (450 MHz, CDCl_3): $\delta = -61.3$. GC-MS: MS (EI+, 70 eV): m/z (%): 222 (100) $[\text{M}]^+$.



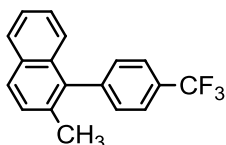
^1H NMR (500 MHz, CDCl_3): $\delta 7.70$ (d, 2 H, $J = 8.0$ Hz), 7.46 (d, 2 H, $J = 8.5$ Hz), 7.30 (m, 3 H), 7.24 (d, 1 H, $J = 7.5$ Hz) 2.29 (s, 3 H). ^{19}F NMR (450 Hz, CDCl_3) $\delta -60.8$. GC-MS: MS (EI+, 70 eV): m/z (%): 236 (100) $[\text{M}]^+$.



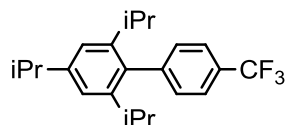
^1H NMR (500 MHz, CDCl_3) $\delta 7.72$ (d, $J = 8.1$ Hz, 2H), 7.31 (d, $J = 8.2$ Hz, 2H), 7.01 (s, 2H), 2.34 (s, 3H), 2.03 (s, 6H). ^{19}F NMR (450 Hz, CDCl_3) $\delta -62.36$. GC-MS: MS (EI+, 70 eV): m/z (%): 264 (100) $[\text{M}]^+$.



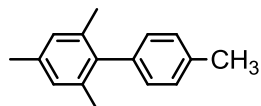
^1H NMR (500 MHz, CDCl_3) δ 7.5 (m, 4H), 7.63 (d, $J = 7.8$ Hz, 2H), 7.78 (d, $J = 8.1$ Hz, 2H), 7.84 (d, $J = 8.4$ Hz, 1H), 7.94 (t, $J = 7.8$ Hz, 2H). ^{19}F NMR (470 MHz, CDCl_3) δ -62.40. GC-MS: MS (EI+, 70 eV): m/z (%): 272 (100) [MZ] $^+$.



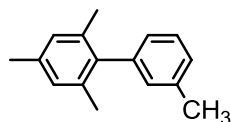
^1H NMR (400 MHz, CDCl_3) δ 7.84 – 7.64 (m, 4H), 7.35 (m, 4H), 7.31 – 7.20 (m, 2H), 2.16 (s, 3H). ^{19}F NMR (376 MHz, CDCl_3) δ -62.46. GC-MS: MS (EI+, 70 eV): m/z (%): 286 (100) [MZ] $^+$.



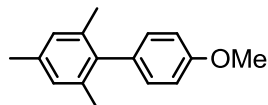
^1H NMR (500 MHz, CDCl_3) δ 7.66 (d, $J = 7.9$ Hz, 2H), 7.31 (d, $J = 7.9$, 2H), 7.23-7.19 (m, 2H), 7.07 (s, 2H), 2.95 (hept, $J = 7.0$ Hz, 1H), 2.50 (hept, $J = 6.9$ Hz, 2H), 1.31 (d, $J = 7.0$, 6H), 1.08 (d, $J = 6.9$ Hz, 12H). ^{19}F NMR (450 Hz, CDCl_3) δ -62.32. GC-MS: MS (EI+, 70 eV): m/z (%): 348 (50) [MZ] $^+$, 249 (100).



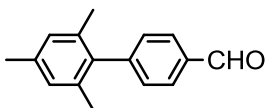
^1H NMR (500 MHz, CDCl_3) δ 7.24 (d, $J = 7.8$ Hz, 2H), 7.04 (d, $J = 7.8$ Hz, 2H), 6.95 (s, 2H), 2.42 (s, 3H), 2.35 (s, 3H), 2.03 (s, 6H). GC-MS: MS (EI+, 70 eV): m/z (%): 210 (90) [MZ] $^+$, 195 (100) [$\text{MZ}-\text{CH}_3$] $^+$.



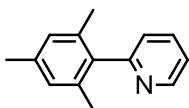
^1H NMR (500 MHz, CDCl_3) δ 7.30 (t, $J = 7.5$ Hz, 1H), 7.14 (d, $J = 7.5$, 1H), 6.96 – 6.91 (m, 4H), 2.38 (s, 3H), 2.33 (s, 3H), 2.01 (s, 6H). GC-MS: MS (EI+, 70 eV): m/z (%): 210 (82) [MZ] $^+$, 195 (100) [$\text{MZ}-\text{CH}_3$] $^+$.



^1H NMR (500 MHz, CDCl_3) δ 7.07 – 7.03 (m, 2H), 6.97 – 6.90 (m, 4H), 3.85 (s, 3H), 2.32 (s, 3H), 2.01 (s, 6H). GC-MS: MS (EI+, 70 eV): m/z (%): 226 (100) [MZ] $^+$.



^1H NMR (500 MHz, CDCl_3) δ 10.06 (s, 1H), 7.94 (d, $J = 8.1$ Hz, 2H), 7.32 (d, $J = 8.1$ Hz, 2H), 6.95 (s, 2H), 2.33 (s, 3H), 1.98 (s, 6H). GC-MS: MS (EI+, 70 eV): m/z (%): 224 (100) [MZ] $^+$.



^1H NMR (500 MHz, CDCl_3) δ 8.71 (m, 1H), 7.74 (m, 1H), 7.28 – 7.20 (m, 2H), 6.92 (s, 2H), 2.32 (s, 3H), 2.01 (s, 6H). GC-MS: MS (EI+, 70 eV): m/z (%): 196 (100) [$\text{MZ}-1$] $^+$, 181 (30) [$\text{MZ}-\text{Me}$] $^+$, 147 (100).

4.5. Mechanistic Studies

a) Reaction of copper salts and (aryl)triethoxysilanes

10 mg of the corresponding Cu salt were added to an NMR tube. Using a Schlenk adaptor for NMR tubes, the sample was kept under N_2 atmosphere. Under a strong current of N_2 , 0.5 mL of DMF, 10 equivalents of $\text{C}_6\text{F}_5\text{-Si(OEt)}_3$ and 1 equivalent of $\text{CF}_3\text{-Ph}$ as internal standard were added via syringe. A capillary filled with acetone- d_6 was added and the NMR tube was closed and wrapped with Teflon tape. The reaction was monitored by ^{19}F NMR.

Formation of $[(\text{C}_6\text{F}_5)\text{Cu}(\text{DMF})]$ from CuF_2 and $(\text{C}_6\text{F}_5)\text{Si(OEt)}_3$

CuF_2 did not react completely after 24 hours at RT. Due to the presence of paramagnetic Cu^{II} , the signals in the ^{19}F were broad. *Meta* and *para* fluorines of $[(\text{C}_6\text{F}_5)\text{Cu}(\text{DMF})]$ were overlapped with *para* and *meta* fluorine atoms of $(\text{C}_6\text{F}_5)\text{Si(OEt)}_3$ and $\text{C}_6\text{F}_5\text{H}$. *Ortho* fluorine atoms were well resolved.

The ^{19}F NMR spectrum is shown in Figure II-1.

Formation of $[(\text{C}_6\text{F}_5)\text{Cu}(\text{bipy})]$ from $[\text{CuF}_2(\text{bipy})]\cdot 3\text{H}_2\text{O}$ and $(\text{C}_6\text{F}_5)\text{Si(OEt)}_3$

A quantitative NMR yield was obtained by integration of the meta fluorine atoms with respect to the internal standard Ph-CF_3 . The signal corresponding to the ortho fluorine atoms is broad, due to fast relaxation.

^{19}F NMR of the Reaction of $[\text{CuF}_2(\text{bipy})]\cdot 3\text{H}_2\text{O}$ with $(\text{C}_6\text{F}_5)\text{Si(OEt)}_3$ at RT. The spectrum was acquired at -50°C . Integrals are referred to an internal standard (Ph-CF_3). The

large signals in the range -164.65 to -164.9 correspond to F_{meta} of C_6F_5H . Six molecules of C_6F_5H per copper are formed in the reaction by hydrolysis with the water molecules in the Cu^{II} reagent. $C_6F_5-C_6F_5$ (0.5 eq. per copper) are also formed according with Scheme II-19 in the main text.

^{19}F NMR (470 MHz, protic DMF, lock signal referenced to an acetone-*d*6 capillary) δ - 110.86 (bs, 2F), -164.53 (t, J_{F-F} = 19.2 Hz, 1F), (-164.94-165.21) (m, 2F). The ^{19}F NMR spectrum is shown in Figure II-2.

Formation of $[(C_6F_5)Cu(PPh_3)_3]$ from $[CuF(PPh_3)_3 \cdot 2MeOH]$ and three equivalents of $C_6F_5-Si(OEt)_3$

A quantitative NMR yield was obtained.

^{19}F NMR (470 MHz, protic DMF, lock signal referenced to an acetone-*d*6 capillary) δ - 110.73 (m, 2F), -163.53 (m, 3F). The ^{19}F NMR spectrum is shown in Figure II-3.

^{31}P NMR (202 MHz, protic DMF, lock signal referenced to an acetone-*d*6 capillary) δ -5.00 (bs).

b) Cu/Pd and Si/Cu/Pd transmetalation experiments

$[(C_6F_5)Cu(bipy)] + trans-[Pd(C_6F_5)(Br)(PPh_3)_2]$

Following the reaction procedure described in the paragraph “*Reaction of Copper salts and aryltris(ethoxy)silanes*”, a solution containing $[(C_6F_5)Cu(bipy)]$ was transferred via syringe to a NMR tube charged with 0.2 equivalents of *trans*- $[Pd(C_6F_5)(Br)(PPh_3)_2]$ under N_2 atmosphere. A capillary filled with acetone-*d*6 was added and the NMR tube was closed and wrapped with Teflon tape. The reaction was monitored by ^{19}F NMR. Upon adding a solution of the copper organometallic to the NMR tube containing the palladium complex, *trans*- $[Pd(C_6F_5)_2(PPh_3)(DMF)]$ was formed in quantitative yield.

trans-[Pd(C₆F₅)(Br)(PPh₃)₂]

^{19}F NMR (470 MHz, protic DMF, lock signal referenced to an acetone-*d*6 capillary) δ - 117.86 (m, 2F), -163.87 (m, 2F), -164.38 (t, J = 20.1 Hz).

^{31}P NMR (202 MHz, protic DMF, lock signal referenced to an acetone-*d*6 capillary) δ 23.60 (m).

trans-[Pd(C₆F₅)₂(PPh₃)(DMF)]

^{19}F NMR (470 MHz, protic DMF, lock signal referenced to an acetone-*d*6 capillary) δ - 112.61 (m, 2F), -166.88 (m, 2F), -167.25 (m, 1F).

^{31}P NMR (202 MHz, protic DMF, lock signal referenced to an acetone-*d*6 capillary) δ 21.88 (q, J_{P-F} = 12.1 Hz).

[(Mes)Cu(bipy)] + *trans*-[Pd(C₆H₄CF₃)(I)(PPh₃)₂]

7.9 mg of [CuF₂(bipy)]·3H₂O were added to a Schlenk flask. The sample was kept under N₂ atmosphere. Under a strong current of N₂, 0.5 mL of DMF, and 73 μL (10 equivalents with respect to the Cu complex) of Mes-Si(OEt)₃ were added via syringe. When the Cu salt was dissolved after stirring at RT, the solution containing [(Mes)Cu(bipy)] was transferred via syringe to a NMR tube charged with 0.2 equivalents of *trans*-[Pd(C₆H₄CF₃)(I)(PPh₃)₂] under N₂ atmosphere. A capillary filled with acetone-*d*₆ was added and the NMR tube was closed and wrapped with Teflon tape. The NMR tube was heated at 110 °C for an hour. After this time, the reaction was checked by ¹⁹F NMR and Mes-C₆H₄-CF₃ was formed in quantitative yield.

[CuF(PPh₃)₃·2MeOH] + *trans*-[Pd(C₆F₅)(Br)(PPh₃)₂] + C₆F₅-Si(OEt)₃

An NMR tube was charged with 5 mg of *trans*-[Pd(C₆F₅)(Br)(PPh₃)₂] (0.0057 mmol) and 24 mg of [CuF(PPh₃)₃·2MeOH] (0.028 mmol) in air. Using a Schlenk adaptor for NMR tubes, the sample was kept under N₂. 0.5 mL of DMF, 15 μL of C₆F₅-Si(OEt)₃ (0.057 mmol) and 1 equivalent of CF₃-Ph (internal standard) were added via syringe under a strong current of N₂. A capillary filled with acetone-*d*₆ was added and the NMR tube was closed and wrapped with Teflon tape. The reaction was monitored by ¹⁹F NMR. The reaction was completed in 20 hours, yielding quantitative formation of *trans*-[Pd(C₆F₅)₂(PPh₃)₂].

***trans*-[Pd(C₆F₅)₂(PPh₃)₂]**

The NMR chemical shifts match with those reported in the literature.⁸⁵

¹⁹F NMR (470 MHz, protic DMF, lock signal referenced to an acetone-*d*₆ capillary) δ -115.25 (m, 2F), -164.05 (m, 3F).

³¹P NMR (202 MHz, protic DMF, lock signal referenced to an acetone-*d*₆ capillary) δ 18.01 (m).

[CuF(PPh₃)₃·2MeOH] + *trans*-[Pd(C₆H₄CF₃)(I)(PPh₃)₂] + Mes-Si(OEt)₃

An NMR tube was charged with 5 mg of *trans*-[Pd(C₆H₄CF₃)(I)(PPh₃)₂] (0.0057 mmol) and 24 mg of [CuF(PPh₃)₃·2MeOH] (0.028 mmol) in air. Using a Schlenk adaptor for NMR tubes, the sample was kept under N₂. 0.5 mL of DMF, 16.5 μL of Mes-Si(OEt)₃ (0.057 mmol) and 1 equivalent of C₆F₆ (internal standard) were added via syringe under a strong current of N₂. A capillary filled with acetone-*d*₆ was added and the NMR tube was closed and wrapped with Teflon tape. The reaction was monitored by ¹⁹F NMR. The reaction was completed upon mixing, yielding quantitative formation of the organic product CF₃-Ph-Mes and [Pd(PPh₃)₂]. The results were confirmed by GC-MS analysis of the reaction crude.

The ³¹P NMR spectrum shows a broad signal at 0 ppm, as a result of a fast exchange between [Pd(PPh₃)_n] and [XCu(PPh₃)₃]. Addition of an excess of I-Ph-CF₃ regenerates complex [Pd(C₆H₄CF₃)(I)(PPh₃)₂] as a sharp signal, showing no exchange with

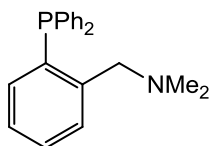
$\text{XCu}(\text{PPh}_3)_3$ in the NMR time scale, and shifts back the signal corresponding to the copper complex to -5 ppm.

c) *Direct Si/Pd transmetalation of bulky groups*

An NMR tube was charged with 7.5 mg of *trans*- $[\text{Pd}(\text{C}_6\text{H}_4\text{CF}_3)(\text{F})(\text{PPh}_3)_2]$ (0.0094 mmol) under N_2 . 0.5 mL of DMF, 14 μL of $\text{Mes-Si}(\text{OEt})_3$ (0.047 mmol) and 1 equivalent of C_6F_6 (internal standard) were added via syringe under a strong current of N_2 . A capillary filled with acetone-*d*6 was added and the NMR tube was closed and wrapped with Teflon tape. The reaction was monitored by ^{19}F NMR. After 24h, the reaction reached equilibrium. 10 % of $\text{CF}_3\text{-Ph-Mes}$ and 70 % of $\text{CF}_3\text{-Ph-H}$ were quantified by integration of the ^{19}F spectrum, in comparison with the internal standard. Both products were identified by spiking the tube with authentic samples. Some unidentified signals were present in the ^{19}F spectrum, accounting for the remaining 20 % of the ^{19}F signal.

4.6. Additional experiments

Copper-catalyzed Hiyama coupling in the presence of P-N ligands



P,N = 1-(2-(diphenylphosphino)phenyl)-N,N-dimethylmethanamine

A screw-capped Schlenk flask with was charged with 12 mg of dry CsF, (1.5 equivalents), 1.2 mg (10% in mmol) of CuI and 2 mg (10% in mmol) of the P-N ligand. The solids were stored under N_2 atmosphere in the flask with a magnetic stir bar. Under a strong current of N_2 , 1 mL of a separately prepared stock solution in DMF was transferred via syringe, containing 0.061 mmol of I-Ph- CF_3 , and 0.12 mmol of $\text{Mes-Si}(\text{OEt})_3$. The flask was heated at 120 $^\circ\text{C}$ until completion of the reaction or specified time. The reaction was monitored by ^{19}F NMR, of samples taken under N_2 atmosphere. *p*-Mes- $\text{C}_6\text{H}_4\text{-CF}_3$ was not obtained as a product of this reaction.

5. References

1. Denmark, S. E.; Baird, J. D. *Chem. Eur. J.* **2006**, *12*, 4954–4963.
2. (a) Denmark, S. E.; Sweis, R. F. *Organosilicon Compounds in Cross-Coupling Reactions*; **2008**; pp. 163–216. Wiley-VCH Verlag GmbH & Co. KGaA, Weinheim, Germany. (b) Denmark, S. E.; Sweis, R. F. *J. Am. Chem. Soc.* **2001**, *123*, 6439–6440. (c) Denmark, S. E.; Smith, R. C.; Chang, W. T.; Muhuhi, J. M.; *J. Am. Chem. Soc.* **2009**, *131*, 3104–3118.
3. (a) (a) Tamao, K.; Kobayashi, K.; Ito, Y. *Tetrahedron Lett.* **1989**, *30*, 6051–6054. For other examples see: (b) Mowery, M. E.; DeShong, P. *J. Org. Chem.* **1999**, *64*, 1684–1688. (c) Manoso, A. S.; Ahn, C.; Soheili, A.; Handy, C. J.; Correia, R.; Seganish, W. M.; DeShong, P. *J. Org. Chem.* **2004**, *69*, 8305–8314.
4. (a) Yoshida, J.; Tamao, K.; Yamamoto, H.; Kakui, T.; Uchida, T.; Kumada, M. *Organometallics* **1982**, *1*, 542–549. Another example: (b) Hosomi, A., Kohra, S., and Tominga, Y. *Chem. Pharm. Bull. Jpn.*, **1988**, *36*, 4622–4625.
5. Pilcher, A. S.; Ammon, H. L.; DeShong, P. *J. Am. Chem. Soc.* **1995**, *117*, 5166–5167.
6. Hatanaka, Y. and Hiyama, T. *J. Org. Chem.* **1988**, *53*, 918–920.
7. Walsh, R. *Acc. Chem. Res.* **1981**, *1537*, 246–252.
8. The Pd-C bond dissociation energy was extracted from: Simoes, J. A. M.; Beauchamp, J. L. *Chem. Rev.* **1990**, *90*, 629–688. The Pd-halogen bond dissociation energy was obtained from: Lan, Y.; Liu, P.; Newman, S. G.; Lautens, M.; Houk, K. N. *Chem. Sci.* **2012**, *3*, 1987. Experimental information concerning Pd-halide dissociation can be obtained herein: Casares, J. A.; Coco, S.; Espinet, P.; Lin, Y. *Organometallics*, **1995**, 3058–3067.
9. (a) Pérez-Temprano, M. H.; Nova, A.; Casares, J. A.; Espinet, P. *J. Am. Chem. Soc.* **2008**, *130*, 10518–10520. (b) Cotter, W. D.; Barbour, L.; McNamara, K. L.; Hechter, R.; Lachicotte, R. J. *J. Am. Chem. Soc.* **1998**, *120*, 11016–11017. (c) Carrasco, D.; Pérez-Temprano, M. H.; Casares, J. A.; Espinet, P. *Organometallics*, **2014**, *33*, 3540–3545. (d) Fuentes, B.; García-Melchor, M.; Lledós, A.; Maseras, F.; Casares, J. A.; Ujaque, G.; Espinet, P. *Chem. Eur. J.* **2010**, *16*, 8596–8599. (e) (a) Casares, J. A.; Espinet, P.; Fuentes, B.; Salas G. *J. Am. Chem. Soc.* **2007**, *129*, 3508.
10. Pauling, L.C. *The Nature of the Chemical Bond*, 3rd edition, **1960**. Cornell University Press, Ithaca, NY.

11. (a) Chuit, C.; Corriu, R. J. P.; Reye, C.; Young, J. C. *Chem. Rev.* **1993**, *93*, 1371–1448. (b) Ramsden, C. A. *Chem. Soc. Rev.*, **1994**, *23*, 111–118. (c) Holmes, R. R. *Chem. Rev.* **1996**, *96*, 927–950. (d) Rendler, S.; Oestreich, M. *Synthesis*, **2005**, 1727–1747.
12. Sugiyama, A.; Ohnishi, Y. Y.; Nakaoka, M.; Nakao, Y.; Sato, H.; Sakaki, S.; Nakao, Y.; Hiyama, T. *J. Am. Chem. Soc.* **2008**, *130*, 12975–12985.
13. Denmark, S. E.; Ober, M. H. *Adv. Synth. Catal.* **2004**, *346*, 1703–1714.
14. Zongker, D.; *Annals of Improbable Research*, **2006**, *12*, 16–21.
15. Gordillo, A.; Ortuño, M. a.; López-Mardomingo, C.; Lledós, A.; Ujaque, G.; De Jesús, E. *J. Am. Chem. Soc.* **2013**, *135*, 13749–13763.
16. Magnusson, E. *J. Am. Chem. Soc.* **1990**, *112*, 7940–7951.
17. Hoffmann, R.; Howell, J. M.; Muetterties, E. L. *J. Amer. Chem. Soc.* **1972**, *94*, 3047–3058.
18. Brook, M. A. *Silicon in Organic, Organometallic and Polymer Chemistry*; Wiley: New York, **2000**.
19. Shukla, K. H.; DeShong, P. *J. Org. Chem.* **2008**, *73*, 6283–6291.
20. (a) Amatore, C.; Grimaud, L.; Le Duc, G.; Jutand, A. *Angew. Chem. Int. Ed.* **2014**, *53*, 6982–6985. Similar findings have been reported for the Suzuki Coupling: (b) Amatore, C.; Jutand, A.; Leduc, G. *Angew. Chem. Int. Ed.* **2012**, *51*, 1379–1382.
21. Grushin, V.; Marshall, W. *J. Am. Chem. Soc.* **2006**, 12644–12645.
22. Shukla, K. H.; DeShong, P. *J. Org. Chem.* **2008**, *73*, 6283–6291.
23. (a) Denmark, S. E.; Regens, C. S. *Acc. Chem. Res.* **2008**, *41*, 1486–1499. (b) Denmark, S. E.; Sweis, R. F.; Wehrli, D. *J. Am. Chem. Soc.* **2004**, *126*, 4865–4875. (c) Denmark, S. E.; Sweis, R. F. *J. Am. Chem. Soc.* **2004**, *126*, 4876–4882. (d) Denmark, S. E.; Smith, R. C. *J. Am. Chem. Soc.* **2010**, *132*, 1243–1245.
24. (a) Tymonko, S. a.; Smith, R. C.; Ambrosi, A.; Denmark, S. E. *J. Am. Chem. Soc.* **2015**, DOI: 10.1021/jacs.5b02515. (b) Tymonko, S. a.; Smith, R. C.; Ambrosi, A.; Ober, M. H.; Wang, H.; Denmark, S. E. *J. Am. Chem. Soc.* **2015**, DOI: 10.1021/jacs.5b02518
25. Denmark, S. E.; Smith, R. C.; Chang, W. T. T. *Tetrahedron*, **2011**, *67*, 4391–4396.
26. Denmark, S. E.; Liu, J. H. C. *Angew. Chem. Int. Ed.* **2010**, *49*, 2978–2986.

27. This is supported by a recent estimation of the total number of publications and patents on cross-coupling reactions through 2010 to April 2014, which affords the following scores and trend: Suzuki Miyaura, 10175/15883 > Heck, 4029/5816 > Sonogashira, 3623/5689 > Stille, 2380/3537 > Negishi, 429/ 737 > Buchwald-Hartwig, 253/498 > Kumada-Corriu, 136/298 > Hiyama-Denmark, 91/172 > carbonyl α -arylation, 113/193. Johansson Seechurn, C. C. C.; Deangelis, A.; Colacot, T. J. *New Trends in Cross-Coupling: Theory and Applications*; Colacot, T. J., Ed.; The Royal Society of Chemistry: Cambridge, **2015**; chapter 1, pp 4.
28. (a) Zhou, H.; Moberg, C.; *J. Am. Chem. Soc.* **2012**, 134, 15992–15999.
29. (a) Gilman, H.; Smart, G. N. *R. J. Org. Chem.* **1954**, 19, 441–450. (b) Smitrovich, J. H.; Woerpel, K. a. *J. Org. Chem.* **1996**, 61, 6044–6046.
30. (a) Bringmann, G.; Gulder, T.; Gulder, T. A. M.; Breuning, M. *Chem. Rev.* **2011**, 111, 563. (b) Kozlowski, M. C.; Morgan, B. J.; Linton, E. C.; *Chem. Soc. Rev.* **2009**, 38, 3193.
31. Wanka, L.; Iqbal, K.; Schreiner P. R. *Chem. Rev.* **2013**, 113, 3516.
32. For stabilization of unstable compounds, see (a) Power, P. P. *J. Organomet. Chem.* **2004**, 689, 3904–3919. (b) Free NHC carbenes are stable due to the steric protection of hindered aryls, see: Melaimi, M.; Soleilhavoup, M.; Bertrand, G. *Angew. Chem. Int. Ed.* **2010**, 49, 8810–8849. Its use is widespread in catalysis; see (c) Kantchev, E. A. B.; O'Brien, C. J.; Organ, M. G.; *Angew. Chem. Int. Ed.* **2007**, 46, 2768–2813.
33. Suzuki, A.; *Angew. Chem. Int. Ed.* **2011**, 50, 6722 – 6737.
34. (a) Giannerini, M.; Fañanás-Mastral, M.; Feringa, B. L. *Nat. Chem.* **2013**, 5, 667–672. (b) Giannerini, M.; Hornillos, V.; Vila, C.; Fañanás-Mastral, M.; Feringa, B. L. *Angew. Chem. Int. Ed.* **2013**, 52, 13329–13333.
35. (a) Dai, C; Fu, G. *J. Am. Chem. Soc.* **2001**, 123, 2719. (b) Organ, M. G.; Abdel-Hadi, M.; Avola, S.; Hadei, N.; Nasielski, J.; O'Brien, C. J.; Valente, C. *Chem. Eur. J.* **2007**, 13, 150. (c) Wolf, C.; Xu, H. *J. Org. Chem.* **2008**, 73, 162. (d) Hartmann, C. E.; Nolan, S. P.; Cazin, C. S. J. *Organometallics*, **2009**, 28, 2915.
36. (a) Çalimsiz, S.; Sayah, M.; Mallik, D.; Organ, M. G. *Angew. Chem. Int. Ed.* **2010**, 49, 2014. (b) Organ, M. G.; Çalimsiz, S.; Sayah, M.; Hoi, K. H.; Lough, A. L. *Angew. Chem. Int. Ed.* **2009**, 48, 2383. (c) Wu, L.; Drinkel, E.; Gaggia, F.; Capolicchio, S.; Linden, A.; Falivene, L.; Cavallo, L.; Dorta, R. *Chem. Eur. J.* **2011**, 17, 12886. (d) Chartoire, A.; Lesieur, M.; Falivene, L.; Slawin, A. M. Z.; Cavallo, L.; Cazin, C. S. J.; Nolan, S. P. *Chem. Eur. J.* **2012**, 18, 4517.
37. Zhao, Q.; Li, C.; Senanayake, C. H.; Tang, W. *Chem. Eur. J.* **2013**, 19, 2261.

38. Hall, D. G. *Structure, Properties, and Preparation of Boronic Acid Derivatives. Overview of Their Reactions and Applications*. Wiley-VCH: Weinheim, Germany, **2006**; pp. 1–99.
39. Szilvasi, T.; Veszprémi, T. *Catalysis* **2013**, *3*, 1984–1991.
40. (a) delPozo, J.; Carrasco, D.; Pérez-Temprano, M. H.; García-Melchor, M.; Álvarez, R.; Casares, J. A.; Espinet, P. *Angew. Chem. Int. Ed.* **2013**, *52*, 2189–2193. (b) delPozo, J.; Casares, J. A.; Espinet, P. *Chem. Commun* **2013**, *49*, 7246–7248.
41. Weber, D.; Gagné, M. R. *Chem. Commun.* **2011**, *47*, 5172–5174.
42. Zhang, J.; Chen, H.; Wang, B.; Liu, Z.; Zhang, Y. *Org. Lett.* **2015**, *17*, 2768–2771.
43. Herron, J. R.; Ball, Z. T. *J. Am. Chem. Soc.* **2008**, *130*, 16486–16487.
44. (a) Herron, J. R.; Russo, V.; Valente, E. J.; Ball, Z. T. *Chem. Eur. J.* **2009**, *15*, 8713–8716. (b) Russo, V.; Herron, J. R.; Ball, Z. T. *Org. Lett.* **2010**, *12*, 220–223.
45. (a) Arimoto, K.; Sensui, I.; Hosomi, A. **1997**, *38*, 3977–3980. (b) Nishihara, Y.; Takemura, M.; Mori, A.; Osakada, K. *J. Organomet. Chem.* **2001**, *620*, 282–286. (c) Nishihara, Y.; Takemura, M.; Mori, A.; Osakada, K. *J. Organomet. Chem.* **2001**, *620*, 282–286.
46. (a) Chinchilla, R.; Nájera, C. *Chem. Soc. Rev.* **2011**, *40*, 5084. (b) Chinchilla, R.; Nájera, C. *Chem. Rev.* **2007**, *107*, 874–922. For an experimental study of the Cu/Pd transmetalation see: (c) He, C.; Ke, J.; Xu, H.; Lei, A. *Angew. Chem. Int. Ed.* **2013**, *52*, 1527–1530. A computational study can be found herein: Sikk, L.; Tammiku-Taul, J.; Burk, P.; Kotschy, A. *J. Mol. Model.* **2012**, *18*, 3025–3033.
47. (a) Semba, K.; Nakao, Y. *J. Am. Chem. Soc.* **2014**, *136*, 7567–7570. (b) Logan, K. M.; Smith, K. B.; Brown, M. K. *Angew. Chem. Int. Ed.* **2015**, DOI: 10.1002/anie.201500396.
48. (a) Rodríguez, N.; Goossen, L. J. *Chem. Soc. Rev.* **2011**, *40*, 5030. Cu/Pd transmetalation is computationally addressed herein: (b) Fromm, A.; Van Wüllen, C.; Hackenberger, D.; Goossen, L. J. *J. Am. Chem. Soc.* **2014**, *136*, 10007–10023.
49. (a) Lesieur, M.; Lazreg, F.; Cazin, C. S. J. *Chem. Commun.* **2014**, *50*, 8927–8929. (b) Coia, N.; Bouyssi, D.; Balme, G. *European J. Org. Chem.* **2007**, 3158–3165. (c) Deng, J. Z.; Paone, D. V.; Ginnetti, A. T.; Kurihara, H.; Dreher, S. D.; Weissman, S. a.; Stauffer, S. R.; Burgey, C. S. *Org. Lett.* **2009**, *11*, 345–347.
50. (a) Pérez-Temprano, M. H.; Casares, J. A.; Espinet, P. *Chem. - A Eur. J.* **2012**, *18*, 1864–1884. (b) Allen, A. E.; MacMillan, D. W. C. *Chem. Sci.* **2012**, *3*, 633.

51. (a) Nakao, Y.; Takeda, M.; Matsumoto, T.; Hiyama, T. *Angew. Chem. Int. Ed.* **2010**, *49*, 4447–4450. (b) Denmark, S. E.; Baird, J. D. *Org. Lett.* **2004**, *6*, 3649–3652.
52. Hirabayashi, K.; Mori, A.; Kawashima, J.; Suguro, M.; Nishihara, Y.; Hiyama, T. *J. Org. Chem.* **2000**, *65*, 5342–5349.
53. Gurung, S. K.; Thapa, S. Vangala, A. S.; Giri, R. *Org. Lett.* **2013**, *15*, 5378
54. Casado, A. L.; Espinet, P. *Organometallics* **2003**, *22*, 1305.
55. Lam, P.Y.S.; Deudon, S.; Averill, K. M.; Li, R.; He, M. Y.; DeShong, P.; Clark, C. G. *J. Am. Chem. Soc.* **2000**, *122*, 7600.
56. Brasche, G.; Buchwald, S. L. *Angew. Chem. Int. Ed.* **2008**, *47*, 1932–1934. (b) Suess, A. M.; Ertern, M. Z.; Cramer, C. J.; Stahl, S. S.; *J. Am. Chem. Soc.* **2013**, *135*, 9797–9804.
57. (a) Ribas, X.; Jackson, D. A. ; Donnadieu, B.; Mahia, J.; Parella, T.; Xifra, R.; Hedman, B.; Hodgson, K. O.; Llobet, A.; Stack, T. D. P. *Angew. Chem. Int. Ed.* **2002**, *41*, 2991–2994.
58. Casitas, A.; Ribas, X. *Chem. Sci.* **2013**, *4*, 2301–2318.
59. Nebra, N.; Grushin, V. V. *J. Am. Chem. Soc.* **2014**, *136*, 16998.
60. Golubeva, E. N.; Gromov, O. I.; Zhidomirov, G. M. *J. Phys. Chem.* **2011**, *115*, 8147–8154.
61. (a) Chmielewski, P. J.; Latos-Grazyński, L.; Schmidt, I. *Inorg. Chem.* **2000**, *39*, 5475–5482. (b) Pawlicki, M.; Kańska, I.; Latos-Grazyński, L. *Inorg. Chem.* **2007**, *46*, 6575–6584. (c) Jacquet, J.; Salanouve, E.; Orio, M.; Vezin, H.; Blanchard, S.; Derat, E.; Desage-El Murr, M.; Fensterbank, L. *Chem. Commun.* **2014**, *50*, 10394–10397.
62. Zhang, H.; Yao, B.; Zhao, L.; Wang, D.; Xu, B.; Wang, M. *J. Am. Chem. Soc.* **2014**, *136*, 6326–6332.
63. (a) Chan, D. M. T.; Monaco, K. L.; Wang, R. P.; Winters, M. P. *Tetrahedron Lett.* **1998**, *39*, 2933. (b) Evans, D. A.; Katz, J. L.; West, T. R. *Tetrahedron Lett.* **1998**, *39*, 2937. (c) Lam, P. Y. S.; Clark, C. G.; Saubern, S.; Adams, J.; Winters, M. P.; Chan, D. M. T.; Combs, A. *Tetrahedron Lett.* **1998**, *39*, 2941. Selected reviews: (c) Qiao, J. X.; Lam, P. Y. S. *Synthesis*, **2011**, 829–856.
64. The copper(II) mediated formation of aryl ethers by Si-O activation of tetraalkoxysilanes has been recently reported: Bhadra S. Dzik W. I. Gooßen, L. J. *Synthesis*, **2013**, *45*, 2387.

65. (a) Ullmann, F.; Bielecki, J. *Chem. Ber.* **1901**, *34*, 2174–2185. (b) Ullmann, F. *Chem. Ber.* **1903**, *36*, 2382–384. (c) Ullmann, F.; Sponagel, P. *Chem. Ber.* **1905**, *38*, 2211–2212. Selected reviews: (d) Hassan, J.; Sévignon, M.; Gozzi, C.; Schulz, E.; Lemaire, M. *Chem. Rev.* **2002**, *102*, 1359–1469.
66. The copper(II) mediated formation of aryl ethers by Si-O activation of tetraalkoxysilanes has been recently reported: Bhadra S. Dzik W. I. Gooßen, L. J. *Synthesis*, **2013**, *45*, 2387.
67. Doshi, A.; Sundararaman, A.; Venkatasubbaiah, K.; Zakharov, L. N.; Rheingold, A. L.; Myahkostupov, M.; Piotrowiak, P.; Jäkle, F. *Organometallics* **2012**, *31*, 1546–1558.
68. (a) Panferova, L. I.; Miloserdov, F. M.; Lishchynskiy, A.; Martínez Belmonte, M.; Benet-Buchholz, J.; Grushin, V. V. *Angew. Chem. Int. Ed.* **2015**, DOI: 10.1002/ange.201500341. (b) Jardine, F. H.; Rule, L.; Vohra, A. G.; *J. Chem. Soc.* **1970**, 238.
69. Armarego, W. L.F.; Chai, C. L. L. *Purification of Laboratory Chemicals* (Fifth Edition). Elsevier, **2003**. ISBN: 978-0-7506-7571-0.
70. C. Amman, P. Meier and A. E. Merbach, *J. Magn. Reson.* **1982**, *46*, 319–321
71. A. H. Norbury, A. L. P. Sinha, *J. Inorg. Nucl. Chem.* **1973**, *35*, 1211–1218.
72. Miyaura, A. Suzuki, *Org. Synth. Coll.* **1993**, Vol. 8, 532, (note 8).
73. E. Lee, D. V. Yandulov, *J. Organometallic Chem.* **2011**, *696*, 4095–4103.
74. Corain, B.; Longato, B.; Favero, G.; Ajò, D.; Pilloni, G.; Russo, U.; Kreissl, F. R. *Inorg. Chim. Acta*, **1989**, *157*, 259–266.
75. O'Brien, Christopher J.; Kantchev, Eric Assen B.; Valente, Cory; Hadei, Niloufar; Chass, Gregory A.; Lough, Alan; Hopkinson, Alan C.; Organ, Michael G. *Chem. Eur. J.* **2006**, *12*, 4743 – 4748.
76. Uson, R.; Fornies, J.; Nalda, J. A.; Lozano, M. J.; Espinet, P.; Albeniz, A. C; *Inorganica Chimica Acta*, **1989**, *156*, 251–256
77. Chai, D. I.; Thansandote, P.; Lautens, M. *Chem. Eur. J.* **2011**, *17*, 8175–8188.
78. Pilon, M. C.; Grushin, V. V. *Organometallics* **1998**, *17*, 1774–1781.
79. Emsley, J.; Arif, M.; Bates, P. A.; Hursthouse, M. B. *J. Chem. Soc. Dalton Trans.* **1987**, 2397–2399.

80. Kazakova, V. V.; Gorbatshevich, O. B.; Skvortsova, S. a.; Demchenko, N. V.; Muzafarov, a. M. *Russ. Chem. Bull.* **2005**, *54*, 1350–1351.
81. Alonso, M. A.; Casares, J. A; Espinet, P.; Soulantica, K.; Orpen, A. G.; Phetmung, H.; *Organometallics* **2003**, *42*, 3856–3864.
82. Krasovskiy, A.; Knochel, P. *Angew. Chemie - Int. Ed.* **2004**, *43*, 3333–3336. (b) Sämann, C.; Dhayalan, V.; Schreiner, P. R.; Knochel, P. *Org. Lett.* **2014**, *16*, 2418–2421. (c) Sämann, C.; Haag, B.; Knochel, P. *Chem. Eur. J.* **2012**, *18*, 16145–16152.
83. Manoso, A. S.; Ahn, C.; Soheili, A.; Handy, C. J.; Correia, R.; Seganish, W. M.; DeShong, P. *J. Org. Chem.* **2004**, *69*, 8305–8314.
84. Zanardi, A.; Mata, J. a.; Peris, E. *Organometallics* **2009**, *28*, 4335–4339.
85. Uson, R.; Fornies, J.; Espinet, P.; Martinez, F.; Tomas, M.; *J. Chem. Soc., Dalton Trans.*, **1981**, 463- 465.

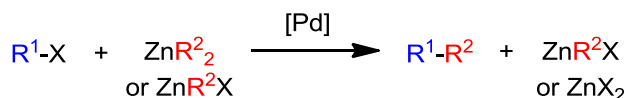
Chapter III

**Study of the secondary
transmetalations in the
Negishi reaction**

1. Introduction

The Negishi reaction is a wide scope and reliable cross-coupling process that can be applied to many substrates and tolerates different functions at the reagents. The performance of zinc organometallics is remarkable, not only in the laboratory scale, in which it has been used for the synthesis of complicated natural products, but also in the larger industrial scale.¹ Particularly, when alkyl–aryl or alkyl–alkyl couplings are involved, it becomes the best choice of all possible cross-coupling reactions, since the transmetalation of alkyl groups has been proved less-efficient and slower with nucleophiles other than the organozincs.²

The Negishi reaction is peculiar in that two types of organometallic reagents are available (ZnRX and ZnR_2). Both are actually used depending on the protocol. The choice of one or the other seems to be totally empirical or based on the ease of access to them.



Scheme III-1. General scheme of the Negishi reaction.

Organometallic complexes of zinc are more polar and nucleophilic than the corresponding boron, tin or silicon counterparts. These natural features turn them into very active transmetalating agents. As a matter of fact, palladium is not the only possible catalyst of these reactions, but also numerous examples with other more electropositive metals can be found, such as Co, Fe or Cu or Ni.³ Indeed, contrary to the common preponderancy of Pd in the manifold of cross-coupling reactions, nickel catalysis plays a central role in the Negishi coupling.⁴

1.1. Background

The use of organozincs in cross-coupling reactions with aryl halides and alkyl halides was first reported in the late 1970s by Negishi and coworkers.⁵ Very close in time, Fauvarque and Jutand disclosed the effective reaction between the Reformatsky reagent $\text{BrZnCH}_2\text{COOEt}$ and organopalladium or organonickel compounds coming from oxidative addition $[\text{M}(\text{Ph})(\text{X})(\text{PPh}_3)_2]$.⁶ This probably constitutes the first report of the study of an isolated Zn/Pd transmetalation. The methodology proved to be efficient also in catalytic conditions with aryl halides. Considering the importance of the Reformatsky reaction,⁷ this work represents one of the first examples of the great potential of zinc organometallics in cross-coupling. In the following years, organozincs consolidated as one of the most effective nucleophiles along with organoboron and organostannanes.⁸

Under a synthetic point of view, the Pd-catalyzed Negishi reaction has been tremendously pushed forward by the development of new catalysts and ligands. The initial involvement of electron-rich and bulky phosphines by the groups of Gregory Fu⁹ and Stephen Buchwald^{10,*} has been followed by the bulky NHC-based PEPPSI palladium precatalysts by Michael Organ's group.¹¹ The latter family of catalysts is widely employed in routine Negishi couplings due to the excellent performance with all kinds of substrates in very mild conditions. As well, new advances in the synthesis of organozincs and catalysts, and the greater mechanistic understanding of all the steps of the coupling have definitely boosted the interest of the Negishi reaction.

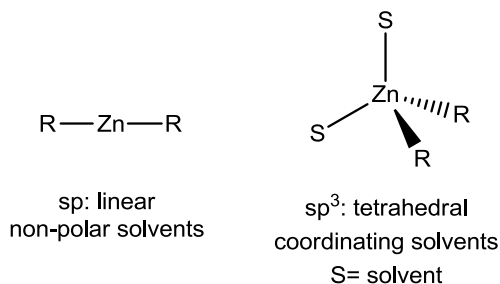
Nevertheless, it has received considerably less attention than the homologous Suzuki reaction, and probably the main reason comes from the initial narrower group tolerance and lower chemical stability of the organozincs. Against this idea, there have been tremendous advances in the synthesis of functionalized organozincs, showing an unprecedented group tolerance and ease of synthesis.¹²

* G. Fu's group has focused on and bulky alkyl phosphines such as PCy_3 or P^tBu_3 , whereas Buchwald's has focused on their own family of bulky biaryl phosphines, and lately in new precatalysts based on this family of ligands that facilitate the generation of Pd^0 active species.

1.2. Structural features of organozincs

a) Diorganozincs

The presence of a completely filled, low-lying $3d$ shell implies that the coordination chemistry of zinc is determined by the $4s$ and $4p$ orbitals. In a typical organozinc compound, the zinc-carbon bonds can be regarded as two equivalent sp -hybridized molecular orbitals, resulting in a linear geometry of the molecule. However, this means that two additional orbitals would be at reach to accept electron density from a Lewis base (for example, a coordinating solvent).¹³



Scheme III-2. Geometry of diorganozincs in different solvents

In non-coordinating solvents, organozincs are non-polar and monomeric linear molecules (Scheme III-2).^{*14} Apparently, they hardly form aggregates via alkyl or aryl bridges by electron-deficient multi-centre bonds, which is the common structural motif in organocopper and organolithium chemistry.[†] The reason for this is attributed to the relatively small electron-deficiency ZnR_2 , which is saturated by two strongly-donating groups. Bridging alkyl groups between zinc atoms are not sufficient to stabilize these aggregates, but they have been proposed to account for the mechanism of the exchange of alkyl groups, which is reported to be very fast via bridging transient species.¹³

* The dipole moment of symmetric diorganozinc compounds in non-polar solvents is therefore zero, as indeed was observed for cyclohexane solutions of ZnMe_2 . See Ref 13.

† ZnPh_2 is an exception of this behavior. The structure in the solid state is a dimer, linked by aryl bridges, see ref 13.

By contrast, coordinating solvents play a very important role in the structure of organozincs. Moderate donors can coordinate to empty orbitals of Zn, leading to 4-coordinate sp^3 tetrahedral structures (Scheme III-2). As it was observed in early works, $ZnMe_2$ can coordinate ethers and other O or N donors.¹³ The ability to coordinate ligands depends on the Lewis acidity of the Zn center. Dialkyl zincs are very rich in electron density, and not very good Lewis acids. All these complexes formed with weak donating solvents such as THF are very labile.^{15,*} By contrast, if the strong Me donor is replaced by the highly-electronegative C_6F_5 group, the corresponding organozinc becomes a better Lewis acid and coordinates THF more strongly. The X-Ray structure of $[Zn(C_6F_5)_2(THF)_2]$ displays a purely tetrahedral geometry, (analogous to that depicted in Scheme III-2).^{16a}

b) *ZnRX-type*

The most common type of organozinc reagents employed in Negishi reactions is $ZnRX$, with only one carbon group and a halogen.[†] In this family the electron-withdrawing halogen atom pulls out electron density, resulting in an increased Lewis acidity of the metal center which now does form aggregate structures in the solid state.[‡] This increased acidity results in a drop of nucleophilicity, but they are still very active transmetalating agents. Nevertheless, this particular feature of $ZnRX$ reagents might play a positive role in the selectivity in some instances, as it will be commented below.

c) *Zincates*

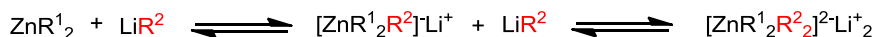
Zincates should be considered with special care. As commented above, organozincs are prone to coordinate Lewis bases and are susceptible towards nucleophilic attack by alkali metal compounds and their halide salts.

* It was found that the adduct $ZnMe_2(THF)_2$ is mainly dissociated in the gas phase. See ref 15.

† This type of organozincs is very commonly employed, since they can be synthesized by direct insertion of Zn dust into a R-X bond (typically I or Br). See ref 13b.

‡ The greater bridging ability of halogens, combined with the enhanced Lewis acidity the zinc center leads to $EtZnCl$ forming structures in which each zinc atom is the center of a tetrahedral structure, coordinated to one ethyl and three chloride ligands. See ref 16b.

R¹ and R² = alkyl, aryl, halide



Zn : sp linear

Zn : sp² trigonal

Zn : sp³ tetrahedral

Scheme III-3. Zincate equilibria in the presence of alkali salts.

As it was shown by ESI-MS and NMR studies, almost all possible species can be detected, suggesting that higher order zincates (4-coordinate) are in equilibrium with the low order ones (3-coordinate), and probably with the neutral species (which cannot be detected, as they are not charged). Some other aggregates have been detected as well.¹⁷

These species were differentiated from ordinary neutral organozincs on the basis of their improved chemical yields (or sometimes the opposite), chemoselectivities and reaction rates for reactions such as Michael addition, reaction with carbonyls or CO₂, and epoxides opening.¹⁸ As it will be discussed later, the Negishi coupling has shown to be very dependent on the formation of these organozincates and the presence of alkali and magnesium salts,¹⁹ to the extent that in some cases, efficient Negishi couplings can be achieved only in the presence of salts or using isolated zincates, whose preparation has been recently reported.²⁰

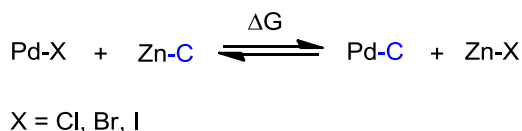
The reason for the enhanced activity reported in certain instances can be explained by the fact that the two additional ligands bound to the organozinc increase the electron density on the Zn metal center. This renders the organozinc more nucleophilic and saturates the Lewis acidity of neutral compound. Additionally, as it was shown, ligands in organozincates are less tightly bound to the metal, thus facilitating the group transfer and transmetalation processes.*

* The Zn-C distances in selected zinc compounds are the following: ZnEt₂(1.948 Å), ZnEtCl (1.946 Å), [ZnEtCl₂]₂²⁻(1.985 Å), [ZnEtBr₃]₂²⁻(2.008 Å). Although the differences are not very large, the elongation of the Zn-C bond can be correlated with the order of the zincate. See ref 16 and 20.

1.3. Nature of the Zn/Pd transmetalation

a) Thermodynamics of the Zn/Pd transmetalation

Following the same logic applied in the previous chapters, a simplistic thermodynamic balance will be employed according to the following Scheme III-4:



Scheme III-4. Thermodynamic balance of the Zn/Pd transmetalation.

The following bonds take part in the process of transmetalation: Zn–C and Pd–X bonds are broken and Pd–C and Zn–X bond are formed. Unfortunately, reliable experimental bond dissociation energies of organozinc compounds are scarce. Nevertheless, a very informative tendency can be obtained from the following experimental values gathered in Table III-1:²¹ The C–Zn bond is of a moderate strength.

Table III-1. Experimental Bond dissociation energies of selected zinc compounds in kcal·mol⁻¹.

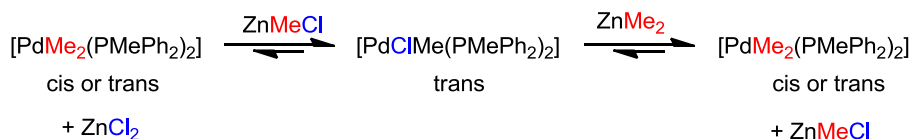
Zn–C Bond	BDE
Me–ZnMe	63.7
Et–ZnEt	52.4
Cl–ZnCl	87.5
I–Zn	36.6
O–Zn	59.8

Table III-2. Calculated bond dissociation energies (kcal·mol⁻¹) of selected Pd compounds.

Bond	BDE
Pd–C	59.0
Pd–Cl	91.9
Pd–Br	81.1
Pd–I	72.8

The same BDE for Pd–X and Pd–Me used in previous chapters will be considered for comparison.²² The involved bonds Pd–X and Pd–C have a very similar strength with regard to that of the Zn–X and Zn–C, particularly if the halogen is Cl.

This would imply the existence of a subtle balance between palladium and zinc organometallics. Our group has studied the equilibrium depicted in Scheme III-5:²⁴



Scheme III-5. Equilibrium between [*trans*-[PdMeCl(PMePh₂)₂]] and ZnMe₂ or ZnMeCl.

As it was found in this study, the equilibrium is displaced towards the products (exergonic) for the more basic and nucleophilic ZnMe₂, whereas the starting reagents are favored (endergonic) if ZnMeCl is used.

Considering that the zinc organometallic will be used in large excess with regard to the palladium catalyst, the transmetalation step of the Negishi reaction is expected to be sufficiently favorable by itself, and no additive is needed to push forward the thermodynamic equilibrium. Additionally, as commented in the General Introduction, the formation of a C–C bond in the irreversible step of reductive elimination will be a decisive push for the total free energy of the reaction.

b) The Pd–Zn interaction

Computational studies have contributed to shed some light in the Negishi reaction.^{23, 24, 25} According to DFT calculations, the group transfer from Zn to Pd is likely to take place through bimetallic Pd–Zn complexes (see Scheme III-6). In some of the computed transition states and intermediates, several of them were found to have very short Pd–Zn distances. They can range from a minor stabilizing interaction to a clear bonding interaction, hence it was proposed that these interactions might be facilitating the transmetalation event as an element that brings the reacting fragments together. Such Pd–Zn interactions were noticed by the group of Álvarez in the formation of allenylzincs from allenylpalladium complexes.²⁶

As commented in the introduction, the Pd^{II}/Zn interaction is presumed to have a great acid/base character, between electron-rich Pd centers and Lewis-acidic Zn centers. As well, closed-shell d⁸–d¹⁰ dispersion forces probably strengthen this

interaction.²⁷ Although there is not a lot of experimental information concerning the role this interaction in the Negishi coupling, computational studies have suggested that it is not only affecting the transmetalation step, but also the reductive elimination and the oxidative addition. The group of Michael Organ has proposed that the presence of ZnBr_2 increases the rate of reductive elimination by binding to the $[\text{PdR}^1\text{R}^2]$ intermediate,^{*} providing additional steric interactions that may aid the expulsion of the cross-coupling products.²⁵ In addition, ZnBr_2 is a rather strong Lewis acid, and the beneficial effect on the elimination rate made by acceptor ligands has been known for long.²⁸

Very interestingly, Alvarez's computational work suggested a detrimental effect of the presence of acid Zn metal centers on the oxidative addition step.^{26b} Pd^0 species are by nature more electron-rich and their interaction with the Zn acids is expected to be stronger than that of Pd^{II} complexes. In a recent paper, these Pd^0 -Zn adducts have been detected by ESI-MS.²⁹ This work provided compelling kinetic evidence of organozincs slowing down the oxidative addition step, due to the formation of these strong Pd^0 -Zn adducts. The authors suggested that the presence of alkali salts might quench these adducts by forming non-acidic zincates and restoring the usual ability of Pd^0 for fast oxidation.

c) Kinetics and nature of the Transition State

If ZnR_2 and ZnRX are compared, ZnMe_2 undergoes transmetalation to Pd at temperatures as low as 203 K, or at 223 K when ZnClMe is used. The reason for this is the increased nucleophilicity of the former, as the two alkyl donors make the zinc center in ZnR_2 very electron-rich.[†] As well, the group of Aiwon Lei has been able to

* Note that ZnBr_2 is a usual byproduct of many Negishi couplings.

† The computational model predicts similar rates for both ZnMe_2 and ZnClMe . The errors might come from the fact that computation predicts PMePh_2 dissociation for the case of the fastest transmetalation with ZnClMe . This has an entropic contribution that is not well modeled by the DFT method, possibly underestimating this activation barrier. However, computational absolute values should never be taken as certain. Nevertheless, the tendencies and the relative energies of the transition states perfectly match the experimental data.

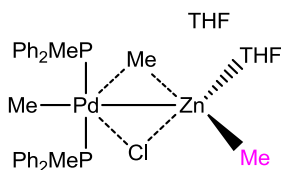
measure the activation parameters of other selected examples through kinetic use of *in situ* IR.³⁰

The only computational model that has been validated by comparison with accurate kinetic data has been carried by our group in collaboration with the group of Ujaque and Lledós.²⁴ Considering the good agreement between the experimental and computational data, we consider this is a good picture of the group exchange, and will be used for further discussion.

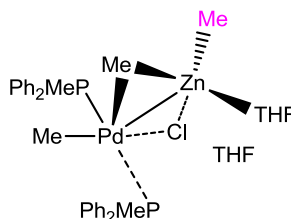
The computational work depicted the transmetalation event as a concerted group exchange between a square-planar palladium complex and a tetrahedral organozinc, with two explicit molecules of solvent coordinated.* It starts with the dissociation of a THF molecule from the organozinc, replaced by the coordination of the halogen to the Zn center. In the TS, it should be highlighted the amphiphilic behavior of zinc organometallics. First, they behave as Lewis basis due to the presence of electron-rich C–Zn bonds, but at the same time they possess low-lying empty orbitals at the Zn atom, which are able to establish additional acid/base interactions by accepting electron density from the Pd complex.

* Two molecules of THF were included in this study, to provide a more accurate depiction of the coordination environment of Zn. However, these molecules are loosely bound to the metal and dissociate readily when the zinc organometallic approaches the palladium center. In some other studies, the role of the solvent is described only as a continuum field.

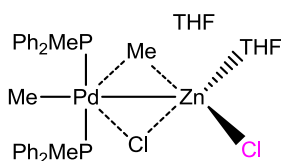
Transmetalation of ZnMe₂ to *trans*;
 $\Delta G_{203\text{K}}^{\ddagger} = 10.7$; d Pd-Zn = 3.110 Å



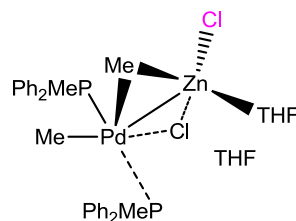
Transmetalation of ZnMe₂ to *cis*;
 $\Delta G_{203\text{K}}^{\ddagger} = 11.8$; d Pd-Zn = 2.707 Å



Transmetalation of ZnClMe to *trans*;
 $\Delta G_{223\text{K}}^{\ddagger} = 16.9$; d Pd-Zn = 3.012 Å



Transmetalation of ZnClMe to *cis*;
 $\Delta G_{223\text{K}}^{\ddagger} = 10.5$; d Pd-Zn = 2.592 Å



Scheme III-6. Scheme of the concerted neutral Pd-Zn transmetalation

This interesting feature could be observed in the computed structures. For the transmetalation using both ZnMe₂ and ZnClMe leading to *trans*-[PdMe₂(PMePh₂)₂], the Pd center displays 5-coordinate trigonal bipyramid geometry, this is: no PMePh₂ is displaced. In this case, the Pd-Zn distance remains around 3.0-3.1 Å. This suggests a weak interaction (if any) between the two metal centers, compared to the sum of the Pd-Zn Van der Waals radii (3.02 Å).³¹

By contrast, in the transition state leading to *cis*-[PdMe₂(PMePh₂)₂], the Pd-P bond distance is very elongated (or even fully dissociated), suggesting that one PMePh₂ has been replaced by the zinc nucleophile. In this case the Pd-Zn bond distance in the computed structure was calculated to be 2.6-2.7 Å. This distance suggests a bonding interaction between the Zn and the Pd center.^{32,*}

* The Pd-Zn distance in the Pd-Zn alloy is 2.65 Å. In this surface, a well-defined Pd/Zn bond is proposed. See ref. 32. Van der Waals radii of Pd: 1.63 Å; Zn: 1.39 Å. See: Bondi, A. *J. Phys. Chem.* **1964**, *68*, 441-451.

Considering that the neutral ligand substitution pathway is faster for ZnMeCl than for ZnMe₂, the only possible explanation for this is that ZnMeCl must replace easier PMePh₂ at the Pd^{II} complex than the more nucleophilic ZnMe₂. How is this possible? In both examples, the basic C–Zn bond attacks the empty LUMO of the Pd complex. At this point, the palladium center should be very rich in energy, as it establishes bonding interaction with up to 6 atoms. The excess of electron density of the palladium center is better alleviated by the empty orbitals of the more acidic ZnMeCl than by those of ZnMe₂, constituting a more efficient metallophilic bond and a more stable TS.* As commented above, the Pd/Zn interaction possesses an important acid/base character, which should be stronger in the case of the more acidic ZnMeCl.

It should be mentioned the impossibility of setting a fully general scene of the Zn/Pd interactions in the transmetalation, due to the fact that not only the group involved in the transfer plays a very important role, but also the other ancillary ligands of the palladium catalyst. The donation ability and the steric bulkiness of the ligands will determine whether effective Zn/Pd interactions are made in the transition state.

1.4. Mechanistic studies of the Zn/Pd transmetalation

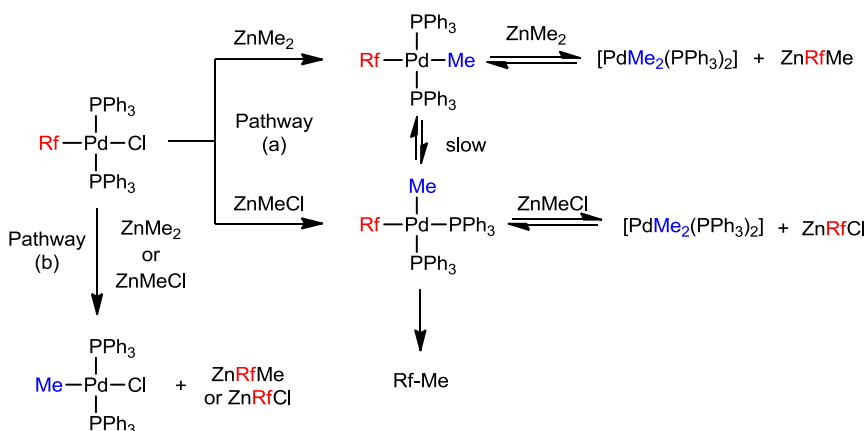
A few mechanistic reports have been published concerning the transmetalation step between the organozinc and the palladium catalyst. Understanding this essential step would help for the development of this reaction and would enhance its synthetic utility.

a) Stereochemical course of the transmetalation

Our research group reported the first detailed experimental observations of transmetalation of an alkylzinc reagent with *trans*-[PdRfCl(PPh₃)₂] (Rf = C₆F₃Cl₂),

* Note that the Pd–Zn bond is significantly shorter in identical intermediates when ZnMeCl is involved, rather than with ZnMe₂. This gives an idea of the relative strengths of the Pd–Zn bonds.

revealing a surprising different behavior of ZnMe_2 and ZnMeCl .^{*,33,33} They could detect by ^{19}F NMR that each methylating reagent afforded stereoselectively a different isomer of the palladium product. In the case of ZnMe_2 , $\text{trans-}[\text{PdRfMe}(\text{PPh}_3)_2]$ was produced, whereas ZnMeCl led initially to $\text{cis-}[\text{PdRfMe}(\text{PPh}_3)_2]$ (Scheme III-7, pathway a).



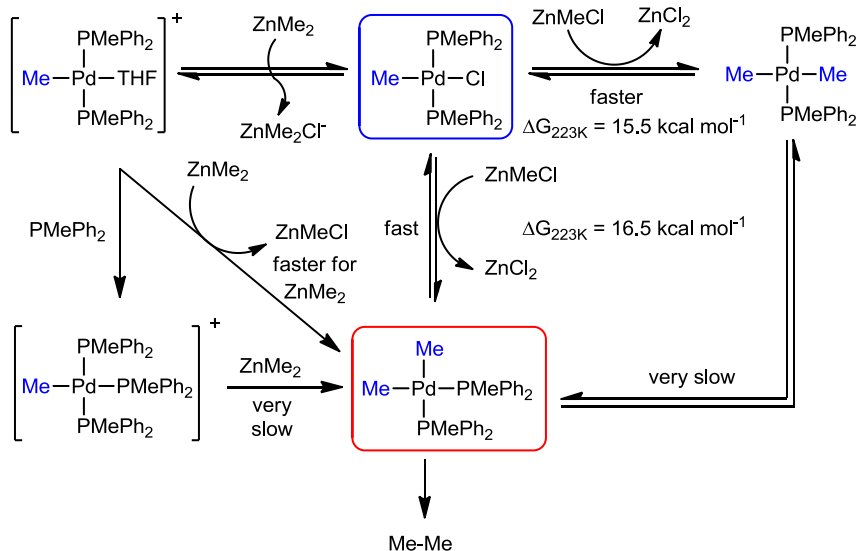
Scheme III-7. Transmetalation outcome between $\text{trans-}[\text{PdRfMe}(\text{PPh}_3)_2]$ and ZnMe_2 or ZnMeCl .

The latter is only the kinetic product, as in the reaction conditions isomerizes to the more stable $\text{trans-}[\text{PdRfMe}(\text{PPh}_3)_2]$ rapidly. This observation was particularly important, because isomerization of $\text{cis-}[\text{PdRfMe}(\text{PPh}_3)_2]$ is a slow process in the absence of ZnMeCl or ZnCl_2 (products of the transmetalation). This means that ZnMeCl and ZnCl_2 are effective catalyst of the isomerization process.

The origin of this Zn-catalyzed isomerization was understood in following research. Casares, Espinet et al. conducted a further study between $\text{trans-}[\text{PdClMe}(\text{PMePh}_2)_2]$ and ZnMeCl to form $\text{trans-}[\text{PdMe}_2(\text{PMePh}_2)_2]$ and $\text{cis-}[\text{PdMe}_2(\text{PMePh}_2)_2]$.^{24b} The kinetic product of this reaction is $\text{trans-}[\text{PdMe}_2(\text{PMePh}_2)_2]$, but it isomerizes very slowly in the absence of ZnMeCl or ZnCl_2 to the thermodynamically more stable $\text{cis-}[\text{PdMe}_2(\text{PMePh}_2)_2]$. However, in the

* This reaction models the transmetalation step of the coupling reaction of ZnMe_2 or ZnMeCl with Rf-I catalyzed by $\text{trans-}[\text{PdRfCl}(\text{PPh}_3)_2]$ to afford Rf-Me .

presence of these reagents, this isomerization became fast via the following sequence: Zn/Pd retrotransmetalation to *trans*-[PdClMe(PMePh₂)₂] and transmetalation to *cis*-[PdMe₂(PMePh₂)₂]. These experiments revealed that the transmetalation in the Negishi reaction is a quickly reversible process.



Scheme III-8. Mechanism of the Zn/Pd reversible transmetalation.

However, the use of ZnMe₂ as transmetalation agent showed an unexpected and relevant mechanistic aspect, not observed for ZnMeCl as nucleophile.^{24a} ZnMe₂ was able to act as Cl⁻ scavenger of *trans*-[PdClMe(PMePh₂)₂], leading to the cationic intermediate *trans*-[PdMe(PMePh₂)₂(THF)]⁺.^{*} From this complex, the transmetalation reaction was noticeably faster than that of the concerted pathways via neutral intermediates. Interestingly, when a tiny amount of ligand PMePh₂ was added, this pathway was inhibited and the cationic species [PdMe(PMePh₂)₃]⁺ could be observed. This complex is very stable and undergoes transmetalation at a much slower rate, sequestering the catalyst.

^{*} In that publication, the fact that this complex was not detected with the better acceptor ZnMeCl was attributed to the greater presence of terminal chloro atoms in that system. These donors would prevent the coordination of the poor THF ligand.

b) Existence of undesired transmetalations

Another key observation made in these studies was the identification of Zn products containing Rf (ZnRfMe and ZnRfCl), coming from undesired Zn/Pd transmetalations (see Scheme III-7, these products can be generated via pathways a and b).³³ These products were detected at the early stage of the reaction no matter which organozinc was employed.

The Rf/Me exchange is the major reaction for ZnMe₂ while it is a minor problem with ZnMeCl. All of these results indicated that ZnR₂ and ZnRX also behave with different kinetic features in the secondary transmetalation step. This unprecedented observation is key for the synthetic outcome and it should be a major determinant in the choice of one Zn organometallic or the other. Secondary transmetalations are responsible for the formation of homocoupling byproducts that reduce the yields and the efficiency of the Negishi reaction in multiple instances (see Scheme III-10).

Following this work, the group of Lei published an experimental and computational investigation of the factors controlling this secondary transmetalation.^{30a} They could observe that the ratio of reductive elimination/secondary transmetalation in the coupling of aryl groups with aryl iodides was affected by the presence of *ortho* substituents in the aromatic ring of both arenes. They concluded that *ortho* substituents in ZnArCl significantly disfavor a second transmetalation. This fact suggested that a judicious design of the coupling should involve a less sterically crowded I–Ar and an *ortho* substituted ZnArCl.

c) The decisive role of additives

As introduced in section 1.2.c), studies in the context of Ni-catalyzed cross-coupling reactions with organozincs revealed a strict dependence on the source or the ZnRX,^{18,19,34} but it was not until the seminal work by the group of Michael Organ was disclosed when the role of salts was considered as a matter of great importance for the success of some of the Negishi cross-coupling reactions.^{35,36} In these pieces of research, they studied the effect of the addition of different salts to the reaction

field and also the need of highly polar solvents (DMI, NMP) in both sp^3 - sp^3 and sp^2 - sp^2 couplings.

When ZnBuBr is used for the coupling depicted in Figure III-1, the presence of additional LiBr was shown to be essential for triggering the catalytic activity. On the contrary, ZnBr₂ was shown to poison the coupling (Figure III-1).³⁵

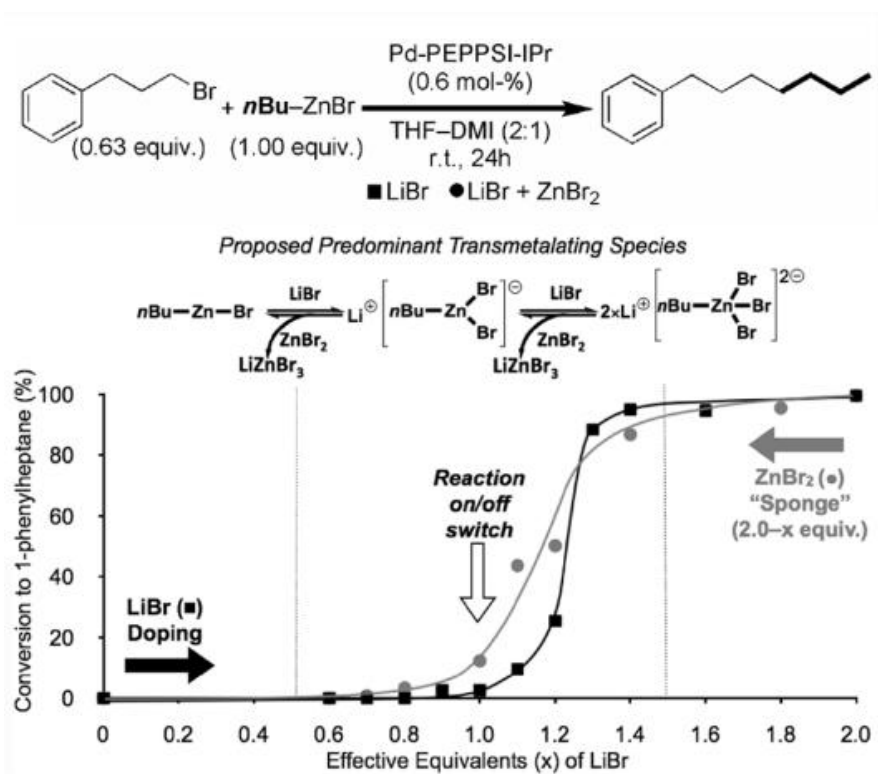


Figure III-1. Titration study in which various stoichiometries of the additives LiBr (x equiv) plus ZnBr₂ were added to the sp^3 - sp^3 Negishi coupling reaction. This figure has been taken as published from reference 34.

In further work, the higher-order zincate ZnBuBr₃²⁻ was identified by ESI-MS and NMR studies upon the addition of several equivalents of LiBr in DMI, which were proposed to be the actual transmetalating species in accordance with the observed stoichiometry of the coupling. The polar solvent was proposed to facilitate the formation of these highly charged species.^{35a} As a matter of fact, when

independently prepared organozincates²⁰ were used, no need for this type of solvents was observed, as the coupling proceeds in THF.^{35b}

When aryl zincs were evaluated in sp^2 - sp^2 couplings, significant differences of reactivity were uncovered. In their reaction conditions, $ZnAr_2$ reagents were efficient transmetalating agents of only one Ar group in the absence of any added salt or polar solvent. The transfer of the second group was found to be dependent on the presence of either a salt (LiBr or $ZnBr_2$ are effective promoters) or a polar solvent. The fact that any salt and the solvent alone can trigger the coupling suggests that an increase in solvent dielectric constant is needed to break down $ZnArX$ aggregates.^{35c}

In all cases, the distinct reactivity was attributed to the differences in the nature of the transmetalation. Alkyl zincs were considered inactive for the group transfer, being higher-order zincates the postulated transmetalating species in sp^3 - sp^3 couplings. In stark contrast, $ZnAr_2$ and $ZnArX$ are active in their neutral form, as long as they do not aggregate. Although the role of additives has demonstrated to be very important for the synthetic outcome, the interpretation given by Organ et al. is only based on reaction yields of catalytic runs. They attributed the lack of reactivity to inefficient transmetalations, but as our group has shown, salt free $ZnMe_2$ and $ZnMeCl$ are extremely active transmetalating species even at low temperature.²⁴ The reasons for the reactivity blackout could be different to those assumed. In this regard, kinetic evidence might point to the role of organozincs as Pd^0 scavengers, switching off the oxidative addition step.²⁹

1.5. The hot spot of the Negishi reaction: sp^3 couplings

Transmetalation of sp^3 groups is usually slower than that of sp^2 or sp moieties.^{*,37} Effective protocols are now available for the Suzuki coupling and others, but as we have seen throughout this introduction, organozincs provide

* This can be deduced from the fact that aryl groups are selectively transferred when $Ar-SnBu_3$ or $Ar-SiMe_3$ are used in the Stille and Hiyama reactions in place of the corresponding alkyl chain. Similarly, sp^3 organoboron reagents are less nucleophilic than the homologous sp^2 counterparts, see ref.37.

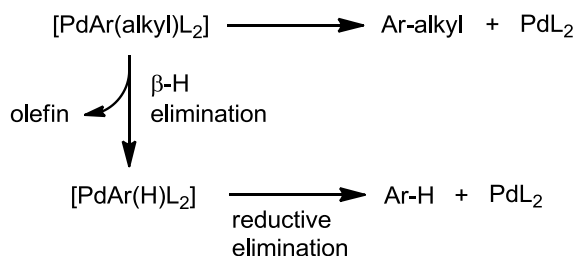
among the fastest transmetalations of all possible nucleophiles, being particularly attractive when sp^3 groups are involved.³⁸

Molecules containing sp^3 fragments are of a tremendous importance in the fields of materials,^{*,39} natural products and drug discovery.⁴⁰ A higher proportion of sp^3 -hybridized carbons results in increased solubility of drugs, a very important property of active molecules in order to become potential candidates towards selected targets. It has been found that compounds having greater fraction of sp^3 -hybridized carbons have greater chances of developing from discovery, through clinical testing, to drugs.^{40,41}

In particular, the number of Csp^3-Csp^3 linkages found in natural products and other complex organic molecules far exceeds the number of arene-carbon linkages, but the formation of Csp^3-Csp^3 bonds can be challenging, particularly if tertiary or quaternary stereocenters are involved. In the past decade, a large amount of progress has been made in this type of coupling since the groundbreaking publication of Gregory Fu and collaborators. They were the first group successful at coupling unactivated alkyl iodides, bromides, chlorides and tosylates with a variety of alkyl organozincs by using Pd_2dba_3 source in combination with the electron-rich and bulky $P(Cyclopentyl)_3$.⁹

There are several reasons why alkyl groups are challenging substrates for Pd-catalyzed cross-coupling reactions. First, alkyl halides or sulfonates lead to relatively slow oxidative additions and reductive eliminations.^{42,43} Second, alkyl-Pd complexes can be subject of β -hydride eliminations.⁴⁴ This secondary reaction reduces the selectivity of the coupling because of the formation of high percentages of undesired C-H side-products (reduction product) along with the desired C-C cross-coupling product.

* Long alkyl chains give flexibility to the structures of materials, increase the solubility of the molecules or help to control and predict properties like the mesophase of liquid crystals. See for instance ref 39.

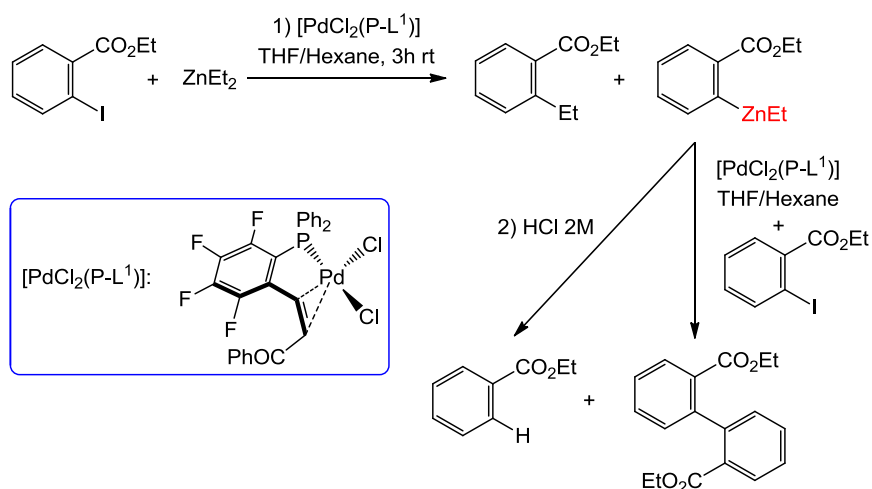


Scheme III-9. Cross-coupling versus Reduction.

In this mechanistic hypothesis the relative rates of transmetalation and reductive elimination versus β -H elimination should be crucial for the formation of the Ar-alkyl (cross-coupling) versus Ar-H (reduction) product (Scheme III-9).

If an alkyl halide or tosylate is employed as the electrophilic substrate, the subsequent $[\text{Pd(alkyl)XL}_2]$ could be prone to β -hydride elimination. This means that fast transmetalations are necessary to minimize the concentration of this conflictive intermediate. In this regard, nucleophiles of boron, tin or silicon perform worse than organozincs.

On the other hand, $[\text{Pd(alkyl)RL}_2]$ will be the catalytic intermediate prior to the reductive elimination step. Since this intermediate can undergo β -hydride elimination as well, the subsequent reductive elimination must be faster than this secondary reaction.⁴⁵ Aiwen Lei's group⁴⁶ and our group⁴⁷ have overcome this problem by using a phosphine ligand with a tethered electron-withdrawing olefin. These ligands have demonstrated to accelerate reductive eliminations of palladium complexes.²⁸ For the $\text{sp}^2\text{-sp}^3$ coupling of aryls with ZnMe_2 , we could demonstrate that reductive elimination was faster than β -hydride elimination, whereas using PPh_3 as ancillary ligand this secondary reaction was not suppressed.



Scheme III-10. Pd-Catalyzed Negishi coupling with a phosphine–EWO ligand.

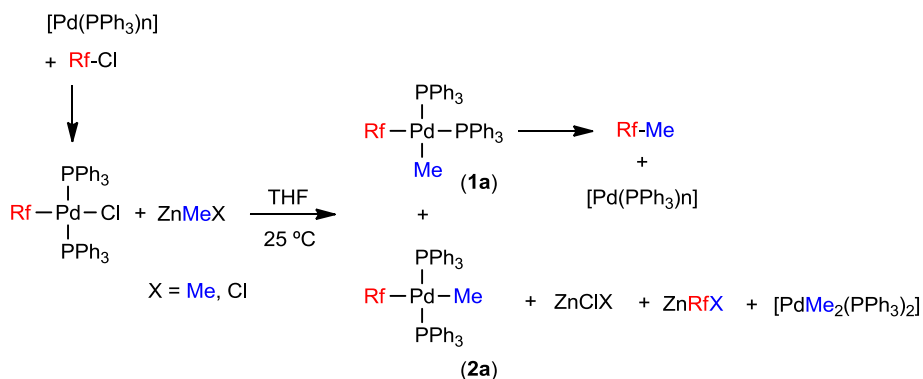
Although the ratio of the desired C–C coupling product and reduction product was very high, the presence of the latter was not completely suppressed.^{46a} The undesired ArH product proceeded from hydrolysis of ZnArEt, formed in secondary transmetalations where Ar is transferred from Pd to Zn. In addition, ZnArEt is able to transmetalate to the intermediate of oxidative addition $[\text{Pd}(\text{Ar})\text{I}(\text{P-L}^1)]$, generating the homocoupling product Ar–Ar (Scheme III-10). Interestingly, the percentage of byproducts formed via undesired transmetalations was much less when ZnEtCl was used instead of ZnEt₂.

2. Organometallic nucleophiles and Pd: What makes ZnMe₂ different?

Some time ago we reported a study on the Pd-catalyzed Negishi coupling of Rf–X (X[−] = halide) with ZnMe₂ (Scheme III-11). The oxidative addition of Rf–Cl to PdL_n (L = PPh₃) produces *trans*-[PdRfCl(PPh₃)₂],^{*} on which transmetalation must occur. It

* The oxidative addition of RfI to Pd(PPh₃)₄ produces initially *cis*-[PdRfI(PPh₃)₂], which then isomerizes to the *trans* isomer. See 49.

was observed in the isolated transmetalation reaction between *trans*-[PdRfCl(PPh₃)₂] and ZnMeX (X = Me, Cl) the formation of *cis* and *trans*-[PdRfMe(PPh₃)₂] ((**1a**) and (**2a**)) and ZnClX. Among the two isomers formed after transmetalation, only the *cis* isomer (**1a**) can undergo reductive elimination of Rf-Me, which can be observed experimentally. Very interestingly, these were not the only products observed, but also a large amount of the exchange products ZnRfX and *cis*-[PdMe₂(PPh₃)₂] (Scheme III-11).^{*33} As commented above, these undesired byproducts have their origin in secondary transmetalations that take place between the zinc organometallic and the palladium catalyst. Understanding of the factors controlling the undesired group exchange is important, so that it can be minimized and ultimately, more efficient synthesis could be designed.

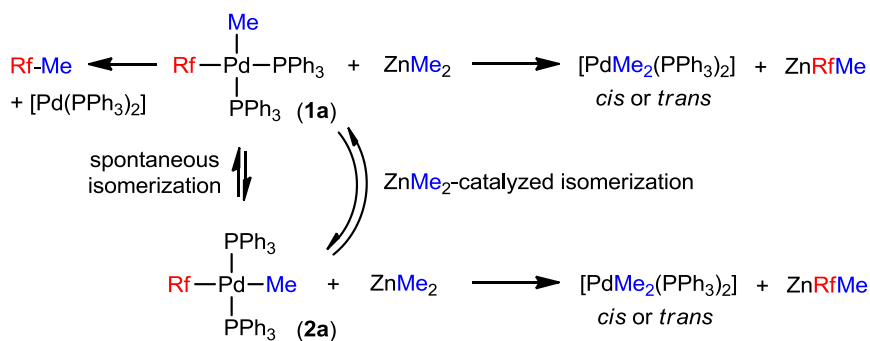


Scheme III-11. Scheme of the early studies on the Negishi reaction published by our group. See ref. 33.

To put some order in the discussion to come, we are considering in this work two categories of transmetalation, depending on the groups undergoing exchange. By “*secondary transmetalations*” we mean transmetalations that exchange two R fragments between Pd and Zn (*carbon for carbon exchanges*), in contrast to the commonly desired transmetalation (*primary transmetalation*) in which an R group on Zn is exchanged for an X group (usually a halide) on Pd (*X for carbon exchange*).

* *trans*-[PdMe₂(PPh₃)₂] that is formed in these reactions isomerizes to the *cis* complex in the reaction conditions.

Regarding the formation of ZnRfMe in the reaction of Scheme III-11, two pathways can be proposed: from complexes *trans* and *cis*-[PdRfMe(PPh₃)₂] (**1a**) and (**2a**) (Scheme III-12), and from the starting material *trans*-[PdRfCl(PPh₃)₂] (**3a**) (Scheme III-13):

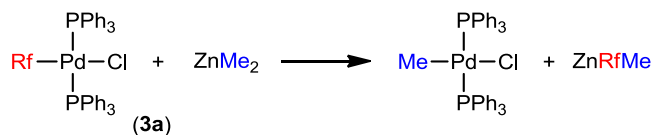


Scheme III-12. Possible reactions of [PdRfMe(PPh₃)₂] complexes with ZnMe₂.

i) Subsequent transmetalation between *cis* or *trans*-[PdRfMe(PPh₃)₂] and the organozinc.* Complexes (**1a**) and (**2a**) can exchange with ZnMe₂ both the Rf group and the methyl group. In the former case, the new species ZnRfMe would be formed. In the latter case, ZnMe₂ would be regenerated and the only possible chemical change in the reagents would be the isomerization of the palladium complex, which is also relevant for the synthetic outcome (see below). It should be noted that these two processes (isomerization and secondary transmetalation) are associated processes, and probably take place from similar intermediates.

ii) By direct Me/Rf exchange between *trans*-[PdRfCl(PPh₃)₂] and ZnMe₂, rather than Me/X exchange (Scheme III-13). This pathway was suggested by Elsevier as the possible origin of homo-coupling products.⁴⁸

* In the case of the *cis* isomer, the selectivity in this transformation would depend on the relative rates of reductive elimination of Rf–Me and this transmetalation (Scheme III-12). This means that if reductive elimination is much faster than the secondary transmetalation, this one would be the only observable reaction, and vice versa.



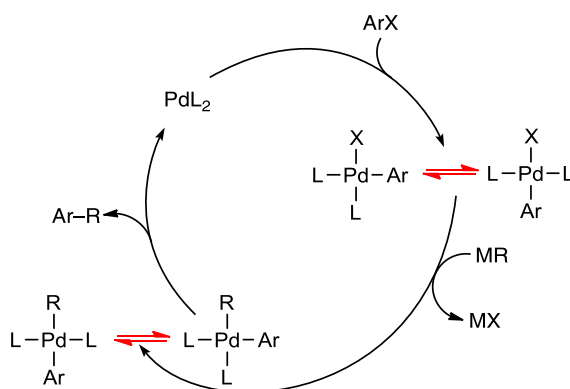
Scheme III-13. Secondary transmetalation of *trans*-[Pd^{Rf}Cl(PPh₃)₂] with ZnMe₂.

There are other possible pathways for the formation of ZnRfX, such as the retrotransmetalation of ZnMeCl with (**1a**) or (**2a**), but they are not significant under low concentration of ZnMeCl existing at the beginning of the reaction.³³ As commented in section 1.4.b) and 1.5, the amount of undesired products presumably formed via undesired transmetalations was much less when ZnRCl was used instead of ZnR₂. In order to understand this difference, it was the purpose of our group to closely examine the differential behavior of these two organometallics. ZnMe₂ will be the subject of study of this doctoral thesis, whereas ZnMeCl and ZnCl₂ will be examined in the Thesis of Desirée María Carrasco (manuscript in preparation).

In this chapter, we will examine the group exchange via pathway *i*) (Scheme III-12). It should be very different to pathway *ii*) (Scheme III-13), because in our case of study, halogens are absent. The nature of the transition states involved in these processes should be different to the common transition states of the usual R/X transmetalation reaction (see Scheme III-6), considering that halogens can assist the group transfer via halogen bridging. A good starting point to analyze this complicated system is to dissect the study starting on the reactivity of complexes [PdR¹R²L₂] with ZnR₂ derivatives. The study of the secondary transmetalation via pathway *ii*) from *trans*-[PdArCl(PPh₃)₂] (**3**) is in an early stage of completion, thus it will not be included in this Thesis. Combined with our previous findings,^{24,33,46} these results would provide a very complete picture of the transmetalation step in the Negishi reaction.

One specific question that we wanted to answer in this study is whether ZnMe₂ would be able to catalyze isomerization reactions of [PdR¹R²L₂] complexes via Me/Me exchange. The *cis/trans* isomerization is known to take place spontaneously in the absence of zinc.^{33,49} Isomerizations are important and can be determinant for

the outcome of the reaction. This problem has been thoroughly discussed in the context of Stille reactions,⁵⁰ but is also operative for other cross-coupling processes. As it was demonstrated in our previous work, both ZnMeCl and ZnCl₂ catalyze this reaction with important synthetic consequences, because reductive elimination of the organic product can only take place at the *cis* isomer.³³



Scheme III-14. A general Pd-catalyzed cross-coupling cycle highlighting the existence of isomers and the importance of isomerization equilibria.

The first block of this chapter will compare the spontaneous and ZnMe₂-catalyzed isomerization of complexes (1) and (2). The ZnMe₂-catalyzed isomerization cannot be measured accurately with experimental techniques in our system, because as it was commented in section 1.4, the fastest process is not the catalytic isomerization, but the Zn/Pd undesired group transfer. As a result, DFT calculations have been carried out to unveil the kinetic feasibility of this process, whereas the spontaneous isomerization has been addressed experimentally. In the second block of this chapter, the secondary transmetalation from complexes (1) and (2) will be evaluated by kinetic measurements and DFT calculations. It is worth reminding that the ZnMe₂-catalyzed isomerization and the secondary transmetalation are associated processes that probably share key intermediates.

The computational work described in the second block of this chapter is still ongoing and have been carried out by Dr. Rosana Álvarez at the University of Vigo. Since the experimental studies show that Rf and Pf behave almost identical (see experimental

part), the group containing less electrons, Pf, was used in the DFT studies, but the results can also be applied to Rf. Both aryls will be used indistinctly in the discussions, or referred to generically as Ar.* On the other hand, we have carried out the calculations for PPh₃ and PMe₃ and the profile of the reaction includes both ligands as valuable information on the well performance of PMe₃ as a model for PPh₃ in this particular system. The calculated structures with PMe₃ allow for an easier observation of structural details in some figures used in this chapter.

2.1. Results and discussion

a) *Non-catalyzed isomerization of trans- and cis-[PdArMe(PPh₃)₂] (Ar = C₆F₅, C₆Cl₂F₃).*

The isomeric complexes *cis*-[PdArMe(PPh₃)₂] (**1**) (Ar = Rf = C₆Cl₂F₃ (**1a**); Ar = C₆F₅ (**1b**)) and *trans*-[PdArMe(PPh₃)₂] (**2**) (Ar = C₆Cl₂F₃ = Rf (**2a**); Ar = Pf = C₆F₅ (**2b**)) can be isolated independently and are sufficiently slow towards coupling to allow for monitoring of the exchange processes they undergo (Figure III-2).^{†,51}

* Rf complexes will be additionally labeled as (**a**), whereas Pf complexes will be labeled as (**b**). When the aryls are treated in a general manner, no additional label will be used.

† In experimental mechanistic studies comparatively inert models offer the possibility to work on catalytic processes that are too fast for conventional reagents. In this respect fluorinated aryls such as C₆F₃Cl₂ (Rf) or C₆F₅ (Pf) are excellent models of conventional aryls, see ref. 51.

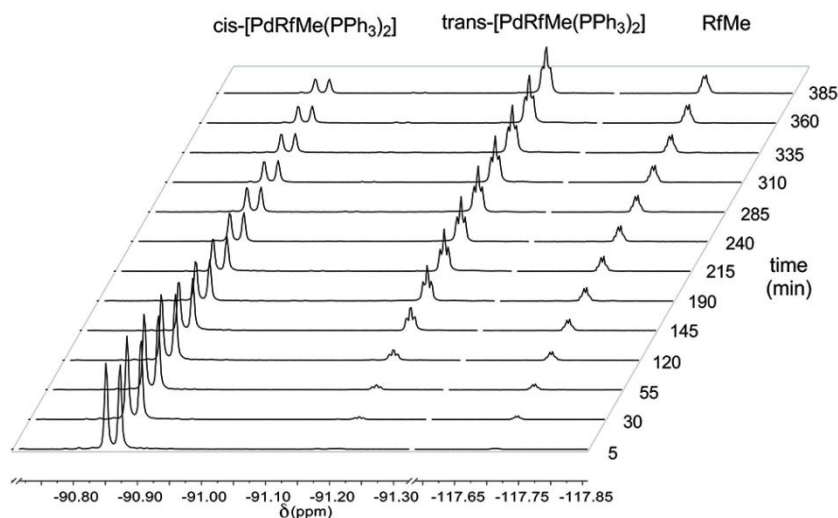
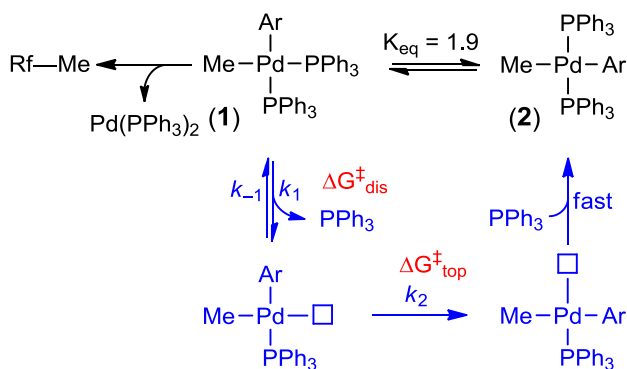


Figure III-2. ^{19}F NMR spectrum (at 470.48 MHz, in THF, 25 °C) of coupling vs. isomerization competence of *cis*-[PdRfMe(PPh₃)₂] (**1a**).

Starting with the *cis* isomer (**1a**), the spectrum shows that formation of the coupling product Rf–Me is slower than isomerization, but fast enough to have to consider it in the kinetic equations of isomerization. The kinetic fitting details are given in the experimental part. The two complexes isomerize in THF solution at room temperature to an equilibrium with $K_{\text{eq}} = 1.9$ (Scheme III-15).³³ This value corresponds to an energy difference of about 0.38 kcal/mol in favor of the more stable *trans* isomer. The observed rate constant of this equilibration, k_{isom} , has an inverse linear dependence on the concentration of added phosphine in the medium, indicating a two step dissociative process, shown highlighted in blue in Scheme III-15, which is similar to that previously proposed for diaryl–palladium complexes.⁴⁹ The rate constants of the individual steps of according to Scheme III-15 were obtained by non-linear-least-square fitting of the data using the program COPASI (see experimental).⁵² A rate determining step value $\Delta G_{\text{top}}^{\ddagger} = 27.7$ kcal/mol was found for the spontaneous isomerization, corresponding to the topomerization step in a three-coordinate intermediate. The behavior of (**1b**) is similar and the experimental data are almost identical (see experimental).



Scheme III-15. Isomerization equilibrium (black) and mechanism (blue) of *cis*-[PdArMe(PPh₃)₂]**(1)** to *trans*-[PdArMe(PPh₃)₂]**(2)** isomerization.

b) *ZnMe₂ catalyzed isomerization of trans- and cis-[PdArMe(PPh₃)₂]*

The catalyzed isomerization reaction $ZnMe_2 + \mathbf{1} = ZnMe_2 + \mathbf{2}$ cannot be experimentally measured separately from the competing non-catalyzed one because, as discussed below, $ZnMe_2$ is a strong methylating reagent and its role as catalyst (in which it is not consumed) will be competing with its activity as reagent (in which it is consumed producing changes in concentration). This problem prevented establishing the reaction conditions required for experimental kinetic studies. Thus, data for the $ZnMe_2$ catalyzed isomerization pathway had to be obtained by DFT methods (wb97XD-PCM-THF/SDD-6-31G*//B3LYP/SDD-6-31G*), which afforded the interesting profile shown in Figure III-3 for Ar = C₆F₅.*

* These calculations also inform on the preliminary molecular interactions in *cis*-**1** and *trans*-**1**, two states that are observed for PMe_3 but cannot be found for the corresponding more crowded PPh₃ complexes, probably because increased steric hindrance is enough to preclude their formation as intermediates.

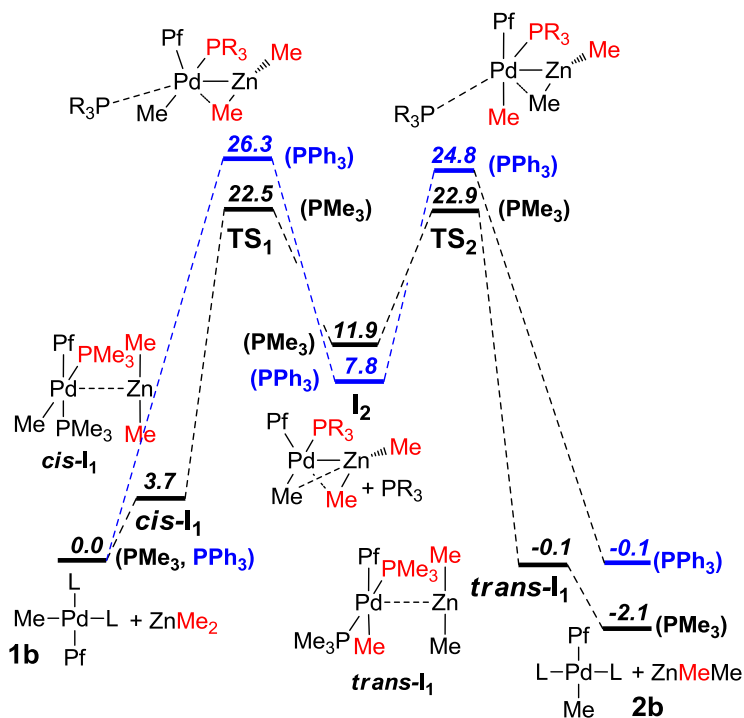


Figure III-3. DFT profile of the ZnMe₂ catalyzed **1b/2b** isomerization. Gibbs energies are shown in kcal/mol (L = PMe₃, black lines; PPh₃, blue lines). NOTES: a) The zeroes for L = PPh₃ or L = PMe₃ should be different in energy and the coincidence of the two zeroes in the figure is artificial, in order to save space. b) The experimental value of the equilibrium fixes the energy of **2b** in THF solution as -0.4, relative to zero for **1b**.

An examination of the profile shows that, in the catalyzed pathway, isomerization and transmetalation are directly connected (see below), as the ZnMe₂ catalyzed isomerization of [PdArMe(PPh₃)₂] occurs via Me/Me transmetalation. Thus this computational study of isomerization provides as well details on the main features of a transmetalation in a system lacking typical bridging groups such as halides. The highest *catalyzed* isomerization barrier corresponds to the transmetalation on the *cis* complex (**1b**) and is in the order of energy (26.3 kcal/mol; note that calculations for these systems have easily 1-3 kcal/mol errors) of the experimental value for the *non-catalyzed* isomerization (27.7 kcal/mol), but still clearly higher than for transmetalations involving halides.²⁴

It is interesting to keep in mind that the ZnMe_2 catalyzed isomerization will follow a law $\text{rate}_{\text{cat}} = k_{\text{cat}}[\text{ZnMe}_2][\text{Pd}]$, while the uncatalyzed isomerization will follow the law $\text{rate}_{\text{cat}} = k_{\text{uncat}}[\text{Pd}]$. The total rate will be $\text{rate}_{\text{total}} = (k_{\text{uncat}} + k_{\text{cat}}[\text{ZnMe}_2])[\text{Pd}]$. For not very different isomerization barriers (k_{cat} and k_{uncat} of similar magnitude, as it is the case) the contribution of the two pathways will dramatically change depending of Pd concentration and obviously the contribution of the catalytic pathway will increase in conditions of high ZnMe_2 concentration ($[\text{ZnMe}_2] \gg [\text{Pd}]$). This is the case of synthetic Pd catalyzed processes, where ZnMe_2 is used as reagent and the initial ZnMe_2/Pd ratio can be easily 10^2 - 10^3 . On the contrary, for small concentrations of ZnMe_2 ($[\text{ZnMe}_2] \ll [\text{Pd}]$), the catalyzed isomerization pathway can be slower than the uncatalyzed one.

The catalyzed isomerization process in Figure III-3, from *cis* (**1b**) to *trans* (**2b**), is beautifully illustrated by sequence of structures shown in Figure III-4.* Since the two profiles are almost symmetrical around the central intermediates I_2 , except for the change of isomer, we comment these details only for the left half of the profile.

* Represented for PMe_3 complexes for better visibility.

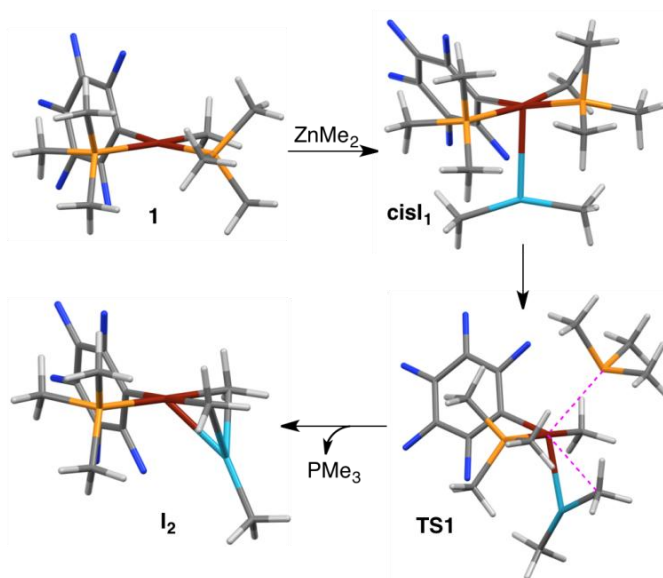


Figure III-4. Snapshots of the computed ZnMe_2 catalyzed isomerization reaction. The structures are represented in capped stick mode using the Mercury software.⁵³ Color code: reddish Pd, light blue Zn, yellow-orange P, deep blue F, grey C and white H.

At the beginning of this pathway, an almost barrierless intermediate structure is observed (*cis-I*₁) suggesting some kind of attractive interaction in the order of 3-4 kcal/mol between the two reacting molecules.^{*,54} Particularly interesting is that the transition state **TS**₁, through which a phosphine substitution by one entering Me–Zn bond is taking place, shows a bipyramidal trigonal coordination for Pd, with the two apical sites occupied by one Me and one PMe_3 ligand; two of the three sites of the equatorial plane are occupied by the C_6F_5 group and the Zn atom of ZnMe_2 ; finally, the third position is in dispute between the leaving PMe_3 , already at a long Pd–P distance, and one Pd–Me bond that, by this time, is already oriented towards that position (this ligand substitution is indicated by two pink dashed lines connecting the exchanging ligands to the Pd center). Increasing involvement of the Me group on Pd and eventual PMe_3 dissociation affords intermediate **I**₂ where the two metals are connected by two Me bridges and a Pd–Zn bond. From that point,

* Taking an approximate value of 8 kcal/mol for the unfavorable entropy contribution on going from 2 molecules getting bonded to give 1 molecule, the calculated estimation of about 3.7 kcal/mol suggests an extremely weak association, whatever its nature. See ref. 54.

recoordination of the phosphine in the appropriate coordination position produces the *trans* isomer found in the calculations, ***cis*-I₁-PMe₃**. The Pd–Zn distance in ***cis*-I₁** is almost identical (2.93 Å, Table III-3) to the sum of the van der Waals radii (3.02Å), which indicates a very minor interaction, perhaps still highly electrostatic in nature and associated with polarization of the electronic clouds of the metals and their ligands. This seems to be supported by the fact that this interaction does not stand changes in Pd coordination: the putative ***cis*-I₁-PPh₃** and ***trans*-I₁-PPh₃**, bearing a more voluminous phosphine ligand, could not be computationally characterized.

Table III-3. Selected geometrical parameters of the computed structures reflecting the changes in bond distances and angles along the isomerization via transmetalation.

Molecule-L	Distance (Å)* [Me ⁰ -Pd/Me ⁰ -Zn] {Me ² -Pd/Me ² -Zn} (Me ¹ -Pd/Me ¹ -Zn)	Distance (Å)* Zn-Pd	Me-Zn-Me largest outer angle (deg)
<i>cis</i> -I ₁ -PMe ₃	[2.10/3.87] {3.71/1.96} (4.02/1.96)	2.93	153.6
TS ₁ -PMe ₃	[2.09/2.95] {2.68/1.99} (4.14/1.94)	2.56	156.0
TS ₁ -PPh ₃	[2.08/2.98] {3.08/1.96} (4.21/1.95)	2.79	156.4
I ₂ -PMe ₃	[2.21/2.17] {2.16, 2.54} (4.23, 1.94)	2.40	146.8 123.4
I ₂ -PPh ₃	[2.12/2.52] {2.28/2.14} (4.23/1.94)	2.42	145.8 124.6
TS ₂ -PMe ₃	[2.12/3.13] {2.42/2.07} (4.19/1.94)	2.44	149.9
TS ₂ -PPh ₃	[2.11/2.88] {2.72/1.98} (4.21/1.95)	2.60	153.2
<i>trans</i> -I ₁ -PMe ₃	[2.12/3.75] {3.74/1.96} (3.93/1.96)	2.90	154.6

Molecule labels are as in Figure 2. Me⁰ is the Me group initially on Pd. Me¹ and Me² are the two Me groups originally on Zn. Me-Pd and Me-Zn stand for the corresponding Csp³-Pd or Csp³-Zn distances.*For comparison $\Sigma r_{\text{cov}}(\text{Pd}+\text{Zn}) = 2.62\text{\AA}$; $\Sigma r_{\text{vdW}}(\text{Pd}+\text{Zn}) = 3.02\text{\AA}$; $\Sigma r_{\text{cov}}(\text{Pd}+\text{Csp}^3) = 2.08\text{\AA}$; $\Sigma r_{\text{vdW}}(\text{Pd}+\text{Csp}^3) = 3.33\text{\AA}$; $\Sigma r_{\text{cov}}(\text{Zn}+\text{Csp}^3) = 2.08\text{\AA}$; $\Sigma r_{\text{vdW}}(\text{Zn}+\text{Csp}^3) = 3.09\text{\AA}$.

A clear bonding interaction between the two metal fragments is found in the transition state **TS₁**, where the Pd–Zn bond distances (2.56 Å for **PMe₃** and 2.79 Å for **PPh₃**) are close to or shorter than the sum of covalent radii (3.02 Å).^{*} Furthermore, one of the Pd–Me distances to the Me groups on Zn is much shorter (2.68 Å for **PMe₃** and 3.08 Å for **PPh₃**) than the other (4.14 Å for **PMe₃** and 4.21 Å for **PPh₃**), supporting engagement in coordination to Pd of one Zn–C bond, rather than involvement of the Zn atom alone. The other Zn–Me bond of **ZnMe₂** is an almost inactive spectator, as supported by the variation of the Zn–Me distances along the way to **I₂**: one of them (Zn–Me¹ in Table III-3) remains essentially unchanged along the process (1.94–1.96 Å), while the other (Zn–Me² in Table III-3) elongates along the process of formation of the Me-bridging system (1.96–2.54 Å). In other words, what we are seeing in **TS₁** is the formation of a bridging Me group involved in a 3-center 2-electron (from now on: 3c-2e) bonding system, at the expense of a Zn–Me bond.

In the next step of the evolution shown in Figure III-4, intermediates **I₂** show the shortest Pd–Zn bonds of each series (2.40 Å for **PMe₃** and 2.42 Å for **PPh₃**), supported by two bridging Me groups. It can also be noted that the Pd–Me distances are shorter (2.16 and 2.21 Å for **PMe₃**; 2.12 and 2.28 Å for **PPh₃**) and the Zn–Me distances are longer (2.17 and 2.54 Å for **PMe₃**; 2.14 and 2.52 Å for **PPh₃**) than before or after this point in the profile; furthermore, the longer Pd–Me distances are associated with the shorter Zn–Me distances in the same bridge. The largest Pd–Me distance is observed *trans* to the **Pf** group in **I₂-(PPh₃)**, but *trans* to the **PMe₃** ligand in **I₂-(PMe₃)**, suggesting a sequence of *trans* influence **PMe₃** > **Pf** > **PPh₃**.

A final noticeable structural change is found in the Me–Zn–Me angle, closing progressively from the initial linearity in free **ZnMe₂** as this fragment progresses towards formation of intermediate **I₂**. This reflects, in simple terms, the increasing involvement in bonding of a second p orbital of Zn (from *sp* towards *sp*² hybridization) as the Zn atom gets involved in more bonds. Yet, the Zn–Me distance

^{*} Note that all these bonds are somewhat longer in the more crowded **TS₁-(PPh₃)** transition state as compared to **TS₁-(PMe₃)**.

for the terminal Me group, not involved in bridges, remains unaltered from its value in free ZnMe_2 .

2.2. What is special in ZnMe_2 (or ZnEt_2) compared to other Zn organometallics?

As commented in the introduction of this chapter, ZnMe_2 is a perfectly symmetric linear molecule (sp hybridization for Zn) in the solid state ($d_{\text{C-Zn}} = 1.927(6) \text{ \AA}$) and in the gas phase.^{14,55} Complexes of ZnMe_2 with OEt_2 or THF are very weak, which suggests that the two strongly electron-donating Me groups make, altogether, a Zn center unusually electron-rich; the other potentially acceptor p orbitals of Zn, well shielded by this electron density, are high in energy and not very prone to participate in bonding. For this reason the Zn center in ZnMe_2 does not show the acidic character found for other Zn compounds (ZnCl_2 , ZnMeCl). Rather on the contrary, Zn in ZnMe_2 seems to act as a Lewis base towards the square-planar Pd acidic center. This electronic richness of the Zn center is not in contradiction with the fact that quantum mechanical calculations in the literature still support polarization of the two identical Zn–Me bonds towards their carbon ends, which develop a considerable negative atomic charge (-1.33).⁵⁶

The Kohn-Sham orbitals shown in Figure III-5 and Figure III-6 nicely support these views,^{*,57} but also lead us to get a more accurate understanding of the initial structural considerations based only on bond distances. The HOMO1 and HOMO2 orbitals (**A**) host the four bonding electrons of ZnMe_2 (Figure III-5) and altogether produce a high electron density in the vicinity of the Zn center. Alternatively, the equivalent orbital combinations **B** (HOMO1+HOMO 2, and HOMO2-HOMO1) allow for an easier identification of the electron density associated with the Zn–Me bond concept, and offer a more visual starting point to understand the orbital and electron density rearrangement during the evolution from *cis*- I_1 towards PMe_3 ligand displacement by a Zn–M bond as entering ligand.

* Only qualitative use of the shape and symmetry of the orbitals is made. For usefulness and some limitations of the meaning of Kohn-Sham orbitals, see ref 57b.

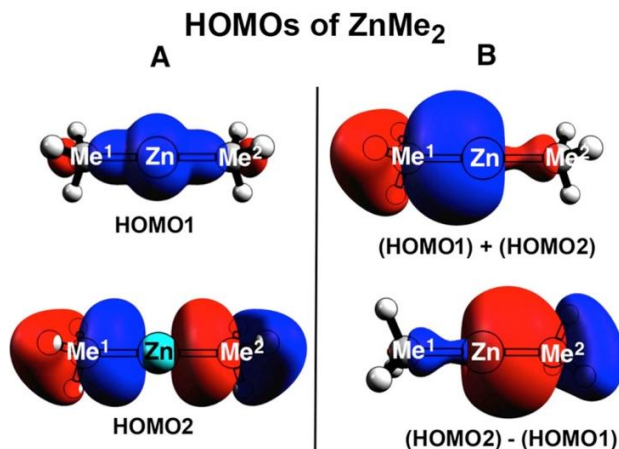


Figure III-5. Selected Kohn-Sham orbitals: **A:** Molecular orbitals HOMO1 and HOMO2 for ZnMe₂. **B:** Alternative (HOMO2 + HOMO1) and (HOMO2 – HOMO1) combinations for ZnMe₂.

This evolution occurs via side-on coordination of one of the two Zn–Me bonds,⁵⁸ which eventually gets polarized towards a 3c-2e Zn–Me–Pd bond, while the other electron pair evolves to be the $\sigma(\text{Zn–Me})$ bond not involved in interaction with Pd. At the early stages of this interaction (*cis*-I₁) the Pd–Zn distance is still a non-bonding distance (2.95 Å, almost identical to the sum of Van der Waals radii (3.02 Å)) but the polarization of the electronic clouds of the Pd and Zn orbitals giving rise to HOMO2/Pd (Figure III-6) already show that the initial contact between ZnMe₂ and the Pd center is beginning to create a 3c-2e Pd/Zn/Me² interaction. In other words, the ligand substitution induced by ZnMe₂ occurs by nucleophilic attack of one of the two $\sigma(\text{Zn–Me}^2)$ bonding electron pairs, fairly high in energy relative to the Pd acceptor orbital, which behaves as entering ligand towards an acceptor MO of the Pd complex. This empty Pd orbital receives the entering ligand in typical associative ligand substitution reactions on Pd. Meanwhile the HOMO1/Pd combination should begin to polarize slightly towards a Pd–Me¹ bonding orbital, although at this stage this can hardly be appreciated in Figure III-5.^{*59}

* Since in a [PdL₄]²⁺ complex with perfect D_{4h} symmetry the LUMO ($d_{x^2-y^2}$) produces zero overlap with σ -ligands approaching in the z direction, the acceptor orbital is an a_{1g} orbital with contributions of the 5s, 5p_z, and 4d_{z²} Pd atomic orbitals: see ref. 59. In this case, with much lower symmetry (C_s for the *cis* complex, C_{2h} for the *trans*), the orbital contribution of Pd

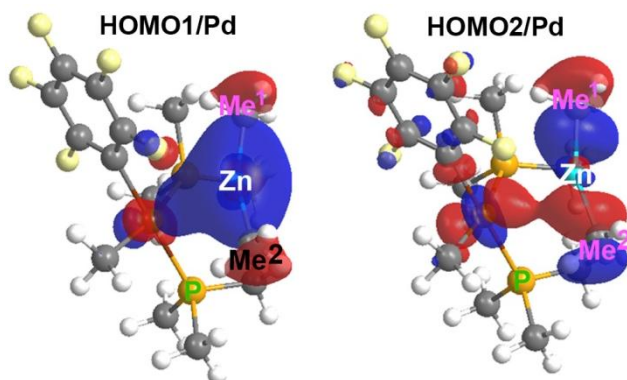


Figure III-6. Selected Kohn-Sham orbitals: Incipient interactions in *cis-I*₁, where shape of the molecular orbitals of the Pd/Zn adduct still reminds those of their ZnMe₂ and Pd parents.

Whereas in the conventional structural representation of Figure III-4 it seems that it is the Zn center that coordinates to the Pd center, this is a naïve and misleading image as it is not the carbon or the Zn centers which are acting as the entering nucleophile, but the electron density of the bond. Figure III-6 shows clearly that, from the very beginning, the interaction is defining involvement of one bond versus the other. In fact, the Pd–Me² is shorter than Pd–Me¹ in *cis-I*₁, and Me¹ is already closer to the PR₃ ligand that will be eventually displaced via the pentacoordinated TS₁. From that point, the implication of the two electrons of the σ(Zn–Me) bond, now fully depending on two metal centers, Zn and Pd, produces a decrease of the electron density on Zn. This stabilizes and makes more acidic the empty p orbitals on Zn, which become an acceptor of electron density from the terminal Pd–Me bond, producing the second Me bridge. With these synergistic interactions, the bimetallic Pd(μ–Me)₂Zn molecular structure is formed.

The electron density is, as discussed, truly responsible for bond formation. This multicenter interaction is difficult to depict but, assuming the typical pictorial representation of molecular structures (based in drawing bonds as bars connecting atomic centers that share bonding electron density), we could say that the Pd

to HOMO2/Pd in *cis-I*₁ contains important contributions of 5s, 4d_{z²} and 5p orbitals with z component, and points toward the z direction. At variance with this, HOMO1/Pd contains 4d_{x²-y²} contribution instead of 4d_{z²}, which makes it fairly inefficient towards Pd/Zn/Me bonding.

coordination in **I**₂ remains essentially square planar, with the two Me groups in the coordination plane and very small deviations from an ideal square plane (all angles are $90 \pm 5^\circ$), in spite of the additional Pd–Zn bond that protrudes below that plane (Figure III-4). In this view the isomerization process is pivoting around the Pd–Zn bond: when the reentering PR₃ splits the Pd–Me bond *trans* to Rf, the *cis* isomer **1b** will be generated; if it splits the Pd–Me bond *trans* to the coordinated phosphine, the *trans* isomer **2b** will be formed.

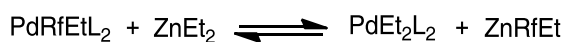
For similar circumstances of factors such as steric hindrance or symmetry, nucleophilic attacks occur more easily for nucleophiles with high energy HOMOs and for electrophiles with low energy LUMOs.* The formation of intermediate **I**₂ by the mechanism discussed above is remarkable in that it occurs by nucleophilic attack to a LUMO in Pd that is not very low in energy, particularly in cases where the existence of two carbon ligands (Me and C₆F₅ in this case) makes the Pd center fairly electron-rich and raises the energy of its LUMO and other orbitals. It is only the high basicity of the Zn–Me bonds in ZnMe₂ that makes this reaction feasible,[†] a behavior that should be less likely with ZnMeCl.

In our recent study of the Negishi cross-coupling reaction of Ar–I and ZnEt₂ to give Ar–Et,⁴⁶ already commented on in the introduction, we observed that important amounts of undesired Et–Et and ZnArEt were formed at early stages of the reaction. This problem was much less visible when the reaction was carried out with ZnEtCl, and also diminished at later stages of the reaction with ZnEt₂ when much of the initial ZnEt₂ had been consumed or transformed in ZnEtCl, drastically diminishing the concentration of ZnEt₂ in solution. The undesired formation of Et–Et

* We are using LUMO for short, but we mean the lowest empty MO that has an appropriate symmetry to give rise to bond formation with the attacking full orbital of the nucleophile, which is not necessarily the LUMO if its symmetry does not provide positive overlapping.

[†] The high basicity refers to high energy of the orbitals hosting the electron density of the Zn–Me bond electron pair. The Zn–Me bond electron pair for ZnMeCl should be lower in energy (less basic). Similar energetic considerations and behavior, including close relationship between basicity and nucleophilicity should be expected for ZnEt₂, but probably not for bulkier dialkyls where the high basicity might not be similarly reflected in high nucleophilicity because of steric hindrance.

and ZnRfEt can be understood from the undesired transmetalation in Scheme III-16, forming $[\text{PdEt}_2\text{L}_2]$:* The stronger nucleophile ZnEt_2 should be much more effective for this attack to Pd than ZnEtCl , and the more electron-rich $[\text{PdEt}_2\text{L}_2]$ should be the least prone to undergo further nucleophilic attack by, for instance, the byproduct ZnRfEt. Consequently, significant contribution of the exchange mechanism calculated and discussed here is expected to contribute very significantly to the undesired conversion of $[\text{PdArEtL}_2]$ to $[\text{PdEt}_2\text{L}_2]$, producing undesired Et–Et homocoupling instead of Ar–Et cross-coupling.



Scheme III-16. Undesired Ar per Et exchange equilibrium.

For comparison we can consider transmetalations involving Pd complexes and ZnCl_2 or ZnRCl and see how they behave differently from those with ZnMe_2 (Figure III-7).²⁴ The electrophilicity of the LUMO of the relatively electron-rich Pd center in $[\text{PdMe}_2\text{L}_2]$ is relatively poor (two Me groups make the Pd center electron-rich, as discussed before for ZnMe_2). On the other hand, the presence of electronegative Cl substituents that withdraw electron density from Zn stabilizes the p orbitals of Zn, which now form more stable complex with the solvent THF (as represented in Figure III-7).[†] Thus the game changes: upon easy equilibrium dissociation of THF, the Zn center becomes the Lewis acid that one usually expects and, at the right of Figure III-7, it is the Pd–Me bond in *trans*- $[\text{PdMe}_2\text{L}_2]$ that attacks the electron-poor Zn center in ZnCl_2 . In other words, the Pd complex is now the nucleophile (through its Pd–Me bonds) and the Zn center is the electrophile. At the left of Figure III-7, the reaction takes place via THF displacement by a Cl ligand to make initially a Pd–Cl–Zn bridge. This makes sense because in *trans*- $[\text{PdMeClL}_2]$ the electronegative Cl substituent has reduced the electron density on Pd, and the lone pairs in Cl are

* In that case L_2 was a chelating phosphine-(electron withdrawing olefin) ligand.

† ZnRX complexes coordinate strongly Lewis bases. Although ZnMe_2 is linear, ZnRX complexes are tetrahedral and coordinate X groups of their neighbors in the solid state. See: ref 16b.

more nucleophilic than the Pd–Me bond with reduced nucleophilicity. In addition, a more stable non-deficient single bridged intermediate is formed.

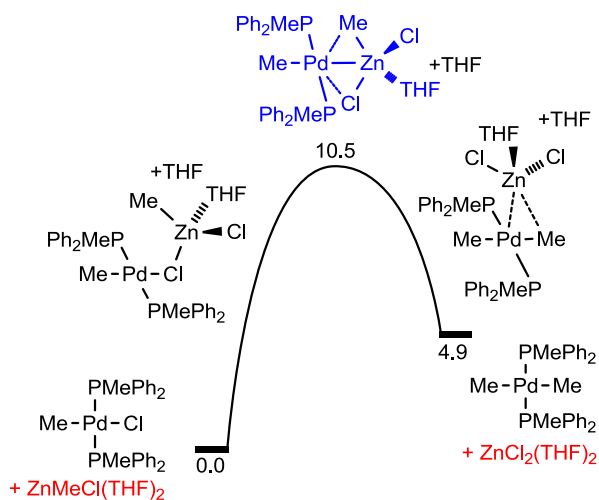


Figure III-7. Transmetalation sequence calculated for the interconversion of *trans*-[PdMeClL₂] + ZnMeCl in *trans*-[PdMe₂L₂] + ZnCl₂. Gibbs energies in kcal/mol. See reference 10.

It is worth commenting the role of the Zn–Pd metallophilic interaction observed in many structures of this work.* It should be noted that the major component of it are not closed-shell d^{10} - d^8 dispersion forces. This kind of interaction cannot be expected for light elements not submitted to relativistic effects, such as Zn and yet we find in this work that the Pd–Zn interaction is very strong. Hence our initial suggestion on the importance of metallophilic interactions in the Au/Pd system should perhaps be taken with caution, although metallophilic interactions can still be important in facilitating the initial approximation of the two metal centers. In any case, the strength of the Pd–Zn interactions is definitely associated with the formation of 3c-2e bonds.

* Metallophilic interactions are usually in the order of energy of weak H-bonds.

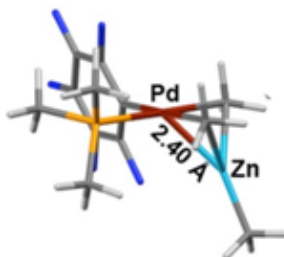


Figure III-8. Structure of $[(\text{Me}_3\text{P})\text{Pd}(\mu\text{-Me})_2\text{ZnMe}]$. The Pd–Zn distance (2.40 Å) is noticeably shorter than the sum of Van der Waals radii (3.02 Å).

All these examples illustrate the complex interplay of electronic effects in metal compounds, which are particularly intricate for transition metal complexes, and the subtle variations of the role of a metal center as a function of its substituents. Letting aside the steric effects that strongly correct the nucleophilicity and electrophilicity values in comparison to the acidity values, Zn changes from acidic center in ZnCl_2 to basic in ZnMe_2 , and the acidity of square-planar Pd^{II} complexes associated with their acceptor molecular orbitals varies importantly with the nature of the ligands.

2.3. Conclusions

The results of this investigation have revealed some interesting peculiarities of ZnMe_2 (and presumably ZnEt_2 but no other ZnR_2 with bulkier R groups) that make it very different from ZnRX (X = halide). Moreover, the common transmetalation intermediates found in the calculations support that transmetalation and catalyzed isomerization are associated processes, and also show that the formation of short Pd–Zn bonds is a common feature of these nucleophiles.

ZnMe_2 and ZnMeCl are very different nucleophiles for the transmetalation of Me groups to Pd, and presumably to other transition metals. In the former, the metal center behaves as a basic, highly nucleophilic center and the Me–Zn bond is able to react, even with fairly electron-rich Pd complexes such as $[\text{PdR}_2\text{L}_2]$, to produce L substitution and form $[\text{LRPd}(\mu\text{-Me})(\mu\text{-R})\text{ZnMe}]$ intermediates from which transmetalation or isomerization can follow. In contrast, the metal center at ZnMeCl

is acidic and has the tendency to react, in isomerization and transmetalation reactions, via intermediates or transition states using non deficient Pd(μ -Cl)Zn bridges.

The bridged structures with at least one electron-deficient component (Me, Et bridges) formed in the Pd/Zn transmetalation reactions show covalent intermetallic distances noticeably shorter than the sum of the Van der Waals radii, regardless of the possible metallophilic nature of the metal or not, because its origin is the 3c-2e nature of the deficient bond.

3. Study of Zn/Pd secondary (R^2 for R^1)

transmetalations of $[PdR^1R^2]$ complexes

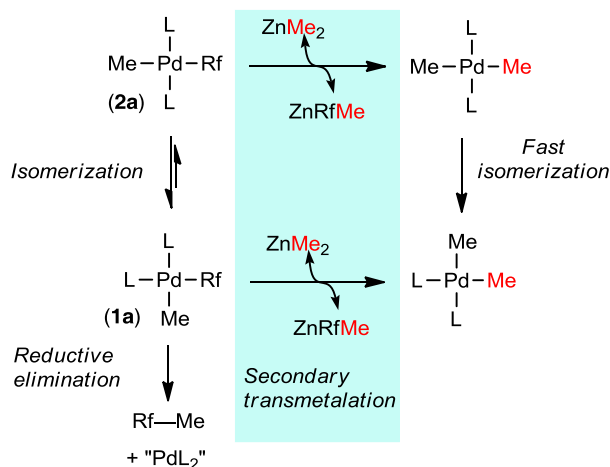
$[PdR^1R^2L_2]$ complexes are well-known intermediates in cross-coupling reactions. If the coupling deals with substrates disfavoring the reductive elimination step (e.g. electron-withdrawing groups in the carbon fragments),* these intermediates will likely accumulate in solution. As commented in the introduction, reductive eliminations involving sp^3 carbon atoms are usually slow.^{42,43} As a result, when using these fundamental groups in catalysis, undesired transmetalation may become a serious competition to the expected cross-coupling reaction, generating an efficient pathway to undesired products.⁶⁰

3.1. Results and discussion

The reactions of *cis* and *trans*- $[PdMeRf(PPh_3)_2]$ with $ZnMe_2$ in THF at 298 K were studied monitoring the Rf/Me exchange by ^{19}F and ^{31}P NMR. When a large excess of $ZnMe_2$ is employed (>20 equivalents, as it is common in Negishi cross-coupling reactions, see experimental), the transmetalation equilibrium is shifted towards the formation of $ZnRfMe$, *cis* and *trans*- $[PdMe_2(PPh_3)_2]$. Eventually, *trans*-

* Note, for instance, that perhalogenated *cis*- $[PdAr_2L_2]$ complexes are very stable towards Ar–Ar reductive elimination, which only takes place with very high activation energies. See ref. 60.

$[\text{PdMe}_2(\text{PPh}_3)_2]$ is transformed into *cis*- $[\text{PdMe}_2(\text{PPh}_3)_2]$ via fast isomerization in the reaction conditions (Scheme III-17).*



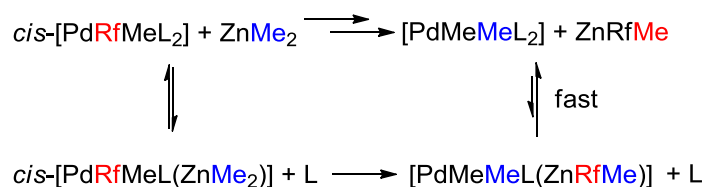
Scheme III-17. Secondary transmetalations involving complexes (1) and (2) eventually form *cis*- $[\text{PdMe}_2\text{L}_2]$.

The experimental study of the reaction of ZnMe_2 with *cis*- $[\text{PdMeRf}(\text{PPh}_3)_2]$ (**1a**) reveals that the presence of free $[\text{PPh}_3]$ retards the formation of ZnRfMe . The reaction rates used for quantitative kinetic purposes have been measured in experiments with added PPh_3 in all cases order to make certain of the good accuracy of the values.[†] The process is roughly order minus one (slope -0.9, see experimental part) with respect to $[\text{PPh}_3]$, consistent with a mechanism in which the first step is the substitution of one phosphine ligand by a molecule of ZnMe_2 , producing an intermediate $[\text{PdRfMeL-ZnMe}_2]$, prior to the transmetalation step. Consequently, the kinetic model of substitution of PPh_3 by ZnMe_2 and subsequent

* The structures of both isomers of $[\text{PdMe}_2(\text{PPh}_3)_2]$ were confirmed by ^1H and ^{31}P NMR. An alternative synthesis of *trans*- $[\text{PdMe}_2(\text{PPh}_3)_2]$ is included in the experimental part.

[†] The rate of the reactions (with or without added PPh_3) is also sensitive to the presence of Pd^0 (presumably $\text{Pd}(\text{PPh}_3)_2$ formed after reductive elimination of (**1a**)), which is eager to coordinate more PPh_3 to produce $[\text{Pd}(\text{PPh}_3)_3]$. The consequence is that, since the transmetalation is retarded by free PPh_3 , the formation of Pd^0 by reductive elimination speeds up the transmetalation reaction artificially. This effect would mislead the interpretation of the reaction rates measured in the absence of added PPh_3 and imposes the use of initial rates method for kinetic purposes.

Rf/Me exchange represented in the equations of Scheme III-18 was used to fit the data (see experimental).



Scheme III-18. Proposed sequence of reactions producing Me/Rf exchange between complex (**1a**) and ZnMe₂. For calculated structures see Figure III-9.

The rate constants of the individual steps were obtained by non-linear-least-square fitting of the data using the program COPASI,⁵² The experimental activation energies ($\Delta G^\ddagger_{298\text{K}}$) for the phosphine substitution step and for the Rf/Me exchange for complex (**1a**) are 22.4 kcal/mol and 25.9 kcal/mol, respectively. In a related case, the allenyl/Me transmetalation in the formation of allenylzincs from allenylpalladium has been postulated to occur through ligand substitution, and DFT calculations have shown that it is energetically feasible.²⁶

The Rf/Me group transfer of (**1**) and ZnMe₂ via ligand substitution was evaluated by DFT calculations. A direct pathway not implying ligand substitution by ZnMe₂ via concerted pentacoordinate transition states was also evaluated. The experimental evidence suggests that the ligand substitution pathway is the only significant contribution to the reaction rate between (**1**) and ZnMe₂, although a minor participation of the direct transmetalation cannot be excluded. Figure III-9 gathers the computational experimental and computational $\Delta G^\ddagger_{298\text{K}}$ of the two possible mechanisms:

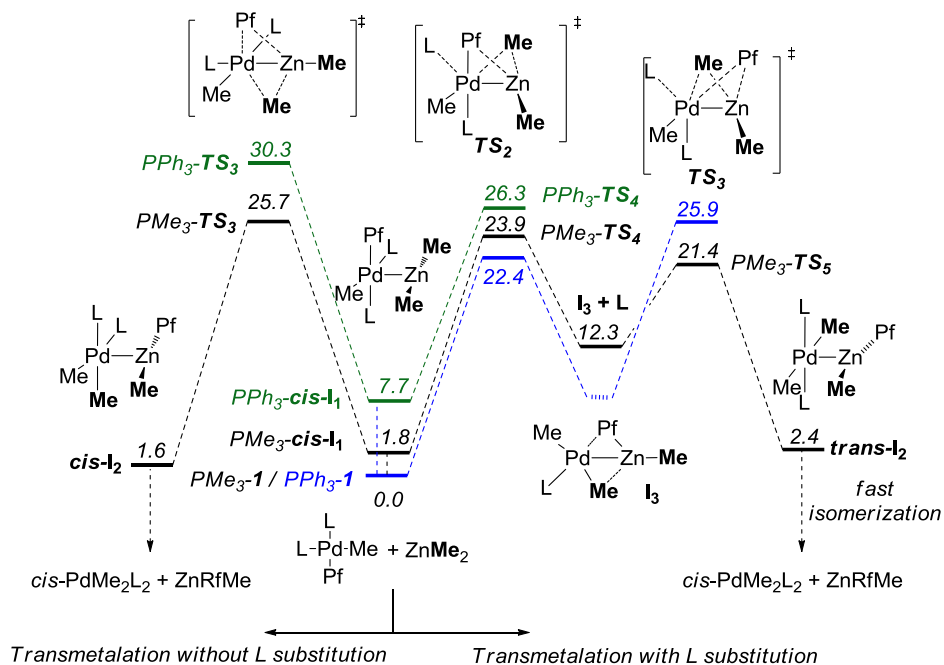


Figure III-9. Calculated (black L = PMe_3 , green L = PPh_3) and experimental (blue, L = PPh_3) profile of the secondary transmetalation: reaction between $\text{cis}[\text{PdArMe}(\text{L})_2]$ (**1**) and ZnMe_2 , (Rf = experimental, Pf = computational).

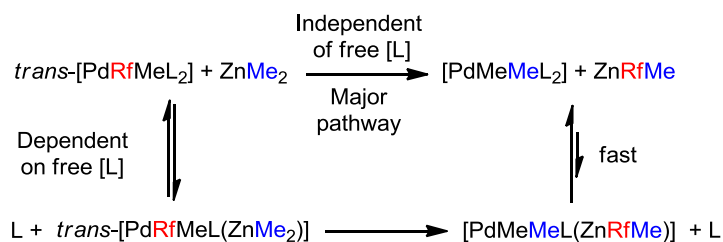
The calculated reaction mechanism for the secondary transmetalation of (**1a**) (Figure III-9) involves as first step a loose interaction between ZnMe_2 and (**1b**) to form cis-I_1 .^{*} This intermediate is common to the ZnMe_2 -catalyzed isomerization of (**1**) and (**2**) studied in the first block of this chapter.[†] From this adduct, the secondary transmetalation can take place directly through TS_3 (*Transmetalation without L substitution*, it will be commented later in detail), or through the calculated lower energy pathway involving the substitution of one ligand by ZnMe_2 (through TS_4) and subsequent Rf/Me exchange between the Pd and Zn centers (TS_5) (*Transmetalation with L substitution*). This pathway can be described as a double substitution process

^{*} The Pd and Zn reagents are engaged in a Van der Waals complex in cis-I_1 and cis-I_2 , and the same can be stated for trans-I_1 and trans-I_2 in Figure III-10. The nature of these intermediates has been discussed in the first part of this chapter, because they are common intermediates of the ZnMe_2 -catalyzed isomerization of (**1**) and (**2**).

[†] $\text{TS}_3\text{-PPh}_3$ has not been located yet. Further computational work is ongoing.

and leads inversion of the stereochemistry at the palladium center. According to the high activation energy found for the transmetalation without L substitution (30.3 kcal/mol), this alternative pathway is not competitive for the *cis* isomer in very nice agreement with the experimental observations.

The reaction of *trans*-[PdRfMe(PPh₃)₂] (**2a**) with ZnMe₂ was studied under the same experimental conditions. In contrast with the reaction of the *cis* isomer, the dependence of the reaction rate on (**2a**) on [PPh₃] is small, and the experimental order of the secondary transmetalation reaction on [PPh₃] is -0.35. These data suggest that there are two competitive pathways, one of them independent of phosphine concentration, and another (slower but not negligible) that depends on the phosphine concentration (Scheme III-19).



Scheme III-19. Proposed sequence of reactions producing Me/Rf exchange between complex (**2a**) and ZnMe₂. For calculated structures see Figure III-10.

The experimental data fit well into this model for (**2a**), although only a lower limit for the experimental activation energy of the major direct Rf/Me exchange (without phosphine substitution) can be obtained, and also an upper limit for that of the less contributing mechanism involving PPh₃ substitution.* The lower limit of the experimental activation energies via direct exchange is >23.7 kcal·mol⁻¹, whereas the overall energy of the mechanism involving PPh₃ substitution is <25.0 kcal·mol⁻¹.

* A maximum rate limit without ligand substitution was estimated assuming that this is the only pathway operating under the maximum concentration of PPh₃ used (7 equivalents with regard to the Pd complex). Assuming this maximum value for the fitting, a minimum value for the overall rate of the pathway involving ligand substitution can be obtained (see experimental part).

Note that the activation energy of direct pathway must be smaller than that of the stepwise mechanism.

The DFT-calculated pathways and the experimental and computed $\Delta G_{298\text{K}}^\ddagger$ are also shown in Figure III-10. As in the calculated pathway for the *cis* isomer, the transmetalation without ligand substitution takes place with conservation of Pd stereochemistry, leading to *trans*-[PdMe₂(PPh₃)₂]. These are concerted substitutions in which the Zn–Me and Pd–Rf bonds are broken while the Zn–Rf and Pd–Me bond are formed in one single step. The new C–Pd bond is formed in the same position where Rf–Pd was, as expected from an associative substitution. This type of transition state has been found in the study of the primary transmetalation of *trans*-Pd complexes with ZnMe₂ (see Scheme III-6).²⁴ The stepwise mechanism involves a rate limiting substitution of L(PMe₃ or PPh₃) via **TS**₇, leading to the tetracoordinate bimetallic intermediate **I**₄. This intermediate evolves by concerted Rf/Me exchange with concomitant re-coordination of PMe₃, giving rise to the final product *cis*-[PdMe₂L₂].

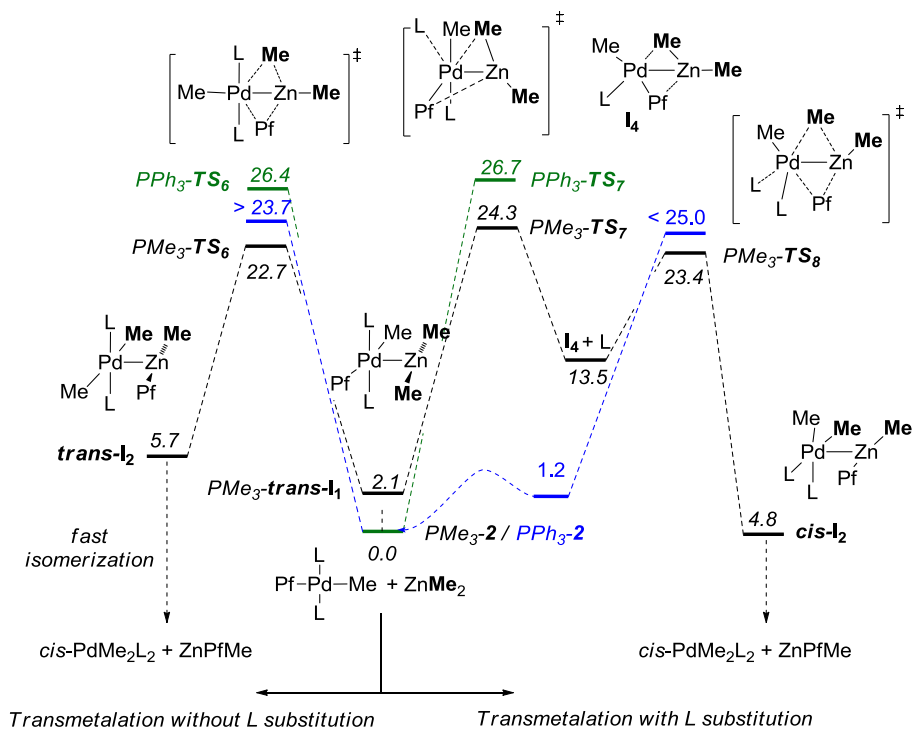


Figure III-10. Calculated (black L= PMe₃, green L= PPh₃) and experimental (blue, L= PPh₃) profile of the secondary transmetalation: reaction between *trans*-[PdArMe(L)₂] (**2a**) and ZnMe₂, (Rf = experimental, Pf= computational).

The DFT calculations in Figure III-10 reflect very well the experimental findings that the transmetalations without L substitution (TS₆-PPh₃, $\Delta G^\ddagger = 26.4$ kcal/mol) and with L substitution (TS₇-PPh₃, $\Delta G^\ddagger = 26.7$ kcal/mol) are competitive for the *trans* isomer (**2b**)*.

As can be deduced from the experimental data (in blue in Figure III-9 and Figure III-10) and also in good agreement with the computational data, the Rf/Me exchange is somewhat faster from complex (**2a**) than from complex (**1a**). The greater efficiency of the direct Rf/Me exchange in the *trans* isomer (**2a**) can be understood considering that the large *trans*-effect of the methyl group directs the

* *trans*-I₁ and TS₈-PPh₃ have not been located yet. Further computational work is ongoing. It is likely that the energy of TS₈-PPh₃ is lower than TS₇-PPh₃ if the same tendency of PMe₃ is maintained. If this is not eventually the case, the energy of TS₈-PPh₃ should be used for comparison with TS₆-PPh₃.

substitution to the Rf group, whereas in the case of complex (**1a**), the Me ligand stabilizes the TS of the substitution of PPh₃, favoring the transmetalation with L substitution.

3.2. Conclusions

As it was observed along the complete study of the reaction of [PdR¹R²L₂] complexes with ZnMe₂, several observations with synthetic consequences for the Negishi cross-coupling reaction can be noted:

The undesired group exchange between (**1**) and (**2**) with ZnMe₂ takes place at an appreciable rate at room temperature. This means that both intermediates should be removed efficiently from the reaction field in order to minimize the rate of the undesired group exchange with ZnMe₂. Reductive elimination only takes place from (**1**), and spontaneous and ZnMe₂-catalyzed isomerization reaction rates are in the same order of magnitude of the secondary transmetalation.

It was reported in our early work that primary transmetalation between (**3**) and ZnMe₂ yields preferably (**2**) and only minor quantities of (**1**).³³ Thus, complex (**2**) is meant to accumulate in solution in these conditions and it is likely that it will generate most of the undesired group exchange taking place via [PdR¹R²L₂] intermediates.* The addition of free ligand slows down the secondary transmetalation of (**1**) with ZnMe₂, but in the case of (**2**) only to a limited extent. Considering that (**2**) will be the major species formed with ZnMe₂ as transmetalating agent, the impact of the addition of free ligand on the secondary transmetalation is expected to be minor.

With all this information in hand, we can contribute to design more efficient Negishi synthesis. In order to minimize the effect of undesired transmetalations, (**1**) and (**2**) should not accumulate in the reaction conditions. In this regard, two simple strategies can be proposed:

* The ongoing study of the secondary transmetalation between (**3**) and ZnMe₂ will conclude whether the formation of ZnRfMe takes place preferably at [PdR¹R²L₂] or at [PdR¹XL₂] complexes.

- Use of chelating ligands: only *cis* complexes will be present in the reaction field, preventing the accumulation of *trans* isomers that cannot undergo reductive elimination and block the catalytic cycle.
- Use of ligands able to promote fast reductive eliminations: As already discussed, the secondary transmetalation is competition with the reductive elimination in the case of *cis* intermediates. Should the latter reaction be sufficiently accelerated, the undesired group exchange would be greatly minimized.

These two features are very nicely combined in the phosphine-olefin ligands that we have used in sp^2 - sp^3 Negishi coupling with great results.⁴⁶ In combination with the optimum transmetalating agent (it turned out to be ZnMeCl instead of ZnMe₂), the amount of undesired products was greatly diminished, leading to excellent yields in challenging cross-coupling reactions that usually lack of good selectivity due to the sluggish coupling of sp^3 groups.

4. Experimental section

4.1. General Methods

All reactions were carried out under N₂ or Ar in THF dried using a Solvent Purification System (SPS). NMR spectra were recorded on Bruker ARX 300, AV 400 or AV 500 instruments equipped with variable-temperature probes. Chemical shifts are reported in ppm from tetramethylsilane (¹H), 85% H₃PO₄ (³¹P), and CCl₃F (¹⁹F), with positive shifts downfield, at ambient probe temperature unless otherwise stated. The temperature for the NMR probe was calibrated with an ethylene glycol standard (high temperature) and with a methanol standard (low temperature).⁶¹ In the ¹⁹F and ³¹P NMR spectra registered in non-deuterated solvents, a coaxial tube containing acetone-*d*₆ was used to maintain the lock ²H signal, and the chemical shifts are reported from the CCl₃F signal in deuterated acetone. The compounds *cis*-[PdArMe(PPh₃)₂] (Ar = Rf = C₆Cl₂F₃, **1a**; Pf = C₆F₅, (**1b**)) and *trans*-[PdArMe(PPh₃)₂] (Ar = Rf = C₆Cl₂F₃, (**2a**); Pf = C₆F₅, (**2b**)) were prepared as reported in the literature for (**1a**) and (**2a**),³³ but using C₆F₅Li in the case of (**1b**) and (**2b**).

4.2. Synthesis of the complexes

***trans*-[PdMe₂(PPh₃)₂].** *Trans*-[PdClMe(PPh₃)₂] (200 mg, 0.30 mmol) and PPh₃ (77.6 mg, 0.30 mmol) were dissolved in 30 mL of THF in a two necked flask and stirred until all the solid was totally dissolved. The solution was cooled to (-80 °C), and then, ZnMe₂ (1.5 mL, 1.5 mmol, 2M in toluene) was added dropwise. When the addition was finished, extra ZnMe₂ was added fastly (1.5 mL, 1.5 mmol, 2M in toluene). The reaction was stirred at (-80 °C) for two hours. Precooled hexane at (-80 °C) was added to force a white solid to precipitate. It was filtered and washed with hexane (2x 5 mL) and dried under reduced pressure. Yield 140 mg (71 %). The solid must be checked at 210 K and in the presence of added PPh₃ (1 equivalent), in order to prevent isomerization of the complex to *cis*-[PdMe₂(PPh₃)₂].

¹H NMR (400 MHz, THF-*d*₈, 210K) δ 7.71 (q, *J* = 5.8 Hz, 2H), 7.62 – 7.48 (m, 13H), 7.41 (m, 21H), -0.89 (t, *J* = 5.4 Hz, 6H). ³¹P {¹H} NMR (162 MHz, THF-*d*₈, 210K) δ 42.84 (s). Anal. Calcd for C₃₈H₃₆PPd: C, 69.04; H, 5.49. Found: C, 68.79; H 5.32.

4.3. Spontaneous isomerization of *cis*-[PdArMe(PPh₃)₂] (**1**) to *trans*-[PdArMe(PPh₃)₂] (**2**)

a) Kinetic experiments

In a standard experiment a NMR tube cooled to -80 °C was charged with *cis*-[PdRfMe(PPh₃)₂] (**1a**) (10 mg, 1.13x10⁻² mmol), PPh₃ (0 to 6 mg; 0 to 2.3x10⁻² mmol), and THF (0.60 mL). When the mixture got dissolved a coaxial capillary containing acetone-*d*₆ was added and the sample was placed into the NMR probe thermostated at 25 °C. Temperature equilibration of the sample was reached after 5 minutes inside the NMR probe. Evolution of the reaction was monitored by ³¹P NMR

or by ^{19}F NMR spectroscopy. Concentration-time data were acquired by integration of the ^{19}F NMR signals.

The initial rates of the isomerization reaction under different concentration of phosphine were measured as the slope of the first data points of the plot concentration of *trans*-[PdRfMe(PPh₃)₂] vs. time. Note that the disappearance of the starting compound *cis*-[PdRfMe(PPh₃)₂] is due to the isomerization but also to the reductive elimination of Rf-Me. The experimental values are collected in Table III-4.

The experiment with complexes containing C₆F₅ instead of C₆Cl₂F₃, **1b**, was carried out similarly. For the sake of comparison the values obtained in both experiments are included. Note the high similarity of the rates. Consequently other experiments were carried out only on the C₆Cl₂F₃ derivatives, which have simpler ^{19}F NMR spectra. Also for simplicity and calculation time economy the DFT calculations were carried out only on the C₆F₅ complexes. Figure III-11 and Figure III-12 show the dependence of the observed rate constant on the concentration of triphenylphosphine and the observed reaction order of the reaction on the concentration of triphenylphosphine.

Table III-4. Experimental values for the isomerization processes.⁽¹⁾

Isomerization of <i>cis</i> -[Pd(C ₆ F ₃ Cl ₂)Me(PPh ₃) ₂]					
[PPh ₃] M	r ₀ (M·s ⁻¹)	Ln(r ₀)	Ln[L] (M)	[<i>cis</i> -PdRfMeL ₂] M	k <i>cis</i> -> <i>trans</i> (r ₀ / [<i>cis</i> -PdRfMeL ₂] ₀)
0	1.60·10 ⁻⁶	-13.34		0.0183	8.73·10 ⁻⁵
2.12·10 ⁻³	1.61·10 ⁻⁷	-15.64	-6.16	0.0180	8.97·10 ⁻⁶
4.69·10 ⁻³	6.56·10 ⁻⁸	-16.54	-5.36	0.0184	3.56·10 ⁻⁶
6.75·10 ⁻³	4.54·10 ⁻⁸	-16.91	-5.00	0.0189	2.40·10 ⁻⁶
19.5·10 ⁻³	1.87·10 ⁻⁸	-17.79	-3.93	0.0177	1.05·10 ⁻⁶
30.0·10 ⁻³	8.00·10 ⁻⁹	-18.64	-3.50	0.0187	4.26·10 ⁻⁷
Isomerization of <i>cis</i> -[Pd(C ₆ F ₅)Me(PPh ₃) ₂]					
[PPh ₃] M	r ₀ (M·s ⁻¹)	Ln(r ₀)	Ln[L] (M)	[<i>cis</i> -PdPfMeL ₂]	k <i>cis</i> -> <i>trans</i> (r ₀ / [<i>cis</i> -PdPfMeL ₂] ₀)
0	1.63·10 ⁻⁶	-13.32		0.0199	8.19·10 ⁻⁵
0.0054	9.8·10 ⁻⁸	-16.14	-5.22	0.0197	4.97·10 ⁻⁶
0.0127	3.12·10 ⁻⁸	-17.28	-4.37	0.0207	1.50·10 ⁻⁶

(1) L = PPh₃; Rf = C₆Cl₃F₂; Pf = C₆F₅.

Cis/trans-isomerization of *cis*-[Pd(C₆Cl₃F₂)Me(PPh₃)₂]: Dependence on [PPh₃]

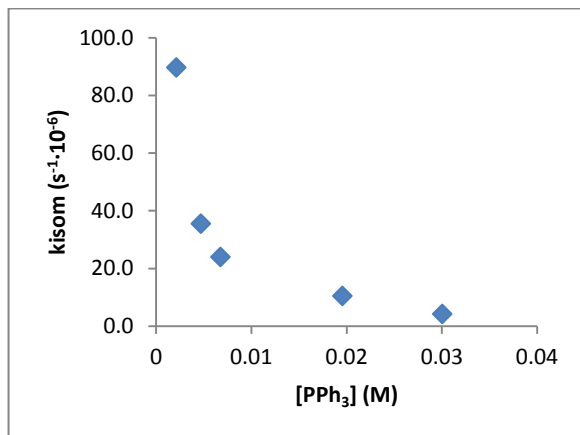


Figure III-11. Plot of the rate of formation of *trans*-[Pd(C₆Cl₃F₂)Me(PPh₃)₂] vs. [PPh₃], starting from *cis*-[Pd(C₆Cl₃F₂)Me(PPh₃)₂].

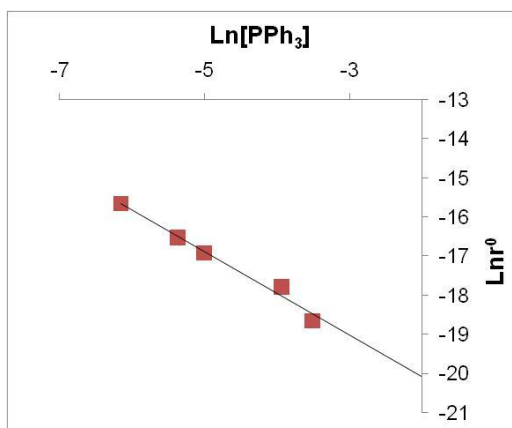


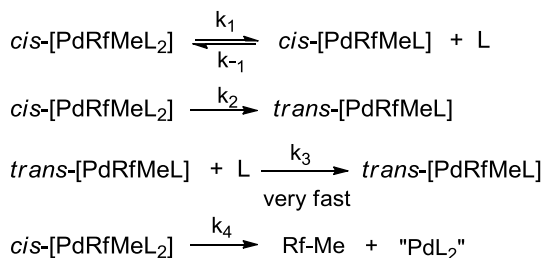
Figure III-12. Plot of the logarithmic rate of formation of *trans*-[Pd(C₆Cl₃F₂)Me(PPh₃)₂] vs. Ln[PPh₃] starting from *cis*-[Pd(C₆Cl₃F₂)Me(PPh₃)₂]. Reaction order on [PPh₃], $\gamma = -1.067x - 22.22$; $R^2 = 0.985$.

Table III-5. Confidence intervals of the linear regression shown in Figure III-12.

	Slope	Interception
<i>cis-trans</i> isomerization	(-0.83) - (-1.31)	(-21.04) - (-23.40)

Kinetic models and non-linear fitting (shown for Rf; the same for Pf)

The experimental data of concentration/time for the isomerization reaction obtained under different concentrations of PPh₃ can be fitted to the reaction sequence in Scheme III-20. Since the cross-coupling product Rf-Me was observed and reliably integrated in the ¹⁹F NMR spectra, a fourth equation was added to account for this process.



Scheme III-20. Proposed pathway of the isomerization of (1a) to (2a)

The fitting of rate constants was performed with the aid of the software "COPASI".⁵² Only data points (concentration vs. time of all the species) concerning up to 12% of conversion were used for the fitting. This allows considering the reaction as irreversible. At long reaction times, Pd(0) complexes are formed and behave as ligand scavengers and other decomposition products start to appear. Values of the concentration versus time plots at different [PPh₃] were used to feed the parameter estimation mode of COPASI. Standard deviations (σ) of the fitted rate constants are given by COPASI. Values are expressed with their interval confidence and a coverage factor of 2 (level of confidence 95%); $X_i \pm 2\sigma$.

k_1 , k_{-1} , k_2 and k_4 were fitted to the experimental data. An arbitrary value of 1000 was assigned to k_3 . This reaction is subsequent to a slow equilibrium and since it is meant to be very fast, no suitable values for the kinetic constant can be obtained with a data fitting. When the modeling was tested with values over 1000 for k_3 , the other constants remained unaffected. The values obtained for the rate constants k_1 and k_{-1} show a covariance > 0.99 , meaning that both parameters cannot be independently extracted from the experimental data points. Considering this fact, the ratio k_1/k_{-1} (K_{eq}) was calculated by fitting all the parameters simultaneously, choosing the values that provided the lowest statistic uncertainty for the model, obtaining a value of $K_{eq} = 2.0 \cdot 10^{-5}$. This value was introduced in the software as a bond for the independent values of k_1 and k_{-1} for further refinement.

Table III-6. Experimental kinetic constants.

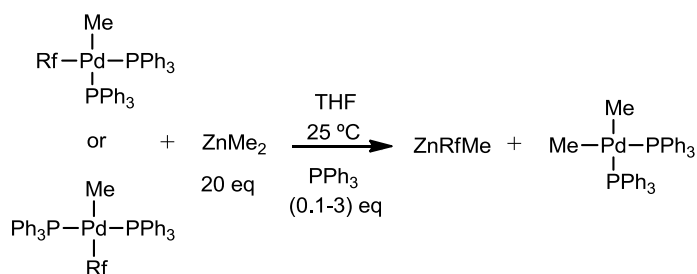
rate constant	Value (s ⁻¹)
k_1	$(9.9 \pm 1.0) \cdot 10^{-5}$
k_{-1}	4.7 ± 0.6
k_2	$(1.3 \pm 0.1) \cdot 10^{-3}$
k_4	$(9.8 \pm 0.1) \cdot 10^{-6}$

4.4. Transmetalation reaction between *cis*-[PdArMe(PPh₃)₂] (**1**) or *trans*-[PdArMe(PPh₃)₂] (**2**) and ZnMe₂

a) Kinetic experiments

In a standard experiment a solution of palladium complex *trans*-[PdRfMe(PPh₃)₂] (**2a**) or *cis*-[PdRfMe(PPh₃)₂] (**1a**) (10 mg, 1.13×10^{-2} mmol) and PPh₃ (0 to 6 mg; 0 to 2.3×10^{-2} mmol) in THF (0.40 mL) was prepared in a RMN tube and cooled to -80 °C. A solution of ZnMe₂ 2M in toluene (0.20 mL, 0.40 mmol) was added plus cold THF to make 0.60 mL of final volume. Then a coaxial capillary containing acetone-*d*₆ was added, and the sample was placed into the NMR probe thermostated at 25 °C. The kinetic experiments were followed by ³¹P NMR or ¹⁹F NMR and Temperature equilibration of the sample was reached after 5 minutes inside the NMR probe. Evolution of the reaction was monitored by ³¹P NMR or by ¹⁹F NMR spectroscopy. Concentration-time data were acquired by integration of the ¹⁹F NMR signals.

Transmetalation studies in the presence of added PPh₃



Scheme III-21. Transmetalation reaction between *trans*-[PdRfMe(PPh₃)₂] or *cis*-[PdRfMe(PPh₃)₂] and ZnMe₂ in the presence of different [PPh₃].

Table III-7. Experimental values for transmetalation kinetic studies. Complex *cis*-[PdRfMeL₂] (**1a**).

[PPh ₃] M	r ₀ (M·s ⁻¹)	<i>cis</i> -[PdRfMeL ₂]	[ZnMe ₂]	k obs
16.2·10 ⁻³	3.62·10 ⁻⁸	0.0197	0.6667	2.76·10 ⁻⁶
13.1·10 ⁻³	4.63·10 ⁻⁸	0.0197	0.6667	3.53·10 ⁻⁶
7.3·10 ⁻³	6.38·10 ⁻⁸	0.0197	0.6667	4.86·10 ⁻⁶
4.8·10 ⁻³	1.00·10 ⁻⁷	0.0195	0.6667	7.70·10 ⁻⁶
3.3·10 ⁻³	1.82·10 ⁻⁷	0.0198	0.6667	1.38·10 ⁻⁵
1.4·10 ⁻³	3.23·10 ⁻⁷	0.0196	0.6667	2.47·10 ⁻⁵

Table III-8. Experimental values for transmetalation kinetic studies. Complex *trans*-[PdRfMeL₂] (**2a**).

[PPh ₃] M	r ₀ (M·s ⁻¹)	<i>trans</i> -[PdRfMeL ₂]	[ZnMe ₂]	k obs
16.7·10 ⁻³	2.26·10 ⁻⁷	0.0197	0.6667	1.72·10 ⁻⁵
6.2·10 ⁻³	3.29·10 ⁻⁷	0.0196	0.6667	2.51·10 ⁻⁵
3.3·10 ⁻³	4.14·10 ⁻⁷	0.0197	0.6667	3.16·10 ⁻⁵
1.5·10 ⁻³	5.53·10 ⁻⁷	0.0197	0.6667	4.20·10 ⁻⁵
10.1·10 ⁻³	2.92·10 ⁻⁷	0.0196	0.6667	2.23·10 ⁻⁵
138.6·10 ⁻³	5.70·10 ⁻⁸	0.0198	0.6667	4.33·10 ⁻⁶

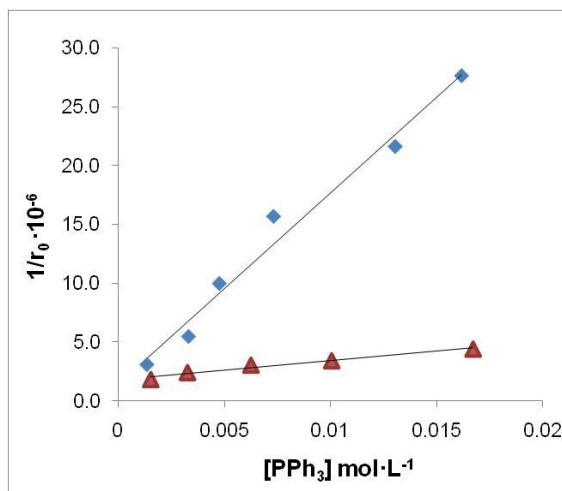
**Figure III-13.** Plot of the reversal of the rate of formation of ZnRfMe vs. [PPh₃] starting from *trans*-[PdRfMe(PPh₃)₂] (red spots, $y = 1.6 \cdot 10^8 x + 1.8 \cdot 10^6$; $R^2 = 0.97$) or *cis*-[PdRfMe(PPh₃)₂] (blue spots, $y = 1.6 \cdot 10^9 x + 0.1 \cdot 10^7$; $R^2 = 0.98$).

Table III-9. Confidence intervals of the linear regression.

	Slope	interception
<i>cis</i> -[PdRfMe(PPh ₃) ₂]	(1.3·10 ⁹ – 1.9·10 ⁹)	(-1.6·10 ⁶ – 4.5·10 ⁶)
<i>trans</i> -[PdRfMe(PPh ₃) ₂]	(1.1·10 ⁸ – 2.2·10 ⁸)	(13·10 ⁶ - 23·10 ⁶)

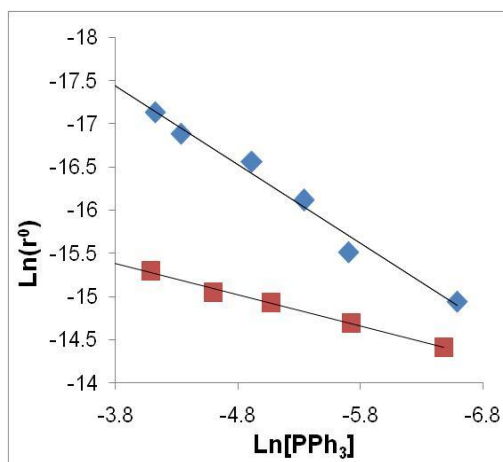


Figure III-14. Representation of $\ln[r^0]$ (formation of ZnRfMe) vs. $\ln[\text{PPh}_3]$ from (**2a**) (red spots, $y = -0.362x - 16.75$; $R^2 = 0.993$) or (**1a**) (blue spots, $y = -0.909x - 20.89$; $R^2 = 0.980$). The slope represents the kinetic order of the reactions on $[\text{PPh}_3]$.

Table III-10. Confidence intervals of the linear regression of Figure III-14.

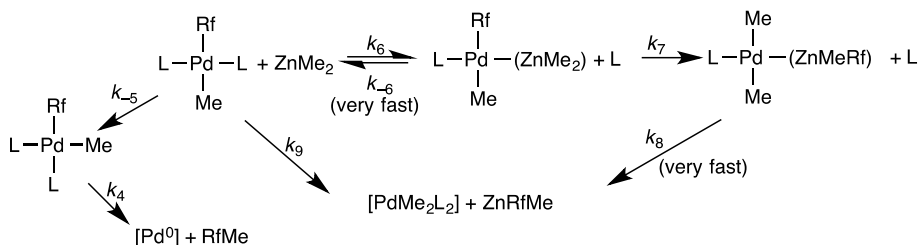
	Slope	interception
<i>cis</i> -[PdRfMe(PPh ₃) ₂]	(-1.09) - (-0.73)	(-21.83) - (-19.96)
<i>trans</i> -[PdRfMe(PPh ₃) ₂]	(-0.42) - (-0.31)	(-17.04) - (-16.47)

Proposed models

The fitting of rate constants was performed with the aid of the software “COPASI”.⁵² Only data points (concentration vs. time of all the species) concerning up to 12% of conversion were used for the fitting. This allows considering the reaction as irreversible. At long reaction times, Pd(0) complexes are formed and behave as ligand scavengers and other decomposition products start to appear. Values of the concentration versus time plots at different $[\text{PPh}_3]$ were used to feed the parameter estimation mode of COPASI. Standard deviations (σ) of the fitted rate constants are given by COPASI. Values are expressed with their interval confidence and a coverage factor of 2 (level of confidence 95%); $X_i \pm 2\sigma$.

Transmetalation from the *trans* isomer

The following model is proposed for the isomerization of (**2a**):



Scheme III-22. Proposed model for the transmetalation reaction between *trans*-[PdRfMe(PPh₃)₂] and ZnMe₂.

Rate constants k_6 , k_{-6} , k_7 and k_9 were fitted according to the proposed model of Scheme III-22. Constant k_{-5} was fixed for every experiment at different [PPh₃], as the experimental value obtained in the *cis-trans* isomerization modeling ($k_{-5} = 2.46 \cdot 10^{-5} \text{ s}^{-1}$). k_8 is subsequent to a slow equilibrium and since it is meant to be very fast, no suitable values can be obtained with a data fitting. When the modeling was tested with values over 1000 for k_8 , the other constants remained unaffected. k_4 was fixed according to the literature data ($k_4 = 8.9 \cdot 10^{-6} \text{ s}^{-1}$).³³

The fitting showed a covariance of 0.998 for the pair of variables k_7 and k_9 , meaning that this pair of values cannot be simultaneously calculated with the data available. Independently of k_7 and k_9 , k_6 has a value of $0.135 \cdot k_{-6}$ for $k_{-6} > 0.1$, so the substitution of the ligand L = PPh₃ in *trans*-[PdRfMeL₂] can be kinetically envisioned as a fast pre-equilibrium with an equilibrium constant of $K_6 = 0.135$.

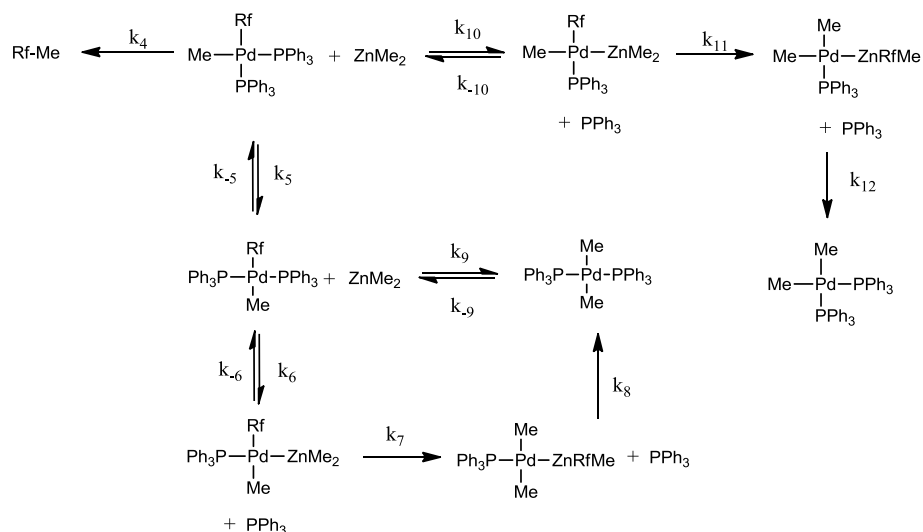
A maximum value for k_9 was estimated assuming that under the maximum concentration of [PPh₃] used, the transformation through k_6 were negligible, obtaining $k_9 = 2.4 \cdot 10^{-5} \text{ mol}^{-1} \text{ s}^{-1}$. Conversely, assuming this maximum value for k_9 , a minimum value for $k_7 = 2.12 \cdot 10^{-5} \text{ s}^{-1}$ was obtained.

Table III-11. Fitted rate constants according to Scheme III-22.

	Values (st dv)
k_6	13.50 (0.05) ($\text{mol}^{-1} \cdot \text{s}^{-1}$)
k_{-6}	100 (s^{-1}) (fixed)
k_7	2.12 (0.01) $\cdot 10^{-5}$ (s^{-1})
k_8	1000 ($\text{mol}^{-1} \cdot \text{s}^{-1}$) (fixed)
k_9	$2.49 \cdot 10^{-5}$ ($\text{mol}^{-1} \cdot \text{s}^{-1}$) (fixed)
k_4	$8.90 \cdot 10^{-6}$ (s^{-1}) (fixed)
k_{-5}	$2.46 \cdot 10^{-5}$ (s^{-1}) (fixed)

Transmetalation from the *cis* isomer

The following model is proposed for the isomerization of (1a):



Scheme III-23. Proposed model for the transmetalation reaction between *cis*-[PdRfMe(PPh₃)₂] and ZnMe₂.

Table III-12. Fitted rate constants according to Scheme III-23.

	Values
k_{10}	$(2.5 \pm 0.1) \cdot 10^{-4} \text{ (mol}^{-1} \cdot \text{s}^{-1}\text{)}$
k_{-10}	$4.2 \pm 0.1 \text{ (s}^{-1}\text{)}$
k_{11}	$(4.5 \pm 1) \cdot 10^{-4} \text{ (s}^{-1}\text{)}$
k_{12}	$1000 \text{ (mol}^{-1} \cdot \text{s}^{-1}\text{)}$
k_4	$8.90 \cdot 10^{-6} \text{ (s}^{-1}\text{)}$
k_5	$4.67 \cdot 10^{-5} \text{ (s}^{-1}\text{) (fixed)}$
k_{-5}	$2.46 \cdot 10^{-5} \text{ (s}^{-1}\text{) (fixed)}$

Rate constants k_{10} , k_{-10} and k_{11} were fitted according to the proposed model of Scheme III-23. Constants k_5 and k_{-5} were fixed for every experiment at different [PPh₃], as the experimental value obtained in the *cis-trans* isomerization modeling ($k_5 = 4.67 \cdot 10^{-5} \text{ s}^{-1}$, $k_{-5} = 2.46 \cdot 10^{-5} \text{ s}^{-1}$). k_4 was fixed according to the literature data ($k_4 = 8.9 \cdot 10^{-6} \text{ s}^{-1}$).³³ k_{12} is subsequent to a slow equilibrium and since it is meant to be

very fast, no suitable values can be obtained with a data fitting. When the modeling was tested with values over 1000 for k_8 , the other constants remained unaffected. Constants k_6 , k_7 , k_8 , k_9 and k_{-9} were fixed as obtained from the transmetalation from the *trans* isomer. Since the transmetalation from the *trans* isomer is faster in the studied range of $[PPh_3]$, these reactions were included to take into account the ZnRfMe formation for the *trans* isomer .

4.5. Computational methods

DFT calculations with the hybrid functionals B3LYP⁶² have been carried out using Gaussian09⁶³ to locate and characterize the stationary points on the potential energy surface. The 6-31G* basis set was used for all atoms with the exception of palladium, for which the Stuttgart-Dresden effective core potential⁶⁴ and the corresponding basis set were used. The optimized geometries have been characterized by harmonic analysis, and the nature of the stationary points has been determined according to the number of negative eigenvalues of the Hessian matrix. Internal reaction coordinates (IRCs) have been carried out from the transition structures to verify the proper connection with reactants and products.⁶⁵ Zero-point vibration energies (ZPVE) and thermal corrections (at 298 K, 1 atm) to the energy have been estimated using the computed frequencies applying the free particle, harmonic oscillator and rigid rotor approximations at the high temperature limit in a canonical ensemble. Solvation effects (to simulate the experimentally used THF) have been also included as single point corrections to the gas-phase free energy of the optimized structures computed with the wB97XD functional⁶⁶ (with dispersion correction) with the self-consistent reaction field (SCRF) method using the polarizable continuum model (PCM)⁶⁷ as implemented in Gaussian09.

Table III-13 gathers the computational results concerning the ZnMe₂-catalyzed isomerization depicted in Figure III-3. The Cartesian coordinates of these structures can be found in the supporting information of the corresponding publication.⁶⁸ Computational results of Figure III-9 and Figure III-10 are still ongoing and will not be included herein.

Calculated energies: (kcal/mol, wB97XD-PCM(THF)/SDD-6-31G*//B3LYP/SDD-6-31G*).

Table III-13. Computational values of all the species participating in Figure III-3.

<i>Label</i>	<i>Enthalpy</i>	<i>TS</i>	<i>Free Energy</i>	ΔG	wB97XD_THF_SP	ΔG
<i>ZnMe₂</i>	-1166449,7	23,0	-1166472,7	--	-1166494,6	--
<i>cis-1-PMe₃</i>	-1140511,3	57,4	-1140568,7	ref	-1140539,0	ref
<i>cis</i> ₁ - <i>PMe₃</i>	-2306970,1	64,6	-2307034,6	6,8	-2307047,4	3,7
<i>TS1-PMe₃</i>	-2306955,2	66,8	-2307022,0	19,4	-2307024,7	22,5
<i>Int-PMe₃</i>	-2017690,8	56,2	-2017747,0	6,2	-2017712,1	11,9
<i>PMe₃</i>	-289265,1	23,2	-289288,3	--	-289310,1	--
<i>TS2-PMe₃</i>	-2306954,7	66,1	-2307020,8	20,7	-2307025,2	22,9
<i>trans</i> ₁ - <i>PMe₃</i>	-2306974,7	65,0	-2307039,8	1,7	-2307050,6	-0,1
<i>ZnMe₂</i>	-1166449,7	23,0	-1166472,7	--	-1166494,6	--
<i>trans-2-PMe₃</i>	-1140515,9	56,3	-1140572,2	-3,5	-1140542,0	-2,1
<i>cis-1-PPh₃</i>	-1862163,6	84,5	-1862248,1		-1862191,4	
<i>ZnMe₂</i>	-1166449,7	23,0	-1166472,7	ref	-1166494,6	ref
<i>cis</i> ₁ - <i>PPh₃</i>	-3028615,3	94,8	-3028710,1	10,7	-3028692,9	7,7
<i>TS1-PPh₃</i>	-3028605,8	94,6	-3028700,4	20,4	-3028673,4	26,3
<i>Int-PPh₃</i>	-2378516,6	71,5	-2378588,1	-1,6	-2378537,1	7,8
<i>PPh₃</i>	-650094,4	40,0	-650134,4	--	-650136,6	--
<i>TS2-PPh₃</i>	-3028604,1	94,9	-3028698,9	21,9	-3028674,4	24,8
<i>trans-2-PPh₃</i>	-1862165,6	85,9	-1862251,5	-3,3	-1862190,0	-0,1
<i>ZnMe₂</i>	-1166449,7	23,0	-1166472,7	--	-1166494,6	--

5. References

1. (a) Magano, J.; Dunetz, J. R. *Chem. Rev.* **2011**, *111*, 2177–2250. (b) Manley, P. W.; Acemoglu, M.; Marterer, W.; Pachinger, W. *Org. Process Res. Dev.* **2003**, *7*, 436–445.
2. Jana, R.; Pathak, T. P.; Sigman, M. S. *Chem. Rev.* **2011**, *111*, 1417–1492.
3. The following reviews contain a detailed picture of Ni chemistry and seminal references can be found therein: (a) Hu, X. *Chem. Sci.* **2011**, *2*, 1867. (b) Phapale, V. B.; Cárdenas, D. J. *Chem. Soc. Rev.* **2009**, *38*, 1598–1607. For the use of other metals than Pd and Ni see the following publications: (c) Hammann, J. M.; Haas, D.; Knochel, P. *Angew. Chem. Int. Ed.* **2015**, *54*, 4478–4481. (d) Thapa, S.; Kafle, A.; Gurung, S. K.; Montoya, A.; Riedel, P.; Giri, R. *Angew. Chem. Int. Ed.* **2015**, *54*, 8236–8240. (e) Reddy, C. K.; Knochel, P. *Angew. Chem. Int. Ed.* **1996**, *35*, 1700–1701.
4. Tasker, S. Z.; Standley, E. A.; Jamison, T. F. *Nature* **2014**, *509*, 299–309.
5. (a) King, A. O.; Okukado, N.; Negishi, E. *J. Chem. Soc. Chem. Commun.* **1977**, 683. (b) Negishi, E.; King, A. O.; Okukado, N. *J. Org. Chem.* **1977**, *42*, 1821–1823.
6. Fauvarque, J. F.; Jutand, A. *J. Organomet. Chem.* **1977**, *132*, C17–C19.
7. Rathke, M. W. *The Reformatsky Reaction. Organic Reactions.* **1975**, *22*, 423–460.
8. Negishi, E. *Acc. Chem. Res.* **1982**, *15*, 340–348.
9. (a) Zhou, J.; Fu, G. C. *J. Am. Chem. Soc.* **2003**, *125*, 12527–12530. (b) Dai, C.; Fu, G. C. *J. Am. Chem. Soc.* **2001**, *123*, 2719–2724. (c) Fu, G. C. *Acc. Chem. Res.* **2008**, *41*, 1555–1564.
10. (a) Han, C.; Buchwald, S. L. *J. Am. Chem. Soc.* **2009**, *131*, 7532–7533. (b) Yang, Y.; Oldenhuis, N. J.; Buchwald, S. L. *Angew. Chem. Int. Ed.* **2013**, *52*, 615–619.
11. (a) Kantchev, E. A. B.; O'Brien, C. J.; Organ, M. G. *Angew. Chem. Int. Ed.* **2007**, *46*, 2768–2813. (b) Organ, M. G.; Avola, S.; Dubovyk, I.; Hadei, N.; Kantchev, E. A. B.; O'Brien, C. J.; Valente, G. *Chem. Eur. J.* **2006**, *12*, 4749–4755.
12. Boudier, A.; Bromm, L. O.; Lotz, M.; Knochel, P. *Angew. Chem. Int. Ed.* **2000**, *39*, 4414
13. (a) Rappoport, Z.; Marek, I. *The chemistry of organozinc compounds*; Ed. Patai Series, Wiley: Chichester, U.K., 2006. (b) Knochel, Paul; Jones, P. *Organozinc Reagents. A practical approach*; Oxford University Press; 1 edition, **2004**.

14. Bacsa, J.; Hanke, F.; Hindley, S.; Odedra, R.; Darling, G. R.; Jones, A. C.; Steiner, A. *Angew. Chem. Int. Ed.* **2011**, *50*, 11685–11687.
15. Thiele, K. H.; *Z. Anorg. Allg. Chem.*, **1962**, 319, 183.
16. For X-Ray structures of selected organozincs see: (a) Weidebruch, M.; Hermdorf, M.; Schäfer, A.; Pool, S.; Saak, W. *J. Organomet. Chem.* **1989**, *361*, 139–145. (b) Guerrero, a; Hughes, D. L.; Bochmann, M. *Organometallics* **2006**, *25*, 1525–1527.
17. (a) Koszinowski, K.; Bo, P. *Organometallics* **2009**, *28*, 100–110. (b) Koszinowski, K.; Böhler, P. *Organometallics* **2009**, *28*, 771–779.
18. (a) Metzger, A.; Bernhardt, S.; Manolikakes, G.; Knochel, P. *Angew. Chem. Int. Ed.* **2010**, *49*, 4665–4668. (b) Uchiyama, M.; Kameda, M.; Mishima, O.; Yokoyama, N.; Koike, M.; Kondo, Y.; Sakamoto, T. *J. Am. Chem. Soc.* **1998**, *120*, 4934–4946.
19. (a) Jin, L.; Liu, C.; Liu, J.; Hu, F.; Lan, Y.; Batsanov, A. S.; Howard, J. a K.; Marder, T. B.; Lei, A. *J. Am. Chem. Soc.* **2009**, *131*, 16656–16657. (b) Ochiai, H.; Jang, M.; Hirano, K.; Yorimitsu, H.; Oshima, K. *Org. Lett.* **2008**, *10*, 2681–2683.
20. MacIntosh, I. S.; Sherren, C. N.; Robertson, K. N.; Masuda, J. D.; Pye, C. C.; Clyburne, J. a C. *Organometallics* **2010**, *29*, 2063–2068.
21. Selected BDEs of zinc compounds are experimental values, except for Zn-I and Zn-Br bonds, which are averaged values: (a) Ruo, Y.-L.; *Comprehensive Handbook of Chemical Bond Energies*; CRC Press; 1 edition, **2007**.
22. The Pd-C bond dissociation energy was extracted from: Simoes, J. a. M.; Beauchamp, J. L. *Chem. Rev.* **1990**, *90*, 629–688. The Pd-halogen bond dissociation energy was obtained from: Lan, Y.; Liu, P.; Newman, S. G.; Lautens, M.; Houk, K. N. *Chem. Sci.* **2012**, *3*, 1987. Experimental information concerning Pd-halide dissociation can be obtained herein: Casares, J. A.; Coco, S.; Espinet, P.; Lin, Y. *Organometallics*, **1995**, 3058–3067.
23. (a) Ribagnac, P.; Blug, M.; Villa-Urbe, J.; Le Goff, X. F.; Gosmini, C.; Mézailles, N. *Chem. Eur. J.* **2011**, *17*, 14389–14393. (b) Yang, Y.; Mustard, T. J. L.; Cheong, P. H. Y.; Buchwald, S. L. *Angew. Chem. Int. Ed.* **2013**, *52*, 14098–14102.
24. (a) García-Melchor, M.; Fuentes, B.; Lledós, A.; Casares, J. A.; Ujaque, G.; Espinet, P. *J. Am. Chem. Soc.* **2011**, *133*, 13519–13526. (b) Fuentes, B.; García-Melchor, M.; Lledós, A.; Maseras, F.; Casares, J. A.; Ujaque, G.; Espinet, P. *Chem. Eur. J.* **2010**, *16*, 8596–8599.
25. Chass, G. a; O'Brien, C. J.; Hadei, N.; Kantchev, E. A. B.; Mu, W.-H.; Fang, D.-C.; Hopkinson, A. C.; Csizmadia, I. G.; Organ, M. G. *Chemistry* **2009**, *15*, 4281–4288.

26. (a) Álvarez, R.; De Lera, A. R.; Aurrecochea, J. M.; Durana, A. *Organometallics* **2007**, *26*, 2799–2802. (b) González-Pérez A. B.; Álvarez, R.; Nieto Faza O.; de Lera, A. R.; Aurrecochea, J. *Organometallics* **2012**, *31*, 2053–2058.
27. Pyykkö, P. *Chem. Rev.* **1997**, *97*, 597–636.
28. See: Pérez-Rodríguez, M.; Braga, A. A. C.; Garcia-Melchor, M.; Pérez-Temprano, M. H.; Casares, J. A.; Ujaque, G.; de Lera, A. R.; Álvarez, R.; Maseras, F.; Espinet, P. *J. Am. Chem. Soc.* **2009**, *131*, 3650–3657, and references therein.
29. Böck, K.; Feil, J. E.; Karaghiosoff, K.; Koszinowski, K. *Chem. Eur. J.* **2015**, *21*, 5548–5560.
30. (a) Liu, Q.; Lan, Y.; Liu, J.; Li, G.; Wu, Y. D.; Lei, A. *J. Am. Chem. Soc.* **2009**, *131*, 10201–10210. (b) Li, J.; Jin, L.; Liu, C.; Lei, A. *Chem. Commun.* **2013**, *49*, 9615–9617. (c) Li, J.; Jin, L.; Liu, C.; Lei, A. *Org. Chem. Front.* **2014**, *1*, 50–53.
31. Van der Waals radii of Pd = 1.63 Å, Zn = 1.39 Å, Au = 1.66 Å, see: Bondi, A. *J. Phys. Chem.* **1964**, *68*, 441–451.
32. Rodriguez, A.; Kuhn, M. *J. Phys. Chem.* **1996**, *100*, 381–389.
33. Casares, J. A.; Espinet, P.; Fuentes, B.; Salas, G. *J. Am. Chem. Soc.* **2007**, *129*, 3508–3509.
34. Valente, C.; Belowich, M. E.; Hadei, N.; Organ, M. G. *European J. Org. Chem.* **2010**, 4343–4354.
35. Achonduh, G. T.; Hadei, N.; Valente, C.; Avola, S.; O'Brien, C. J.; Organ, M. G. *Chem. Commun.* **2010**, *46*, 4109–4111.
36. (a) Hunter, H. N.; Hadei, N.; Blagojevic, V.; Patschinski, P.; Achonduh, G. T.; Avola, S.; Bohme, D. K.; Organ, M. G. *Chem. Eur. J.* **2011**, *17*, 7845–7851. (b) McCann, L. C.; Hunter, H. N.; Clyburne, J. a C.; Organ, M. G. *Angew. Chem. Int. Ed.* **2012**, *51*, 7024–7027. (c) Mccann, L. C.; Organ, M. G. *Angew. Chem. Int. Ed.* **2014**, 4386–4389.
37. Miyaura, N.; Ishiyama, T.; Sasaki, H.; Ishikawa, M.; Satoh, M.; Suzuki, A. **1989**, 314–321.
38. Geist, E.; Kirschning, A.; Schmidt, T. *Nat. Prod. Rep.* **2014**, *31*, 441–448.
39. (a) Lei, T.; Wang, J. Y.; Pei, J. *Chem. Mater.* **2014**, *26*, 594–603. (b) Cordovilla, C.; Coco, S.; Espinet, P.; Donnio, B. *J. Am. Chem. Soc.* **2010**, *132*, 1424–1431.
40. Aldeghi, M.; Malhotra, S.; Selwood, D. L.; Chan, A. W. E. *Chem. Biol. Drug Des.* **2014**, *83*, 450–461.

41. Lovering, F.; Bikker, J.; Humblet, C. *J. Med. Chem.* **2009**, *52*, 6752–6756.
42. Jana, R.; Pathak, T. P.; Sigman, M. S. *Chem. Rev.* **2011**, *111*, 1417–1492.
43. Ariafard, A.; Lin, Z. *Organometallics* **2006**, *25*, 4030–4033.
44. Cárdenas, D. J. *Angew. Chem. Int. Ed.* **2003**, *42*, 384–387.
45. Sköld, C.; Kleimark, J.; Trejos, A.; Odell, L. R.; Nilsson Lill, S. O.; Norrby, P. O.; Larhed, M. *Chem. Eur. J.* **2012**, *18*, 4714–4722.
46. (a) Gioria, E.; Martínez-Ilarduya, J. M.; Espinet, P. *Organometallics* **2014**, *33*, 4394–4400. (b) Gioria, E.; Martínez-Ilarduya, J. M.; García-Cuadrado, D.; Miguel, J. A.; Genov, M.; Espinet, P. *Organometallics* **2013**, *32*, 4255–4261.
47. (a) Luo, X.; Zhang, H.; Duan, H.; Liu, Q.; Zhu, L.; Zhang, T.; Lei, A. *Org. Lett.* **2007**, *9*, 4571–4574. (b) Zhang, H.; Luo, X.; Wongkhan, K.; Duan, H.; Li, Q.; Zhu, L.; Wang, J.; Batsanov, A. S.; Howard, J. A. K.; Marder, T. B.; Lei, A. *Chem. Eur. J.* **2009**, *15*, 3823–3829.
48. Van Asselt, R.; Elsevier, C. J. *Organometallics*, **1994**, *13*, 1972–1980.
49. Casado, A. L.; Casares, J. A.; Espinet, P. *Inorg. Chem.* **1998**, *37*, 4154–4156, and references therein.
50. (a) Pérez-Temprano, M. H.; Gallego, A. M.; Casares, J. A.; Espinet, P., *Organometallics*, **2011**, *30*, 611–617. (b) Cordovilla, C.; Bartolomé, C.; Martínez-Ilarduya, J. M.; Espinet, P. *ACS Catal.* **2015**, 3040–3053.
51. For the use of perhalogenated aryls in other studies and for their NMR spectroscopic features see: Espinet, P.; Albéniz, A. C.; Casares, J. A.; Martínez-Ilarduya, J. M. *Coord. Chem. Rev.* **2008**, *252*, 2180–2208.
52. COmplex PATHway Simulator. Hoops, S.; Sahle, S.; Gauges, R.; Lee, C.; Pahle, J.; Simus, N.; Singhal, M.; Xu, L.; Mendes, P.; Kummer, U. *Bioinformatics* **2006**, *22*, 3067–3074.
53. <http://www.ccdc.cam.ac.uk/Solutions/FreeSoftware/Pages/FreeMercury.aspx>.
54. For an interesting discussion concerning the entropic cost of association of two molecules see: Page, M. *Angew. Chem. Int. Ed.* **1977**, *16*, 449–459.
55. Haaland, A.; Green, J. C.; McGrady, G. S.; Downs, A. J.; Gullo, E.; Lyall, M. J.; Timberlake, J.; Tutukin, A. V.; Volden, H. W.; Østby, K.-A. *Dalton Trans.* **2003**, 4356–4366.
56. Antes, I.; Frenking, G. *Organometallics* **1995**, *14*, 4263–4268.

57. (a) Kohn, W.; Sham, L. J. *Physical Reviews*, **1965**, A1133–A1138. (b) S. Hamel, P. Duffy, M. E. Casida, D. R. Salahub, *J. Electron Spectrosc. Relat. Phenom.*, **2002**, *123*, 345-363, and references therein. Orbitals represented using Chemcraft (Figure III-5, <http://www.chemcraftprog.com/index.html>) or Chemission (Figure III-6, <http://www.chemission.com>).
58. For an early proposal of side-on coordination of C–M (M = Hg) bond as the initial step of transmetalation from a metal nucleophile, and for early studies by Ingold, Reutov, and others see references in: Reutov, O. A. *Rus. Chem. Rev.* **1967**, *36*, 163–174.
59. Purcell, K. F. and Kotz, J. C. *Inorganic Chemistry*, **1977**, Saunders Co., Philadelphia, p. 176.
60. (a) Usón, R.; Fornies, J. *Adv. Organomet. Chem.* **1988**, *28*, 219-297. (b) Alonso, M.A.; Casares, J. A.; Espinet, P.; Martínez-Ilarduya, J. M.; Perez-Briso, C. *Eur. J. Inorg. Chem.* **1998**, *11*, 1745-1753. (c) Espinet, P.; Martínez-Ilarduya, J. M.; Perez-Briso, C.; Casado, A. L.; Alonso, M.A. *J. Organomet. Chem.* **1998**, *551* (1-2), 9-20. (d) Bartolome, C.; Espinet, P.; Villafañe, F.; Giesa, S.; Martin, A.; Orpen, A. G. *Organometallics* **1996**, *15*, 2019-2028
61. Amman, C.; Meier, P.; Merbach, A. E. *J. Magn. Reson.* **1982**, *46*, 319-321.
62. (a) Becke, A. D. *J. Chem. Phys.* **1993**, *98*, 5648. (b) Lee, C.; Yang, W.; Parr, R. G. *Phys. Rev. B: Condens. Matter* **1988**, *37*, 785.
63. Frisch, M. J.; Trucks, G. W.; Schlegel, H. B.; Scuseria, G. E.; Robb, M. A.; Cheeseman, J. R.; Scalmani, G.; Barone, V.; Mennucci, B.; Petersson, G. A.; Nakatsuji, H.; Caricato, M.; Li, X.; Hratchian, H. P.; Izmaylov, A. F.; Bloino, J.; Zheng, G.; Sonnenberg, J. L.; Hada, M.; Ehara, M.; Toyota, K.; Fukuda, R.; Hasegawa, J.; Ishida, M.; Nakajima, T.; Honda, Y.; Kitao, O.; Nakai, H.; Vreven, T.; Montgomery, J. A.; Peralta, J. E.; Ogliaro, F.; Bearpark, M.; Heyd, J. J.; Brothers, E.; Kudin, K. N.; Staroverov, V. N.; Kobayashi, R.; Normand, J.; Raghavachari, K.; Rendell, A.; Burant, J. C.; Iyengar, S. S.; Tomasi, J.; Cossi, M.; Rega, N.; Millam, J. M.; Klene, M.; Knox, J. E.; Cross, J. B.; Bakken, V.; Adamo, C.; Jaramillo, J.; Gomperts, R.; Stratmann, R. E.; Yazyev, O.; Austin, A. J.; Cammi, R.; Pomelli, C.; Ochterski, J. W.; Martin, R. L.; Morokuma, K.; Zakrzewski, V. G.; Voth, G. A.; Salvador, P.; Dannenberg, J. J.; Dapprich, S.; Daniels, A. D.; Farkas, Foresman, J. B.; Ortiz, J. V.; Cioslowski, J.; Fox, D. J., Gaussian 09, Revision B.01, Wallingford CT, 2009.
64. Andrae, D.; Häussermann, U.; Dolg, M.; Stoll, H.; Preuss, H. *Theor. Chim. Acta.* **1990**, *77*, 123-141.
65. (a) Fukui, K. *Acc. Chem. Res.* **1981**, *14*, 363. (b) Gonzalez, C.; Schlegel, H. B. *J. Phys. Chem.* **1990**, *94*, 5523.

66. Chai, J.-D.; Head-Gordon, M. *Phys. Chem. Chem. Phys.* **2008**, *10*, 6615.
67. (a) Tomasi, J.; Persico, M. *Chem. Rev.* **1994**, *94*, 2027. (b) Cossi, M.; Scalmani, G.; Rega, N.; Barone, V. *J. Chem. Phys.* **2002**, *117*, 43. (c) Tomasi, J.; Mennucci, B.; Cammi, R. *Chem. Rev.* **2005**, *105*, 2999.
68. delPozo, J.; Gioria, E.; Casares, J. A.; Álvarez, R.; Espinet, P. *Organometallics* **2015**, *34*, 3120–3128.

Chapter IV

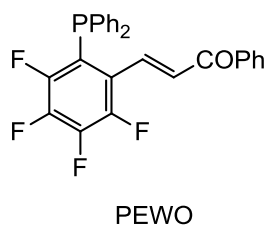
**Unexpected instability of
Pd–Phosphine–Olefin
complexes**

1. Introduction

Pd catalyzed cross-coupling reactions involve several steps: oxidative addition, transmetalation, reductive elimination, and the often overlooked isomerization, but reductive elimination is most decisive because it is typically irreversible and it is this irreversibility that will pull forward the whole catalytic cycle.^{1,2} When reductive elimination is not fast, competitive side-reactions such as homocoupling, β -hydride elimination, or others, will dramatically decrease the yield of the desired cross-coupling reaction.³

Phosphine-(electron-withdrawing olefin) chelating ligands (PEWO ligands) developed by our group and by others,^{4,5,6} have been used in the Pd-catalyzed coupling of alkyls with aryls (see Scheme IV-1). These couplings are usually difficult due to formation of Pd-alkyl intermediates that can undergo fast β -hydride elimination and lead to Ar-H reduction products instead of the desired Ar-alkyl products.³ When the reductive elimination step is made fast enough by the PEWO ligand, secondary reactions such as β -hydride elimination can be minimized or eliminated.^{4,5}

Thus, PEWO ligands are able to reduce the coupling activation energy accelerating typically slow couplings. In this regard, palladium-catalyzed fluorination and trifluoromethylation of aromatic halides is a booming area usually hindered by the high activation energy of the reductive elimination step in Pd^{II} complexes bearing these moieties, such as [Pd(Ar)(F)L₂] and [Pd(Ar)(CF₃)L₂].^{7,8} There are only a few examples of ligands able to promote these transformations.^{9,10} Design of appropriate ligands to facilitate the coupling of fluorinated groups is highly desirable, and some successful reactions have been reported.^{11,12} Having in mind the great potential of PEWOs at developing Pd-catalyzed fluorination and trifluoromethylation, it was our purpose to prepare complexes on which we could study experimentally the critical reductive elimination step of Ar-F and Ar-CF₃. The PEWO ligand in Scheme IV-1, designed in our group, was used.

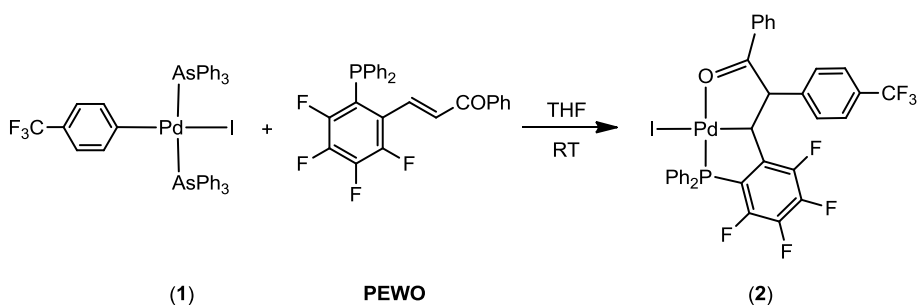


Scheme IV-1. Structure of the phosphine-olefin ligand.

2. Results and discussion

a) Synthesis of the products

In this regard, we envisioned a synthesis for the target compounds $[\text{Pd}(\text{C}_6\text{H}_4\text{CF}_3)(\text{F})(\text{PEWO})]$ and $[\text{Pd}(\text{C}_6\text{H}_4\text{CF}_3)(\text{CF}_3)(\text{PEWO})]$, by displacement of the labile AsPh_3 on the complex $[\text{Pd}(\text{C}_6\text{H}_4\text{CF}_3)(\text{I})(\text{AsPh}_3)_2]$ (**1**), and subsequent fluorination and trifluoromethylation of the product $[\text{Pd}(\text{C}_6\text{H}_4\text{CF}_3)(\text{I})(\text{PEWO})]$ (**2**) according to the procedure described by Grushin.^{8a} Stirring complex $[\text{Pd}(\text{C}_6\text{H}_4\text{CF}_3)(\text{I})(\text{AsPh}_3)_2]$ with one equivalent of PEWO leads to full displacement of AsPh_3 . Unfortunately, complex $[\text{Pd}(\text{C}_6\text{H}_4\text{CF}_3)(\text{I})(\text{PEWO})]$ is not stable, and undergoes a process of migratory insertion of the aryl into the olefin of the ligand, leading to the isolable product (**2**). The structure of this product was confirmed by single crystal X-Ray diffraction.



Scheme IV-2. Reaction of (**1**) with PEWO generates product (**2**).

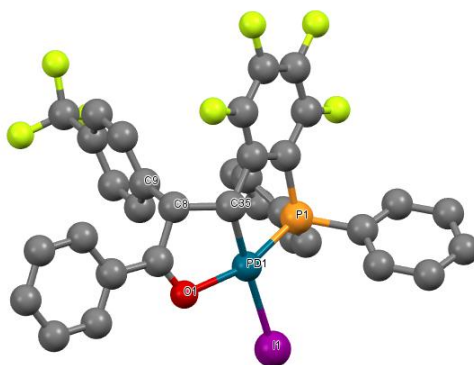
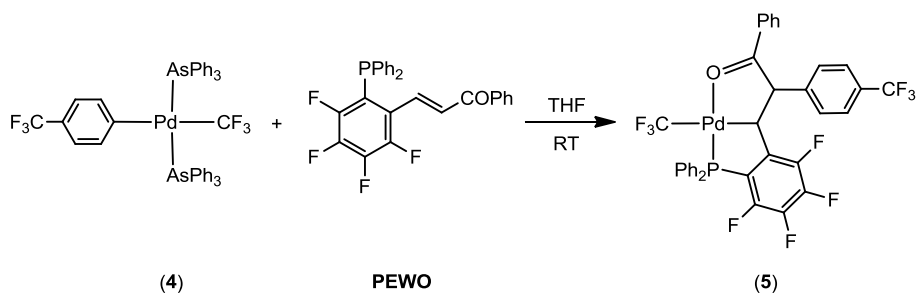


Figure IV-1. X-Ray structure of (2). H atoms are omitted for clarity.

Considering that complex $[\text{Pd}(\text{C}_6\text{H}_4\text{CF}_3)(\text{I})(\text{PEWO})]$ cannot be isolated but AsPh_3 displacement is effective, we prepared the new compounds $[\text{Pd}(\text{C}_6\text{H}_4\text{CF}_3)(\text{F})(\text{AsPh}_3)_2]$ (3) and $[\text{Pd}(\text{C}_6\text{H}_4\text{CF}_3)(\text{CF}_3)(\text{AsPh}_3)_2]$ (4) and studied their reaction with PEWO. The reaction of $[\text{Pd}(\text{C}_6\text{H}_4\text{CF}_3)(\text{F})(\text{AsPh}_3)_2]$ with PEWO leads to a complicate mixture of products that we could not identify, among which $\text{F}-\text{C}_6\text{H}_4\text{CF}_3$ is not present. In a similar fashion to what we observed with (2), $[\text{Pd}(\text{C}_6\text{H}_4\text{CF}_3)(\text{CF}_3)(\text{PEWO})]$ is not stable and rearranged to complex (5).



Scheme IV-3. Ligand displacement reaction of (4) and subsequent aryl migratory insertion after reaction with PEWO ligand.

b) Thermal decomposition studies

Complexes (3) and (4) were decomposed in toluene at 85 °C for several hours. In these conditions, the starting materials are not stable and lead to complicated mixtures of products among which $\text{CF}_3\text{C}_6\text{H}_4-\text{F}$ and $\text{CF}_3\text{C}_6\text{H}_4-\text{CF}_3$ were not detected,

neither in the presence of added PEWO. When complex (5) is heated at 85 °C in toluene (poorly soluble) or CH₂Cl-CH₂Cl, no reductive elimination of CF₃C₆H₄-CF₃ was achieved either.*

2.2. Computational examination of the olefin insertion into the Pd-Aryl bond

As it was found in our studies, aryl-Pd(PEWO) compounds are unstable and tend to rearrange via processes of migratory insertion of the olefin into the Pd-aryl bond. This process takes place at significant rates at room temperature and might be a serious drawback in catalysis. After ligand rearrangement, a palladacycle is obtained and the benefits for coupling of the presence of the acceptor olefin tethered are lost. This process reminds to that reported by Buchwald regarding the bulky biaryl phosphines developed in his group.¹³ Further insights into this process have been obtained by computational means, taking into account both [PdR¹X(PEWO)] and [PdR¹R²(PEWO)] complexes, which are the catalytic intermediates that can undergo this rearrangement. (see experimental section for computational details).

* The major products of these reactions are CF₃C₆H₄-C₆H₄CF₃ and CF₃C₆H₅, detected by GC-MS. When PEWO is present, phosphonium salts were formed, according to the ³¹P NMR spectra. The reactions are not affected by the presence of either 1 or 2 equivalents of EWO when present.

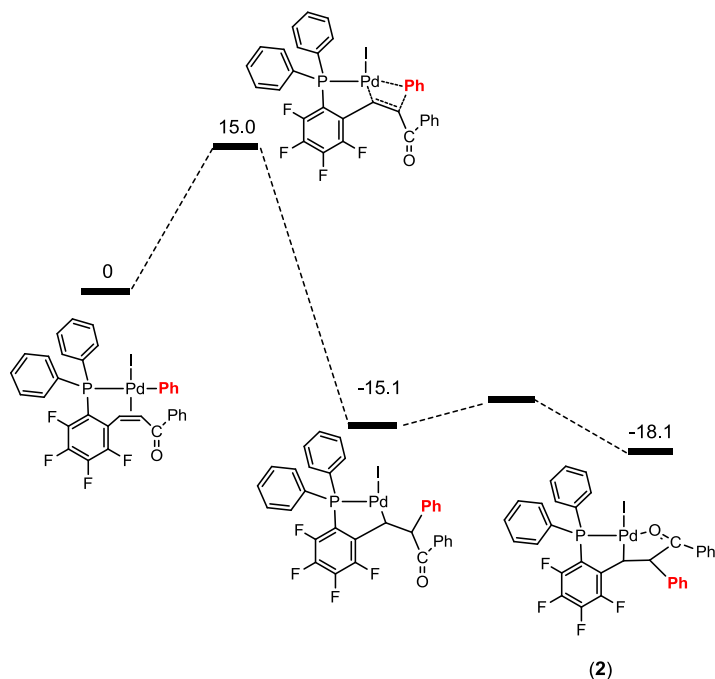


Figure IV-2. Reaction mechanism and activation energies of the olefin insertion process and formation of (2).

The reaction is found to be fast and it is greatly endergonic. The geometry of the starting Pd-olefin complex reveals a usual perpendicular coordination of the olefin in the ground state. In the TS, the olefin has rotated 90 degrees and it is placed parallel to the Pd-Phenyl bond. At this point, the phenyl ring migrates to the β -carbon of the olefin, while a new Pd-alkyl bond is generated with the α -carbon. The insertion leads to an intermediate stabilized by a weak interaction with the α -carbon of the phenyl ring (Pd-C distance: 2.52 Å). Rotation of the ligand and coordination of the carbonyl to the empty position at the palladium center affords product (2). No TS was located in this transformation, but it implies rotation around a Csp^3-Csp^3 bond, thus it is expected to be a fast process. As a whole, the migratory insertion of the olefin into the Pd-C bond implies formally a nucleophilic attack of the anionic aryl ring to the electrophilic olefin.

2.3. Effect of the groups in the migration process

Several groups at the palladium center have been screened computationally, in both $[\text{PdR}^1\text{X}(\text{PEWO})]$ and $[\text{PdR}^1\text{R}^2(\text{PEWO})]$ intermediates in catalysis. In the latter case, the ΔG^\ddagger of the rearrangement can be compared with the activation energies of the reductive elimination of $\text{R}^1\text{-R}^2$. Table IV-1 summarizes the results:

Table IV-1. Effect of the groups on the migratory insertion and reductive elimination.

Substrate		$\Delta G^{\ddagger[a]}$	$\Delta G^{0[a]}$	$\Delta G^{\ddagger[a]}$
X	R ¹	insertion		reductive elimination
I	Ph	15.0	-18.1	-
Cl	Ph	13.3	-24.7	-
OTf	Ph	8.5	-32.3	-
I	Rf	20.0	-13.1	-
Cl	Rf	17.2	-15.1	-
I	Me	19.9	-24.4	-
Ph	Ph	20.8	-13.7	5.5
Rf	Rf	22.1	-8.1	15.7
Me	Ph	21.5	-12.7	10.3
Ph	Me	26.6	-15.3	10.5
Me	Rf	28.7	1.1	16.6
Rf	Me	22.2	-20.1	14.4
CF ₃	Ph	15.8	-17.1	19.6
Ph	CF ₃	39.3	-9.0	21.6

[a] Free energy values in $\text{Kcal}\cdot\text{mol}^{-1}$

The following trends of activation energies of rearrangement can be deduced from this table:

i) Activation energies: $\text{OTf} < \text{Cl} < \text{I}$; Electron-withdrawing X groups accelerate the migratory insertion by making the palladium complex more electrophilic. This

circumstance enhances the σ -donation of the olefin to the palladium center, making it more electron-deficient and more prone to nucleophilic attack by the electron-rich aryl ring.

ii) $\text{Ph} < \text{Me} < \text{Rf} < \text{CF}_3$; this tendency is also expected for C-C reductive elimination. Electron-withdrawing atoms stabilize very importantly the set of orbitals that would translate into lower reactivity towards electrophilic olefins.

iii) $[\text{PdR}^1\text{X}(\text{PEWO})] < [\text{PdR}^1\text{R}^2(\text{PEWO})]$, which is consistent, considering that the latter are more electron-rich.

In $[\text{PdR}^1\text{R}^2(\text{PEWO})]$ complexes, reductive elimination is faster than migratory insertion, except in one case. The activation energy of olefin insertion of complex $[\text{PdPh}(\text{CF}_3)(\text{PEWO})]$ is lower than that of reductive elimination, in very good agreement with the experimental results. In a catalytic cycle, $[\text{PdR}^1\text{X}(\text{PEWO})]$ complexes undergo migratory insertion in competition with the transmetalation step. This fact suggests that the latter should be faster in order to ensure that the catalyst is not decomposed throughout the process. This might be the reason why PEWOs have demonstrated great efficiency with organozincs,^{4,5,6} since they are very fast transmetalating agents. Aiwon Lei's group has reported experimental ΔH^\ddagger of $12.3 \text{ kcal}\cdot\text{mol}^{-1}$ for the transmetalation of aryl groups.¹⁴ Our previous computational studies provided $\Delta G^\ddagger_{203\text{K}}$ of $10\text{-}12 \text{ kcal}\cdot\text{mol}^{-1}$ for the transmetalation of Me.¹⁵ These values suggest that the transmetalation step could be faster than the ligand rearrangement when organozincs are involved. Indeed, Lei's group has studied by kinetic means the aryl-alkyl coupling catalyzed by a very similar ligand.^{6,*} They reported in his work an unidentified catalyst deactivation process that became significant at high number of turnovers. This makes perfect sense if the rate laws of both processes are examined:

$$\text{Transmetalation; Rate}_{\text{trans}} = k_{\text{trans}}[\text{Pd}][\text{Zn}]$$

* The structure of PEWO and the ligand used by Aiwon Lei and collaborators differs only on the fluorine atoms in the aryl ring at which the olefin is tethered. This fluorine atoms render the ligand more electron-poor and make it more soluble.

$$\text{Insertion; Rate}_{\text{inser}} = k_{\text{inser}}[\text{Pd}]$$

Considering these rate laws for not very different activation energies of the insertion and transmetalation, the contribution of these pathways in competition will dramatically change depending on [Zn]. As the nucleophile is present in very high concentrations with regard to the palladium catalyst, the transmetalation step will be faster as long as [Zn] is high. This is consistent with Lei's observation that the catalyst deactivation is significant only after a large number of turnovers, that is, when the concentration of the zinc nucleophile is running low.

Further investigation is ongoing concerning the influence of the ligand rearrangement process in catalysis. However, it is worth commenting the remarkably low activation energy for the reductive elimination process of Ph-CF₃ predicted by the calculations, which is among the lowest described in the literature.^{8,11} This fact indicates that PEWOs are promising ligands for Pd-catalyzed trifluoromethylation, but they should be redesigned in order to prevent competitive undesired processes that may ruin the coupling.

3. Conclusions

New complexes (**3**) and (**4**) have been prepared and are excellent benchmarks for the preparation of complexes bearing F or CF₃ groups with many other ligands by displacement of the labile AsPh₃.

PEWO ligand is unable to promote reductive elimination of Ar-F or Ar-CF₃ bonds. We have unveiled an unexpected ligand rearrangement that takes place at [PdRX(PEWO)] and [PdR¹R²(PEWO)] complexes, and might preclude the use of this ligands in catalysis. Successful couplings with PEWO require that the transmetalation and the reductive elimination steps are faster than this process. The experimental evidences suggest that this is the case when organozincs are used as transmetalation agents. Our computational data indicate that the reductive elimination step is faster than this undesired process (in all cases examined except when CF₃ is involved).

4. Experimental section

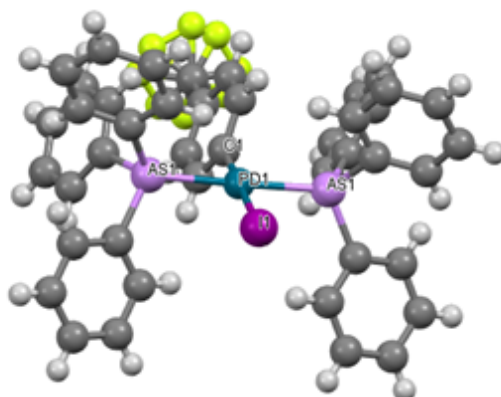
4.1. General methods

All chemicals were purchased from Aldrich, Alfa Aesar, TCI, Deutero, and Pressure Chemical companies. Anhydrous, oxygen-free benzene, benzene- d_6 , toluene, THF, and hexanes were obtained by distillation from Na/OCPh₂. CD₂Cl₂ and CDCl₃ were vacuum-transferred from CaH₂. All solvents for experiments in an inert atmosphere were stored over freshly activated 4 Å molecular sieves in a glove-box. Pd₂(dba)₅¹⁶ and PEWO⁵ were prepared by the literature procedures. Ligand ¹H, ¹⁹F, and ³¹P NMR spectra were recorded on Bruker Avance 400 Ultrashield and Bruker Avance 500 Ultrashield NMR spectrometers. Single crystal X-ray diffraction studies were performed on a Bruker-Nonius diffractometer and a Bruker Apex DUO Kappa 4-axis goniometers equipped with APPEX 2 4K CCD area detectors. An Agilent Technologies 7890A-5975C instrument was used for GC-MS analysis. Elemental analyses were performed by the Microanalysis Center at the Complutense University of Madrid.

4.2. Synthesis of the compounds

trans-[Pd(I)(*p*-C₆H₄CF₃)(AsPh₃)₂] (1)

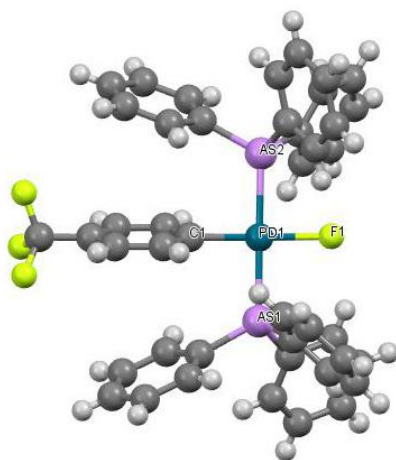
In air, a flask was charged with 1.42 g of Pd₂dba₅ (1.025 mmol), 1.57 g (5.17 mmol) of AsPh₃ and a teflon stir bar, and it was entered into the glovebox. 20 ml of dry THF were added via syringe. The solution was stirred for 40 minutes, obtaining a dark brown solution. After this time, 320 μL of 4-iodobenzotrifluoride (2.15 mmol) were added via syringe. Instantaneous change of the reaction mixture to a dark green suspension was observed. The solution was stirred for further 40 minutes. In air, the solution was filtered through a plug of Celite to remove the palladium black present in the reaction mixture, obtaining a yellow solution. The filtering plug was washed with 10 ml of THF. The solvent was removed under reduced pressure to obtain a yellow powder. It was washed with Et₂O (10 mL x4), manually stirring the washing solution for 2-3 minutes. After the third washing, the pale powder turned into yellow crystals that were suitable for X-Ray diffraction. A new fraction was obtained as yellow crystals that appeared in the washing solution. Yield: 1.6 g (79%). The NMR data is consistent with the reported in the literature.¹⁷



Scheme IV-4. X-Ray structure of *trans*-[Pd(I)(*p*-C₆H₄CF₃)(AsPh₃)₂] (**1**).

[Pd(F)(*p*-C₆H₄CF₃)(AsPh₃)₂] (**3**)

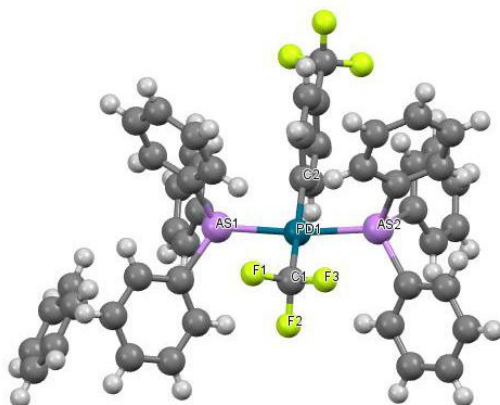
In air, a vial was charged with (**1**) (437 mg, 0.44 mmol) and AsPh₃ (270 mg 0.88 mmol). The vial was transferred into the glovebox. AgF (167.9 mg, 1.32 mmol) was added to the vial. 5 mL of benzene were added with a syringe, obtaining a clear yellow solution with an orange solid suspended. The vial was brought out of the glovebox and was sonicated protected from light. The progress of the reaction was followed by ¹⁹F NMR. After 1 hour sonicating, full conversion of the starting material was observed. In the glovebox, the yellow suspension was filtered with Celite, leading to a very light yellow solution. The solvent was concentrated with an argon flow until around 1 mL of benzene was left. The addition of one or two drops of hexane provoked the formation of a very fine dust of remaining silver salts, that were decanted. Careful addition of hexane to the solution led to the formation of white crystals that were suitable for X-Ray diffraction. Decantation of the solvent allowed for the obtaining a white solid that was dried under reduced pressure. Yield: 340 mg (92%). ¹H NMR (400 MHz, Tol-*d8*) δ 7.77 (m, 12H), 7.03 (m, 18H), 6.83 (d, *J* = 7.5 Hz, 2H), 6.43 (d, *J* = 7.5 Hz, 2H). ¹⁹F NMR (377 MHz, Tol-*d8*) δ -61.43 (s, 3F), -317.06 (bs, 1F). Elemental analysis calculated for C₄₃H₃₄As₂F₄Pd: C, 58.49; H, 3.88. Found: C, 58.68; H, 3.93.



Scheme IV-5. X-Ray structure of *trans*-[Pd(*p*-C₆H₄CF₃)(F)(AsPh₃)₂] (**3**).

***trans*-[Pd(CF₃)(*p*-C₆H₄CF₃)(AsPh₃)₂] (**4**)**

In air, a vial was charged with (**1**) (437 mg, 0.44 mmol) and AsPh₃ (270 mg 0.88 mmol). The vial was transferred into the glovebox. AgF (249,0 mg, 1.96 mmol) was added to the vial. 5 mL of benzene were added with a syringe, obtaining a clear yellow solution with an orange solid suspended. The vial was brought out of the glovebox and was sonicated protected from light. The progress of the reaction was followed by ¹⁹F NMR. After 1 hour sonicating, full conversion of the starting material was observed. In the glovebox, the yellow suspension was filtered with Celite, leading to a very light yellow solution. With a syringe, 200 μL of CF₃SiMe₃ (1.35 mmol) were added to the vial. The solution was stirred for 15 minutes and afterwards, it was concentrated until the final volume of the solution was around 2 mL of benzene. Hexane was added dropwise to the solution. With the first couple of drops, a very fine white powder of silver salts remaining in the solution was formed, that was decanted. The subsequent addition of hexane to the remaining solution drop by drop led to the formation of white crystals that were suitable for X-Ray diffraction. ¹H NMR (400 MHz, Tol-*d8*) δ 7.50 (m, 12H), 7.04 (m, 18H), 6.85 (d, *J* = 7.9 Hz, 2H), 6.47 (d, *J* = 7.9 Hz, 2H). ¹⁹F NMR (377 MHz, Tol-*d8*) δ -10.65 (s, 3F), -61.39 (s, 3F). Elemental analysis calculated for C₄₄H₃₄As₂F₆Pd: C, 56.64; H, 3.67. Found: C, 56.75; H, 3.71.



Scheme IV-6. X-Ray structure of *trans*-[Pd(*p*-C₆H₄CF₃)(CF₃)(AsPh₃)₂] (**4**).

[Pd(II)(PPh₂(C₆F₄CH(C₆H₄CF₃)CHCOPh))] (2**)**

A two necked flask was charged in air with 1.16 g of *trans*-[Pd(II)(*p*-C₆H₄CF₃)(AsPh₃)₂] (1.17 mmol) and 600.6 mg of PPh₂(C₆F₄CH=CHCOPh) (1.30 mmol). Under Ar atmosphere, 25 mL of THF were added via syringe. The solution was stirred at room temperature. After 3 hours stirring, a yellow solid started to precipitate. The progress of the reaction was monitored by ³¹P. After 5 hours, the reaction was finished. In air, the solution was concentrated until 10 mL of THF remained. Then, 40 mL of hexane were added to precipitate the rest of the complex. The yellow powder was filtered and dried under vacuum. Yield 1.19 mg (83%). Suitable crystals for X-Ray diffraction were obtained by slow diffusion of hexane in a saturated solution of the complex in CH₂Cl₂ (Figure IV-1). ¹H NMR (500 MHz, acetone-*d*₆) δ 8.27 (d, *J* = 7.4 Hz, 2H), 8.11 (d, *J* = 7.8 Hz, 2H), 8.03 – 7.90 (m, 2H), 7.78 (t, *J* = 7.4 Hz, 1H), 7.57 (s, 5H), 7.41 (s, 6H), 6.08 (bs, 1H), 5.72 (bs, 1H). ¹⁹F NMR (376 MHz, acetone-*d*₆) δ -25.9 (d, *J* = 8Hz, 3F), -63.1 (s, 3F), -129.00 (m, 1F), -136.4 (m, 1F), -149.0 (td, *J* = 20.7, 6.6 Hz, 1F), -156.7 (t, *J* = 21.7 Hz, 1F). ³¹P NMR (202 MHz, acetone-*d*₆) δ 52.76 (m). Elemental analysis calculated for C₃₄H₂₁F₇IOPPd: C, 48.45; H, 2.51. Found: C, 48.58; H, 2.49.

[Pd(CF₃)(PPh₂(C₆F₄CH(C₆H₄CF₃)CHCOPh))] (5**)**

A two necked flask was charged in air with 201.8 mg of *trans*-[Pd(CF₃)(*p*-C₆H₄CF₃)(AsPh₃)₂] (0.22 mmol) and 100.4 mg of PPh₂(C₆F₄CH=CHCOPh) (0.22 mmol). Under Ar atmosphere, 10 mL of THF were added via syringe. The solution was stirred at room temperature for 30 minutes, and then, it was heated to 60 °C. The progress of the reaction was monitored by ³¹P. After 20 hours, the reaction was finished. In air, the solution was filtered with celite, and it was concentrated under reduced pressure. A brown powder was obtained. The solid was crystallized in THF/hexane. Yield 104.7 mg (62%). 400 MHz, CDCl₃) δ 8.20 – 8.14 (dd, *J* = 8.6 Hz, 1.2 Hz, 2H), 8.01 – 7.89 (m, 4H), 7.72 – 7.65 (dd, *J* = 7.5 Hz, 1.2 Hz, 1H), 7.62 – 7.43 (m,

8H), 7.34 (td, $J = 7.8, 2.7$ Hz, 2H), 7.12 (dd, $J = 13.5, 7.7$ Hz, 2H), 5.98 (bs, 1H), 4.41 (bs, 1H). ^{19}F NMR (376 MHz, CDCl_3) δ -25.87 (d, $J = 8$ Hz, 3F), -62.34 (s, 3F), -126.70 (m, 1F), -135.7 (m, 1F), -147.81 (td, $J = 20.7, 6.6$ Hz, 1F), -153.47 (t, $J = 21.7$ Hz, 1F). ^{31}P NMR (162 MHz, CDCl_3) δ 52.41 (m). Elemental analysis calculated for $\text{C}_3\text{H}_{21}\text{F}_{10}\text{OPPd}$: C, 53.56; H, 2.70. Found: C, 53.69; H, 2.78.

4.3. Decomposition studies

In the glovebox, an NMR tube was charged with 15 mg of the corresponding Pd complex. With a syringe, 0.6 mL of toluene were added. The tube was sealed with a septum and brought out of the glovebox. The sample was heated in an oil bath at 85 °C. The reaction was monitored by ^{19}F NMR until completion was achieved overnight. The remaining solution was filtered through a plug of silica and diluted with hexane to 2 mL of final volume. The sample was analyzed by GC-MS.

4.1. DFT calculations

All calculations have been performed using the Gaussian09 collection of computer programs.¹⁸ We selected the DFT method and employed the PBE functional for the exchange and correlation parts of the density functional.¹⁹ Grimme's correction for the empirical dispersion effects (D3) were included as implemented in Gaussian.²⁰ The electronic environment for all species within the reaction pathway was modeled using the following scheme: for Pd and I, we applied the LANL2DZ basis set augmented by a diffuse type functions.²¹ All other atoms were described by the 6-31G(d,p) basis set. Standard procedures were employed to obtain the geometries and electronic energies for stationary points (minima or transition states) along the reaction paths. Normal mode analysis was performed for each species to verify the nature of the located stationary point. Enthalpies (ΔH , ΔH^\ddagger) and Gibbs' free energies (ΔG , ΔG^\ddagger ; $T = 298.15$ K, $P = 1$ atm) were obtained from the electronic energies (ΔE , ΔE^\ddagger) using standard thermodynamic corrections. Increased atomic grid sizes were used for calculations using M06 functional. Solvent (toluene) effects were calculated through optimization in a SMD model.²²

4.2. Computational optimization

Table IV-2. Activation barriers with selected DFT functionals. Energies in $\text{kcal}\cdot\text{mol}^{-1}$.

Method	d GS(A)	d TS (A)	ΔG^\ddagger
PBEPBE-D3	2.97	2.09	15.02
M06	3.03	2.11	13.30
B3LYP-D3	3.01	2.14	15.50

The activation energies and geometries obtained with PBE are very similar to those obtained with M06 and B3LYP.

5. References

1. Pérez-Temprano, M. H.; Nova, A.; Casares, J. A.; Espinet, P. *J. Am. Chem. Soc.* **2008**, *130*, 10518–10520.
2. Steric and electronic effects of ligands on this fundamental step have been extensively studied: (a) Ozawa, F. Reductive Elimination. In *Fundamentals of Molecular Catalysis*; Kurosawa, H., Yamamoto, A., Eds.; Elsevier: New York, **2003**; Vol. 3, pp 479–511. (b) Birkholz, M.; Freixa, Z.; van Leeuwen, P. W. N. M. *Chem. Soc. Rev.*, **2009**, *38*, 1099–1118. (c) Hartwig, J. F. *Acc. Chem. Res.* **1998**, *31*, 852–860. (d) Hartwig, J. F. *Inorg. Chem.* **2007**, *46*, 1936–1947.
3. (a) Ishiyama, T., Abe, S., Miyaura, N., Suzuki, A. *Chem. Lett.* **1992**, *21*, 691–694. (b) Denmark, S. E.; Wu, Z.; *Org. Lett.* **1999**, *1*, 1495.
4. Gioria, E.; Martínez-Ilarduya, J. M.; Espinet, P. *Organometallics* **2014**, *33*, 4394–4400.
5. Gioria, E.; Martínez-Ilarduya, J. M.; García-Cuadrado, D.; Miguel, J. A.; Genov, M.; Espinet E. *Organometallics* **2013**, *32*, 4255–4261.
6. (a) Luo, X.; Zhang, H.; Duan, H.; Liu, Q.; Zhu, L.; Zhang, T.; Lei, A. *Org. Lett.* **2007**, *9*, 4571–4574. (b) Zhang, H.; Luo, X.; Wongkhan, K.; Duan, H.; Li, Q.; Zhu, L.; Wang, J.; Batsanov, A. S.; Howard, J. A. K.; Marder, T. B.; Lei, A. *Chem. Eur. J.* **2009**, *15*, 3823–3829. (c) Shi, W.; Luo, Y.; Luo X.; Chao, L.; Zhang, H.; Wang, J.; Lei, A.; *J. Am. Chem. Soc.* **2008**, *130*, 14713–14720.
7. Grushin, V. V; Marshall, W. J. *Organometallics* **2007**, 4997–5002.
8. (a) Grushin, V.; Marshall, W.; *J. Am. Chem. Soc.*; **2006**, *128*, 12644–12645. (b) Bakhmutov, V. I.; Bozoglian, F.; Gómez, K.; González, G.; Grushin, V. V; Macgregor, S. A; Martin, E.; Miloserdov, F. M.; Novikov, M. A.; Panetier, J. A.; Romashov, L. V. *Organometallics* **2012**, *31*, 1315–1328. (c) Algarra, G.; Grushin, V. V.; Macgregor, S. A. *Organometallics* **2012**, *31*, 1467–1476.
9. Examples of Ar-F reductive elimination in Pd. (a) Watson, D.; Su, M.; Teverovskiy, G.; Zhang, Y.; García-Fortanet, J.; Kinzel, T.; Buchwald S.; *Science*, **2009**, *325*, 1661–1664. (b) Lee, H.; Milner, P.; Buchwald, S.; *Org. Lett.*, **2013**, Vol. 15, No 21, 5602–5605.
10. Other example of Ar-CF₃ reductive elimination in Pd: Cho, E.; Senecal, T.; Kinzel, T.; Zhang, Y.; Watson, D.; Buchwald S.; *Science*, **2010**, *328*, 1679–1681.
11. Nielsen, M. C.; Bonney, K. J.; Schoenebeck, F. *Angew. Chem. Int. Ed.* **2014**, *53*, 5903–5906.

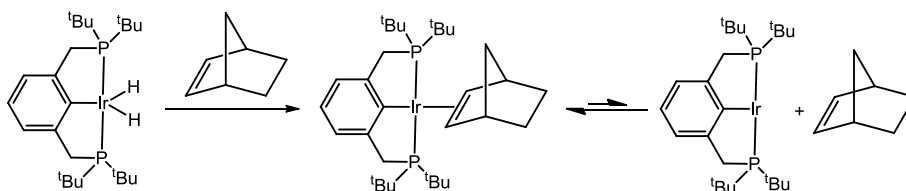
12. For recent examples of polyfluorinated groups in catalysis, see: (a) Ohashi, M., Doi, R.; Ogoshi, S.; *Chem. Eur. J.*, **2014**, *20*, 2040–2048. (b) Zhang, H-H.; Dong, J.; Hu, Q-S.; *Eur. J. Org. Chem.* **2014**, 1327–1332. (c) Bruno, C. N., Niljianskul, N., Buchwald, S. L.; *J. Org. Chem.* **2014**, *79*, 4161–4166.
13. Milner, P. J.; Maimone, T. J.; Su, M.; Chen, J.; Müller, P.; Buchwald, S. L. *J. Am. Chem. Soc.* **2012**, *134*, 19922–19934.
14. Li, J.; Jin, L.; Liu, C.; Lei, A. *Chem. Commun.* **2013**, *49*, 9615–9617.
15. (a) García-Melchor, M.; Fuentes, B.; Lledós, A.; Casares, J. A.; Ujaque, G.; Espinet, P. *J. Am. Chem. Soc.* **2011**, *133*, 13519–13526. (b) Fuentes, B.; García-Melchor, M.; Lledós, A.; Maseras, F.; Casares, J. A.; Ujaque, G.; Espinet, P. *Chem. Eur. J.* **2010**, *16*, 8596–8599.
16. Ushkov, A. V.; Grushin, V. V. *J. Am. Chem. Soc.* **2011**, *133*, 10999.
17. delPozo, J.; Carrasco, D.; Pérez-Temprano, M. H.; García-Melchor, M.; Álvarez, R.; Casares, J. A.; Espinet, P. *Angew. Chem. Int. Ed.* **2013**, *52*, 2189–2193.
18. Gaussian 09, Revision D, M. J. Frisch, G. W. Trucks, H. B. Schlegel, G. E. Scuseria, M. A. Robb, J. R. Cheeseman, G. Scalmani, V. Barone, B. Mennucci, G. A. Petersson, H. Nakatsuji, M. Caricato, X. Li, H. P. Hratchian, A. F. Izmaylov, J. Bloino, G. Zheng, J. L. Sonnenberg, M. Hada, M. Ehara, K. Toyota, R. Fukuda, J. Hasegawa, M. Ishida, T. Nakajima, Y. Honda, O. Kitao, H. Nakai, T. Vreven, J. A. Montgomery, Jr., J. E. Peralta, F. Ogliaro, M. Bearpark, J. J. Heyd, E. Brothers, K. N. Kudin, V. N. Staroverov, R. Kobayashi, J. Normand, K. Raghavachari, A. Rendell, J. C. Burant, S. S. Iyengar, J. Tomasi, M. Cossi, N. Rega, N. J. Millam, M. Klene, J. E. Knox, J. B. Cross, V. Bakken, C. Adamo, J. Jaramillo, R. Gomperts, R. E. Stratmann, O. Yazyev, A. J. Austin, R. Cammi, C. Pomelli, J. W. Ochterski, R. L. Martin, K. Morokuma, V. G. Zakrzewski, G. A. Voth, P. Salvador, J. J. Dannenberg, S. Dapprich, A. D. Daniels, Ö. Farkas, J. B. Foresman, J. V. Ortiz, J. Cioslowski, D. J. Fox, Gaussian, Inc., Wallingford CT, **2009**.
19. Perdew, P.; Burke, K.; Ernzerhof, M.; *Phys. Rev. Lett.*, **1996**, *77*, 3865–68.
20. Grimme, S.; Ehrlich, S.; Goerigk, L.; *J. Comp. Chem.* **2011**, *32*, 1456–65.
21. (a) Hay, P. J.; Wadt, W. R.; *J. Chem. Phys.* **1985**, *82*, 299. (b) Roy, L. E.; Hay, P. J.; Martin, R. L.; *J. Chem. Theory Comput.* **2008**, *4*, 1029.
22. Marenich, A. V.; Cramer, C. J.; Truhlar, D. G.; *J. Phys. Chem. B* **2009**, *113*, 6378.

Chapter V

**Mechanism of the N–H
oxidative addition/reductive
elimination of anilines**

1. Introduction

The reaction of $[(PCP)IrH_2]$ with a hydrogen acceptor such as norbornene or tert-butylethylene, is known to generate $[(PCP)Ir]$, a very reactive 14-electron species, which undergoes oxidative addition of a variety of bonds, such as C–H,¹ C–O,² C–F,³ or C–C.⁴



Scheme V-1. Generation of active species for oxidative addition of several important bonds.

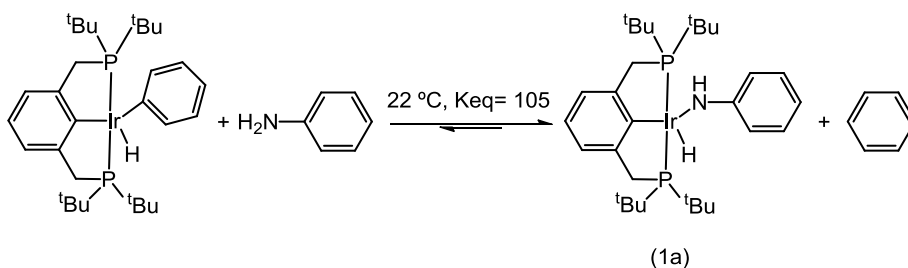
Similarly, this coordinatively unsaturated species allows for oxidative addition of N–H bonds of anilines and benzamides. It was reported several years ago that reaction of $[(PCP)IrH_2]$ and norbornene with 1.2 equiv of aniline in *p*-xylene solvent at room temperature gave the anilide hydride $[(PCP)IrH(NHPh)]$ (**1a**) in 95% yield by N–H oxidative addition.⁵

Despite the fact that anilines undergo facile activation with the classical aromatic PCP ligand, NH_3 turns out to be a more complicated substrate. In most cases, Werner coordination complexes are favored and only a few examples of N–H activation of NH_3 are reported.⁶ The complex $[(PCP)IrH(NH_2)]$ was demonstrated to be thermodynamically unstable, as it undergoes reductive elimination at room temperature to generate the σ -complex $[(PCP)Ir(NH_3)]$.⁵

Ligand design has boosted the power of these unsaturated species, allowing for the activation of NH_3 . More electron-rich auxiliary ligands, such as alkyl PCP or PSiP are reactive enough to activate this reluctant substrate.⁶ NH_3 is abundant and inexpensive, thus catalytic reactions that utilize ammonia are considered among the ten current greater challenges for catalytic chemistry.⁷

Despite the importance of this reaction, only few studies have been devoted to understand the mechanisms of N–H oxidative addition⁸ and its microscopic reverse, reductive elimination.⁹ Comparatively, there is more information concerning C–H activation using Ir complexes.^{1,5} Mechanistic studies could have a strong influence and trigger the development of new metal-catalyzed transformations of amine and related compounds.¹⁰ A deeper understanding of this step would have an impact in transformations such as olefin hydroamination¹¹ or coupling with arenes,¹² very important processes in both the laboratory and industrial scale.

Although N–H and C–H bonds exhibit similar homolytic bond strengths, [(PCP)IrH(NHPh)] and [(PCP)IrH(Ph)] complexes are quite different. Whereas C–H oxidative addition/reductive elimination is fast in the NMR time scale at -20 °C, N–H activation is slow even at RT. Also, the thermodynamics of N–H activation are more favorable than those of C–H addition of arenes, as a Keq of 105 is found when aniline and complex [(PCP)IrH(Ph)] are reacted (Scheme V-2) Other thermodynamic studies with (POCOP)Ir complexes showed the same tendency, higher thermodynamic stability of Ir–NH adducts compared with Ir–CH adducts.



Scheme V-2. Equilibrium between C–H and N–H addition products.

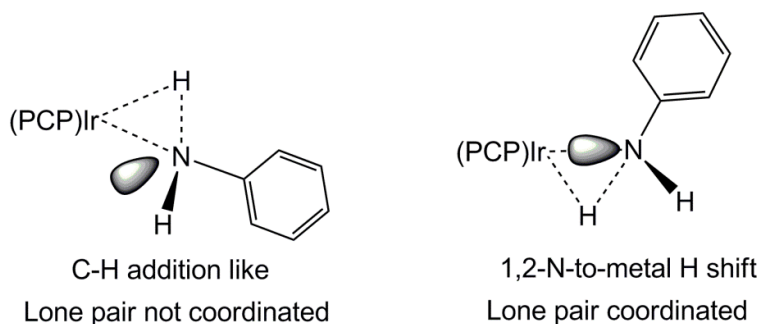
This higher stability lies on the fact that the Ir–N bond is stronger than the Ir–C bond. Anilide–Ir bonds show π -donation from the lone pair of the N atom to the empty orbital of the metal, which contributes to increase the strength of the bond.

However, there are good reasons to consider that the kinetics of N–H addition are influenced by factors very different from those that determine C–H addition. Unlike hydrocarbons, this lone pair not only affects the thermodynamics of the

process, but also can readily coordinate changing the nature of the transition state. Two possible scenarios can be envisioned:

(a) N–H activation may be concerted like the C–H activation, considering that the lone pair is not coordinated to the metal center. Firstly, the reaction would proceed via coordination of the σ N–H bond to the metal center, followed by concerted N–H activation.^{1,5}

(b) The lone pair remains coordinated to Ir, and oxidative addition takes place as a 1,2-N-to-metal shift, either as a proton or hydride.



Scheme V-3. Nature of the transition state of the N–H oxidative addition.

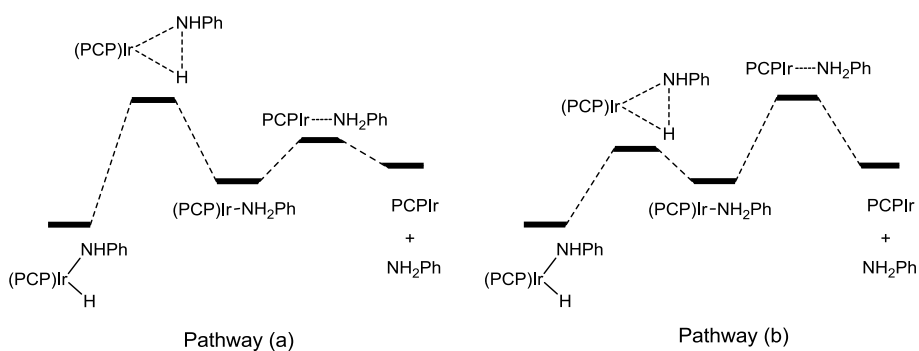
Essentially, the nature of this transition state could be defined by the role of the lone pair in the transition state. It is difficult to answer to this fundamental question, considering that there are not many experiments that can distinguish unambiguously between these two possible pathways. Thus, DFT calculations might provide better insights into the actual mechanism of this process. By these means, the transition state of the C–H addition has been extensively studied by the group of Goldman, but the absence of the lone pair makes it comparatively easier.¹³

As mentioned above, complex $\sigma\text{-}[(\text{PCP})\text{Ir}^{\text{I}}\text{-NH}_3]$ is the thermodynamic product of the reaction when NH_3 is involved instead of any aniline.⁵ At the same time, complexes $\sigma\text{-}[(\text{POCOP})\text{Ir}^{\text{I}}\text{-NH}_2\text{Ar}]$ have been identified as transient species of the reaction of $[(\text{POCOP})\text{Ir}(\text{C}_2\text{H}_4)]$ with different anilines.⁸ Based on these facts, the σ -complex $[(\text{PCP})\text{Ir}^{\text{I}}\text{-NH}_2\text{Ph}]$ could be proposed to be the species that undergoes

oxidative addition to form the Ir^{III} species. However, so far there is no evidence confirming that this σ -[(PCP)Ir–Aniline] complex is the initial species that undergoes oxidative addition, nor in the case of the POCOP ligand. The fact that these species are detected does not prove that the aniline remains coordinated to the metal center in the transition state.

Experimental studies can provide information about the nature of the potential energy surface of the process (which means, the relative energies of every step of the mechanism) and the intermediates that take part in the reaction. Kinetic and thermodynamic measurements have been conducted with the aim of unveiling the complete energetic profile of the oxidative addition and the reductive elimination of anilines. Our initial efforts focused on reductive elimination (microscopic reverse of oxidative addition), since the anilide hydride (**1a**) is stable, thus it allows for an easier experimental study.

So far there is no quantitative experimental information unveiling the relative energies of all the species that take part in this reaction. Two possible situations with different rate limiting steps can be proposed for the N–H reductive elimination of anilines:



Scheme V-4. Free energy surface for the reductive elimination of PhNH₂ from [(PCP)Ir(H)(NHPh)]. Scenario (a): Oxidative addition/reductive elimination is the rate limiting step. Scenario (b): Ligand coordination/dissociation is the rate limiting step.

A good example of these two possible scenarios was reported in 2003 by the group of Parkin. C–H activation of benzene by [Me₂Si(C₅Me₄)₂]M complexes showed

very different rate limiting steps for Mo and W in the same system. C–H oxidative addition was found to be faster than C₆H₆ dissociation for the tungsten system, whereas dissociation is favored over the molybdenocene complexes.¹⁴ In that work, each scenario was determined by thorough analysis of the Kinetic Deuterium Isotope Effects.

If (a) is the actual scenario, the resting state of this reaction would be the starting material [(PCP)Ir(H)(NHP)]. In principle, no intermediate should be observed under the reaction conditions. Conversely, if oxidative addition is examined, the resting state would be σ -[Ir^I-NH₂Ph] and it would accumulate during the course of the reaction.

Alternatively, if ligand coordination/dissociation is rate limiting and scenario (b) is lower in energy, the resting state would be the most stable species of the resulting equilibrium between [(PCP)Ir(H)(NHP)] and σ -[Ir^I-NH₂Ph], as they would be in fast exchange before rate-limiting ligand dissociation. This one would be [(PCP)Ir(H)(NHP)], as this is the only species experimentally detected in the reaction depicted in Scheme V-2. If oxidative addition is considered, [(PCP)Ir-NBE] would be most stable species before the rate determining TS, and no other intermediate should be observed along with the final product.

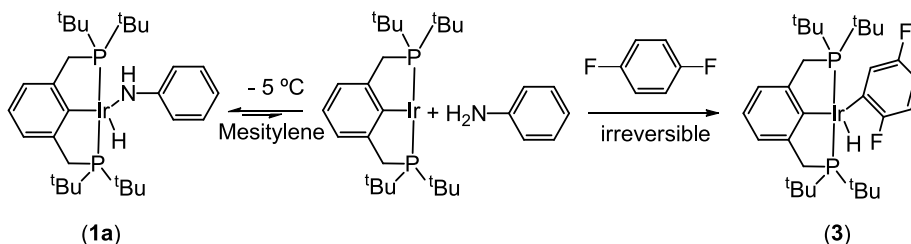
Herein we report a study of the N–H oxidative addition and reductive elimination of N–H bonds to [(PCP)Ir] complexes. Kinetic studies of substituted anilines are evaluated, towards the understanding of this transition state and the nature of the process. Computational studies have been conducted by our laboratory, and they will be used for the discussion. Nevertheless, they will not be included explicitly herein as they have been carried out by Tian Zhou and Prof. Krogh-Jespersen in the Goldman group.

2. Results and discussion

2.1. Study of the reductive elimination of [(PCP)Ir(H)(NHPH)]

Different ligands that could trap [(PCP)Ir^I] were used to make the reductive elimination of aniline an irreversible reaction, thus allowing us to get kinetic information about the process.

With the aim of using a trapping ligand that could not coordinate to [(PCP)Ir(H)(NHPH)] prior to reductive elimination, 1,4-difluorobenzene (from now on DFB) was tested. DFB itself is a very poor ligand for Ir^{III}, however, it forms a very stable Ir^{III} adduct by C–H activation of the Ir^I species that are formed after reductive elimination (Scheme V-5). Concentration-time data were acquired by integration of the ³¹P NMR spectra (see experimental).



Scheme V-5. Study of aniline elimination with DFB as trapping ligand.

If reductive elimination follows a dissociative pathway, the rate of elimination must be independent of the concentration of DFB at high concentration of this trapping ligand (saturation kinetics). As it was confirmed, the rate is independent of [DBF] from $8 \cdot 10^{-2}$ – $5 \cdot 10^{-1}$ M. From these values, kinetic constant of the elimination was averaged and a value of $\Delta G^\ddagger = 20.8 \text{ kcal} \cdot \text{mol}^{-1}$ at $-5 \text{ }^\circ\text{C}$ was obtained.

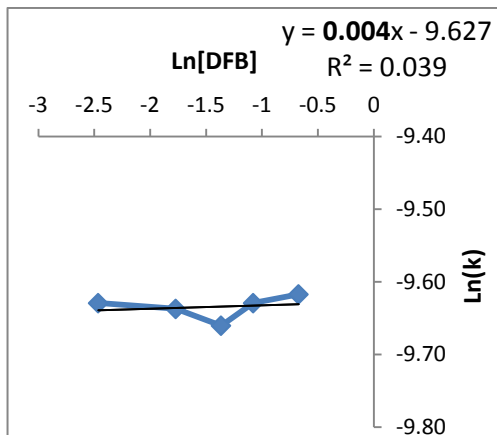
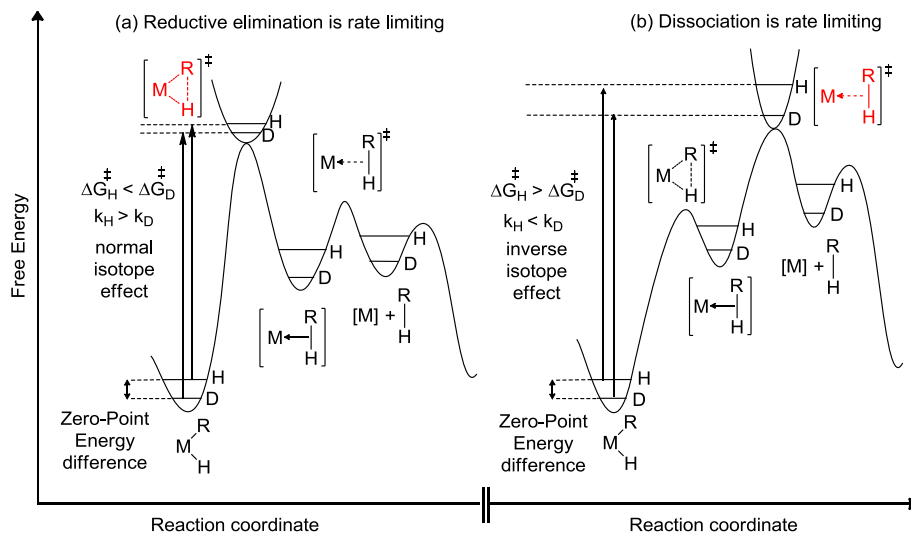


Figure V-1. Dependence on [DFB] of the reaction rate of reductive elimination.

a) Kinetic Isotope Effect

When one studies C–H, N–H or O–H bond activations, the measurement of kinetic isotope effects (KIEs) is a powerful and common technique for studying the reaction mechanism.¹⁵ As it was commented before, very clear information concerning the rate limiting step (see Scheme V-4) can be obtained from the relative rates of elimination of both isotopic species. Complex (**1a-d7**) was prepared with deuterated aniline and the rates of elimination in the reaction with DFB were obtained (Scheme V-5).

Scheme V-6 illustrates the two possible free energy surfaces of the reductive elimination of PhNH₂ from [(PCP)Ir(H)(NHPh)] and the expected Zero-Point Energies differences of the M–H(D) bonds in ground state and that of the rate limiting transition state of each scenario.



Scheme V-6. Representation of the Kinetic isotope effect in the two possible scenarios of the potential energy surface.

If oxidative addition/reductive elimination is rate limiting (Scheme V-6, scenario (a)), the kinetic isotope effect of any of this two possible sides of the transition state would be greatly affected by the isotope (H or D) involved in the reaction, because N–H bond breaking would take place at the rate limiting step.

If reductive elimination is examined within this scenario, one should consider the higher strength of Ir–D bond in comparison with Ir–H bond. As a result, lower zero-point energy of the Ir–D bond is predicted. The transition state for reductive elimination involves cleavage of the M–H bond, so the zero-point energy differences between the two isotopic species should diminish in the transition state, since the bond force constant decreases during a bond breaking process. The final consequence is that reductive elimination of [(PCP)Ir(D)(NPh)] should result in a slower reaction rate than that of [(PCP)Ir(H)(NPh)], thus normal KIEs are predicted. Normal isotope effects have been measured for mononuclear, rate-determining alkane reductive eliminations (KIE=1.7).¹⁶

If oxidative addition is considered, the KIE should be larger than that of the reductive elimination, considering the greater relative stability of N–D and N–H bonds in comparison with Ir–D and Ir–H bonds.¹⁷ Greater differences in the zero-

point energy at the ground state imply greater differences between the isotopic rates.

However, if ligand coordination/dissociation is rate limiting (Scheme V-6, scenario b), the prediction should be very different and inverse values of KIE are expected (<1). In the reported examples for the C–H reductive elimination,¹⁸ the origin of the inverse effect has been explained as a result of an equilibrium between the hydrido aryl (or alkyl) complex and a σ -complex of the metal with the arene (alkane), prior to complete dissociation of the σ -complex in a subsequent step of higher energy. In the case of the N–H elimination, a similar result would be expected. The Zero-Point Energy difference at the rate determining transition state would be greater than that of the Ir–H(D) ground state, because full N–H(D) bond formation would be accomplished before the rate limiting step. This is the same as saying that deuterium prefers to be located in the stronger bond (the higher frequency oscillator), which is C–D (or N–H) versus M–D (Scheme V-6).

On the other hand, oxidative addition would be only affected by secondary Kinetic Isotope Effect, which is of less importance (smaller isotopic differences are expected, usually ranged from 0.8 - 1.2).¹⁹ Inverse isotope effects have been reported for reductive eliminations from metal complexes $[M(R)(H)]$, where R = aryl²⁰ or alkyl, in which formation of a σ -M–(C–H) complex is rate limiting²¹

DFT calculations were conducted by us to predict the KIE values of every possible scenario:

Table V-1. KIE calculations, taking into account only the specified TS.

Rate limiting step	KIE oxidative addition	KIE reductive elimination
N–H activation (a)	5.9	1.6
Aniline coordination/release (b)	1.1	0.4

Experimental measurement of the KIE was carried out by comparing the rates of the reductive elimination of both isotopic species $[(PCP)Ir(H)(NHPh)]$ and

[(PCP)Ir(D)(NDPh)]-*d*7 in the presence of DFB (Scheme V-5).²² The obtained value of the KIE was 1.7, consistent with ox/ad reductive elimination as rate limiting step. Consistently with the fact that ligand coordination/dissociation is not rate limiting, the rate of reductive elimination showed no dependence on the concentration of free aniline.

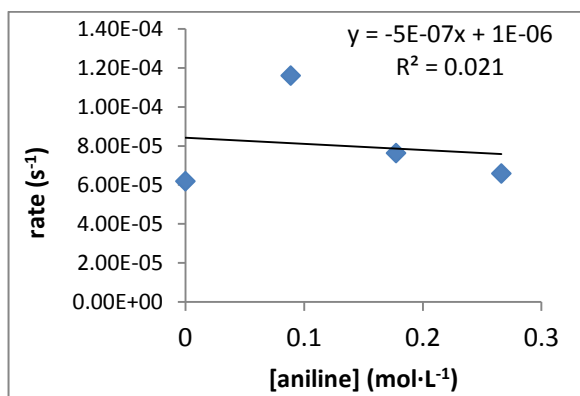
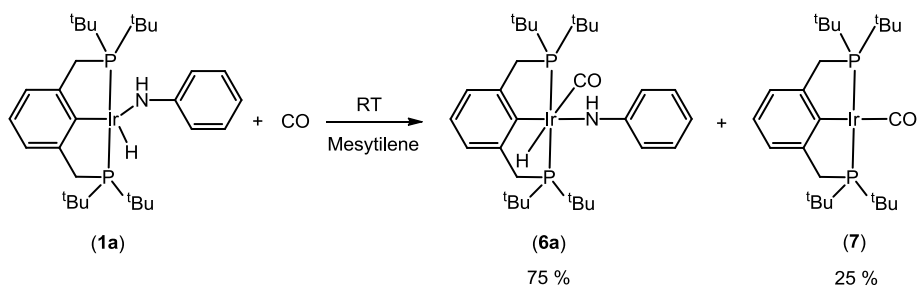


Figure V-2. Plot of the rate of the reductive elimination of (**1a**) at different aniline concentrations.

b) Reductive elimination with small coordinating ligands

When small ligands such as PEt_3 or CO were used to trap the Ir^{I} species formed after reductive elimination, coordination of the ligand can occur prior to the elimination. This provides a way to study whether or not reductive elimination takes place from 6-coordinate complexes and to get values of reaction rates, which can be compared with those of elimination from 5-coordinate complexes.

Evacuation of the atmosphere of a frozen sample of **(1a)** and subsequent introduction of a CO atmosphere provided instantaneously complexes **(6a)** and **(7)** at RT. The ratio between these complexes does not change with time.

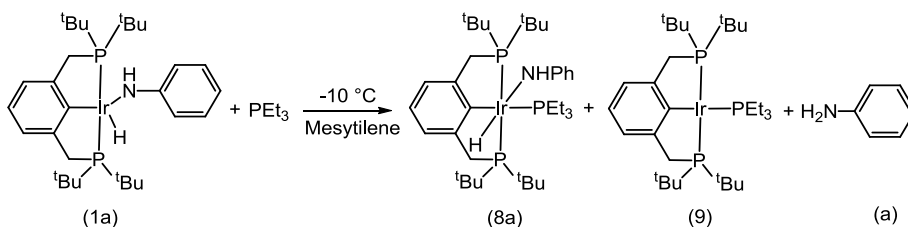


Scheme V-7. Reaction of **(1a)** with CO.

Complex **(6a)** was described in the original work in which the N–H oxidative addition to PCP–Ir complexes was reported.⁵ Along with this product, complex **(7)** is formed, suggesting that reductive elimination might take place from a different isomer of a 6-coordinate $[(\text{PCP})\text{Ir}(\text{H})(\text{NHPPh})(\text{CO})]$. This reductive elimination might be very fast, precluding the detection of any other isomer.

A similar study was repeated with PEt_3 , which is easier to handle and also a strong and small ligand. The reaction of **(1a)** with PEt_3 was monitored at $-10\text{ }^\circ\text{C}$. Complex **(9)** is formed along the reaction course after N–H reductive elimination. Also, a complex consistent with the formulation $[(\text{PCP})\text{Ir}(\text{H})(\text{NHPAr-R})(\text{PEt}_3)]$ is detected in the ^{31}P NMR and ^1H NMR. The multiplicity of the Ir–H signal, as a quartet, points to a cis configuration of the PEt_3 and both phosphorus of the PCP ligand and the hydride. Considering the high *trans* influence of the hydride ligand,

the most likely configuration of complex **(8a)** would imply PEt_3 to be trans to the PCP ligand.



Scheme V-8. Reaction of **(1a)** with PEt_3 .

Significantly faster rates of formation of **(9)** were obtained at $-10\text{ }^\circ\text{C}$ than those of formation of **(3)** (Scheme V-5) when DFB is used to promote the reductive elimination from the 5-coordinate complex. This fact suggests that reductive elimination from a 6-coordinate complex would be faster than elimination from a 5-coordinate. It has to be taken into account that reductive elimination cannot take place from **(8a)**, because the anilide and the hydride are not in cis disposition to each other. It is likely that reductive elimination takes place from an undetected isomer.

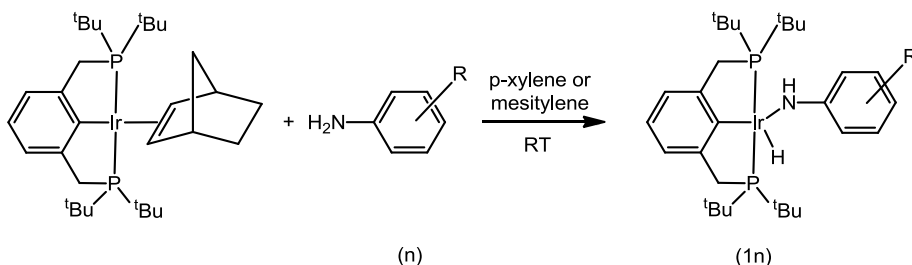
Complex **(1a)** is still present in the reaction in the presence of extra PEt_3 , thus the actual scenario could be more complicated and other equilibria such as ligand coordination/dissociation or isomerization seem to be present. For this reason, all the kinetic information that was obtained could not be correlated with the true barrier of the reductive elimination from a 6-coordinate complex. Unfortunately, further experimentation should be conducted to get quantitative values of the rates, which would allow for accurate comparison of the reaction rates between elimination from a 5-coordinate and 6-coordinate complexes.

Similar results were obtained for the (POCOP)Ir system. PMe_3 coordinates at $-40\text{ }^\circ\text{C}$ prior to reductive elimination; yet not additional information about the rates is given in this work.⁸

The fact that reductive elimination might be faster in the 6-coordinate complex than in the 5-coordinate one could be an important factor trying to unveil the nature of the transition state of the elimination from the 6-coordinate complex. Classical concerted H–H and C–H eliminations have been reported to be slower in square planar (4-coordinate) and octahedral (6-coordinate) than in the respective 3 or 5-coordinate structures.²³ In these systems, ligand dissociation is required prior to reductive elimination. Consequently, this faster pathway for reductive elimination in the 6-coordinate complex might point to a non-concerted reductive elimination, thus suggesting a non-concerted H-migration. However, this affirmation needs further experimentation: accurate kinetic data is needed for comparison, and at this point, dissociation of an arm of the pincer ligand cannot be discarded.

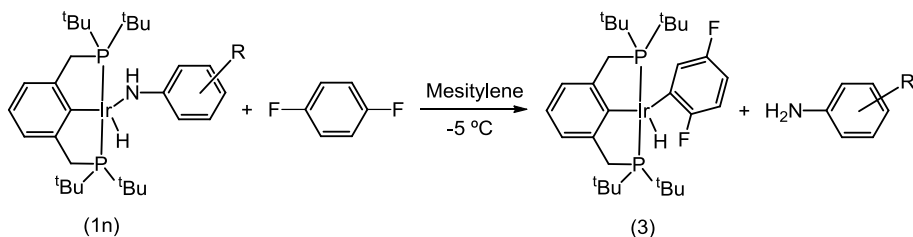
c) Role of the electronic properties of the aniline

With the aim of getting a closer understanding of the electronic effects of the anilines in the reductive elimination reaction, different substituents on the aromatic ring of the aniline were tested. [(PCP)Ir(NBE)] was treated with substituted anilines bearing electron-withdrawing and electron-donating groups. In all cases, the corresponding complex [(PCP)Ir(H)(NHAr–R)] was obtained in quantitative yields, except for anilines (**f**), (**g**) and (**h**) (see Table V-2). A complex σ -[(PCP)Ir–NH₂Ar] was never isolated as the stable final product. This is opposed to what was reported for [(POCOP)Ir] complexes, where complexes σ -[Ir^I–NH₂Ar] were favored with electron-rich anilines. This fact stands out the ability of the PCP ligand to stabilize the oxidation state (III) for Ir.⁸ Spectroscopic and experimental details of all the [(PCP)Ir(H)(NHAr–R)] complexes can be found in the supporting information.



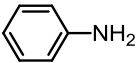
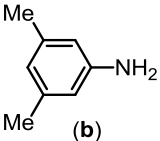
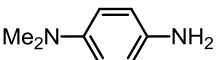
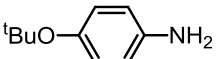

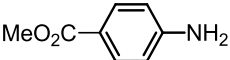
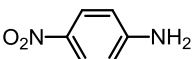
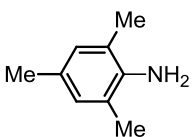
Scheme V-9. Synthesis of [(PCP)Ir(H)(NHAr–R)] complexes.

ΔG^\ddagger values of the reductive elimination of a number of different $[(PCP)Ir(H)(NHAr-R)]$ were obtained in the presence of DFB. As demonstrated above, the obtained ΔG^\ddagger 's correspond to the true barriers of reductive elimination.



Scheme V-10. Reductive elimination of $[(PCP)Ir(H)(NHAr-R)]$.

Table V-2. Experimental ΔG^\ddagger s for the reductive elimination of substituted anilines.

Aniline	K (s ⁻¹)	ΔG^\ddagger [a] kcal·mol ⁻¹	Hammett σ^{24}
 (a)	$(8.1 \pm 0.4) \cdot 10^{-5}$	20.8	0
 (b)	$(9.6 \pm 0.5) \cdot 10^{-5}$	20.6	-0.14
 (c)	$(2.4 \pm 0.1) \cdot 10^{-4}$	20.1	-0.66
 (d)	$(1.6 \pm 0.1) \cdot 10^{-4}$	20.3	-0.34
 (e)	$(1.8 \pm 0.1) \cdot 10^{-4}$ [b]	22.6 ^[b]	0.54
 (f)	$(6.7 \pm 0.3) \cdot 10^{-5}$ [b]	23.2 ^[b]	0.45
 (g)	-	- Decomposition	-
 (h)	-	- No N-H activation	-

[a] The values were obtained as an average of three runs. The values of ΔG^\ddagger are given in kcal·mol⁻¹. The errors of were calculating by propagating those of the rate constants. In all cases, the error was smaller than 0.01. [b] the reaction is too slow at -5 °C, these ΔG^\ddagger were obtained at 25 °C.

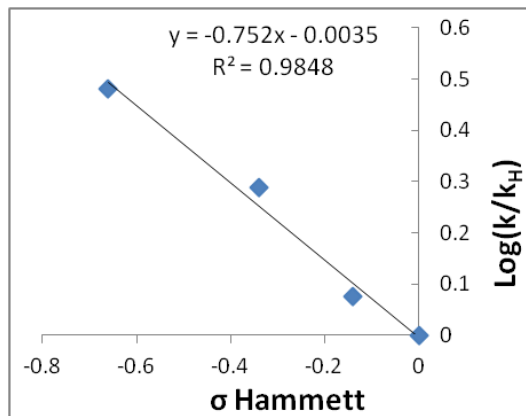
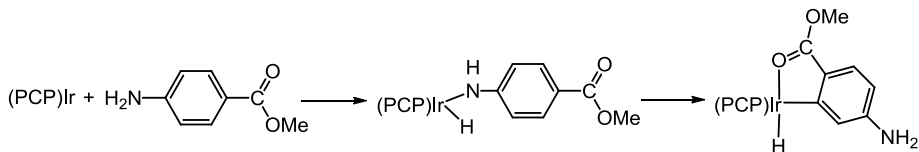


Figure V-3. Hammett plot of the reductive elimination of substituted anilines.

The Hammett plot shows a moderate dependence on the electronic nature of the aniline (slope = -0.75). As deduced from the values, the more electron-withdrawing the aniline, the complex $[(PCP)Ir(H)(NHAr-R)]$ eliminates more slowly. This implies that the electron density in the transition state is decreased, with regard to the ground state $[(PCP)Ir(H)(NHAr-R)]$. The obtained values are consistent with what was observed for (POCOP)Ir complexes.²⁵

Anilines (**e**) and (**f**) are not fitted in the linear plot, because these eliminations are too slow at -5 °C and have been measured at RT. In the case of aniline (**f**) since the thermodynamically stable product is not $[(PCP)Ir(H)(NH-Ph-CO_2Me)]$ (**1f**) but $[(PCP)Ir(H)(2,5-CO_2Me-Ph-NH_2)]$ (see below), accurate kinetic data could not be obtained for its elimination.

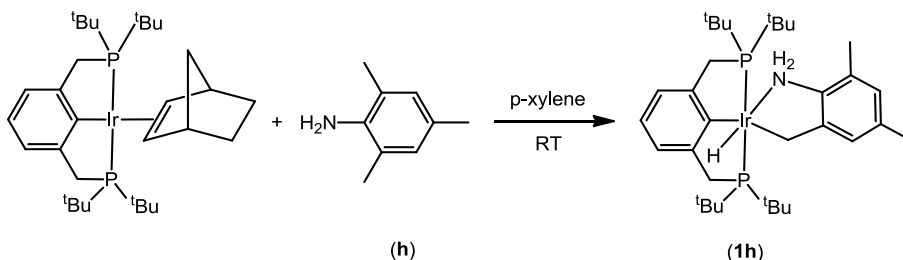
When $[(PCP)Ir(NBE)]$ was treated with aniline (**f**), initial monitoring of the reaction showed that the NH activation product is the major one after 1 hour. In 24 hours, the complex rearranged, leading to a 6-coordinate complex of C-H activation at the meta position and coordination of the carbonyl.



Scheme V-11. Rearrangement of $[(PCP)Ir(H)(NHAr-CO_2Me)](1f)$.

In the case of aniline (**g**), the complex $[(PCP)Ir(H)(NH(4-Ph-NO_2))](1g)$ was detected in the early stage of reaction, but within minutes, Ir metal was formed and no trace of the Ir–H moiety was detected. As the metal center is reduced, probably a Single Electron Transfer (SET) process is taking place, prompted by the NO_2 group acting as a radical stabilizer.

Bulky anilines such as mesityl aniline (**h**) do not undergo N–H oxidative addition. Instead, C–H activation of the ortho methyls takes place. The product is stable, and does not rearrange even at 100 °C for several days (see experimental part for characterization data).

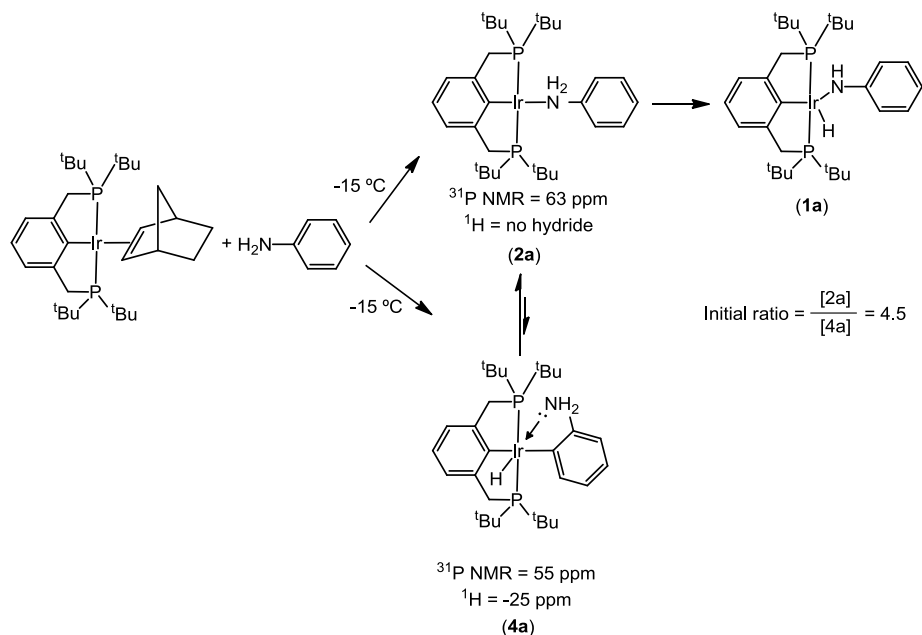


Scheme V-12. Reaction of $[(PCP)Ir(NBE)]$ with mesityl aniline.

2.2. Study of the oxidative addition

Information concerning oxidative addition of anilines would be very useful to design new catalytic processes that involve N–H oxidative addition to a metal center. However, this oxidative addition is experimentally more difficult to study, considering the thermodynamic instability of σ - $[(PCP)Ir-Aniline]$ complexes, and the fast rates displayed by this reaction.

According to the mechanistic proposal, the σ complex $[(PCP)Ir(NH_2Ph)]$ should be the resting state of the oxidative addition. To the $[(PCP)Ir(NBE)]$ complex, 2 equivalents of aniline were added to a frozen sample at $-196\text{ }^\circ\text{C}$. Then, the solvent was thawed and the reaction was monitored by NMR at $-15\text{ }^\circ\text{C}$. At this temperature, oxidative addition takes place slow enough, and 2 intermediates could be observed in the ^{31}P and ^1H NMR in a 4.5:1 ratio.



Scheme V-13. Reaction of $[(PCP)Ir(NBE)]$ with aniline. Detected intermediates by ^1H and ^{31}P NMR.

The assignment of the complexes is based on the NMR data. **(2a)** is the major product of the reaction. It shows a singlet in ^{31}P NMR and no hydride in the ^1H NMR. **(4a)** is the other signal detected in ^{31}P , which shows a triplet in the ^1H NMR at -25 ppm, consistent with C–H activation of the aryl group.

The same experiment was reproduced with a bulkier aniline, 3,5-dimethylaniline. In principle, this aniline would not undergo oxidative addition in the meta or para position due to the two methyl groups that protect these positions. However, it is still possible to observe the C–H activation intermediate,

although in a lower relative quantity. This fact strongly supports the assigned structure of complex (**4a**). The abnormal downfield chemical shift of the hydride (-25 ppm) suggest significant coordination of the N lone pair to the iridium center (behaving as a 6-coordinate complex) and the hydride and aryl ring disposed in cis stereochemistry.^{26*}

The concentration of (**2a**) and (**4a**) decreases at the same time that the one of (**1a**) increases. The ratio (**2a**)/(**4a**) (initially 4.5) increases with time, so that this suggest that (**4a**) is a kinetic product of the reaction.

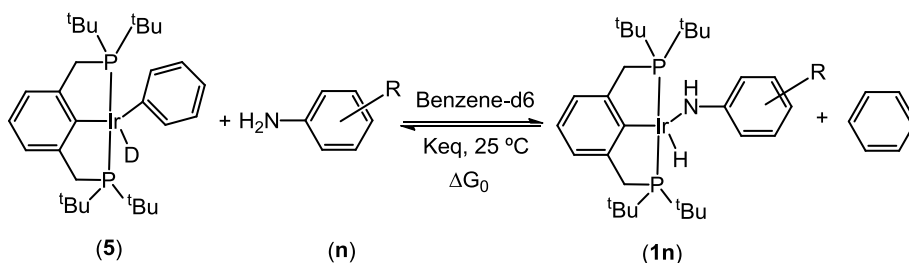
As discussed above, the rate of formation of (**1a**) corresponds to the true rate of oxidative addition. At -15 °C, the obtained rate constant provided a value for $\Delta G^\ddagger = 19.3 \text{ kcal}\cdot\text{mol}^{-1}$, as an average of three measurements.

2.3. Equilibration of [(PCP)Ir(H)(Ph)] with anilines and

[(PCP)Ir(H)(NHAr-R)]

The reaction of (**5**) with different anilines was carried out in order to obtain the relative stabilities of (**5**) and the N-H activation product (**1n**). This information can be combined with the elimination rates in order to get the relative rates of oxidative addition and a full picture of the reaction profile implying species that do not contain aniline (see Scheme V-15).

* The ^1H chemical shift of the hydride of the complex [(PCP)Ir(Ph)(H)] is -45 ppm. If this chemical shift is compared to that of complex (**4a**), the data suggest that the structure of the iridium center resembles more to a 6-coordinate complex than to a 5-coordinate one. A similar phenomenon was found for complex (**1h**). This behavior is reproduced by the previously synthesized complex [(PCP)Ir(H)($\kappa^2\text{-O}_2\text{C-C}_6\text{H}_4\text{NO}_2$)] (-24.85 ppm), in which the aryl ring and the hydride are cis to each other. The analogous complex in which the aryl ring and the hydride are trans shows a different chemical shift for the hydride (-8.93). This consideration has been used for the stereochemical assignment of complexes (**1h**) and (**4a**). See ref 26.



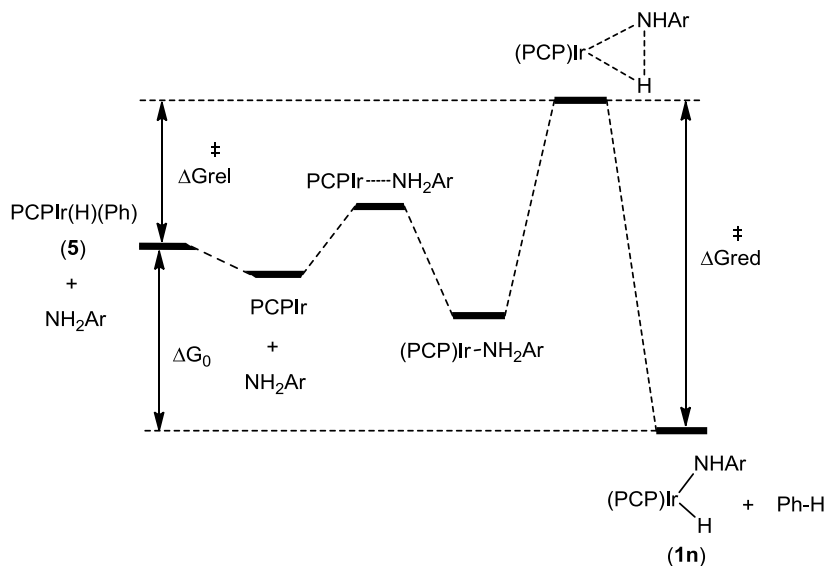
Scheme V-14. Relative stability of the C–H and N–H activation products.

The equilibration was carried out in situ, generating **(5)** via reduction of $[(\text{PCP})\text{IrH}_2]$ with norbornene in benzene- d_6 in the presence of 1 equivalent of the corresponding aniline. The sample was monitored by ^1H and ^{31}P NMR until equilibration was reached (after 3h). Integration of the ^{31}P NMR spectra allowed us for the quantification of the Keq for all the substituted anilines at 25°C (see experimental for details).

Table V-3. Relative stabilities of the N–H activation adducts to the C–H activation adducts with substituted anilines.

Aniline	Keq (25°C)
Ph-NH_2 (a)	105.0 ¹
3,5-Me-C ₆ H ₄ -NH ₂ (b)	233
<i>p</i> -Me ₂ N-C ₆ H ₄ -NH ₂ (c)	60
<i>p</i> - ^t BuO-C ₆ H ₄ -NH ₂ (d)	191
<i>p</i> -F ₃ C-C ₆ H ₄ -NH ₂ (e)	58170
<i>p</i> -MeO ₂ C-C ₆ H ₄ -NH ₂ (f)	-

The relative ΔG^\ddagger from the $[(\text{PCP})\text{Ir}(\text{H})(\text{Ph})]$ to the transition state of the oxidative addition could be calculated for *p*-F₃C-C₆H₄-NH₂ (**e**), using these ΔG_0 and the experimental ΔG^\ddagger values for the reductive elimination as illustrated in Scheme V-15. For this particular case, all the magnitudes are calculated at 25°C and therefore they can be compared. With the rest of the anilines, Keq should be obtained at -5°C to obtain the full profile of the reaction.



Scheme V-15. Full profile of N-H activation by [(PCP)Ir] complexes.

Table V-4. Relative energies of the N-H activation profile with CF₃-C₆H₄-NH₂ at 25 °C.

Aniline	Keq	ΔG_0	$\Delta G^{\ddagger}_{red}$ ^[a]	$\Delta G^{\ddagger}_{relative}$ ^[b]
CF ₃ -Ph-NH ₂ (e)	58170	-2.8	22.6	19.8

[a] The values of all ΔG are given in kcal·mol⁻¹. [b] $\Delta G^{\ddagger}_{rel} = \Delta G_0 + \Delta G^{\ddagger}_{red}$.

With regard to the thermodynamics of the process, the values are expected and fully consistent with the reported tendency for (POCOP)Ir complexes.⁸ Electron-withdrawing anilines provide more stable [Ir^{III}(H)(NHAr)] complexes than electron-rich anilines. As it was discussed therein, in low-spin d⁶ Ir^{III} complexes all the d_π orbitals are filled, thus there is repulsive interaction between the filled Ir π(d_{xy}) orbital and the filled Nπ (p_y) orbital. As the aniline becomes more electron-deficient, the energy of the Nπ orbital is lowered and the destabilizing interaction is reduced.²⁷ An alternative view is that electron-withdrawing substituents stabilize the negative charge on the anilide ligand, enhancing the electrostatic interaction between the metal and the anilide group and resulting in a greater Ir-N bond strength.

2.4. Additional experiments

The dynamic behavior of [(PCP)Ir(H)(NHAr-R)] complexes was examined with variable temperature NMR techniques to see whether the rate of reductive elimination/oxidative addition could be determined using line-broadening techniques. When complex **1a** was studied from -40°C to RT in mesitylene-*d*12, no broadening of the hydride at -38.1 ppm was observed. However, at higher temperature (75°C) the signal broadened and considerable loss of ^1H and ^{31}P signal was observed. Cooling down the sample back to RT did not recover the sharpness of the signal. Free aniline was detected, consistently with (**1a**) decomposition at high temperatures.

To prove if the signal was broadened due to the presence of free aniline, to a pure sample of (**1a**), 10 equivalents of free aniline were added. The signal broadened immediately.

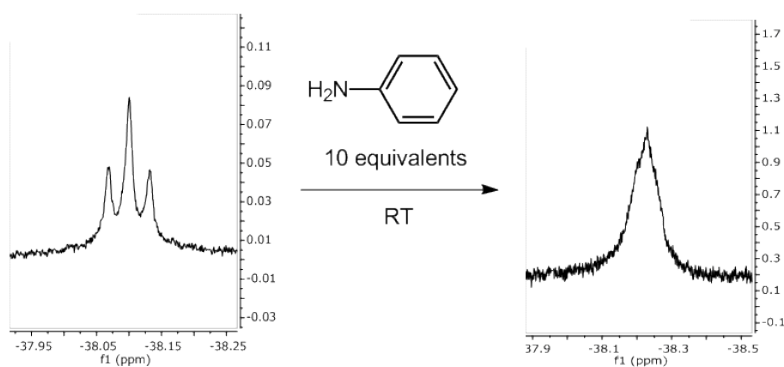


Figure V-4. Complex (**1a**) in the presence of 10 equivalents of free aniline.

It is not clear why this broadening takes place in the presence of free aniline. As it was demonstrated, the rate of reductive elimination does not depend on the concentration of free aniline. A possible explanation is that the protons of free aniline undergo chemical exchange with those of complex (**1a**).

Additional studies with complex (**1c**) were carried out to see if the bulkier and hence more protected aniline might help to stabilize the complex at higher

temperatures. It turned out to be more stable but some free aniline and somewhat broadened signals were obtained after heating at high temperatures.

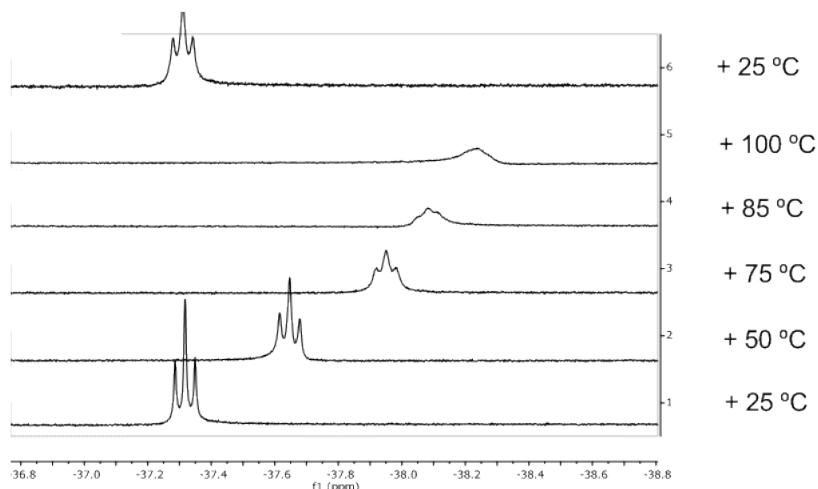


Figure V-5. From bottom to top. Variable temperature NMR of complex 1c in mesitylene-*d*12.

3. Conclusions

The mechanisms of N–H oxidative addition/reductive elimination of N–H bonds of anilines to 14-electron [Ir(PCP)] complexes have been evaluated by means of experimental studies and DFT calculations (not included herein).

We have been able to unveil the previously unknown shape of the potential energy surface of the process by the study of the KIE of the reductive elimination of [(PCP)Ir(H)(NHA*r*–R)] in the presence of DFB. We have proven that oxidative addition/reductive elimination is the rate limiting step. The study of the reversal oxidative addition at low temperatures allowed us for the detection in solution of the transient 4-coordinate σ -[(PCP)Ir^I–NH₂Ar] and other kinetic products.

Hammett plot of the reductive elimination of substituted [(PCP)Ir(H)(NHA*r*–R)] and equilibration of these complexes in the presence of benzene have revealed that faster oxidative additions and slower reductive eliminations take place in the

presence of electron-withdrawing groups. Consequently, electron-deficient [(PCP)Ir(H)(NHAr-R)] complexes show increased stabilities with respect to [(PCP)Ir(H)(Ph)], which result from stronger Ir-N bonds than those of electron rich anilides.

Although the role of the lone pair in the transition state cannot be established by any experimental measurement, the differences between the C-H activation and the N-H oxidative addition/reductive elimination suggest that there is a significant contribution of lone pair to Ir donation in the TS. DFT calculations will play a crucial role in determining the actual scenario.

4. Experimental section

4.1. General Considerations

All reactions were carried out under argon atmosphere in a dry box or using standard Schlenk techniques. All the anilines were purchased from Aldrich. Liquid anilines were dried over CaH_2 and vacuum-transferred to yield colorless liquids in a high vacuum line, which were stored in a $-40\text{ }^\circ\text{C}$ glovebox freezer. Solid anilines were purified by crystallization in hexanes. Solvents were degassed in a high vacuum line. They were dried in the glovebox over activated alumina and stored over molecular sieves. All other reagents were purchased from commercial suppliers and used without further purification. NMR spectra were acquired on 400 or 500 MHz Varian VNMR NMR spectrometers. ^1H and ^{13}C spectra are referenced to residual solvent peaks. ^{31}P NMR chemical shifts were referenced to a 85% H_3PO_4 external reference. $[(\text{PCP})\text{IrH}_2]^{28}$ and $[(\text{PCP})\text{IrHCl}]^{29}$ were prepared according to published methods. All other chemicals were used as received from commercial suppliers.

4.2. General synthesis of complexes $[(\text{PCP})\text{Ir}(\text{H})(\text{NHAr})]$

In a glovebox, 5 mg of $[(\text{PCP})\text{IrH}_2]$ were weighed in a vial, and 1 equivalent of the corresponding aniline was added, via syringe if the aniline is liquid, or weighed in the same vial if solid. Both reagents were dissolved in 200 μL of *p*-xylene. 3 mg (3 equivalents) of norbornene were dissolved in 200 μL of *p*-xylene. Both solutions were mixed together and transferred to a J-Young NMR tube. Within minutes, the initial brown solution became dark. The solvent and volatiles (norbornene, aniline excess, and norbornane) were removed in the vacuum line under reduced pressure. The remaining solid was dissolved in *p*-xylene-*d*10 or mesitylene-*d*12. These samples were used for the variable temperature NMR studies in mesitylene-*d*12.

(1a) $[(\text{PCP})\text{Ir}(\text{H})(\text{NHPH})]$

^1H NMR (300 MHz, *p*-xylene-*d*10) δ 7.16-6.91 (m, 5H, aniline H), 6.81 (d, $J_{\text{HH}} = 7.2$ Hz, 2H, PCP m-H), 6.63 (t, $J_{\text{HH}} = 7.2$ Hz, 1H, PCP p-H), 4.90 (s, 1H, N-H), 3.16 (d of vt, $J_{\text{PH}}=3.6$ Hz, $J_{\text{HH}}=17.1$ Hz, 2H, CH_2), 3.08 (d of vt, $J_{\text{PH}}=3.6$ Hz, $J_{\text{HH}}=17.1$ Hz, 2H, CH_2), 1.22 (t, $J_{\text{PH}}=6.45$ Hz, 18H, $\text{C}(\text{CH}_3)_3$), 1.16 (t, $J_{\text{PH}}=6.30$ Hz, 18 H, $\text{C}(\text{CH}_3)_3$), -38.21 (t, $J_{\text{PH}}=12.6$ Hz, 1H, Ir-H). ^{31}P NMR (121.4 MHz, *p*-xylene-*d*10): δ 66.81 (s).

(1b) $[(\text{PCP})\text{Ir}(\text{H})(\text{NHPH-CF}_3)]$

^1H NMR (500 MHz, *p*-xylene-*d*10) δ 7.49 (d, $J = 8.5$ Hz, 2H, aniline), 7.16-7.01 (overlapped with the solvent signal, 3H, PCP), 6.52 (d, $J = 8.7$ Hz, 2H, aniline), 3.96 (s, 1H, N-H), 3.24 (d of vt, $J_{\text{PH}}=3.8$ Hz, $J_{\text{HH}}=16.8$ Hz, 2H, CH_2), 3.16 (d of vt, $J_{\text{PH}}=3.8$ Hz, $J_{\text{HH}}=16.8$ Hz, 2H, CH_2), 1.20 (t, $J_{\text{PH}}=6.8$ Hz, 18H, $\text{C}(\text{CH}_3)_3$), 1.17 (t, $J_{\text{PH}}=6.8$ Hz, 18 H, $\text{C}(\text{CH}_3)_3$), -43.24 (t, $J = 13.1$ Hz, 1H, IrH). ^{31}P NMR (202.4 MHz, *p*-xylene-*d*10) δ 68.49 (d, $J = 12.6$ Hz). ^{19}F NMR (470 MHz, *p*-xylene-*d*10) δ -58.76 (s).

(1c) [(PCP)Ir(H)(3,5-NHPh-(CH₃)₂)]

¹H NMR (400 MHz, *p*-xylene-*d*10) δ 7.40-7.00 (overlapped with the solvent signal, 3H), 6.64 (s, 2H), 6.40 (s, 1H), 5.29 (s, 1H N-H), 3.30 (d of vt, *J*_{PH}=3.6 Hz, *J*_{HH}=16.8 Hz, 2H, CH₂), 3.12 (d of vt, *J*_{PH}=3.8 Hz, *J*_{HH}=16.8 Hz, 2H, CH₂), 1.34 (t, *J*_{PH}=6.45 Hz, 18H, C(CH₃)₃), 1.26 (t, *J*_{PH}=6.30 Hz, 18H, C(CH₃)₃) -37.29 (t, *J* = 12.6 Hz, 1H). ³¹P NMR (162 MHz, *p*-xylene-*d*10) δ 67.50 (s).

(1d) [(PCP)Ir(H)(4-NHPh-N(CH₃)₂)]

¹H NMR (400 MHz, *p*-xylene-*d*10) δ 7.06 (overlapped with the solvent signal, bs, 1H), 6.82 (d, *J* = 8.7 Hz, 2H), 6.69 (d, *J* = 8.7 Hz, 2H), 6.52 (bs, 2H), 6.17 (s, 1H N-H), 3.22 (q of vt, *J*_{HH} = 16.3, *J*_{PH} 3.8 Hz, 4H), 2.83 (s, 6H, NMe), -33.62 (t, *J* = 12.1 Hz, 1H IrH). ³¹P NMR (162 MHz, *p*-xylene-*d*10) δ 65.84.

(1e) [(PCP)Ir(H)(4-NHPh-O^tBu)]

¹H NMR (400 MHz, *p*-xylene-*d*10) δ 7.30-7.01 (overlapped with the solvent signal, 3H), 6.99 – 6.89 (m, 4H), 5.64 (s, 1H NH), 3.24 (d of vt, *J*_{PH}=3.5 Hz, *J*_{HH}=16.4 Hz, 2H, CH₂), 3.12 (d of vt, *J*_{PH}=3.5 Hz, *J*_{HH}=16.4 Hz, 2H, CH₂), 1.33 (t, *J*_{PH}=6.4 Hz, 18H, C(CH₃)₃), 1.26 (t, *J*_{PH}=6.4 Hz, 18 H, C(CH₃)₃), -35.44 (t, *J*_{PH} = 12.4, 1H). ³¹P NMR (162 MHz, *p*-xylene-*d*10) δ 66.72.

(1f) [(PCP)Ir(H)(4-NHPh-CO₂Me)]

¹H NMR (400 MHz, *p*-xylene-*d*10) δ 8.15 (d, *J* = 8.7 Hz, 2H), 7.30-7.00 (overlapped with the solvent signal, 3H), (6.50 (d, *J* = 8.8 Hz, 2H), 4.17 (s, 1H NH), 3.86 (s, 3H CO₂Me), 3.22 (dt, *J* = 9.8, 3.8 Hz, 15H), 1.21 (t, *J*_{PH}=6.3 Hz, 18H, C(CH₃)₃), 1.17 (t, *J*_{PH}=6.3 Hz, 18 H, C(CH₃)₃), -43.74 (t, *J*_{PH} = 13.1 Hz, 1H). ³¹P NMR (162 MHz, *p*-xylene-*d*10) δ 68.40 .

(1h) [(PCP)Ir(H)(CH₂Ph-2-NH₂-3,5-Me)]

¹H NMR (400 MHz, *p*-xylene-*d*10) δ 7.46 – 7.42 (m, 1H), 7.36 (d, *J* = 7.3 Hz, 2H), 7.18 (d, *J* = 7.2 Hz, 1H), 6.56 (s, 1H), 4.31 (s, 2H NH₂), 3.71 (t, *J* = 7.2 Hz, 2H IrCH₂), 3.54 (dt, *J*_{HH} = 16.7 , *J*_{PH} 4.3 Hz, 2H), 3.35 (dt, *J*_{HH} = 16.7, 3.0 Hz, 2H), 2.33 (s, 3H), 1.83 (s, 3H), 1.42 (t, *J*_{PH}=6.1 Hz, 18H, C(CH₃)₃), 1.08 (t, *J*_{PH}=5.8 Hz, 18 H, C(CH₃)₃), -20.76 (t, *J*_{PH} = 17.4 Hz, 1H IrH). ³¹P NMR (162 MHz, *p*-xylene-*d*10) δ 42.21.

The fact that no coupling is detected between the hydride and the Ir-CH₂ supports the assignment of the structure described in the main text.

4.3. Kinetic runs

Protic mesitylene was used in all the kinetic runs, otherwise stated. The NMR was previously tuned and shimmed with a sample of pure mesitylene-*d*12. Concentration-time data were acquired by integration of the ³¹P NMR using a calibrated capillary with a solution of OPPh₃ in mesitylene-*d*12 as internal standard. In order to assure full temperature equilibration, only the data acquired after 5

minutes were used. Kinetic constants were obtained using initial rates method, thus data points of the first 20% of the reaction were used in each run. Three runs were carried out for each determination and the values were averaged. Errors were determined by assuming an absolute error of 5% on all NMR integrations and propagating accordingly, as it has been applied in the literature in the determination of rate constants by NMR integration.³⁰

4.4. Study of the reductive elimination

a) Reductive elimination kinetics in the presence of DFB

15 mg [(PCP)IrH₂] was weighed in a vial inside a glovebox. The solid was dissolved in 1000 μ L of mesitylene. With a syringe, the appropriate amount of the corresponding aniline was added, or it was weighed in the vial prior to the addition of the solvent (1.2 equivalents). A separate solution of 9 mg of norbornene in 350 μ L of mesitylene was prepared. Both solutions were mixed. A color change was observed after a few minutes from orange to a very dark solution. This is indicative of the formation of the corresponding [(PCP)Ir(H)(NHAr)]. With a syringe, 450 μ L of this solution were added to 3 NMR tubes and closed with a septum. Each sample was frozen with a liquid nitrogen bath, and 50 μ L of a 1.7 M solution of difluorobenzene (10 equivalents) in mesitylene were added with a syringe. The final concentration of [(PCP)Ir(H)(NHAr)] in each sample is 0.017 M. The NMR tube was thawed and immediately inserted in a NMR probe thermostated at the appropriate temperature.

b) Temperatures of the NMR probe

Reductive eliminations of (1a) [(PCP)Ir(H)(NHPh)], (1c) [(PCP)Ir(H)(3,5-NHPh-(CH₃)₂)], (1d) [(PCP)Ir(H)(4-NHPh-N(CH₃)₂)], (1e) [(PCP)Ir(H)(4-NHPh-O^tBu)] were carried out with the NMR probe thermostated at -5 °C.

Reductive eliminations of (1b) [(PCP)Ir(H)(NHPh-CF₃)], (1f) [(PCP)Ir(H)(4-NHPh-CO₂Me)], were carried out with the NMR probe thermostated at 25 °C.

c) Reductive elimination in the presence of CO

A 0.017 M solution of [(PCP)Ir(H)(NHPh)] in mesitylene was prepared in a J-Young tube. In a high vacuum line, the solution was degassed and frozen in a bath of liquid nitrogen. The Ar atmosphere was replaced with 1 atm of CO. The sample was thawed and immediately inserted in the NMR probe at RT.

d) Reductive elimination in the presence of PET₃

Three samples of 0.017 M of [(PCP)Ir(H)(NHPh)] in mesitylene were prepared in NMR tubes, and closed with septa. Each sample was frozen in a liquid nitrogen bath, and 50 μ L of a 3.4 M solution of PET₃ in mesitylene were added with a syringe. The NMR tube was thawed and immediately inserted in a NMR probe thermostated at -15°C.

4.5. Study of the oxidative addition

A fresh sample of [(PCP)IrNBE] has to be prepared in each run. This complex is not stable and reacts slowly with the solvent. 5 mg of [(PCP)IrH₂] and 3 mg of norbornene were weighed in a vial. Both solids were dissolved in 400 μ L of mesitylene and transferred to a NMR tube, sealed with a septum. The sample was frozen in a liquid nitrogen bath. 100 μ L (2 equivalents) of a stock solution of aniline (16 μ L/mL, 2 equivalents) were added to the NMR tube via syringe. The final concentration of [(PCP)Ir(NBE)] in each sample is 0.017 M. The NMR tube was thawed and immediately inserted in a NMR probe thermostated at -15°C.

4.6. Equilibration of [(PCP)Ir(H)(Ph)] (5) with anilines and [(PCP)Ir(H)(NHA_r-R)] (1n)

In a glovebox, 5 mg of [(PCP)IrH₂] were weighed in a vial, and 1 equivalent of the corresponding aniline was added, via syringe if the aniline is liquid, or weighed in the same vial if solid. 3 mg of norbornene were dissolved in 400 μ L of benzene-*d*₆. The NBE solution was transferred to the vial with a syringe, and when everything was dissolved, to a J-young NMR tube. Each sample was checked by NMR after 1 hour. In all cases, equilibration was reached after 3 hours at RT. All the equilibrium constants were obtained by ³¹P NMR integration

4.7. DFT calculations

All calculations have been performed using the Gaussian09 collection of computer programs.³¹ We selected the DFT method and employed the M06-L model developed by Zhao and Truhlar for the exchange and correlation parts of the density functional.³² This functional has been used previously to describe the same system and showed the best agreement with our experimental results.³³ The electronic environment for all species within the reaction pathway was modeled using the following scheme: for Ir, we applied the LANL2TZ basis set augmented by a diffuse f-type function (exponent = 0.07645).³⁴ All other atoms were described by the 6-311G(d,p) basis set. Standard procedures were employed to obtain the geometries and electronic energies for stationary points (minima or transition states) along the reaction paths. Normal mode analysis was performed for each species to verify the nature of the located stationary point. Enthalpies (ΔH , ΔH^\ddagger) and Gibbs' free energies (ΔG , ΔG^\ddagger ; T = 298.15 K, P = 1 atm) were obtained from the electronic energies (ΔE , ΔE^\ddagger) using standard thermodynamic corrections. Increased atomic grid sizes were used for numerical integrations to enhance computational stability and accuracy of geometry optimizations and vibrational frequency calculations (grid=ultrafine option). Solvation effects were not considered explicitly in the calculations, since the experiments were carried out in non-polar hydrocarbons. A specific solvent dependence was not encountered in any of the experiments and a few selected calculations in which the general effects of a surrounding solvent were included via a continuum dielectric model revealed only very minor changes in reaction barrier heights (< 1 kcal/mol).

5. References

1. Kanzelberger, M.; Singh, B.; Czerw, M.; Krogh-Jespersen, K.; Goldman, A. S.; *J. Am. Chem. Soc.* **2000**, *122*, 11017-11018.
2. (a) Kundu, S.; Choi, J.; Wang, D.; Choliy, Y.; Emge, T. J.; Krogh-Jespersen, K.; Goldman, A. S.; *J. Am. Chem. Soc.* **2013**, *135*, 5127-5143. (b) Choi, J. Choliy, Y.; Zhang, X.; Emge, T. J.; Krogh-Jespersen, K. Goldman, A. S.; *J. Am. Chem. Soc.* **2009**, *131*, 15627–15629.
3. Choi, J.; Wang, D.; Kundu, S.; Choliy, Y.; Emge, T. J.; Krogh-Jespersen, K.; Goldman, A. S.; *Science*, **2011**, 1545-1548.
4. Laviska, D. A.; Guan, C.; Emge, T. J.; Wilklow-Marnell, M. Brennessel, W. W.; Jones, W. D.; Krogh-Jespersen, K.; Goldman, A. S.; *Dalton Trans.*, **2014**, *43*, 16354–16365.
5. Kanzelberger, M.; Zhang, X.; Emge, T. J.; Goldman, A. S.; Zhao, J.; Incarvito, C.; Hartwig, J. F. *J. Am. Chem. Soc.* **2003**, *125*, 13644.
6. (a) Zhao, J.; Goldman, A. S.; Hartwig, J. F.; *Science*, **2005**, *307*, 1080-1082. (b) Morgan, E.; MacLean, D. F.; McDonald, R.; Turculet, L.; *J. Am. Chem. Soc.* **2009**, *131*, 14234–14236.
7. Haggin, J.; *Chem. Eng. News.*; **1993**, *71*, 23.
8. (a) Sykes, A. C.; White, P.; Brookhart, M. *Organometallics*, **2006**, *25*, 1664. (b) Averkiev, B. B.; Truhlar, D. G. *Catal. Sci. Technol.* **2011**, *1*, 1526-1529. (c) Huang, Z.; Zhou, J. S.; Hartwig, J. F. *J. Am. Chem. Soc.* **2010**, *132*, 11458–11460.
9. (a) Glueck, D.; Winslow, L.; Bergman, R. G. *Organometallics*, **1991**, 1462–1479. (b) Huang, Z.; Zhou, J. S.; Hartwig, J. F. *J. Am. Chem. Soc.* **2010**, *132*, 11458–11460.
10. Sevov, C. S.; Zhou, J.; Hartwig, J. F. *J. Am. Chem. Soc.* **2014**, *136*, 3200–3207.
11. Sevov, C. S.; Zhou, J.; Hartwig, J. F.; *J. Am. Chem. Soc.*, **2012**, *134*, 11960-11963.
12. For a recent example see: (a) Kim, H.; Shin, K.; Chang, S. *J. Am. Chem. Soc.* **2014**, *136*, 5904–5907. For selected reviews see: (b) Collet, F.; Lescot, C.; Dauban, P. *Chem. Soc. Rev.* **2011**, *40*, 1926–1936. (c) Roundhill, D. M. *Chem. Rev.* **1992**, *92*, 1–27.
13. Krogh-Jespersen, K.; Czerw, M.; Zhu, K.; Singh, B.; Kanzelberger, M.; Darji, N.; Achord, P. D.; Renkema, K. B.; Goldman, A. S. **2002**, 10797–10809.

14. Churchill, D. G.; Janak, K. E.; Wittenberg, J. S.; Parkin, G. J. *Am. Chem. Soc.* **2003**, *125*, 1403–1420.
15. (a) Simmons, E. M.; Hartwig, J. F. *Angew. Chem. Int. Ed.* **2012**, *51*, 3066–3072. (b) Gómez-Gallego, M.; Sierra, M. a. *Chem. Rev.* **2011**, *111*, 4857–4963.
16. (a) Abis, L.; Sen, A.; Halpern, J. J. *Am. Chem. Soc.* **1978**, *100*, 2915–2916. (b) Michelin, R. A. *Inorg. Chem.* **1983**, *22*, 1831–1834.
17. Deprez; N. R.; Sanford; M. S. *J. Am. Chem. Soc.* **2009**, *131*, 11234.
18. For a fundamental explanation of Kinetic Isotope effects in C-H bond activation with transition metals see: Jones, W. D.; *Acc. Chem. Res.* **2003**, *36*, 140–146, and references therein.
19. Gómez-Gallego, M.; Sierra, M. a. *Chem. Rev.* **2011**, *111*, 4857–4963.
20. Jones, W. D.; Feher, F. J. *J. Am. Chem. Soc.* **1985**, *107*, 620–631.
21. Buchanan, J. M.; Stryker, J. M.; Bergman, R. G. *J. Am. Chem. Soc.* **1986**, *108*, 1537.
22. $KIE = \log(kH/kD)$.
23. Saillard, J.; Hoffmann, R.; *J. Am. Chem. Soc.* **1984**, *106*, 2006–2026.
24. Hansch, C.; Leo, a; Taft, R. W. *Chem. Rev.* **1991**, *91*, 165–195.
25. Sykes, A. C.; White, P.; Brookhart, M.; *Organometallics* **2006**, *25*, 1664–1675.
26. Zhang, X.; Kanzelberger, M.; Emge, T. J.; Goldman, A. S. *J. Am. Chem. Soc.* **2004**, *126*, 13192–13193.
27. Krogh-Jespersen, K.; Czerw, M.; Zhu, K.; Singh, B.; Kanzelberger, M.; Darji, N.; Achord, P. D.; Renkema, K. B.; Goldman, A. S. *J. Am. Chem. Soc.* **2002**, *124*, 10797.
28. Gupta, M.; Hagen, C.; Kaska, W. C.; Cramer, R. E.; Jensen, C. M. *J. Am. Chem. Soc.* **1997**, *119*, 840–841.
29. Moulton, C. J.; Shaw, B. L. *J. Chem. Soc., Dalton Trans.* **1976**, 1020–1024.
30. Milner, P. J.; Maimone, T. J.; Su, M.; Chen, J.; Müller, P.; Buchwald, S. L. *J. Am. Chem. Soc.* **2012**, *134*, 19922–19934.
31. Gaussian 09, Revision D, M. J. Frisch, G. W. Trucks, H. B. Schlegel, G. E. Scuseria, M. A. Robb, J. R. Cheeseman, G. Scalmani, V. Barone, B. Mennucci, G. A. Petersson, H. Nakatsuji, M. Caricato, X. Li, H. P. Hratchian, A. F. Izmaylov, J. Bloino, G. Zheng, J.

L. Sonnenberg, M. Hada, M. Ehara, K. Toyota, R. Fukuda, J. Hasegawa, M. Ishida, T. Nakajima, Y. Honda, O. Kitao, H. Nakai, T. Vreven, J. A. Montgomery, Jr., J. E. Peralta, F. Ogliaro, M. Bearpark, J. J. Heyd, E. Brothers, K. N. Kudin, V. N. Staroverov, R. Kobayashi, J. Normand, K. Raghavachari, A. Rendell, J. C. Burant, S. S. Iyengar, J. Tomasi, M. Cossi, N. Rega, N. J. Millam, M. Klene, J. E. Knox, J. B. Cross, V. Bakken, C. Adamo, J. Jaramillo, R. Gomperts, R. E. Stratmann, O. Yazyev, A. J. Austin, R. Cammi, C. Pomelli, J. W. Ochterski, R. L. Martin, K. Morokuma, V. G. Zakrzewski, G. A. Voth, P. Salvador, J. J. Dannenberg, S. Dapprich, A. D. Daniels, Ö. Farkas, J. B. Foresman, J. V. Ortiz, J. Cioslowski, D. J. Fox, Gaussian, Inc., Wallingford CT, **2009**.

32. Zhao, Y.; Truhlar, D. G.; *Theo. Chem. Acc.* **2008**, 120, 215.

33. Averkiev, B. B.; Truhlar, D. G. *Catal. Sci. Technol.* **2011**, 1, 1526-1529.

34. (a) Hay, P. J.; Wadt, W. R.; *J. Chem. Phys.* **1985**, 82, 299. (b) Roy, L. E.; Hay, P. J.; Martin, R. L.; *J. Chem. Theory Comput.* **2008**, 4, 1029.

Resumen en español

La etapa de transmetalación en procesos catalizados por paladio: Estudio del papel del nucleófilo clásico, de los ligandos, y del potencial en síntesis de un tercer metal.

1. Introduction

Las reacciones de acoplamiento cruzado catalizadas por paladio han cambiado la manera en la que los químicos diseñan las síntesis en la actualidad. Estos procesos ocupan por derecho propio un espacio central en la construcción de moléculas complejas tanto en entornos académicos como en la industria. Para el diseño de procesos eficientes basados en estas reacciones, la gran comprensión alcanzada sobre el mecanismo por el cual transcurren ha tenido una importancia fundamental.

Las reacciones de acoplamiento cruzado tienen lugar entre un electrófilo orgánico y un nucleófilo organometálico, para lo cual es necesario el empleo de un catalizador, habitualmente de paladio, capaz de realizar de manera eficiente las siguientes etapas: adición oxidante, transmetalación y eliminación reductora. Las etapas de adición oxidante y eliminación reductora son etapas independientes del nucleófilo empleado y son comunes (salvo en los casos de complicaciones asociadas) a todas las variantes de procesos catalizados por paladio, mientras que la etapa de transmetalación es muy dependiente del nucleófilo escogido y suele condicionar en gran medida el proceso en su conjunto. La elección de un tipo de nucleófilo u otro limita las posibles condiciones de reacción y la tolerancia a grupos funcionales de la síntesis. Por un lado, el empleo de nucleófilos muy reactivos (litiados o magnesianos) permite reacciones en condiciones muy suaves, pero tiene una baja tolerancia a grupos funcionales y, en ocasiones, produce una baja selectividad del proceso. Por el contrario, el empleo de nucleófilos poco reactivos, como borónicos o silanos, requiere el uso de condiciones más drásticas y el empleo de aditivos que potencien su reactividad (fluoruros o bases), pero poseen una tolerancia muy alta a todo tipo de grupos funcionales presentes en la reacción. Adicionalmente, su baja reactividad los hace estables al aire y almacenables. Es destacable que el mecanismo por el cual transcurre la etapa de transmetalación es muy diferente en función del nucleófilo empleado.

2. Metodología

El propósito fundamental de esta Tesis Doctoral, ha sido comprender y mejorar la etapa de transmetalación en varios sistemas de interés. En los Capítulos I y II se ha realizado el estudio de la reacción de Stille y de Hiyama respectivamente con grupos voluminosos. Cuando este tipo de sustratos están implicados, las reacciones de acoplamiento cruzado se vuelven mucho más lentas e ineficaces. En ambos capítulos se ha estudiado el efecto de la presencia de un metal adicional del grupo XI (oro y cobre, respectivamente) en la etapa de transmetalación, y se ha estudiado el papel de los ligandos auxiliares en los catalizadores en la eficiencia del proceso sintético. Cabe destacar que esta metodología ha permitido desarrollar procesos multimetálicos muy eficientes sin precedente en la bibliografía, en condiciones de reacción suaves y con materiales sencillos y disponibles.

La reacción de Negishi es ampliamente utilizada en síntesis orgánica para el acoplamiento de grupos alquilo, debido a que los alquilzincs son reactivos ideales por su gran reactividad en la etapa de transmetalación. Sin embargo, esta reacción a menudo se ve dificultada por transmetalaciones competitivas indeseadas que dan lugar a subproductos y disminuyen la eficiencia de la síntesis. En el Capítulo III por medio de medidas cinéticas y experimentos computacionales, hemos llevado a cabo el estudio del papel del ZnMe_2 (un nucleófilo habitual de la reacción de Negishi) en la formación de estos subproductos, y en otras reacciones con el catalizador de paladio que son relevantes para el transcurso sintético.

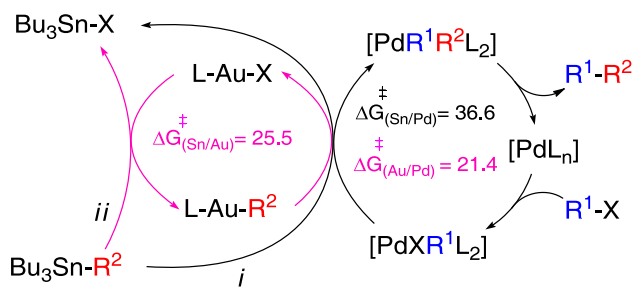
El Capítulo IV contiene el trabajo realizado a lo largo del Doctorado en una línea de investigación distinta de la principal de esta Tesis Doctoral, y que se está realizando también en el grupo de la Universidad de Valladolid. Este trabajo consiste en la investigación por medio de técnicas experimentales y computacionales de un ligando fosfina-olefina diseñado en nuestro grupo con el propósito de incrementar la reactividad de los catalizadores de paladio para procesos muy complicados. Parte de este trabajo ha sido realizado en colaboración con el Dr. Vladimir V. Grushin en el Instituto Catalán de Investigaciones Químicas (ICIQ) en Tarragona.

Por último, en el Capítulo V se detalla el estudio del mecanismo de adición oxidante de enlaces N-H de anilinas a complejos de iridio con ligandos pincer [Ir(PCP)]. El mecanismo de esta reacción ha sido examinado por medio de técnicas cinéticas y computacionales. El resultado de este trabajo ayudará a desarrollar procesos catalíticos que incluyan esta activación, como la adición de amoníaco a olefinas. Este trabajo ha sido realizado en la universidad de Rutgers, (Nueva Jersey, Estados Unidos) bajo la supervisión del Profesor Alan Goldman para optar a la Mención Internacional de esta Tesis Doctoral.

3. Resumen de los resultados

3.1. Capítulo I: La reacción de Stille cocatalizada por oro

La reacción de Stille ha sido ampliamente estudiada en nuestro grupo y presenta una aplicabilidad alta para la síntesis de principios activos como fármacos, cosméticos y otros productos de alto valor añadido, debido a su alta tolerancia de grupos funcionales, su selectividad y su buen rendimiento. Cuando los organoestannanos habituales empleados como nucleófilos son voluminosos, la etapa de transmetalación Sn/Pd es muy lenta y el ciclo catalítico se vuelve ineficaz. En presencia de catalizadores de oro se abre una nueva transmetalación Sn/Au/Pd que transcurre por estados de transición más bajos en energía, permitiendo así la obtención de biarilos voluminosos con buen rendimiento. El estudio computacional de las transmetalaciones Sn/Au, Au/Pd y Sn/Pd confirma que para la transferencia de grupos voluminosos, la vía catalizada por oro es sensiblemente más rápida que la vía clásica sin mediación del cocatalizador.



Esquema Resumen-1. Caminos de reacción: (i) Reacción de Stille clásica (ii) Reacción de Stille cocatalizada por complejos de oro.

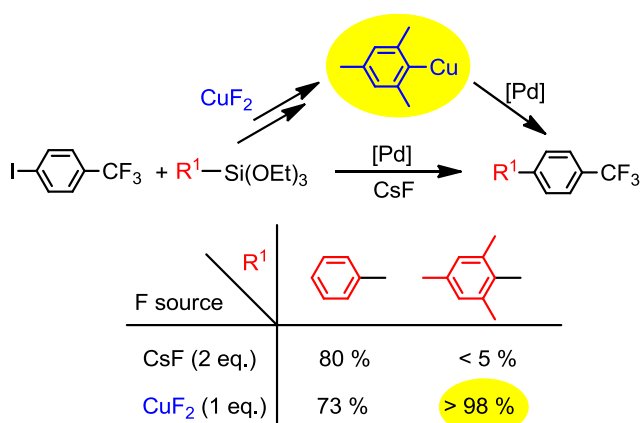
En caso de que los catalizadores de oro y paladio presenten ligandos diferentes, se produce una reorganización de los mismos en el medio de reacción que puede ser decisiva para el éxito o el fracaso de la reacción de acoplamiento cruzado. Ambos metales presentan requerimientos estéricos y electrónicos diferentes, por lo que la combinación de ligandos, y la elección de la posición inicial de los mismos es importante para el desarrollo sintético. Se han estudiado estos intercambios de ligandos desde un punto de vista mecanístico, permitiendo establecer las combinaciones óptimas para ambos metales.

3.2. Capítulo II: Reacción de Hiyama bimetalica con grupos voluminosos promovida por CuF_2

Entre la variedad de reacciones de acoplamiento cruzado habitualmente empleadas, la reacción de Hiyama es particularmente interesante debido a la gran estabilidad de los nucleófilos de silicio, la alta compatibilidad con todo tipo de grupos funcionales y la nula toxicidad de los subproductos de reacción. Aunque esta reacción se ha empleado en la síntesis de moléculas muy complicadas, hasta el momento es mucho menos popular que las reacciones homologas de Suzuki o Negishi. Una grave limitación en su aplicación es que la reacción de Hiyama es ineficaz a la hora de acoplar grupos voluminosos.

Hemos desarrollado un sistema bimetalico Pd/ CuF_2 (catalítico en paladio pero estequiométrico en CuF_2) capaz de realizar el acoplamiento de silanos muy

voluminosos de manera muy eficiente y selectiva. El proceso tolera arilos con todo tipo de grupos funcionales como piridinas o aldehídos, que son problemáticos con otras metodologías de síntesis. El catalizador mixto $[\text{PdCl}_2(\text{IDM})(\text{AsPh}_3)]$ demostró ser el más efectivo de todos los ensayados. Entre sus ventajas, destacan su gran facilidad de síntesis y su gran actividad. A pesar del aparente inconveniente del uso de una fuente de arsénico en el catalizador, la facilidad de purificación de los productos finales permite obtenerlos esencialmente libres de As y Pd (concentraciones de ambos metales < 1 ppm).



Esquema Resumen-2. Representación de las ventajas de la reacción de Hiyama promovida por CuF_2 frente a otros activadores clásicos (CsF). Mientras que CsF solo es efectivo con arilos no voluminosos, el CuF_2 permite la obtención de sustratos impedidos con rendimientos excelentes.

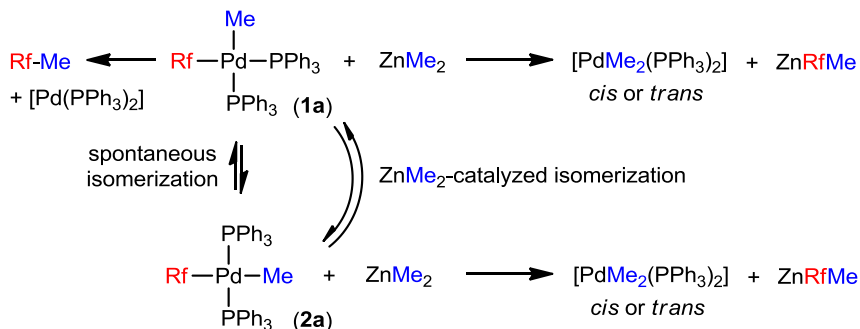
Adicionalmente, se ha realizado un estudio mecanístico del proceso para comprender el origen de la gran selectividad encontrada. La reacción comienza por la activación del silano por el CuF_2 , generando un arilo de cobre (II) intermedio. El organometálico de Cu^{II} es inestable y se desproporciona para dar lugar a un arilo de Cu^{I} , y otro de Cu^{III} que es reducido a Cu^{I} en presencia de exceso de silano. Los organometálicos de Cu^{I} son capaces de transmetalar el arilo voluminoso al catalizador de Pd^{II} , en el cual tiene lugar el acoplamiento. En estas condiciones de reacción, el CuF_2 es transformado íntegramente en Cu^{I} -arilo, y no es necesario el empleo de ninguna otra fuente de fluoruro adicional. En este sentido, el sistema es

muy conveniente, pues el CuF_2 es, además, una fuente de F^- más barata que las empleadas habitualmente en la reacción de Hiyama clásica.

3.3. Capítulo III: Estudio de la transmetalación secundaria en la reacción de Negishi

El acoplamiento de grupos alquilo tiene una gran importancia en la química de síntesis, pues estos grupos son los más habituales en moléculas con todo tipo de aplicaciones; sin embargo, su empleo en síntesis presenta dificultades con nucleófilos poco reactivos como borónicos o estannanos. La reacción de Negishi es ampliamente utilizada para este propósito, debido a que los organozincicos empleados como nucleófilos en la reacción de Negishi son agentes transmetalantes muy activos.

En este apartado, hemos llevado a cabo el estudio de la reacción entre complejos de paladio del tipo $[\text{PdArMe}(\text{PR}_3)_2]$ y ZnMe_2 por medio de medidas cinéticas y computacionales. Estos complejos de paladio son intermedios conocidos del ciclo catalítico de la reacción de Negishi, y su reacción con ZnMe_2 da lugar a los subproductos indeseados del tipo ZnArMe , por intercambio Ar/Me (transmetalación secundaria). A través de los mismos intermedios que en el caso de la transmetalación secundaria, el ZnMe_2 puede catalizar los procesos de isomerización *cis/trans* de los intermedios de paladio a través de intercambios Me/Me. Tal cual se detalla en texto principal, este proceso puede tener una gran relevancia en el transcurso de la síntesis. Los intercambios Ar/Me y Me/Me se ha estudiado de manera independiente.

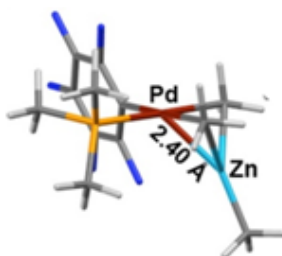


Esquema Resumen-3. Reacciones de complejos $[\text{PdRfMe}(\text{PPh}_3)_2]$ con ZnMe_2 .

La isomerización *cis/trans* de complejos $[\text{PdArMe}(\text{PR}_3)_2]$ a través de intercambios Me/Me puede ser catalizada por ZnMe_2 , o puede ocurrir espontáneamente (esto es, en ausencia de ZnMe_2). Ambos procesos tienen lugar en competencia. El mecanismo no catalizado ha sido examinado experimentalmente por medio de técnicas cinéticas, y ocurre a través de la disociación de un ligando neutro, seguido de una etapa de topomerización y recoordiación del ligando. Por el contrario, la isomerización catalizada por ZnMe_2 no puede ser estudiada con facilidad por técnicas cinéticas clásicas, por lo que ha sido estudiado por técnicas DFT. Comparando los valores de las energías de activación calculadas con los obtenidos experimentalmente, es posible que, en determinadas condiciones, ambos procesos (espontáneo y catalizado) tengan lugar a velocidades competitivas, ya que sus constantes de velocidad son parecidas, pero en condiciones de alta concentración del reactivo-catalizador ZnMe_2 es de esperar que la isomerización catalizada sea muy predominante.

El estudio computacional ha mostrado que el ZnMe_2 se comporta como un centro fuertemente básico, lo cual contrasta con el comportamiento típicamente ácido del Zn en el ZnMeCl . Esta característica hace que ambos nucleófilos se comporten de maneras muy diferentes en el contexto de la reacción de Negishi, como se ha comprobado en trabajos anteriores. En los estados de transición y en ciertos intermedios encontrados computacionalmente como participantes del proceso de intercambio Me/Me, se encuentran distancias Zn-Pd muy cortas, significativamente inferiores a los radios de Van der Waals de ambos centros

metálicos, sugiriendo una gran interacción entre los metales. Estas distancias están relacionadas con la formación de enlaces deficientes de 3-centros 2-electrones.



Esquema Resumen-4. Estructura calculada de un intermedio de la reacción de intercambio de Me por Me entre complejos $[\text{PdArMe}(\text{PR}_3)_2]$ y ZnMe_2 .

El análisis cinético del intercambio indeseado de Ar por Me ha revelado un comportamiento diferente de los isómeros *cis* y *trans* de complejos $[\text{PdArMe}(\text{PR}_3)_2]$ ($\text{PR}_3 = \text{PPh}_3$) en el intercambio Ar/Me con ZnMe_2 . El isómero *cis* intercambia su grupo a través de intermedios de paladio tetracoordinados, en los cuales la primera etapa es la sustitución de una molécula de PPh_3 por ZnMe_2 , mientras que el isómero *trans* realiza el intercambio a través de estados de transición pentacoordinados, sin sustitución de PPh_3 . El estudio ha mostrado que la velocidad de este intercambio indeseado es significativa a temperatura ambiente y que es necesario evitar la acumulación de intermedios del tipo $[\text{PdArMe}(\text{PR}_3)_2]$ por medio de ligandos que induzcan la eliminación reductora y que favorezcan configuraciones *cis* (ligandos quelato).

3.4. Capítulo IV: Inestabilidad inesperada de los complejos Pd–fosfina–olefina

El desarrollo de procesos de fluoración y trifluorometilación de haluros de arilo catalizados por paladio presenta muchos problemas debido a que la etapa clave de eliminación reductora es muy lenta. Considerando la gran importancia de esta área de investigación, el desarrollo de ligandos capaces de acelerar esta reacción es muy deseable. Ligandos fosfina que presentan una olefina aceptora en su estructura

(PEWOs) se han mostrado efectivos para este propósito en trabajos anteriores en nuestro grupo de investigación. El objetivo de este trabajo, se centró en sintetizar y estudiar la eliminación reductora de complejos $[\text{PdAr}(\text{F})(\text{PEWO})]$ y $[\text{PdAr}(\text{CF}_3)(\text{PEWO})]$. La síntesis de estos complejos no ha sido posible, debido a una reacción inesperada de inserción migratoria de la olefina del ligando en el enlace $\text{Pd}-\text{Ar}$, produciendo complejo paladaciclo desde el cual no tiene lugar la eliminación reductora. Por medio de un estudio computacional, se ha caracterizado el proceso de reorganización de los complejos de paladio del tipo $[\text{PdR}^1\text{X}(\text{PEWO})]$ y $[\text{PdR}^1\text{R}^2(\text{PEWO})]$ y se ha comparado con el proceso competitivo de eliminación reductora de los segundos.

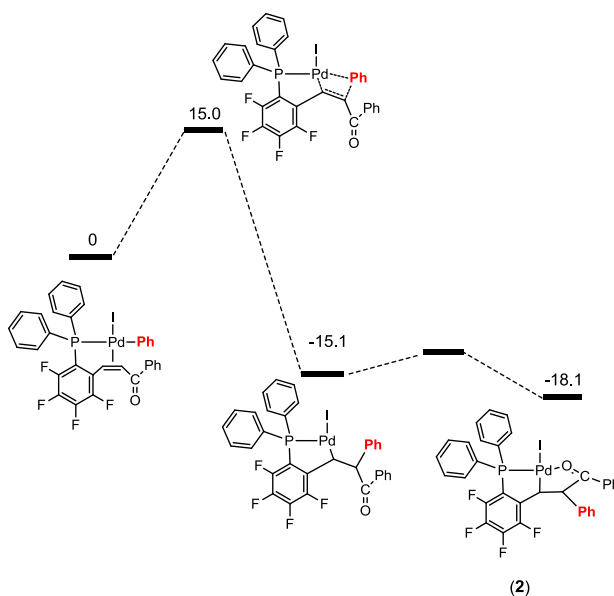


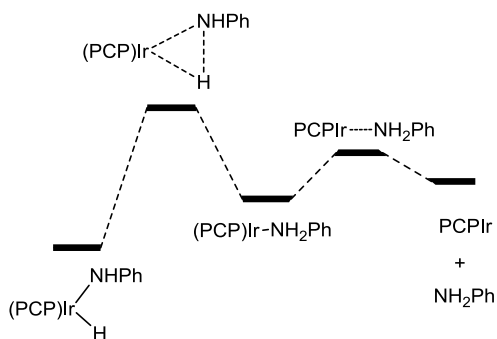
Figura Resumen-1. Proceso de inserción migratoria de la olefina del ligando PEWO en el enlace $\text{Pd}-\text{Ph}$ del complejo $[\text{PdPh}(\text{I})(\text{PEWO})]$.

Los datos obtenidos sugieren que los procesos de eliminación reductora son más rápidos que los procesos de inserción migratoria excepto cuando el grupo CF_3 está implicado. En los complejos que presentan este grupo, la tendencia se invierte, en concordancia con los resultados experimentales. El estudio computacional sugiere que los sistemas catalíticos basados en PEWO requieren que la etapa de transmetalación sea más rápida que la reorganización del complejo intermedio

[PdR¹X(PEWO)] para ser efectivos. En este sentido, los organozincos utilizados en la reacción de Negishi han proporcionado resultados satisfactorios en trabajos anteriores debido a su gran actividad para la transmetalación.

3.5. Capítulo V: Estudio de la adición oxidante/eliminación reductora de enlaces N–H

Las especies insaturadas de [Ir^I(PCP)] son muy reactivas, y son capaces de dar procesos de adición oxidante de enlaces N–H de anilinas, así como de otros muchos enlaces. Comprender los mecanismos por los cuales tienen lugar estos procesos es importante para el desarrollo de catálisis con aminas y amoniaco, que son de mucho interés para multitud de aplicaciones. La etapa inversa de eliminación reductora ha sido estudiada por medio de técnicas cinéticas clásicas, marcaje isotópico y computación.* Ha sido posible comprender la superficie de energía potencial del proceso, y obtener datos cuantitativos de las barreras de activación medibles experimentalmente, así como la detección de intermedios de reacción previamente desconocidos.



Esquema Resumen-5. Superficie de energía potencial de la eliminación reductora/adición oxidante de enlaces N–H a complejos [Ir(PCP)].

La reacción transcurre a través de una etapa limitante para la velocidad de reacción de eliminación reductora del enlace N–H, seguido por una coordinación

* Los resultados obtenidos son igualmente aplicables en el sentido de la adición oxidante, de acuerdo al principio de reversibilidad microscópica.

reversible y comparativamente rápida del par electrónico de la anilina a las especies [Ir(PCP)]. Los grupos dadores de densidad electrónica aceleran la etapa de eliminación reductora, mientras que el impedimento estérico severo en torno al enlace N–H protege a la anilina frente a su activación.

4. Conclusiones generales

Aunque la temática abordada en esta Tesis Doctoral es diversa, los estudios abordados en ella se han centrado en la comprensión y mejora de la etapa de transmetalación en reacciones de acoplamiento catalizadas por paladio. Los resultados obtenidos permiten concluir:

Complejos de metales del grupo XI (Au y Cu) son capaces de transmetalalar grupos con gran impedimento estérico a paladio más rápidamente que los derivados correspondientes de tributilestannano y tetraetoxisilano. Basándonos en esta idea, hemos diseñado sistemas bimetálicos muy efectivos para la obtención de biarilos altamente impedidos.

Hemos estudiado el papel de los ligandos auxiliares en catálisis con más de un metal, examinando los procesos dinámicos de intercambio de los mismos entre los metales y su papel en la efectividad de la síntesis. El resultado obtenido resalta la importancia de la buena elección de los ligandos a la hora de diseñar procesos multimetálicos, pues las necesidades electrónicas y estéricas de los metales participantes son muy diferentes.

Los intercambios indeseado Me/Me y Ar/Me entre complejos del tipo [PdArMeL₂] y el ZnMe₂ ocurren a temperatura ambiente pueden ser responsables de productos indeseados. El empleo de ligandos quelato que induzcan la eliminación reductora puede minimizar el papel de estas reacciones secundarias en procesos de síntesis.

Los ligandos fosfina–olefina aceptora no son capaces de promover la eliminación reductora de Ar–F o Ar–CF₃, debido a un proceso competitivo de reorganización del ligando más rápido que la eliminación reductora.

El Capítulo V, al margen de esta línea principal de trabajo, ha sido realizado en el grupo de Alan Goldman (Rutgers University, Estados Unidos) como parte de la actividad de tesis doctoral tendente a la obtención de Mención Internacional.

